12-13-2022 10:00 AM

Seismic Site Characterization and Response in Metropolitan Vancouver

Jamal Assaf, *The University of Western Ontario*

Supervisor: El Naggar, Hesham M., *The University of Western Ontario*
Joint Supervisor: Molnar, Sheri, *The University of Western Ontario*
A thesis submitted in partial fulfillment of the requirements for the Doctor of Philosophy degree in Civil and Environmental Engineering
© Jamal Assaf 2022

Recommended Citation

Abstract

Metropolitan (Metro) Vancouver is the largest city in British Columbia and has the highest earthquake risk in Canada due to vulnerability of persons and infrastructure located near the Cascadia subduction zone. The effects of local geology on seismic waves (site effects) play a major role in determining surface shaking levels and seismic hazard. Site effects are typically accounted for in ground motion prediction by inclusion of important seismic site characteristics. This thesis first evaluates the seismic site characteristics across Metro Vancouver then facilitates the development of a region-specific site amplification model.

To evaluate site characteristics in Metro Vancouver, a comprehensive database of seismic site condition measures is compiled to develop important predictive site characteristic models for site-specific and regional application. Non-invasive surface wave measurements are conducted to obtain the depth to glacial till (z_{gl}) and deep shear wave velocity (Vs) profiles with their uncertainties in the Fraser River Delta (FRD). A model to predict z_{gl} based on the 2nd peak frequency of the microtremor horizontal-to-vertical spectral ratio (MHVSR) is proposed. Seismic Cone Penetration Testing (SCPT) soundings are compiled to derive a CPT-to-Vs model using traditional linear and nonlinear regressions along with two machine learning approaches and a combination of CPT parameters. Machine learning approaches show slightly improved prediction accuracy compared to traditional regression due to the availability of a large database. A comprehensive Vs database is collected from available invasive and acquired non-invasive *in situ* measurements in the region. Generic Vs-depth relationships of post-glacial, glacial and rock geologies are developed. A comprehensive Vs_{30}, the time-averaged shear wave velocity to depth 30 m, database is established from direct Vs measurements and via conversion of other *in situ* measurements using the developed predictive models. Region-specific Vs_{30} prediction models are developed based on mapped geology and topographic slope or z_{gl}.

To facilitate the development of a region-specific site amplification model, one-dimensional (1D) site response analyses (SRA) of the Metro Vancouver region are conducted. Input time histories for the three earthquake source types are scaled at 2 and 10

% probability of exceedance in 50 years consistent with the national probabilistic seismic hazard model. The predicted linear and nonlinear SRA de/amplification spectra at 8 selected sites are compared to a site amplification model for a western North America (WNA) ground motion model (GMM). The WNA amplification model overestimates or underestimates linear site amplification for deep and shallow sites in Metro Vancouver respectively. For thick post-glacial sediments in the FRD and North Shore, stronger nonlinearity is predicted than exists in the WNA amplification model. Potential sources of 1D SRA uncertainties in Metro Vancouver are quantified via sensitivity analysis. The 1D SRA accomplished in this thesis are an important step towards developing a region-specific site amplification model that can be combined with developed site characteristics mapping to produce the first 1D site amplification map for Metro Vancouver.

Summary for Lay Audience

Seismic hazard quantification is a first step towards making informed decisions in urban planning and engineering applications to reduce the impact of earthquakes. Seismic site effects or the effect of near surface geology on the seismic waves plays a major role in determining the shaking hazard at the surface. Seismic site characteristics are metrics that correlate well with observed site effects. These characteristics include the variation of the soil stiffness with depth, shear wave velocity (Vs) depth profile, Vs_{30} (the time-averaged shear wave velocity to 30 m depth), and depths to glacial sediments and rock.

This thesis provides predictive models to spatially map important site characteristics in Metro Vancouver and facilitates the development of region-specific models to account for site effects. Cost-effective non-invasive measurements are conducted to obtain measures of site characteristics (Vs profiles, z_{gl}) in the Fraser River Delta (FRD). A model to map z_{gl} based on non-invasive measurements is proposed for shallow sites. Available geotechnical field measurements (seismic cone penetration testing, SCPT) are compiled to derive a Vs predictive model from CPTs using traditional and machine learning regression approaches. The findings promote the use of machine learning approaches in geotechnical applications when a large database is available. A comprehensive Vs database is collected from existing and acquired measurements and average Vs of different sediments are presented. Further, the predictive models are applied to available measurements to propose a model to produce the first Vs_{30} map for Metro Vancouver. A Vs_{30} map is an essential input to many applications involving emergency response, urban planning, and risk studies.

Finally, numerical simulations are conducted to predict site-specific surface ground motions inclusive of 1D site effects. Earthquake loading for different types of earthquakes is determined and propagated through soil models to predict site amplification. Comparison of the site-specific amplification with those predicted from a ground motion prediction equation applicable to the region is inconsistent and confirms our site-specific modelling is required to predict accurate ground motions in Metro Vancouver. Recommendations for

developing a new model that better captures Metro Vancouver soil response during earthquakes are provided.

Co-Authorship Statement

This thesis includes original results of the research conducted by the candidate under the supervision of Dr. Hesham El Naggar (Civil & Environmental Engineering) and Dr. Sheri Molnar (Earth Sciences). This thesis is presented in Integrated Article format and the following manuscripts have been published, submitted, or prepared for submission, to peer-reviewed journals.

Preliminary results presented in Chapters 3 were published in the 12th Canadian Conference on Earthquake Engineering Proceedings and superseded by Assaf et al. (2022):

Assaf, J., Molnar, S., El Naggar, M.H., Sirohey, A. (2019). Seismic Site Characterization at Strong Motion Stations in Metro Vancouver, 12th Canadian Conference of Earthquake Engineering, Quebec City, Quebec. 8 pages.

Assaf, J., Molnar, S., El Naggar, M.H., Sirohey, A. (2022). Seismic site characterization in Fraser River Delta in Metropolitan Vancouver. Soil Dynamics and Earthquake Engineering 161:107384. https://doi.org/https://doi.org/10.1016/j.soildyn.2022.107384

Material presented in Chapter 4 is published in Soil Dynamics and Earthquake Engineering journal:

Assaf, J., Molnar, S., El Naggar, M.H. (2023a). CPT-Vs Correlations for Post-glacial Sediments in Metropolitan Vancouver. Soil Dynamics and Earthquake Engineering 165:107693. https://doi.org/10.1016/j.soildyn.2022.107693

Material presented in Chapter 5 is prepared for submission to Bulletin of Seismological Society of America:

Acknowledgments

I would like to express my sincere gratitude to Dr. Hesham El Naggar and Dr. Sheri Molnar for their continuous support throughout this thesis work. I appreciate all the knowledge and the motivation they provided me with during every stage in this long journey. Their exemplary dedication on a professional level and their kindness on a personal level will always inspire me throughout my life.

Thank you to the examining committee, Dr. Miroslav Nastev, Dr. Bing Li, Dr. Aly Ahmed, and Dr. Jinfei Wang for their time examining this thesis and providing thoughtful comments and suggestions.

I would like to thank my friends from the Geotechnical Research Center at the Civil & Environmental Engineering department and from the Good Vibrations and Excitation group at Earth Science department for sharing this journey with me and making me feel I belong to both departments.

Finally, Thank you to my parents and siblings for their unconditional love and support. To my uncle's family in London, thank you for being there for me since day one in Canada. Thank you to all my extended family in Calgary for their continuous support and belief in me.

Table of Content

List of Tables

List of Figures

List of Abbreviations and Symbols

AMEN   Assaf, Molnar, El Naggar

B/C   NBC site class boundary between B and C

CanadaSHM6 The 6th Generation Seismic Hazard Model of Canada

CENA   Central Eastern North America

Dmin   Small-strain damping

FRD   Fraser River Delta

f_0 Fundamental site frequency

$f_{0,HVSR}$ Fundamental peak frequency from MHVSR

$f_{1,HVSR}$ 2nd peak frequency from MHVSR

$f_{m,pgl}$ Theoretical fundamental resonant frequency of post-glacial sediments

GMM   Ground Motion Model

GSC   Geologic Survey of Canada

HRFK   High-resolution frequency wavenumber

MAM   Microtremor Array Measurement

MASW   Multichannel analysis of surface waves

Metro   Metropolitan

MHVSR   Microtremor horizontal to vertical spectral ratio

MLR   Multi-linear regression

MSPAC	Modified Spatial Auto Correlation
MRD	Modulus reduction and damping curves
M_w	Moment magnitude
NBCC	National Building Code of Canada
NGA-West2	Next Generation Attenuation (NGA) GMM development for shallow crustal earthquakes in Western North America (West), second database (West2)
NGA-Sub	Next Generation Attenuation (NGA) GMM development for interface earthquakes (Subduction, Sub)
NLR	Nonlinear least square regression
PGA	Peak ground acceleration
PGA_r	Peak ground acceleration at rock level
POE	Probability of Exceedance
PSA	Pseudo-spectral acceleration (5 % damping)
PSHA	Probabilistic seismic hazard analysis
Vs	Shear wave velocity
Vs(z)	Shear wave velocity depth (z) profile
Vs_z	Time-averaged shear-wave velocity to a depth (z) in meters
Vs_{zp}	Time-averaged shear-wave velocity to the maximum profile depth (zp)
Vs_{30}	Time-averaged shear-wave velocity of the top 30 meters

RFR	Random Forest regression (RFR)
S/CPT	Seismic/ Cone Penetration Test
SRA	Site response analysis
Vp	Compressional wave velocity
Vr	Rayleigh wave phase velocity
Vr_λ	Phase velocity equivalent to a specific wavelength Rayleigh wave (λ in meters)
T_0	Natural site period
UHS	Uniform Hazard Spectrum
WNA	Western North America
XGBR	Extreme Gradient Boosting regression
z	Depth
z_{gl}	Depth to glacial sediments
z_{brk}	Depth to bedrock
zp	Maximum depth of shear wave velocity profile
ε	error between measurement and prediction
λ	wavelength (m)
ν	Poisson's ratio
ρ	Density

σ   standard deviation

μ   log-normal mean

Chapter 1

1   Introduction

Metro Vancouver with over 2.5 million inhabitants is the largest city in British Columbia (BC) and has the highest earthquake risk in Canada due to its proximity to the Cascadia subduction zone (Adams & Cassidy, 2002). Natural Resources Canada (NRCan) states that 60% of Canada's earthquakes occur along BC's coast. The total estimated direct losses (related to property and infrastructure) and indirect losses (e.g., related to supply chain interruptions and infrastructure disruptions) due to a magnitude 9.0 earthquake in British Columbia is very high, ~$75 billion (AIR 2013). To reduce the impact of earthquakes in Metro Vancouver, a better understanding of the seismic hazard is required.

The seismic hazard in any region is dictated by three main factors: earthquake source, path, and site effects. Earthquake source effects are a result of the seismotectonic setting of the region (e.g., potential earthquake magnitudes, occurrence rates, etc.), while path effects are mainly related to the distance between the earthquake source and the site. Site effects are a consequence of interactions between near surface geology with the arriving seismic waves at the site and play a major role in determining the levels of shaking and hazard at the surface. Thus, accurate characterization of seismic site effects is an essential task to quantify the overall seismic hazard in a region.

Regional site effects are typically accounted for when the mapping of site characteristics (e.g., shear wave velocity in top 30 m, Vs_{30}) is included in the seismic hazard analysis. Seismic microzonation mapping identifies spatial variation in seismic hazard due primarily to local seismic site conditions, typically for an urban city or region. A variety of seismic site characteristic measures exist currently (e.g., Vs_{30}) and their mapping are important inputs for many regional applications such as emergency response, urban planning, and risk studies. While there exists some studies on seismic site characterization mapping in Metro Vancouver, there is no Vs_{30} map for the region. The work reported in this thesis is part of the Metro Vancouver seismic microzonation mapping project (2017-2024) which aims to

generate the first suite of comprehensive seismic microzonation maps for the entire region, including site amplification inclusive of basin effects, and liquefaction and landslide hazard potential maps. A major focus of this study is to utilize the most comprehensive regional compilation of non-invasive and invasive measurements to date to derive region-specific predictive models to map important seismic site characteristics such as Vs, Vs_{30} and depth to glacial sediments. A region-specific Vs_{30} mapping prediction model is developed based on geologic mapping and depth to glacial sediments. Another important focus of this thesis is to facilitate the development of region-specific site amplification model via one-dimensional (1D) site response analysis (SRA) at two chosen seismic hazard levels (2% and 10% probability of exceedance in 50 years) for different earthquake source types. The eventual application of the region-specific site amplification model given the developed regional site characteristic maps (e.g., Vs_{30} map) will improve regional estimation of the seismic hazard in Metro Vancouver.

1.1   Purpose of Study

The main objective of this thesis is to develop region-specific prediction models for mapping important seismic site characteristic metrics in Metro Vancouver and facilitate the development of a region-specific site amplification model. Regional prediction of site-specific ground motions for Metro Vancouver is more complex than anywhere else in Canada and is a major reason why its seismic microzonation mapping has lagged behind that of other cities. The specific set of objectives for this study are as follows:

1- Investigate the applicability of emerging non-invasive seismic (surface wave and microtremor) testing methods to quantify important site effect metrics such as the depth to glacial sediments (z_{gl}) and Vs depth profiling [Vs(z)] in the Fraser River Delta (FRD).

2- Derive a region-specific cone penetration test (CPT)-to-Vs relationship from compiled SCPT measurements. A region-specific CPT-to-Vs model is required to

improve prediction of Vs(z) and Vs_{30} from available CPT measurements in the region.

3- Compile a Vs(z) database to assess the distribution of Vs(z) for different sediment types in Metro Vancouver. Use the Vs(z) database and the CPT-to-Vs model derived in Objective 2 to establish a comprehensive Vs_{30} database from which to develop a region-specific Vs_{30} prediction model for Metro Vancouver.

4- Conduct linear and nonlinear one-dimensional (1D) site response analyses (SRA) using input time histories representative of the regional probabilistic seismic hazard (i.e., three earthquake source types) in Metro Vancouver to facilitate development of a region-specific site amplification model.

To accomplish the thesis objectives, the following tasks were completed:

1- Over multiple summer field campaigns, I performed non-invasive microtremor and surface wave seismic testing across the Fraser River Delta (FRD) and MHVSR method testing at locations where z_{gl} is available. I derived a relationship between the 2nd MHVSR peak frequency ($f_{1,HVSR}$) and z_{gl}. I performed joint inversion of Rayleigh-wave fundamental-mode dispersion estimates and MHVSR fundamental peak frequency ($f_{0,HVSR}$) to obtain deep Vs(z) including uncertainties at 16 FRD sites and validated them with nearby Vs(z) from other methods.

2- I compiled available SCPT measurements in Metro Vancouver and examined the applicability of existing CPT-to-Vs relationships to predict Vs from CPT data. I established five region-specific CPT-to-Vs models using multiple regression and machine learning approaches and different CPT parameter combinations. I proposed and validated a final region-specific CPT-to-Vs model.

3- I compiled the most comprehensive Vs(z) database for Metro Vancouver to date from various open and proprietary data sources. I converted Vs_{5-29}, CPT profiles, and Rayleigh wave fundamental-mode dispersion estimates (Vr_{λ}) to Vs_{30} and

thereby assemble the most comprehensive regional Vs_{30} database to date. I developed two hybrid proxy-Vs_{30} prediction models based on combinations of seismic site condition metrics: geology, topographic slope, or z_{gl}. I propose use of the region-specific geology-z_{gl} model to predict Vs_{30} for regional seismic microzonation mapping.

4- I used the compiled Vs(z) database to recommend key sites for regional 1D SRA and to identify the appropriate reference site condition for Metro Vancouver. I performed regional probabilistic seismic hazard analyses (PSHA) using NRCAN's 6th-generation seismic hazard model of Canada (CanadaSHM6) to select and scale input earthquake time histories for SRA. I developed input time histories at two seismic hazard levels (2% and 10% POE in 50 years) for each of the three earthquake source types. I conducted linear and nonlinear SRA at 8 selected sites and SRA sensitivity analyses of the effect of Vs variability on site amplification. I compared my predicted Metro Vancouver site amplification from 1D SRA to amplification of western North America. I provided recommendations to develop a region-specific site amplification model in future.

1.2 Organization of Thesis

This thesis is produced in accordance with the guidelines of the School of Graduate and Postdoctoral Studies. Different chapters of the thesis have been published in, submitted, or prepared for submission to peer-reviewed journals. The thesis consists of seven chapters that are briefly described in this section.

Chapter 2 presents an overview of the seismotectonic setting of southwestern BC. Different *in situ* measures of local site conditions to quantify seismic site effects and important seismic site characteristics are summarized. Previous studies on seismic site characterisation and local site effects in Metro Vancouver are presented along with their limitations.

Chapter 3 presents the non-invasive seismic field testing accomplished in the FRD over multiple field campaigns, including the single-station MHVSR method to obtain amplification spectra and site peak frequencies, and active- and passive-source surface wave array testing to obtain dispersion estimates. A relationship to predict z_{gl} for shallow FRD sites from $f_{1,HVSR}$ is developed. Joint inversion of $f_{0,HVSR}$ and Rayleigh-wave fundamental-mode dispersion curves is performed to obtain the deepest constrained Vs(z) at 16 FRD sites. The developed Vs(z) are validated with available Vs(z) obtained by other *in situ* invasive and non-invasive Vs(z) methods.

Chapter 4 describes development of several CPT-to-Vs models specific to Metro Vancouver from SCPT(z) measurements. Different regression approaches and CPT parameter combinations are evaluated; the machine learning model based on basic CPT parameters is recommended to predict Vs(z) and validated in comparison with invasive *in situ* Vs(z) measurements.

Chapter 5 presents compilation of a comprehensive Vs(z) database from various data sources in Metro Vancouver. Generic Vs(z) relationships specific to post-glacial, glacial and rock geologies are developed. A comprehensive Vs_{30} database from direct Vs(z) measurements is compiled and augmented with Vs_{30} from other *in situ* measurements such as CPT and dispersion curves from surface wave testing. The compiled Vs_{30} database is utilized to develop two proxy-based Vs_{30} prediction models based on geology and topographic slope or z_{gl}. A final model to map Vs_{30} in Metro Vancouver is proposed.

Chapter 6 describes local site conditions in developing layered 1D soil models and selection of the reference ground condition(s) for linear and nonlinear SRAs throughout Metro Vancouver. PSHAs are conducted to derive input ground motions at the 2 and 10 % POE in 50 years compatible with the CanadaSHM6. Input motion selection and scaling methodology for the three earthquake source types is presented. 1D site de/amplification spectra at 8 selected sites are compared with a site amplification model for western North America. Parametric studies are performed to gauge SRA modelling uncertainties in Metro Vancouver and provide future recommendations.

Chapter 7 summarizes the main findings of this thesis and presents recommendations for future research.

1.3   Original Contributions

This study aims to provide improved evaluation of seismic site characteristics and site effects with their spatial distribution in Metro Vancouver from a combination of newly acquired and existing *in situ* measurements. The original contributions of this study are:

1- Developed a model to map z_{gl} for shallow FRD sites based on $f_{1,HVSR}$.

2- Demonstrated the robustness of joint inversion of Rayleigh-wave fundamental-mode dispersion estimates and $f_{0,HVSR}$ from combined surface wave and microtremor *in situ* testing in retrieving constrained deep Vs profiles up to 220 m depth in the FRD.

3- Developed region-specific models to predict Vs(z) from CPT data and illustrated the usefulness of applying machine learning regression approaches in geotechnical applications, specifically in developing CPT-to-Vs correlations, given a large database is available.

4- Compiled the most comprehensive Vs(z) database for Metro Vancouver to date from existing and newly acquired invasive and non-invasive testing and thereby established a comprehensive Vs_{30} database for Metro Vancouver from direct Vs(z) measurements and other *in situ* measurements.

5- Developed Vs_{30} mapping prediction models for Metro Vancouver based on geology and topographic slope or z_{gl}.

6- Developed region-applicable input time histories of the three earthquake source types for 1D SRA scaled to two reference site conditions and consistent with the probabilistic seismic hazard of the CanadaSHM6 model.

7- Determined generally poor agreement between predicted region-specific site amplification via 1D SRA with that of an available western North America site amplification model. A region-specific site amplification model for Metro Vancouver will be required to achieve seismic microzonation (amplification) hazard mapping in future.

1.4 References

Adams, J., & Cassidy, J. (2002). The Case for an Advanced National Earthquake Monitoring System for Canada's Cities at Risk. 7th US National Conference on Earthquake Engineering. Boston, USA. 10 pages.

AIR Worldwide (2013). Study of Impact and the Insurance and Economic Cost of a Major Earthquake in British Columbia and Ontario/Québec. Report Commissioned by the Insurance Bureau of Canada. Boston. AIR.

Natural Resources Canada. Earthquake Hazards and Risks, https://earthquakescanada.nrcan.gc.ca/hazard-alea/earthquake_hazards_risks, last accessed September 2022.

Kolaj, M., Adams, J., Halchuk, S. (2020). The 6th Generation seismic hazard model of Canada. 17th World Conference on Earthquake Engineering, Sendai, Japan, Paper 1c-0028.

Chapter 2

2   Literature Review

Accurate seismic hazard assessment for Metro Vancouver is a challenging task due to its variable local geology and complex seismicity associated with the Cascadia subduction zone. The effects of surface topography and subsurface geology on propagating seismic waves (i.e., earthquake site effects) play a major role in achieving accurate ground motion prediction for the region. A brief description of the seismo-tectonic setting in southwestern British Columbia is first presented in this chapter. The physics of seismic site effects, methods to quantify site effects, and important site characteristics are then discussed. Finally, a summary of previous studies related to seismic site characterization and effects in Metro Vancouver is presented.

2.1   Seismo-tectonic Settings in Cascadia Subduction Zone

Due to its location near to the Cascadia subduction zone, the highly populated city of Vancouver and southwest BC are one of the most seismically active regions in Canada (Adams et al., 2002). The 1000 km long Cascadia subduction zone spans Vancouver Island to northern California, where the oceanic Juan de Fuca and Explorer plates are subducting beneath the continental North American plate with the developed interface boundary ~150 km west of Vancouver (Rogers et al., 1998). This active tectonic setting of southwest BC leads to frequent seismic activity that arises from three different sources: shallow crustal earthquakes (depth ~ 20 km) within the continental North American Plate, deeper intraslab (depth 45 - 65 km) earthquakes within the subducting Juan de Fuca plate, and interface earthquakes of the Cascadia subduction boundary with a maximum considered M_W of 9.2-9.3 (Rogers et al., 1998) (Figure 2-1). The central region of Vancouver Island, which is almost aseismic today, was the location of the largest known on-land crustal earthquake in Canada (M 7.3) on June 23, 1946 (Rogers and Hasegawa, 1978). The three largest intraslab earthquakes, 1949 M_W 7, 1965 M_W 6.5 and 2001 M_W 6.8, occurred at over 50 km depth beneath Puget Sound, Washington, within the

subducting Juan de Fuca plate (Rogers 2015). While no large Cascadia interface events have been recorded north of Oregon, tsunami and other paleoseismic evidence confirms the most recent great interface earthquake (estimated M 9.0) occurred January 26 1700 at 9 pm (Satake et al., 1996) and has a recurrence time of around 500 years (Goldfinger et al., 2012).
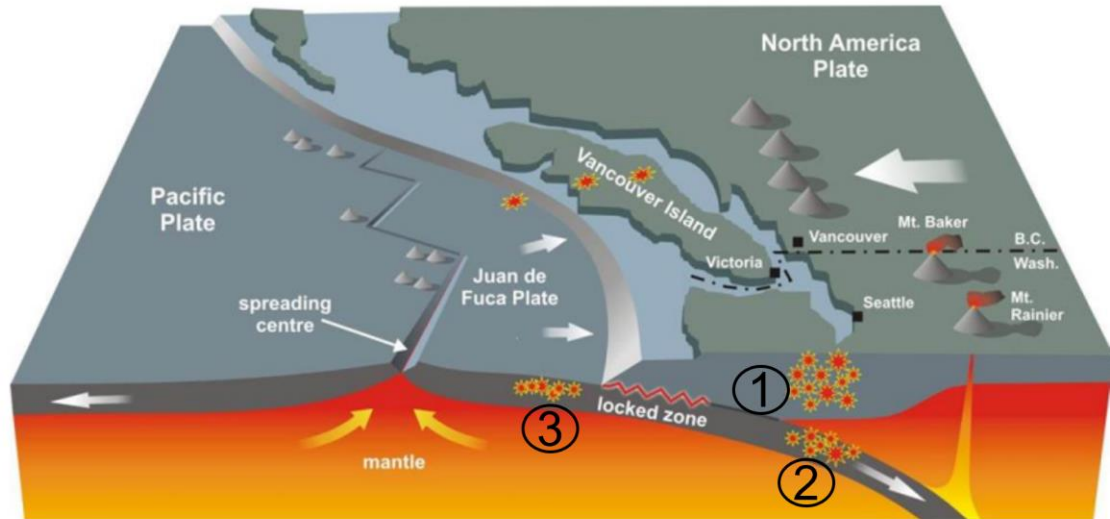
Figure 2-1: Cartoon cross-section of the Cascadia subduction zone in southwest British Columbia showing the three sources of earthquakes that contribute to seismic hazard: 1) crustal earthquakes in the North American plate, 2) deeper intraslab earthquakes in the subducting Juan de Fuca plate and 3) large subduction interface earthquakes that occur where the two plates are currently locked in contact in the offshore region. (Modified from Rogers et al. 2015).

All three earthquake sources are capable of producing damaging earthquakes; however, the differences in their seismicity (hypocentre locations, maximum considered magnitude, occurrence rates) leads to their different contribution to the overall seismic hazard. The seismic hazard is often determined from a Probabilistic Seismic Hazard Analysis (PSHA) that accounts for uncertainties in different components involved in the seismic hazard (Cornell 1968; McGuire 2004). The uniform hazard spectrum (UHS) at a site represents

ground motions at different spectral periods corresponding to the same target probability of exceedance (POE) hazard levels. A disaggregation analysis (Bazzurro and Cornell 1999) can separate the relative contributions of different earthquake sources to the overall UHS at a site. While the overall seismic hazard continually evolves as more paleoseismic evidence, earthquake recordings, and improved GMMs are incorporated (Adams 2019), the contributions of the three earthquake source types in southwestern BC to the UHS are generally well understood from disaggregation analysis. For ground motions at the 2 % in 50 years probability of exceedance, a typical probability level considered for design of new buildings, intraslab events in the Juan de Fuca plate are the largest contributor to the seismic hazard in Vancouver for periods shorter than 0.5 s (Rogers et al. 2015). At longer periods, subduction interface earthquakes dominate the hazard. Shallow crustal earthquakes contribute the most at shorter periods but never exceed the more frequent intraslab and larger magnitude interface source contributions. Contributions of the short-period-dominant intraslab and long-period-dominant interface earthquakes to the overall hazard decreases eastward across Metro Vancouver as the distance from the Cascadia subduction zone increases. The understanding of the contributions of the three earthquake sources to the overall hazard in Metro Vancouver is essential for all seismic hazard applications, and specifically for selecting and scaling appropriate input earthquake time histories as will be discussed in Chapter 6.

2.2   Seismic Site Effects Quantification

Several physical phenomena lead to alteration of seismic waves as they interact with the local site conditions (geology) as shown in Figure 2-2. Due to the natural geologic sedimentation process, ground stiffness and density increases with depth. The decrease in Earth's seismic impedance (wave speed x density) towards the ground surface causes impedance contrast (broadband) amplification of the seismic waves due to conservation of energy (Aki and Richards, 1980, Shearer and Orcutt 1987). In case a strong impedance contrast (> ~3) exists between two layers, resonance phenomena occurs and results in very high amplitudes due to wave reverberation. Other factors such as subsurface geometry or surface topography can lead to de/amplification due to focusing and defocusing effects of

the arriving waves. In specific basin geometries, waves can get trapped at the basin edge generating large amplitude surface waves (e.g., Bard and Bouchon 1985, Adams et al. 2019). Broadband and resonance amplification (Figure 2-2.1 and 2-2.2) are categorized as 1D site effects, manifesting due to upward shear wave propagation through the local soil column.
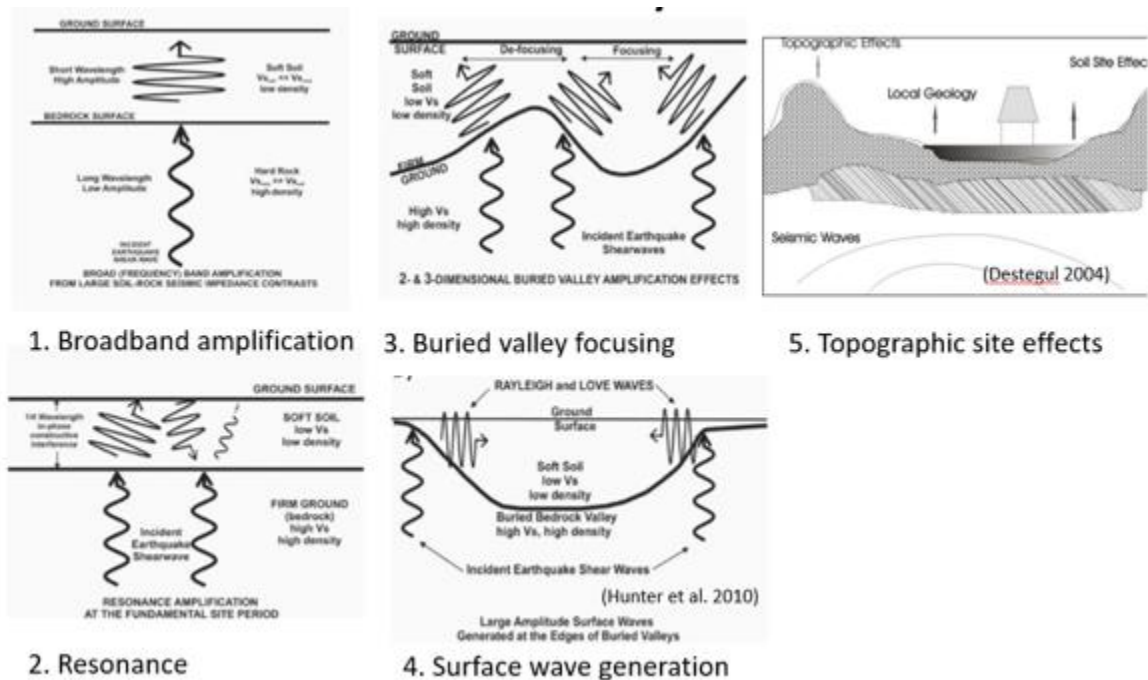
Figure 2-2: Physical phenomena leading to seismic site effects (Modified from Hunter et. al 2010, and Destegul 2004).

Table 2-1 provides a list of methods developed to quantify seismic site effects. Methods based on earthquake recordings (observations) such as Standard soil-base-to-surface Spectral Ratios (SSR) and Surface-to-Borehole Spectral Ratios (SBSR) are the preferred methods to determine site (whole soil column) amplification. However, the applicability of empirical methods is limited to cases where earthquake recordings are obtained at a reference outcrop site or at depth in a borehole. Other empirical methods based on multiple earthquake recordings and compatible ground motion models (GMMs) can be utilized to obtain reliable site amplification (δS2S and GIT in Table 2-1). A recent promising

empirical method (C-HVSR) corrects MHVSR amplification spectra to site amplification spectra in two stages or using two different spectral adjustments (Kawase et al., 2018). The potential of the C-HVSR method is implied in the ease of collecting MHVSR measurements in regions where available earthquake recordings are scarce. Analytical methods to calculate the linear amplification spectrum of vertically propagating horizontally polarized shear (SH) transfer function given 1D subsurface models of Vs, density, and material damping properties at the site have been proposed (e.g., Haskell 1960). Similarly, the square-root-impedance (SRI, e.g., Joyner et al. 1981, Boore 2003) uses transmissivity-and-reflectivity ray theory to provide rapid approximation of linear site amplification. Numerical one-dimensional 1D site response analysis (SRA) is commonly used to simulate SH and can accounts for dynamic nonlinear soil behavior through shear modulus reduction and damping curves.

Table 2-1. Different methods to quantify seismic site effects (adapted from Zhu et al. 2022).

Method Name	Description	Requirement(s)	Reference condition	Methodology
SSR	Standard spectral ratio	Simultaneous earthquake recordings at the site and a nearby outcrop rock site (free of site effects)	Outcrop rock	Two earthquake recordings
SBSR	Surface-to-borehole spectral ratio	Simultaneous recordings at collocated surface-downhole pair	Rock at depth	Two earthquake recordings
δS2S	Site-to-site variability from GMM residuals	Multiple stations with earthquake recordings from multiple events to which the selected GMM is applicable	Single site or a set of sites	Multiple earthquake recordings
GIT	General inversion technique	Multiple stations with earthquake recordings from multiple events	Single site or a set of sites	Multiple earthquake recordings
SH Transfer function	SH transfer function	1D site model (density and velocity profiles, damping parameter)	Last considered layer (elastic half-space)	Analytical
SRI	Square-root impedance	1D site model (density and velocity profiles, damping parameter)	Last considered layer (elastic half-space)	Analytical

SRA/GRA	Site/Ground response analysis	1D site model (density, velocity and damping profiles, modulus reduction, and damping curves)	Outcrop rock or rock at depth	Numerical modeling
C-HVSR	Corrected horizontal-to-vertical spectral ratio	Vertical correction functions (and site parameters) and HVSR function	Outcrop rock or rock at depth	Empirical prediction
f (site characteristics)	Generic models	Site characteristics (e.g., Vs_{30}, f_0, $Z_{1.0}$, and $Z_{2.5}$)	Variable	Empirical prediction

The availability of a large database of earthquake recordings in a region permits development of generic ground motion models (GMMs) that provide the mean or median surface ground motions with their variability; these GMMs are generally referred to as ergodic models (e.g., NGA West-2, Bozorgnia et al., 2014; NGA Subduction; Bozorgnia et al., 2022). Seismic site effects terms (Generic models, Table 2-1) in these ergodic GMMs are typically derived from regression analysis of the observed site effects and measured site characteristics at the seismic stations (e.g., the time-averaged Vs to a depth of 30 m, Vs_{30}). Thus, *in situ* measures of seismic site characteristics are essential inputs for both developing new site effects models and applying existing ones to a certain region or site.

Borcherdt (1994) proposed Vs_{30} as a quantitative site characteristic measure to capture site effects, and further determined site de/amplification factors for six seismic site classifications (A-F) based on Vs_{30}. Vs_{30} has since become the most common site term parameter in seismic hazard assessment (GMMs) and the basis of seismic site designation in seismic design codes worldwide. An alternative *in situ* seismic site characteristic measure growing in popularity and adoption as a site term in GMMs to capture seismic amplification is the fundamental site frequency (f_0) or natural site period ($T_0 = 1/f_0$) (e.g., Di Alessandro et al. 2012, Ghofrani and Atkinson 2014, Hassani and Atkinson 2016, Hashash et al. 2020). Several studies have recently shown that f_0 correlates equally or even better than Vs_{30} with observed site amplification in specific cases (e.g., Hassani et al. 2018; Zhu et al. 2020). Additional seismic site characteristic metrics such as the depth to a Vs of 1.0, 1.5, or 2.5 km/s ($Z_{1.0}$, $Z_{1.5}$, or $Z_{2.5}$, respectively) have been included in GMMs to better capture long-period amplification related to deep sedimentary basins (Day et al. 2008).

The use of combinations of seismic site characteristics measures is considered desirable to fully account for seismic site effects. Figure 2-3 shows the results of a questionnaire answered by 71 research seismologists, geophysicists, and geotechnical engineers from around the world (albeit biased to Europe) about their perception/opinion of the most important site characteristics or indicators for effective site characterization (Cultrera et al. 2021). The questionnaire responses identified that the most important and/or mandatory metrics (> 50 %) for accurate site characterization, in order of priority, are: f_0, $Vs(z)$, Vs_{30}, geology, depth to seismic bedrock, site class, and depth to engineering bedrock.
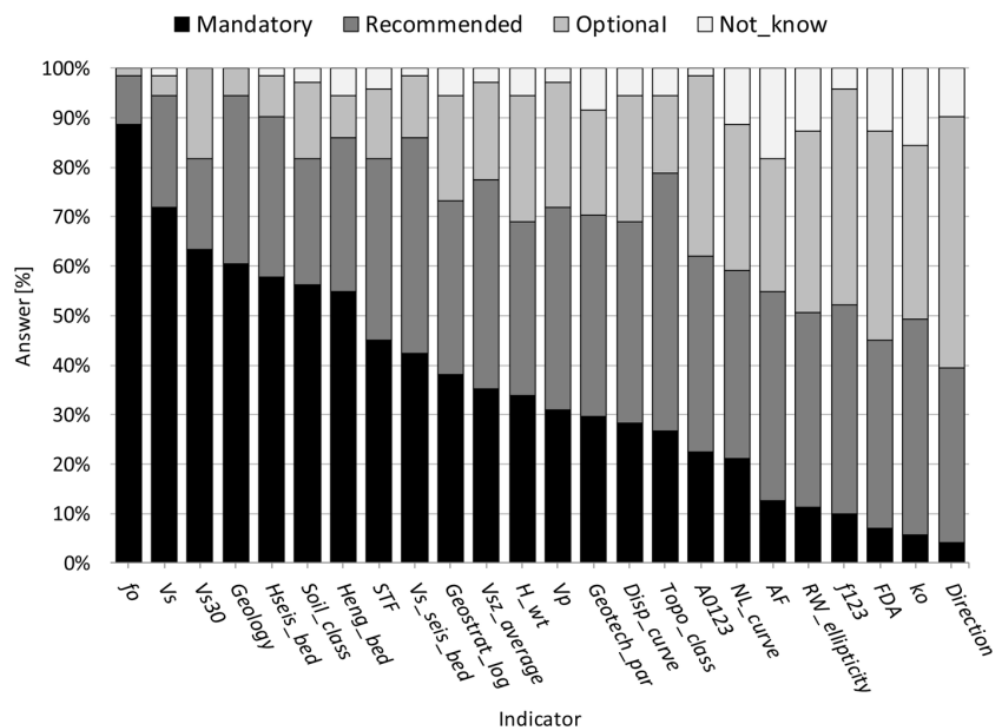
Figure 2-3. Order of importance in seismic site characterization measures from a worldwide (Europe-centric) questionnaire (Cultrera et al. 2021)

2.3 Seismic Site Characterization

The importance of seismic site characteristics (e.g., Vs profiles, Vs_{30}, f_0, depths to impedance contrasts) to accurately quantify site effects have promoted the development of several *in situ* methods to measure or estimate these metrics.

Vs profiles required for numerical site response analysis or Vs_{30} determination are typically measured *in situ* using invasive (e.g., down-hole, cross-hole, and suspension P-S logging) or non-invasive methods (e.g., seismic reflection and refraction, surface wave, and microtremor methods) (Hunter and Crow, 2015). Invasive profiling methods provide high-resolution Vs measurements, e.g., every 1 m depth increment, and therefore better identify minor or subtle changes in Vs with depth. In contrast, non-invasive Vs profiling methods sample larger soil volumes and provide an average Vs estimate throughout this volume. Non-invasive surface wave methods have become popular methods and widely adopted to infer Vs profiles due to their time- and cost-efficiency. Active-source multichannel analysis of surface waves (MASW) and passive-source microtremor array measurements (MAM) are commonly used seismic array techniques that exploit the dispersive nature of surface waves to obtain an experimental dispersion curve (phase velocity frequency spectrum) at a site, from which a Vs profile can be derived using inversion. Some of the challenges associated with non-invasive methods are the inversion non-uniqueness and the inclusion and propagation of uncertainties in Vs profiles (Vantassel and Cox 2021). To address some of this uncertainty, inverted Vs profiles in some cases are communicated by considering a suite of lowest misfit models, e.g., (100 or 1000 profiles). The Inter-PACIFIC project demonstrated that the Vs variability from non-invasive surface wave methods and invasive methods is comparable for both simple and more complex geologic settings (Garofalo et al. 2016a, b) and differences in Vs_{30} from both methods were generally less than 4%.

In lieu of direct Vs measurements, many correlative relationships have been developed to predict Vs from other readily available *in situ* invasive testing method measures, i.e., Vs proxies. These other *in situ* measures that approximate Vs include the number of blow counts (N) obtained from standard penetration testing (SPT), undrained shear strength (s_u) obtained from testing soil samples in a geotechnical laboratory or field-vane measurements (e.g., Seed et al. 1986, Wair et al. 2012), and cone penetration testing (CPT) (e.g., Andrus et al. 2007, McGann et al. 2015, Salsabili et al. 2022). Seismic site designation of the 2005-2015 NBCC included three site characteristic measures (Vs, s_u, N_{60}) that when averaged for the top 30 m could be used to determine the seismic site classification and thereby the

seismic design ground motions; the released but not yet enforced 2020 NBCC permits site designation using Vs_{30} directly (design motions are specific to a Vs_{30} value and not the average within a site class) and maintains use of N_{60} and s_u for site class designation. Hence, the seismic site characteristic metric to achieve seismic microzonation mapping in Canada was NBCC site class and has shifted towards Vs_{30} directly.

The importance of Vs_{30} maps for regional seismic hazard and risk studies (e.g., ShakeMaps and FEMA's HAZUS loss maps in the United States), promoted new methods to estimate Vs_{30} from widely available proxies. These proxies include the mapped surficial geology (e.g., Wills and Clahan 2006), topographic slope (e.g., Allen and Wald 2007), and terrain classification (e.g. Yong et al. 2012, Iwahashi et al. 2018) or their combination (Ahdi et al. 2017; Foster et al. 2019). Proxy-based Vs_{30} prediction methods are generally anchored on *in situ* Vs_{30} measurements and geostatistical frameworks to establish correlations between Vs_{30} and the selected readily available proxies. Additionally, regional average (generic) Vs profiles determined for different sediment types can be applied to predict Vs or Vs_{30} from borehole stratigraphy or three-dimensional (3D) geological models at a specific site or for a region (e.g., Motazedian et al. 2011; Rosset et al. 2015, Nastev et al. 2016; Foulon et al. 2018; Salsibili et al. 2021).

While Vs profiles may also be used to predict another important site characteristic, f_0, via the analytical expression of shear wave resonance in a single soil layer over an elastic half-space (Haskell 1960),

$$f_0 = \frac{Vs_{avg}}{4h} \qquad \textbf{Eq. 2-1}$$

where h is soil thickness and Vs_{ave} is the soil's average Vs, they are often limited in depth and don't reach the resonator depth associated with f_0. The single-station microtremor horizontal-to-vertical spectral ratio (MHVSR) method has become the most popular method to retrieve resonance frequencies at a site due to its easy and cost-effective application (Molnar et al. 2022). When a sufficiently strong impedance contrast exists at depth, the MHVSR's fundamental peak frequency ($f_{0,HVSR}$) can be used to approximate the

shear-wave resonant frequency (f_0) (Field and Jacob 1993). MHVSRs have also been used to map other important site characteristics such as the depth to bedrock or stiff sediments using $f_{0,HVSR}$ when the region-specific correlation between $f_{0,HVSR}$ and h is known (e.g., Molnar et al. 2022). Additionally, the complementary inversion of the site's MHVSR peak frequency(ies) and dispersion curve has been proven to better constrain the layered models especially at greater depths (e.g., Molnar et al. 2022).

2.4   Site Characteristics and Effects in Metro Vancouver

Several research programs have been implemented to gather information on seismic site characteristics in Metro Vancouver and specifically in the FRD. The Geologic Survey of Canada (GSC), in cooperation with other public and private agencies, conducted an extensive testing program during the 1980s and 1990s to characterize the subsurface conditions and seismic hazard in the region, in particular to the FRD (e.g., Clague et al., 1998). The GSC performed over 500 Vs(z) in the FRD via invasive downhole and SCPT testing and non-invasive shear-wave refraction and compressional-wave reflection surveys that are publicly available in Hunter et al., (2016). With the emergence of surface wave methods in the 2000's, Xia et al. (2000) compared Vs in the top 30 m from MASW testing with downhole Vs measurements at 8 GSC sites in the FRD. Molnar et al. (2010, 2012) compared Vs profile probability distributions obtained from Bayesian inversion of MAM-derived dispersion estimates with the average Vs of co-located invasive methods. They demonstrated that the low frequency dispersion estimates from MAM testing provide reliable Vs profiles to significant depth in the FRD; the average relative difference in Vs is 5% to 120 m depth and 25% to 60 m depth at two sites. Jackson (2017) was the first to generate Vs profiles from joint inversion of MHVSR peak frequency(ies) and dispersion estimates from MAM testing for 13 sites across Metro Vancouver (not the FRD). This thesis will produce the first set of Vs profiles obtained via joint inversion of MHVSR peak frequencies and combined MAM and MASW dispersion estimates (Molnar et al. 2020) for 16 FRD sites. While extensive Vs(z) testing has been performed in the FRD, there is a limited amount of Vs(z) information available outside the FRD (Monahan and Levson 2001).

The need for regional-scale site characteristics in Metro Vancouver have promoted limited seismic hazard mapping projects. The Geomap Vancouver poster (Turner et al., 1998) shows the distribution of major geologic units and conveys their characteristics relevant to engineering and land-use planning. These characteristics included landslide susceptibility (slope angle, historical events) and liquefaction susceptibility (geology material and age, degree of saturation). Hunter et al. (2002) generated example seismic microzonation hazard maps for the FRD based on the over 500 Vs(z), including NBCC site class, site amplification factor, and T_0. Additionally, Monahan (2017) produced the first seismic site class map of Metro Vancouver based on surficial geology mapping and borehole and Vs data that he compiled from available and private sources. Unlike the 2015 National Building Code of Canada (NBCC), the NBCC 2020 currently allows direct use of measured Vs_{30} values instead of site classes for determining design ground motions. Thus, the availability of a Vs_{30} map, rather than a site class map, provides a more accurate representation of site effects in Metro Vancouver.

Although Metro Vancouver lies in a seismically active region, the scarcity of earthquake recordings represents a challenge for accurate seismic hazard assessment. A total of 12 earthquakes have been recorded in Metro Vancouver since 1976 and all produced weak ground motions (< 5.5 % g, where g is the acceleration of gravity). Limited recordings from earthquakes prior to 2002 had good signal-to-noise ratio at frequencies > 0.5 Hz (Cassidy et al. 1997, Rogers et al. 1998, Cassidy and Rogers 1999, Cassidy and Rogers 2004) and indicated amplification between 1.5-4 Hz (0.25-0.67 s period) near the edge of the FRD that is up to a factor of 6 relative to firm soil. Near the center of the delta where post-glacial soft sediments are thickest, peak amplification of 2-5 around 1 Hz relative to firm soil were measured. At higher frequencies, little or no amplification or even slight attenuation was observed (Cassidy and Rogers 2004). Newer recordings, except for the 2015 earthquake recordings, mainly consisted of surface waves and had limited high frequency content as the earthquakes were located far from Metro Vancouver (Molnar et al., 2020, Assaf et al. 2022). None of the available recordings provide full amplification spectrum at both low and high frequencies. Three boreholes under the Port Mann bridge east of Metro Vancouver

are instrumented at three depths; their recordings of the 2015 M_W 4.7 intraslab earthquake presented a rare opportunity to evaluate and validate linear empirical and theoretical site amplification in the region (Molnar et al., 2020).

Due to limited available earthquake recordings in Metro Vancouver, some numerical modeling studies of site effects or amplification in the FRD have been conducted. Atkinson and Cassidy (2000) compared linear SRI amplification via the quarter-wavelength approach with SSRs from the 1996 Duvall, Washington, and 1997 Georgia Strait earthquakes. They found a broadband amplification in the FRD of at least 3 to 6 relative to a reference condition with a Vs of 3.7 km/s at seismogenic depths (8 km). Finn et al. (2003) showed that 2D modelled linear amplification, in comparison to 1D modelling, improved the prediction of low amplitude recorded ground motions specifically for sites with thin post-glacial sediment deposits. Molnar et al. (2014a, b) used a finite-difference code and a 3D velocity structure of the Georgia Basin with a minimum Vs of 625 m/s to examine 3D site amplifications for long-period ground motion for shallow crustal and deep intraslab scenario earthquakes. They found that long period amplification (> 2 s) is a factor of 3-4 in Metro Vancouver. Recently, Kim (2019) produced a site amplification map for the FRD from equivalent linear and nonlinear site response analyses using crustal earthquake recordings from the NGA-West2 database (Ancheta et al. 2014). Kim (2019) generated 21 1D models with the same soil layering and assigned Vs from the Hunter et al. (2016) database, and derived amplification functions based on PGA on rock (PGA_r) and T_0. Kim (2019) included 10 profiles with depth to bedrock between 50 and 200 m; however, the shallowest known depth to bedrock in the FRD is 200 m (Britton et al. 1995). For producing the site amplification map, Kim (2019) calculated the natural period (T_0) from the available Vs profiles. None of the used Vs profiles extends to the bedrock depth, and thus T_0 calculated from shallow Vs profiles underestimates the actual T_0 related to bedrock depth.

2.5   Summary

An overview of the seismic hazard in Metro Vancouver is presented in this chapter with details on the three earthquake source types that contribute to the hazard. Various methods

to quantify seismic site effects and their limitations are summarized along with the most important site characteristics. Invasive and non-invasive *in situ* methods to obtain site characteristics such Vs profiles, Vs_{30}, $f_{0,HVSR}$, and depths to impedance contrasts are discussed. Finally, previous work on seismic site characterization and effects in Metro Vancouver, mainly in the FRD, is presented.

While numerous testing expeditions have been conducted in the FRD, the capabilities of non-invasive testing in retrieving important site characteristics have not been fully explored. Previous non-invasive Vs profiling methods were limited to either active- or passive source testing and further did not examine correlations between depths to impedance contrasts and peak frequencies. Outside the FRD, there is very limited known information on Vs of sediments which hinders development of a Vs_{30} map for the region. The development of a Vs_{30} map for Vancouver requires additional data outside the FRD to complement the existing available measurements. Regarding numerical modelling of site effects, previous work was mainly limited to the FRD and did not consider all three earthquake source types in Metro Vancouver simultaneously.

2.6   References

Adams, J. (2019). "A 65-year history of seismic hazard estimates in Canada". 12th Canadian Conference on Earthquake Engineering, Québec City, Québec., Paper 192-cSSQ-149.

Adams, J., & Cassidy, J. (2002). The Case for an Advanced National Earthquake Monitoring System for Canada's Cities at Risk. 7th US National Conference on Earthquake Engineering. Boston, USA. 10 pages.

Adams, B. M., Osborne, N. M., & Taber, J. J. (2003). The basin-edge effect from weak ground motions across the fault-bounded edge of the Lower Hutt Valley, New Zealand. Bulletin of the Seismological Society of America, 93(6), 2703-2716.

Ahdi, S. K., Stewart, J. P., Ancheta, T. D., Kwak, D. Y., & Mitra, D. (2017). Development of VS profile database and proxy-based models for VS30 prediction in the Pacific Northwest region of North America. Bulletin of the Seismological Society of America, 107(4), 1781-1801.

Allen, T.I., Wald, D. (2007). Topographic Slope as a Proxi for Seismic Site-Conditions (VS30) and Amplification Around the Globe. US Geological Survey Open-File:69. https://doi.org/10.1785/0120060267

Andrus, R. D., Mohanan, N. P., Piratheepan, P., Ellis, B. S., & Holzer, T. L. (2007). Predicting shear-wave velocity from cone penetration resistance. Proceedings of the 4th International Conference on Earthquake Geotechnical Engineering, 1454.

Ancheta, T.D., Darragh, R.B., Stewart, J.P., Seyhan, E., Silva, W.J., Chiou, B.S-J., Wooddell, K.E., Graves, R.W., Kottke, A.R, Boore, D.M., Kishida, T. & Donahue, J.L. (2014). "NGAWest2 Database," Earthquake Spectra, **30**(3): 989–1005.

Assaf., J., Sirohey, A., Ghofrani, H., Molnar, S. (2022). Compilation and systematic processing of earthquake and microtremor HVSR amplification at Metro Vancouver strong-motion stations. ISSN 2816-6027. (https://metrovanmicromap.ca)

Atkinson, G.M., and Cassidy, J.F. (2000). "Integrated Use of Seismograph and Strong-Motion Data to Determine Soil Amplification: Response of the Fraser River Delta to the Duvall and Georgia Strait Earthquakes," Bulletin of the Seismological Society of America, **90**(4): 1028–1040.

Bazzurro, P., & Allin Cornell, C. (1999). Disaggregation of seismic hazard. Bulletin of the Seismological Society of America, 89(2), 501-520.

Boore, D., (2003). Simulation of ground motion using the stochastic method. Pure and applied Geophysics, 160:3-4, 635–676.

Borcherdt, R.D. (1994). Estimates of Site-Dependent Response Spectra for Design (Methodology and Justification). Earthquake Spectra 10:617–653

Bozorgnia, Y., Abrahamson, N. A., Ahdi, S. K., Ancheta, T. D., Atik, L. al, Archuleta, R. J., Atkinson, G. M., Boore, D. M., Campbell, K. W., S-J Chiou, B., Contreras, V., Darragh, R. B., Derakhshan, S., Donahue, J. L., Gregor, N., Gulerce, Z., Idriss, I. M., Ji, C., Kishida, T., … Youngs, R. R. (2022). NGA-Subduction research program. Earthquake Spectra, 38(2). https://doi.org/10.1177/87552930211056081

Bozorgnia, Y., Abrahamson, N. A., al Atik, L., Ancheta, T. D., Atkinson, G. M., Baker, J. W., Baltay, A., Boore, D. M., Campbell, K. W., Chiou, B. S. J., Darragh, R., Day, S., Donahue, J., Graves, R. W., Gregor, N., Hanks, T., Idriss, I. M., Kamai, R., Kishida, T., … Youngs, R. (2014). NGA-West2 research project. Earthquake Spectra, 30(3). https://doi.org/10.1193/072113EQS209M

Bard, P. Y., & Bouchon, M. (1985). The two-dimensional resonance of sediment-filled valleys. Bulletin of the Seismological Society of America, 75(2), 519-541.

Clague, J.J., Luternauer J.L., Mosher D.C. (1998): Geology and Natural Hazards of the Fraser River Delta, British Columbia, Geological Survey of Canada, Bulletin 525. 270 pages

Cassidy, J.F., Rogers, G.C., and Weichert, D.H. (1997). Soil response on the Fraser Delta to the Mw=5.1 Duvall, Washington, earthquake. Bulletin of the Seismological Society of America, 87: 1354-1361

Cassidy, J.F., and Rogers, G.C. (1999). Seismic site response in the greater Vancouver, British Columbia, area: Spectral ratios from moderate earthquakes. Canadian Geotechnical Journal, 36(2): 195–209.

Cassidy, J.F., and Rogers, G.C. (2004). Variation in ground shaking on the Fraser River delta (Greater Vancouver, Canada) from analysis of moderate earthquakes. 13th World Conference on Earthquake Engineering, (1010): 7.

Cornell, C. A. (1968). Engineering seismic risk analysis. Bulletin of the seismological society of America, 58(5), 1583-1606.

Cultrera, G., Cornou, C., Di Giulio, G., & Bard, P. Y. (2021). Indicators for site characterization at seismic station: recommendation from a dedicated survey. Bulletin of Earthquake Engineering, 19(11), 4171-4195.

Day, S. M., Graves, R., Bielak, J., Dreger, D., Larsen, S., Olsen, K. B., ... & Ramirez-Guzman, L. (2008). Model for basin effects on long-period response spectra in southern California. Earthquake Spectra, 24(1), 257-277.

Destegul, U., (2004). Sensitivity Analysis of Soil Site Response Modeling in Seismic Microzonation for Lalitpur, Nepal. MSc. Thesis, Enschede, 135 pp.

Di Alessandro, C., Bonilla, L. F., Boore, D. M., Rovelli, A., & Scotti, O. (2012). Predominant-period site classification for response spectra prediction equations in Italy. Bulletin of the Seismological Society of America, 102(2). https://doi.org/10.1785/0120110084

Foster, K. M., Bradley, B. A., McGann, C. R., & Wotherspoon, L. M. (2019). A VS30 map for New Zealand based on geologic and terrain proxy variables and field measurements. Earthquake Spectra, 35(4). https://doi.org/10.1193/121118EQS281M

Garofalo, F., Foti, S., Hollender, F., Bard, P. Y., Cornou, C., Cox, B. R., Ohrnberger, M., Sicilia, D., Asten, M., di Giulio, G., Forbriger, T., Guillier, B., Hayashi, K., Martin, A., Matsushima, S., Mercerat, D., Poggi, V., & Yamanaka, H. (2016a). InterPACIFIC project: Comparison of invasive and non-invasive methods for seismic site characterization. Part I: Intra-comparison of surface wave methods. Soil Dynamics and Earthquake Engineering, 82. https://doi.org/10.1016/j.soildyn.2015.12.010

Garofalo, F., Foti, S., Hollender, F., Bard, P. Y., Cornou, C., Cox, B. R., Dechamp, A., Ohrnberger, M., Perron, V., Sicilia, D., Teague, D., & Vergniault, C. (2016b). InterPACIFIC project: Comparison of invasive and non-invasive methods for seismic

site characterization. Part II: Inter-comparison between surface-wave and borehole methods. Soil Dynamics and Earthquake Engineering, 82. https://doi.org/10.1016/j.soildyn.2015.12.009

Goldfinger, C., Nelson, C. H., Morey, A. E., Johnson, J. E., Patton, J. R., Karabanov, E. B., ... & Vallier, T. (2012). Turbidite event history—Methods and implications for Holocene paleoseismicity of the Cascadia subduction zone (No. 1661-F). US Geological Survey.

Ghofrani, H., Atkinson, G.M. (2014). Site condition evaluation using horizontal-to-vertical response spectral ratios of earthquakes in the NGA-West 2 and Japanese databases. Soil Dynamics and Earthquake Engineering **67**:30–43. doi: 10.1016/J.SOILDYN.2014.08.015

Halchuk, S., Adams, J., Kolaj, M. and Allen, T., (2019). June. Deaggregation of NBCC 2015 seismic hazard for selected Canadian cities. In 12th Canadian Conference on Earthquake Engineering (p. 9).

Hashash, Y. M. A., Ilhan, O., Hassani, B., Atkinson, G. M., Harmon, J., & Shao, H. (2020). Significance of site natural period effects for linear site amplification in central and eastern North America: Empirical and simulation-based models. Earthquake Spectra, 36(1). https://doi.org/10.1177/8755293019878198

Haskell, N. A. (1960). Crustal reflection of plane SH waves. Journal of Geophysical Research, 65(12), 4147-4150.

Hassani, B., and G. M. Atkinson (2018). Site-effects model for central and eastern North America based on peak frequency and average shear-wave velocity, Bull. Seismol. Soc. Am. 107, 338-350.

Hunter, J. A., Benjumea, B., Harris, J. B., Miller, R. D., Pullan, S. E., Burns, R. A., & Good, R. L. (2002). Surface and downhole shear wave seismic methods for thick soil site investigations. Soil Dynamics and Earthquake Engineering, 22(9-12), 931-941.

Hunter, J. A., Burns, R. A., Good, R. L., & Pelletier, C. F. (2016). Fraser River Delta – A compilation of shear wave velocities and borehole geophysics logs in unconsolidated sediments of the Fraser River Delta, British Columbia. Geological Survey of Canada Open File:1–112.

Hunter, J.A., Crow, H.L. (2015). Shear wave velocity measurement guidelines for Canadian seismic site characterization in soil and rock. Natural Resources Canada. doi: 10.4095/297314

Iwahashi, J., Kamiya, I., Matsuoka, M., Yamazaki, D., (2018). Global terrain classification using 280 m DEMs: segmentation, clustering, and reclassification. Progress in Earth and Planetary Science 5, 1. https://doi.org/10.1186/s40645-017-0157-2

Jackson, F., Molnar, S., Ghofrani, H., Atkinson, G.M., Cassidy, J.F., Assatourians, K. (2017). Ground Motions of the December 2015 M 4.7 Vancouver Island Earthquake: Attenuation and Site Response. Bulletin of the Seismological Society of America 107:2903–2916

Jackson, F. (2017). "Assessment of Earthquake Site Amplification and Application of Passive Seismic Methods for Improved Site Classification in the Greater Vancouver Region, British Columbia". Electronic Thesis and Dissertation Repository. 4938. https://ir.lib.uwo.ca/etd/4938

Joyner, W.B., Warrick, R.E., Fumal, T.E. (1981). The effect of Quaternary alluvium on strong ground motion in the Coyote Lake, California, earthquake of 1979. Bulletin of the Seismological Society of America 71: 1333–1349.

Kawase, H., Nagashima, F., Nakano, K., Mori, Y. (2018). Direct evaluation of S-wave amplification factors from microtremor H/V ratios: Double empirical correction to "Nakamura" method. Soil Dynamics and Earthquake Engineering 126: 105067.

Kramer, S.L., (1996). Geotechnical Earthquake Engineering, Prentice Hall. 653p

McGann, C. R., Bradley, B. A., Taylor, M. L., Wotherspoon, L. M., & Cubrinovski, M. (2015). Development of an empirical correlation for predicting shear wave velocity of Christchurch soils from cone penetration test data. Soil Dynamics and Earthquake Engineering, 75. https://doi.org/10.1016/j.soildyn.2015.03.023

McGuire, R.K. (2004). Seismic Hazard and Risk Analysis (Engineering Monographs on Miscellaneous Earthquake Engineering Topics). Oakland, CA: Earthquake Engineering Research Institute.

Molnar, S., Dosso, S.E., Cassidy, J.F. (2010). Bayesian inversion of microtremor array dispersion data in southwestern British Columbia. Geophysical Journal International **183**:923–940. doi: 10.1111/j.1365-246X.2010.04761.x

Molnar, S., Ventura, C., Finn, W., Taiebat, M., Dosso, S., Cassidy, J.F. (2012). Evaluation of shear-wave velocity profiles from ambient vibration array recordings in SW British Columbia, Canada. In: Proceedings of the fifteenth world conference on earthquake engineering, Lisbon, Portugal, Paper 3175, 2012

Molnar, S., Cassidy J.F., Olsen, K.B., Dosso, S.E. and He, J. (2014a). "Earthquake Ground Motion and 3D Georgia Basin Amplification in Southwest British Columbia: Deep Juan de Fuca Plate Scenario Earthquakes," Bulletin of the Seismological Society of America, **104**(1): 301–320.

Molnar, S., Cassidy J.F., Olsen, K.B., Dosso, S.E. and He, J. (2014b). "Earthquake Ground Motion and 3D Georgia Basin Amplification in Southwest British Columbia: Shallow Blind-Thrust Scenario Earthquakes," Bulletin of the Seismological Society of America, **104**(1): 321–335

Molnar, S., Assaf, J., Sirohey, A., & Adhikari, S. R. (2020). Overview of local site effects and seismic microzonation mapping in Metropolitan Vancouver, British Columbia, Canada. Engineering Geology, 270, 105568. https://doi.org/https://doi.org/10.1016/j.enggeo.2020.105568

Molnar, S., Sirohey, A., Assaf, J., Bard, P.-Y., Castellaro, S., Cornou, C., Cox, B., Guillier, B., Hassani, B., Kawase, H., Matsushima, S., Sánchez-Sesma, F. J., & Yong, A. (2022). A review of the microtremor horizontal-to-vertical spectral ratio (MHVSR) method. Journal of Seismology, 26(4), 653–685. https://doi.org/10.1007/s10950-021-10062-9

Monahan, P.A. (2017). Soil hazard map of the Lower Mainland of British Columbia for assessing the earthquake hazard due to lateral ground shaking. APEGBC, UBC, BC ministry of education, June 2017. In: Seismic retrofit guidelines. third ed. volume 9; 2005. Part III, 1pp.

Motazedian, D., Hunter, J.A., Pugin, A., Crow, H. (2011). Development of a Vs30 (NEHRP) map for the city of Ottawa, Ontario, Canada. Canadian Geotechnical Journal 48:458–472. https://doi.org/10.1139/T10-081

Nastev, M., Parent, M., Ross, M., Howlett, D., & Benoit, N. (2016). Geospatial modelling of shear-wave velocity and fundamental site period of Quaternary marine and glacial sediments in the Ottawa and St. Lawrence Valleys, Canada. Soil Dynamics and Earthquake Engineering, 85, 103-116.

Salsabili, M., Saeidi, A., Rouleau, A., Nastev, M. (2022). Development of empirical CPTu-Vs correlations for post-glacial sediments in Southern Quebec, Canada, in consideration of soil type and geological setting. Soil Dynamics and Earthquake Engineering 154:107131. https://doi.org/https://doi.org/10.1016/j.soildyn.2021.107131

Satake, K., Shimazaki, K., Tsuji, Y., and Ueda, K. (1996). Time and size of a giant earthquake in Cascadia inferred from Japanese tsunami records of January 1700; Nature, v. 379, p. 246-249

Seed, B.H., Wong, T.R., Idriss, I.M., Tokimatsu K (1986). Moduli and Damping Factors for Dynamic Analyses of Cohesionless Soils. Journal of Geotechnical Engineering 112:1016–1032. https://doi.org/10.1061/(ASCE)0733-9410(1986)112:11(1016)

Rogers, G.C. (1998). Earthquakes and earthquake hazard in the Vancouver area; in Geology and Natural Hazards of the Fraser River Delta, British Columbia, (ed.) J.J. Clague, J.L. Luternauer, and D.C. Mosher; Geological Survey of Canada, Bulletin 525.

Rogers, G., Halchuk, S., Adams, J., & Allen, T. (2015). 5th Generation (2015) Seismic Hazard Model for Southwest British Columbia. The 11th Canadian Conference on Earthquake Engineering, 1–10

Rosset, P., Bour-Belvaux, M., Chouinard, L. (2015). Microzonation models for Montreal with respect to Vs30. Bulletin of Earthquake Engineering 13:2225–2239. https://doi.org/10.1007/s10518-014-9716-8

Turner, R.J.., Clague, J.J., Groulx, B.J., Journeay, M.J. (1998). GeoMap Vancouver Geological Map of the Vancouver Metropolitan Area Geological Survey of Canada Open File 3511.

Vantassel, J.P., Cox, B.R. (2021). A procedure for developing uncertainty-consistent Vs profiles from inversion of surface wave dispersion data. Soil Dynamics and Earthquake Engineering **145**:106622. doi: https://doi.org/10.1016/j.soildyn.2021.106622

Wair, B., DeJong, J., Shantz, T. (2012). Guidelines for estimation of shear wave velocity profiles. Berkeley: Pacific Earthquake Engineering Research Center, University of California PEER report no 2012/08

Wills, C.J., Clahan, K.B. (2006). Developing a Map of Geologically Defined Site-Condition Categories for California. Bulletin of the Seismological Society of America 96:1483–1501. https://doi.org/10.1785/0120050179

Yong, A., Hough, S.E., Iwahashi, J., Braverman, A. (2012). A Terrain-Based Site-Conditions Map of California with Implications for the Contiguous United States. Bulletin of the Seismological Society of America 102:114–128. https://doi.org/10.1785/0120100262

Zhu, C., Pilz, M., & Cotton, F. (2020). Which is a better proxy, site period or depth to bedrock, in modelling linear site response in addition to the average shear-wave velocity?. Bulletin of Earthquake Engineering, 18(3), 797-820.

Zhu, C., Cotton, F., Kawase, H., Haendel, A., Pilz, M., Nakano, K. (2022). How well can we predict earthquake site response so far? Site-specific approaches. Earthquake Spectra. 2022;38(2):1047-1075. doi:10.1177/87552930211060859

Chapter 3

3 Seismic Site Characterization in Fraser River Delta in Metropolitan Vancouver

In this chapter, seismic site characteristics, specifically depth to stiff glaciated Pleistocene sediments (z_{gl}) and shear wave velocity (Vs) profiles, of the FRD are determined from non-multi-method invasive seismic testing. A z_{gl} predictive model based on $f_{1,HVSR}$ is developed for shallow FRD sites ($z_{gl} \leq 56$ m) and is compared to existing MHVSR peak frequency-sediment thickness models developed in other regions in the world. At 16 FRD sites, a combination of active- and passive-source surface wave array methods are performed to obtain the Rayleigh wave fundamental-mode dispersion curve which is jointly inverted with the MHVSR fundamental peak frequency ($f_{0,HVSR}$) using three parametrization models with varied layering. The jointly inverted Vs profiles with their uncertainties are presented for the 16 sites and compared with existing proximal Vs profiles measured by other *in situ* Vs profiling methods.

3.1 Introduction

British Columbia (BC) is located in one of the most seismically active regions of Canada (Rogers et al. 1998). Southwestern BC, including Metropolitan (Metro) Vancouver, has the highest seismic risk in Canada due to the complex geologic and tectonic setting of the region (Adams and Halchuk 2002). The Holocene post-glacial (mainly alluvium) sediments and Pleistocene glacial and interglacial deposits of the Fraser River Delta (FRD), located in southern Metro Vancouver, are known to significantly alter the characteristics of seismic ground motions as observed from weak-motion earthquake recordings (Cassidy et al. 1997, Cassidy and Rogers 1999, Cassidy and Rogers 2004, Jackson et al. 2017, Molnar et al. 2020). Thus, accurate estimation of the surface ground motions to ensure the safety of local communities can only be achieved through robust incorporation of local site effects.

Local site effects describe the effects of near surface geology on the propagation of seismic waves in the upper few hundred meters of the soil column (Borcherdt 1970). The variation

of subsurface ground stiffness, described by shear wave velocity (Vs), and surface and subsurface geometry of the sediments at a site can modify the amplitude, frequency and duration of seismic waves. Borcherdt (1994) proposed the time-averaged Vs to a depth of 30 m (Vs_{30}) as a quantitative measure to assign subsurface site conditions into one of six seismic site classes with associated site foundation factors of surface-to-bedrock de/amplification. Vs_{30} site classification is prevalent in seismic hazard analysis (i.e., the most common site term parameter in ground motion models or GMMs) and adopted by many seismic design codes worldwide. An alternative measure of site amplification growing in popularity and use in GMMs is the fundamental site frequency (f_0) or natural site period ($T_0 = 1/f_0$) (Di Alessandro et al. 2012, Ghofrani and Atkinson 2014, Hassani and Atkinson 2016, Hashash et al. 2020). Inclusion of simple site effect parameters (Vs_{30} or f_0) in GMMs captures the average site effects of global ground motion databases and do not necessarily represent the local site conditions at a specific site or local region. Alternatively, the knowledge of Vs variation with depth and the dynamic properties of soils allows for a more accurate quantification of site- and region-specific seismic response.

In the Canadian guidelines of *in situ* Vs profiling methods for seismic site characterization (Hunter and Crow 2015), methods are categorized into two main groups: invasive (e.g., down-hole, cross-hole, and suspension P-S logging) and non-invasive (e.g., seismic reflection and refraction, surface wave, and microtremor methods). Typically, invasive profiling methods provide high-resolution Vs measurements, e.g., every 1 m depth increment, and therefore better identify minor or subtle changes in Vs with depth. In contrast, non-invasive Vs profiling methods sample larger soil volumes and provide an average Vs estimate throughout this volume. Specifically, non-invasive surface wave methods have been developed and widely used to infer Vs profiles due to their time- and cost-efficiency. Active-source multichannel analysis of surface waves (MASW) and passive-source microtremor array measurements (MAM) are techniques commonly used to extract surface wave phase velocity estimates at each selected frequency, i.e., the site's dispersion curve. While performing MASW or MAM testing is relatively simple, the identification of fundamental- and higher-mode dispersion curves, the inversion non-

uniqueness, and the inclusion and propagation of uncertainties in Vs profiles (Vantassel and Cox 2021) can be challenging, especially at sites with complex geologic conditions (e.g., Vs reversals, and lateral variability). Inversion of the site dispersion curve determines a suite of layered earth models for which the theoretical (forward) dispersion curve fits the experimental one; optimization inversion techniques seek the minimum misfit Vs profile whereas global search techniques and/or Monte Carlo sampling are used to capture Vs profile uncertainty (e.g., Molnar et al. 2010, Wathelet et al. 2020). The uncertainty in inverted Vs profiles is often communicated by considering a suite of lowest misfit models, e.g., 33 (Hollender et al. 2018), 50 (Griffiths et al. 2016, Teague and Cox 2016), 100 (Giulio et al. 2012), and 1000 profiles (Teague et al. 2018, Deschenes et al. 2018, Bilson Darko et al. 2020), noting there is no global standard and thus considerable variation in the inversion methodology of the provided examples.

There is significant published literature documenting agreement of non-invasive Vs profiling (often a modelled Vs profile from inversion of surface wave dispersion estimates) with that of invasive Vs profiling. The Inter-PACIFIC project, a blind-test comparison of invasive and non-invasive Vs profiling amongst different practitioner teams and for three sites of varying ground stiffness (soft, stiff, and rock), demonstrated that the Vs variability from non-invasive surface wave methods and invasive methods is comparable for both simple and more complex geologic settings (Garofalo et al. 2016a). The differences in Vs_{30} from both methods were generally less than 4% and coefficient of variation (COV) of Vs with depth from invasive and non-invasive surface wave methods was similar, ranging between 0.1 and 0.2 at the soft and stiff sites, respectively, and ranges between 0.1 and 0.6 for the rock site (Garofalo et al. 2016a). In Canada, the FRD has been the testing ground for comparison of Vs profiling methods with good agreement between spectral analysis of surface waves (SASW) vs. seismic cone penetration test (SCPT) at 15 sites (Woeller et al. 1993). The variability between MASW and downhole Vs at 8 sites (Xia et al. 2000) was 8-26%, and Vs variability of 5% to 120 m depth and 25% to 60 m depth between MAM testing and the average of co-located invasive methods at two sites (Molnar et al. 2010, 2012). We note that validation of non-invasive Vs profiling methods (SASW, MASW,

MAM) in comparison with invasive methods is limited to individual surface wave array methods. It is now recommended to combine active- and passive-source surface wave array methods to obtain dispersion estimates over a wider frequency bandwidth and thereby obtain the Vs profile over a greater depth range (e.g., Garofalo et al. 2016a, Foti et al. 2018).

Single station MHVSR measurements have been widely used for seismic microzonation and earthquake site characterization applications (Molnar et al. 2022). When a sufficiently strong impedance contrast exists at depth, the MHVSR's fundamental peak frequency ($f_{0,HVSR}$) can be used to approximate the shear-wave resonant frequency ($f_{0,SH}$) (Field and Jacob 1993, Lachet and Bard 1994) and/or the fundamental-mode Rayleigh wave ellipticity (f_{Ellip}) (Poggi and Fäh 2010). In terms of amplitudes, there is a growing consensus that MHVSR amplitudes have a weak correlation with site amplification (relative to soil base or rock), despite some empirical and numerical studies that show amplitudes of MHVSR peak frequencies scales well with the strength of the impedance contrast, and thus somehow linked to site amplification (Albarello and Lunedei 2011, Oubaiche et al. 2012). In Canadian studies, however, MHVSRs are observed to provide reliable measures of both $f_{0,HVSR}$ and amplitude ($A_{0,HVSR}$) in comparison to observed earthquake soil-to-rock amplification in British Columbia (Molnar and Cassidy 2006) and earthquake HVSR amplification in Ontario (Braganza et al. 2017), Alberta (Farrugia et al. 2018) and British Columbia (Molnar et al. 2020). However, the MHVSR amplification is observed to be lower than the very high earthquake HVSR amplification of weak ground motions for Ottawa soil sites (Adams 2007; Khaheshi Banab et al. 2012). MHVSRs have been used to map the depth of the bedrock or stiff sediments using $f_{0,HVSR}$ with empirical knowledge of the Vs variation with depth (e.g., Seht and Wohlenberg 1999, Delgado et al. 2000, Parolai et al. 2002, Hinzen et al. 2004, D'Amico et al. 2008, Gosar and Lenart 2010, Tün et al. 2016, Molnar et al. 2018, Moon et al. 2019). The presence of multiple MHVSR peaks is typically related to secondary impedance contrasts and less likely to be higher resonance modes (Molnar et al. 2022). Many studies have pointed out that the correlation between secondary MHVSR peaks and the depths to shallow interfaces with a strong impedance contrast is in fact of geologic origin (e.g., Guéguen et al. 2000, García-Fernández and

Jiménez 2012, Macau et al. 2015, Castellaro 2016, Wotherspoon et al. 2018, Teague et al. 2018, Oubaiche et al. 2016, Rohmer et al. 2020, Rahimi et al. 2020). Fewer studies have found good agreement between secondary MHVSR peaks and higher modes of f_0 (e.g., Bodin et al. 2001, Goetz 2009). Additionally, MHVSR peak frequencies or its full spectrum may be inverted separately or jointly with the site dispersion curve to infer Vs profiles, with varying levels of success. The complementary inversion of MHVSRs with dispersion curves has been proven to help constrain the layered earth models, especially at greater depths (e.g., Molnar et al. 2018, Pratt 2018).

The FRD in Metro Vancouver is a relatively lowland region compromising Holocene-aged deltaic silts and sands, with thicknesses up to 300 m, that have been deposited since the last glaciation 11,000 years ago (Luternauer and Hunter 1996). The Vs of these deltaic sediments increases with depth from a minimum of ~ 70 m/s at the surface to about 500 m/s at 300 m (Hunter et al. 2016). The FRD post-glacial sediments overlay glaciated sediments mostly comprised of ice-compacted till and glaciomarine silts and sands from repeated glaciations. The average Vs of glacial sediments is ~ 475 m/s ranging between 400-1200 m/s with a poorly defined depth dependency (Hunter et al. 1999, Monahan and Levson 2001). Beneath the central FRD, post-glacial and glacial sediments have a maximum known thicknesses of about 300 m and 500 m, respectively (Clague et al. 1998). Late-Cretaceous to Tertiary sedimentary bedrock of the Georgia basin, with Vs of ~ 1000 to ~ 2500 m/s (Hunter et al. 1999), outcrops along the North Shore and in the northern cliffs of Stanley Park dipping about 12° to the south (Armstrong 1984) and are found at depths of 200 to 1000 m underneath the FRD (Britton et al. 1995). Mafic intrusions (basaltic dykes) within the sedimentary rock sequences also outcrop within the Metro Vancouver area, e.g., Queen Elizabeth Park, the highest topographic location within city of Vancouver (Armstrong 1984, Armstrong 1990). At the northern extent of Metro Vancouver, outcropping granitic Coast Mountain plutonic rocks mark the northern limit of the Georgia sedimentary basin (Armstrong 1984).

The overall subsurface architecture of the FRD is therefore dominated by two major seismic impedance contrasts between post-glacial deltaic and glaciated sediments (impedance contrast strength of ~1.5 to 3) and between glaciated sediment and sedimentary bedrock (impedance contrast strength ~2 to 3) (Hunter et al. 2016). The depths to these two major impedance contrasts control the resonant frequencies of FRD sites and play a major role in its soil amplification. Atkinson and Cassidy (2000) reported that the theoretical linear site response in FRD is primarily controlled by the thickness of post-glacial sediments and is less sensitive to the variability in glacial sediments thickness. Similarly, Ventura et al. (2004) and Onur et al. (2004) compared T_0 from theoretical site response and observed MHVSRs at 27 strong-motion accelerograph stations and found that the variation in the thickness of post-glacial sediments thickness has greater impact on the site T_0 than that of the glacial sediments. Moreover, the post-glacial/glacial boundary is often used as the half-space for site response modelling in geotechnical engineering applications (e.g., liquefaction assessment). This is mostly driven by the fact that Vs profiles that penetrate into stiff glacial sediments correspond to seismic site class C reference conditions (Vs_{30} = 450 m/s) selected for the 5th generation seismic hazard model for Canada (Adams et al. 2015) and that Vs and other material properties of the deeper glaciated sediments are less understood. Earthquake recordings at strong-motion stations show ground motion amplitudes are highest at the edge of the FRD, where the thickness of post-glacial sediments rapidly decreases to a few meters (Cassidy and Rogers 2004). Finn et al. (2003) showed that 2D site response modelling for select FRD strong-motion stations, in comparison to 1D modelling, improved the prediction of recorded ground motions specifically for sites with thinner post-glacial sediment deposits. The thickness of post-glacial sediments, or depth (z) to stiff glacial (gl) sediments, z_{gl}, is therefore a very important parameter in the framework of seismic hazard estimation and site effects characterization in the FRD.

In this study, seismic site effect metrics for sites in the FRD are explored. Datasets specific to the FRD region are accessed for this study from the recently-compiled comprehensive geodatabase of the Metro Vancouver seismic microzonation project (Molnar et al. 2020, Adhikari and Molnar 2021), consisting of existing borehole lithology and Vs depth profiles

from a variety of invasive and non-invasive *in situ* testing complemented by targeted non-invasive *in situ* testing (single station MHVSR, MAM and MASW dispersion methods) performed during four field campaigns of the project. First, z_{gl} is considered in relation with the theoretical resonant frequency of post-glacial sediments ($f_{m,pgl}$) determined from Vs profiles that log into glacial sediments (known z_{gl}) and the observed MHVSR 2nd peak frequency ($f_{1,HVSR}$) at locations where z_{gl} is known. We develop a model to predict z_{gl} based on $f_{1,HVSR}$ and compare it to existing $f_{0,HVSR}$-sediment depth models worldwide. This study also presents the non-invasive active-source MASW and passive-source MAM testing and combined dispersion curves for 16 FRD sites, of which 8 are co-located with strong-motion station sites. The extracted dispersion curves (with data uncertainties) are jointly inverted with $f_{0,HVSR}$ using three model parametrizations with varied layering. The jointly inverted Vs profiles are obtained using the most comprehensive set of non-invasive *in situ* datasets for the FRD to date. The reliability of the inverted Vs profiles with their uncertainties are evaluated compared to nearby Vs profiles from other *in situ* methods. The developed z_{gl} predictive model and inverted Vs profiles provide important input to 1D and 2D site response modelling at delta edge sites and seismic hazard mapping in the FRD. In addition, the developed Vs profiles of the 8 strong-motion stations can be used in the future to correlate earthquake ground motion recordings with seismic site metrics.

3.2   Vs Profile and z_{gl} Datasets of the Metro Vancouver Seismic Microzonation Project

A variety of geodatasets have been compiled (e.g., borehole lithology, depth profiles of Vs, (S)CPT and SPT measurements), and complemented by non-invasive seismic testing (MHVSR, MASW and MAM), into a comprehensive regional geodatabase (Adhikari and Molnar 2021) for the Metro Vancouver seismic microzonation mapping project (Molnar et al. 2020). The geodatasets used in sections 3.3 and 3.4 of this study are presented here. For section 3.3, 32 unique locations where existing Vs profiles sample the FRD sediments and log into stiff glaciated sediments are compiled from Hunter et al. (2016) and other geotechnical reports. The 32 Vs profiles are compiled from a variety of *in situ* invasive and non-invasive Vs profiling methods: 20 downhole, 5 SCPT, and 7 surface shear wave

refraction. The total number of Vs profiles is 39 as there are 2 Vs profiles for each refraction testing site, from forward and reverse refraction shot gathers. For these 39 Vs profiles, z_{gl} is determined from lithological information or by a sharp increase in Vs; 25 Vs profiles have corresponding borehole lithology and other geophysical testing or CPT measurements. The lithological information, if available, must clearly demonstrate transition from sandy or silty deltaic sediments to gravelly or till-like glaciated sediments (most often reported as diamicton). For borehole logs where the lithological description is not provided, contrasts in Vs and/or electrical conductivity (Hunter et al. 2016) are used to determine z_{gl}. The Metro Vancouver project's single station microtremor measurements (MHVSR) are performed at 13 sites where existing Vs profiles of Hunter et al. (2016) and z_{gl} are available, and at 4 other locations where z_{gl} is known (Mustard and Roddick 1992) but no Vs profile exists. The locations of the 32 unique Vs profile locations and the 17 co-located or proximal (within 100 m) MHVSR measurements are shown in Fig. 3-1 underlain by the regional surficial geology map (Dunn and Ricketts 1994). Active-source MASW and passive-source MAM measurements performed at 16 seismic array sites within the FRD (Fig. 3-1) as part of the Metro Vancouver project are analyzed in section 3.4 to determine the fundamental-mode Rayleigh wave dispersion curve and jointly invert with MHVSR peak frequencies to obtain 16 new non-invasive Vs profiles. The locations where z_{gl} is approximately less than 50 m (Monahan 2005) are also plotted in Fig. 3-1 as a mappable approximation of the FRD edges. Fig. 3-2 shows lithologic cross-sections beneath the FRD from Clague et al. (1998) with z_{gl} and glaciated sediment thicknesses based on boreholes and geophysical surveys with projected locations of MHVSR testing from Fig. 3-1.
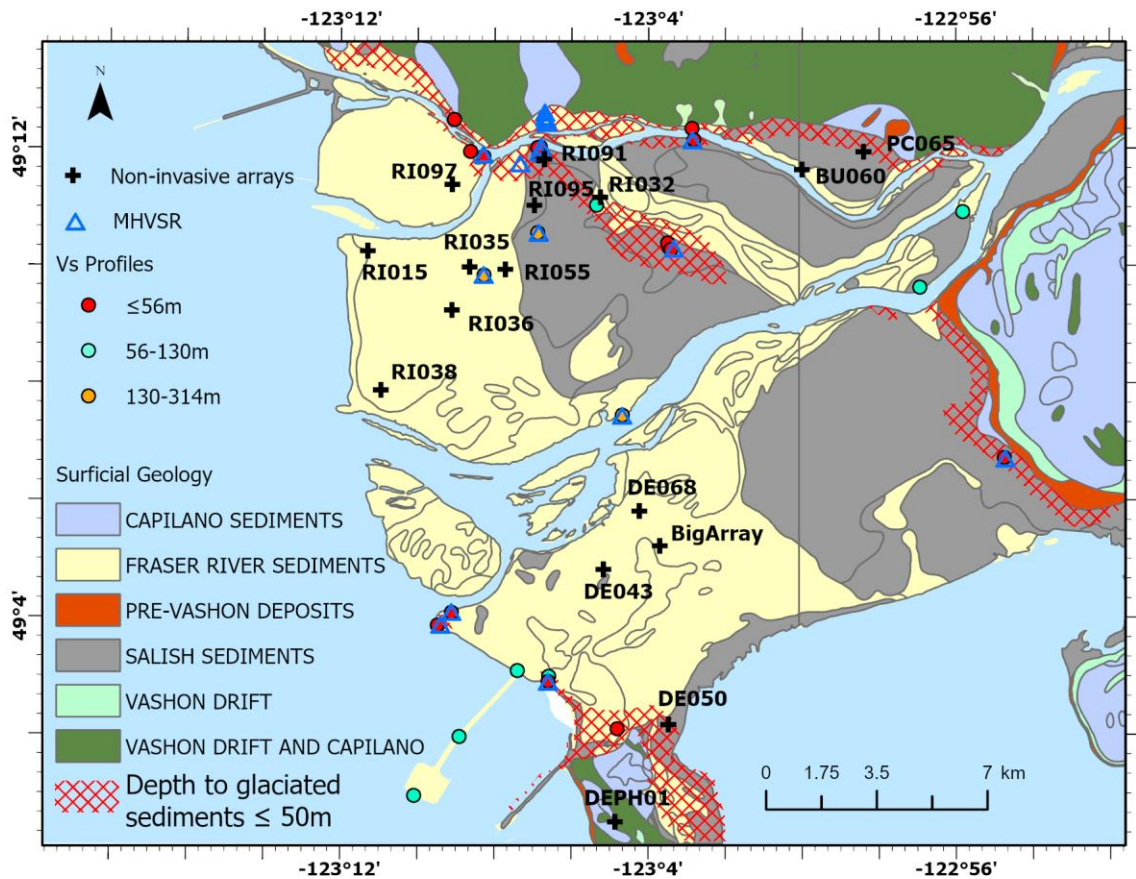
Figure 3-1 Regional surficial geology map showing locations of performed MHVSRs (blue triangles) at locations where depth to stiff glacial sediments is known. Locations of Vs profiles that log into stiff glacial sediments are shown with circles colored by maximum profile depth. Non-invasive seismic array sites are shown with black crosses. The approximate boundaries where z_{gl} is expected to be less than 50 m are also shown (Monahan 2005).
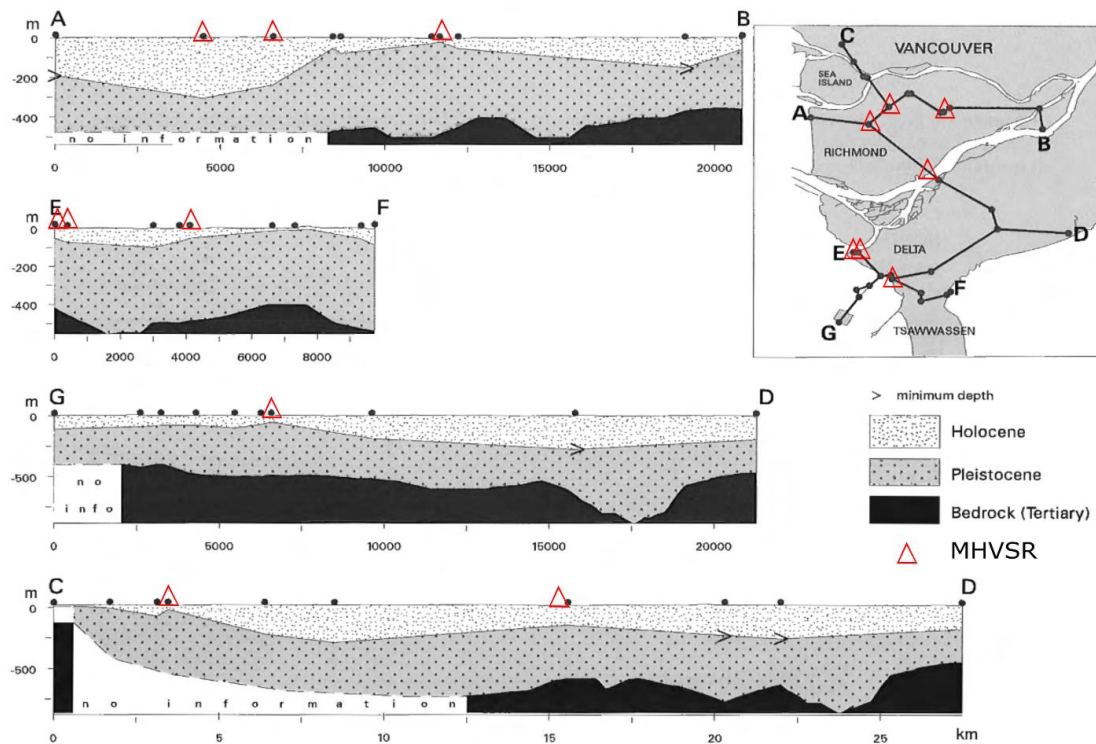
Figure 3-2: Cross-sections showing variation in the thickness of post-glacial (Holocene) and glacial (Pleistocene) deposits beneath the FRD based on borehole lithology and geophysical surveys (modified from Clague et al. 1998); note different vertical depth scales. zgl is known only below borehole locations (designated by black dots); zgl values between borehole locations were inferred by Clague et al. (1998). Locations of microtremor measurements proximal to the borehole location (Fig. 3-1) are referenced on the relevant cross-section using red triangles.

3.3   Relationship Between z_{gl} and Resonant Frequencies

HVSRs from microtremor and weak-motion earthquake recordings at many FRD sites commonly exhibit two peaks (Onur et al. 2004, Molnar et al. 2013, Molnar et al. 2020), $f_{0,HVSR}$ and $f_{1,HVSR}$ that are in the range of about 0.15 to 0.6 Hz and about 0.6 to 5 Hz, respectively. Previous 1D site response modelling in the FRD (Harris et al. 1998, Onur et al. 2004, Molnar et al. 2013) demonstrated that the full soil column's modelled fundamental frequency ($f_{0,SH}$) corresponding to the deeper glacial sediments-bedrock interface at 200 to

800 m depth (Britton et al. 1995) is in good agreement with the observed $f_{0,HVSR}$ range. Although we measure $f_{0,HVSR}$ at many FRD sites in this study, a model to predict the depth to bedrock from $f_{0,HVSR}$ is currently not available, mainly due to the few boreholes that log into the deep bedrock. Notably, previous studies generally did not focus on $f_{1,HVSR}$. Molnar et al. (2013) noted the modelled higher modes of the 1D linear transfer function at one FRD site were not observed in the MHVSR and earthquake SH/V ratios. The origin of the 2nd peak in the MHVSR ($f_{1,HVSR}$) of FRD sites was therefore not yet well understood. After collecting over 2,000 MHVSR measurements across Metro Vancouver (Molnar et al. 2020; Sirohey and Molnar 2021), we know that the MHVSR $f_{1,HVSR}$ occurs at frequencies related to the post-glacial/glacial impedance contrast (z_{gl}) at depths ranging from a few meters to over 300 m. From weak ground motion recordings of past earthquakes in the region, the highest surface motions in Metro Vancouver were observed near the FR delta edge at intermediate frequencies (1.5-4.0 Hz; Cassidy and Rogers 2004) similar to $f_{1,HVSR}$ rather than $f_{0,HVSR}$, which makes the understanding of these higher frequency peaks of significant importance.

To study the correlation between $f_{1,HVSR}$ and z_{gl}, the relationship between the theoretical fundamental resonant frequency of post-glacial sediments ($f_{m,pgl}$ or $1/T_{m,pgl}$) and z_{gl} is first investigated. To calculate $f_{m,pgl}$, both z_{gl} and Vs profile of post-glacial sediments to a depth equal to z_{gl} are needed. We calculate $f_{m,pgl}$ for a range of assumed z_{gl} values using the average Vs depth profile of the FRD post-glacial sediments determined by Hunter and Christian (2001) to 90 m:

$$\text{Vs}(z) = 71.22 + 35.26z^{0.4362} \pm 2\sigma_{Vs} \qquad for\ z \leq 90\ m \qquad \textbf{Eq. 3-1}$$

where z is the depth in meters and σ_{Vs} is one standard deviation (19.4 m/s). The theoretical resonant period (T_0) of a layer with thickness H overlying a half-space can be calculated as 4tt (Seht and Wohlenberg 1999), where tt is the shear-wave travel time within the soil layer, i.e., $T_0 = 4H/Vs_{avg}$. The theoretical tt of post-glacial sediments ($tt_{m,pgl}$) is

$$tt_{m,pgl} = \int_0^{z_{gl}} \frac{dz}{Vs(z)}$$ **Eq. 3-2**

Substituting Eq. (3-1) in Eq. (3-2), $T_{m,pgl}$ and consequently $f_{m,pgl}$ are obtained by numerical integration for a range of z_{gl} between 2 and 350 m, which is the expected range of z_{gl} in the FRD. Although Eq. 3-1 is developed for FRD sediments at $z \leq 90$ m, its power law gradient functional form is well determined and can be extended to predict Vs at greater depth within FRD sediments, noting uncertainty in Vs continually increases with depth past the 90 m limit of the model. We also calculate $f_{m,pgl}$ using Vs profiles and z_{gl} at the 39 available Vs profiles that fully sample the post-glacial sediments (shown as colored circles in Fig. 3-1). These 39 Vs profiles are used by Hunter and Christian (2001) to develop their Vs(z) relationship and therefore occur within the Vs(z) distribution of Eq. 3-1. $T_{m,pgl}$ $(1/f_{m,pgl})$ of each Vs profile was calculated by

$$T_{m,pgl} = \sum \frac{4H_i}{Vs_i}$$ **Eq. 3-3**

where H_i and Vs_i are the thickness and the Vs of layer i, respectively.

Single station MHVSR measurements were performed using Tromino® seismometers at or close to 13 of the 39 Vs profile locations (within 100 m; Fig. 3-1), and at an additional 4 locations where z_{gl} is known from boreholes. Microtremor recordings were conducted during daytime hours with a minimum recording duration of 30 minutes. Appropriate soil-sensor coupling and protection against weather conditions such as wind were applied. The recordings were divided into time windows of 60 seconds duration using Geopsy software (v. 2.9.1, Wathelet et al. 2020). Transients in the time series were removed first using an anti-triggering algorithm then by manual removal of time windows that produced anomalous MHVSR spectra. The selected time windows were 5% cosine tapered and Fourier transformed into the frequency domain before applying a smoothing Konno-Ohmachi filter with a coefficient of 40 to the amplitude spectra. For each selected time window, the ratio of the quadratic mean of the horizontal component spectra to the vertical

component spectrum is calculated and then averaged over all selected time windows. Peak frequencies are picked using Geopsy from the MHVSR curves such that the amplitude of the peaks are larger than 2 according to SESAME criteria for clarity (Bard et al. 2004). These peak frequencies represent the average values as calculated from individual windows with constraints placed on the frequency range in which to look for peaks in Geopsy. We note that $f_{0,HVSR}$ determined from Tromino seismometers in the FRD was validated using Guralp 40T broadband seismometers which have a flat instrument response to 0.03 Hz (Molnar et al. 2020).

Fig. 3-3 compares the experimental MHVSRs with $f_{0,HVSR}$ and $f_{1,HVSR}$ conducted 22 m and 19 m away from downhole Vs at FD92-2 (shallow site example, $z_{gl} = 32$ m) and BH13-01 (deep site example, $z_{gl} = 313.9$ m), respectively. The calculated $f_{m,pgl}$ at both sites using Eq. 3-3 based on the borehole lithology (z_{gl}) and the downhole Vs profiles is also shown in Fig. 3-3. $f_{m,pgl}$ at FD92-2 agrees with $f_{1,HVSR}$ while at BH13-01, $f_{m,pgl}$ is close to or merged with $f_{0,HVSR}$. The MHVSR peak frequencies and their spectra for the 17 measurements are listed in Table A-1 and shown in Figure A-1, respectively, in Appendix A. Figure 4-4 shows our compilation of theoretical $f_{m,pgl}$ from the 39 Vs profiles and experimental $f_{1,HVSR}$ from the 17 MHVSR sites according to z_{gl} in comparison to $f_{m,pgl}$ predicted using the existing Hunter and Christian (2001) Vs(z) relationship ($z_{gl} = 2\text{-}350$ m) for the FRD. In general, the relationship between z_{gl} and $f_{m,pgl}$ from the existing FRD Vs(z) model and our selected 39 Vs profiles are similar, as expected. For frequencies greater than ~1 Hz, both theoretical $f_{m,pgl}$ and experimental $f_{1,HVSR}$ correspond to similar z_{gl} values. An observed $f_{1,HVSR}$ below ~1 Hz is rare, only 3 MHVSR measurements provide an $f_{1,HVSR}$ value below 1 Hz. It is observed that for shallower sites ($z_{gl} \leq 56$ m or frequencies ≥ 1 Hz), $f_{1,HVSR}$ and $f_{m,pgl}$ are similar for the known z_{gl}, while at the 3 deepest sites (frequencies < 1 Hz), $f_{1,HVSR}$ deviates from $f_{m,pgl}$. We hypothesize that this deviation is attributed to the strength of the impedance contrast at different depths. For example, the average post-glacial Vs from Eq. 3-1 at depths of 20 m and 100 m are 212 and 369 m/s, respectively. Considering the average Vs of glaciated sediments in the FRD is 480 m/s as calculated from invasive Vs profiles (Hunter el al. 2016), the impedance contrast strength at 20 m and 100 m are 2.26 and 1.3,

respectively. The impedance contrast strength decreases at deeper depths as Vs of the post-glacial sediments increases. Retrieval of $f_{0,HVSR}$ or $f_{1,HVSR}$ is known to improve when a strong impedance contrast exists; deeper impedance contrasts might not be strong enough to excite $f_{1,HVSR}$, unlike for shallower contrasts. Moreover $f_{m,pgl}$ decreases with increasing depth eventually merging with the full soil column f_0 making the separation between these two resonance peaks difficult (e.g., Fig 3-3b). At shallower sites (Fig 3-3a), the two resonance peaks are well separated ($f_{0,HVSR}$ around 0.2-0.5 Hz and $f_{1,HVSR}$ above 1 Hz). Based on this rationale and Fig. 3-4 comparisons, $f_{1,HVSR}$ is considered to correlate well with $f_{m,pgl}$ only for shallow depths or when $f_{1,HVSR}$ is ≥ 1 Hz.

A power-law gradient model has been widely used for mapping depth to impedance contrast from $f_{0,HVSR}$. To develop a relationship between z_{gl} and $f_{1,HVSR}$, a non-linear regression is employed using the same power-law gradient model with $f_{0,HVSR}$ replaced by $f_{1,HVSR}$, i.e.,:

$$z_{gl} = af_{1,HVSR}^{-b} \qquad \textbf{Eq. 3-4}$$

where *a* and *b* are the unknown regression coefficients, given the ($f_{1,HVSR}$, z_{gl}) data pairs in Fig. 4-4 for $z_{gl} \leq 56$ m (i.e., removing the three $f_{1,HVSR}$ outliers below 1 Hz). The determined power-law regression model (N=14, $R^2 = 0.88$) is

$$z_{gl} = 54.72f_{1,HVSR}^{-1.34} \quad \text{for} \quad f_{1,HVSR} \geq 1 \text{ Hz} \qquad \textbf{Eq. 3-5}$$

This model is extrapolated: (1) at frequencies < 1 Hz (grey dashed line in Fig. 4) to highlight the model's deviation from the experimental $f_{1,HVSR}$ values, and (2) at frequencies > 3.347 Hz (black dashed line in Fig. 3-4) as no ($f_{1,HVSR}$, z_{gl}) pairs exist at these high $f_{1,HVSR}$ and shallow z_{gl} values. Our z_{gl} predictive model matches well with $f_{m,pgl}$ from the existing FRD Vs(z) model over the 1-8 Hz bandwidth.

The predictive z_{gl} model for the FRD (Eq. 3-5) is compared to 9 different published $f_{0,HVSR}$-sediment thickness models that use the same functional form (Eq. 3-4) from different regions of the world in Fig. 3-5. Table 3-1 reports the model coefficients and properties of

these $f_{0,HVSR}$-sediment thickness models. Our model estimates the depth to stiff glaciated sediments using $f_{1,HVSR}$ while the other models reported in Table 3-1 describe the relationship between $f_{0,HVSR}$ and the depth to bedrock. In general, both the existing FRD Vs(z) model and our predictive z_{gl} model of this study predict shallower conditions, or lower equivalent averaged Vs, at a certain frequency compared to other models. This is due to the different stiffness of the geologic layers considered in the model development; the average Vs to bedrock depth used in other models includes stiffer sediments and should be higher than the average Vs to glacial (till-like) sediments considered in this study.

The models developed in this study are mostly comparable to the Delgado et al. (2000) model ($a = 55.11$, $b = -1.256$), which is proposed to estimate soft soil thickness for the Segura River valley in Spain, and to a lesser extent, the model developed for soft glaciomarine sediments thickness in the Ottawa region in Canada ($a = 55$, $b = -1.02$; Motazedian et al. 2011, Molnar et al. 2018). Interestingly, the Vs range in the Segura river study is 85 m/s at the surface and increases to about 200 m/s at 20 m (Delgado et al. 2000), which is very similar to the Vs(z) relationship of post-glacial sediments in the FRD (~ 71 m/s at surface and 212 m/s at 20 m from Eq. 3-1). The similarity in Vs with depth for the FRD (Canada) and the Segura River valley (Spain) sediments, presumably due to their similar deltaic depositional environments, further explains the closest agreement between our predictive z_{gl} model and that of Delgado et al. (2000). This observation supports the application of peak frequency-thickness relationship developed using data from one region to another with a similar geologic setting and Vs(z) relationship.

The use of our developed z_{gl} predictive model (Eq. 3-5) should be limited to zones where z_{gl} is expected to be less than 50-60 m, i.e., FRD edge locations (Monahan 2005) shown in Fig. 3-1. The extrapolation of the z_{gl} model to frequencies higher than experimental $f_{1,HVSR}$ data used in model development (> 3.347 Hz) can be considered with caution; small z_{gl} values are expected but the rate of change in z_{gl} and hence $f_{1,HVSR}$ will be significant at the FRD edge. In contrast, use of our predictive z_{gl} model might significantly under predict z_{gl} when $f_{1,HVSR}$ is < 1 Hz and is not recommended at these low frequencies. The predictive z_{gl}

model developed here based on $f_{1,HVSR}$ is important for estimating and mapping the thickness of shallow post-glacial FR sediments generally at the edges of the delta, where soil amplification during past earthquakes was the highest in the FRD (Cassidy and Rogers 2004). Finn et al. (2003) showed that using 2D site response modelling, in comparison to 1D modelling, in the FRD improved the prediction of recorded ground motions specifically for sites with shallow post-glacial sediment thickness. Thus, more extensive 1D and 2D site response modeling studies can make use of our z_{gl} predictive model to define the FRD geometry.
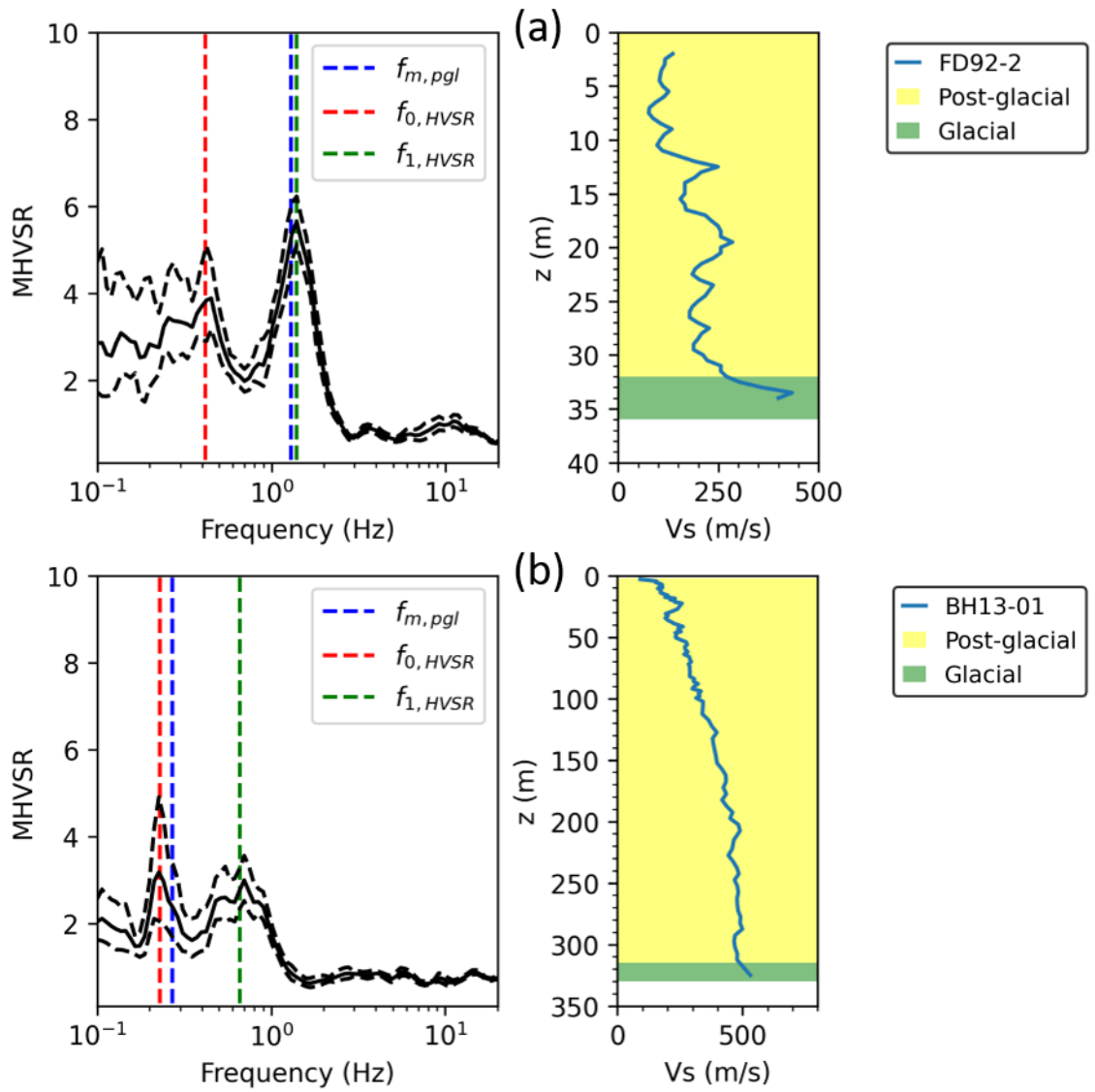
Figure 3-3: Experimental MHVSR peak frequencies with $f_{m,pgl}$ via Eq. 3 for downhole Vs profiles (a) FD92-2 with z_{gl} = 32 m and (b) BH13-01 with z_{gl} = 313.9 m.
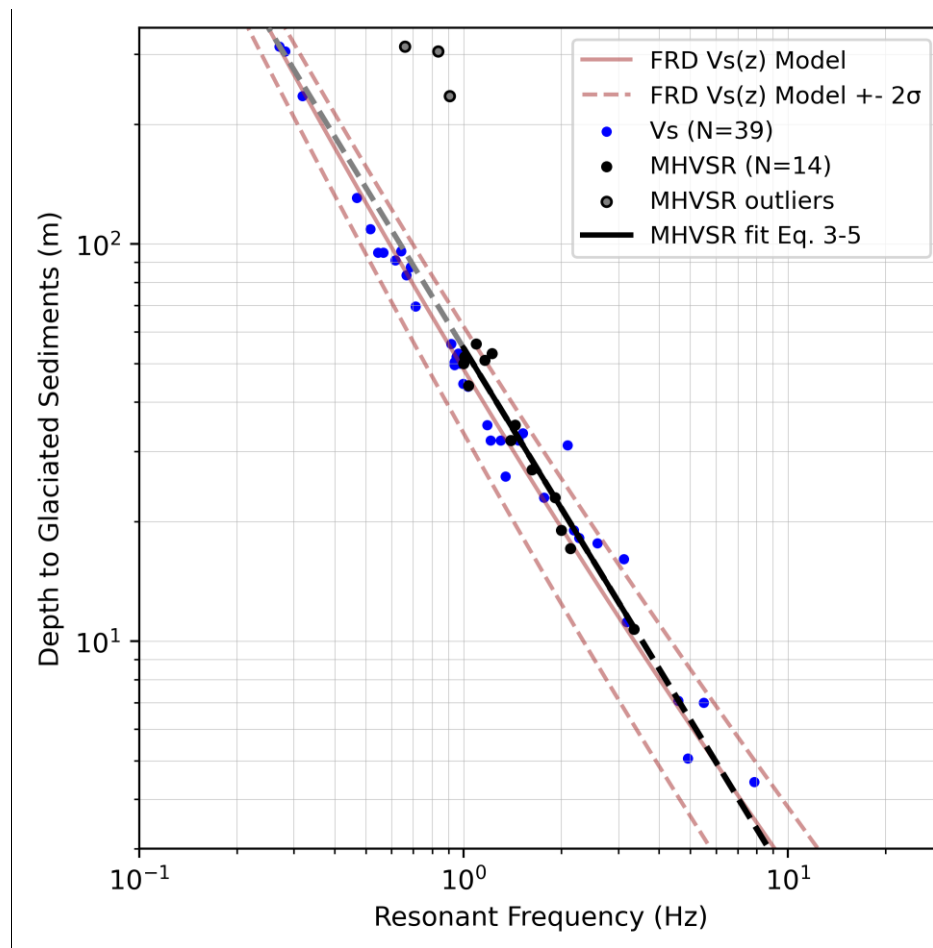
Figure 3-4: Relationship between resonant frequencies ($f_{m,pgl}$ and $f_{1,HVSR}$) with z_{gl}. The blue circles show $f_{m,pgl}$ determined from the 39 Vs profiles that log into glaciated sediments which are a subset of $f_{m,pgl}$ determined from the existing FRD Vs(z) relationship (pink lines). A powerlaw model (solid black line) is fit to the experimental $f_{1,HVSR}$ data (black circles) which is extrapolated to higher (black dashed line) frequencies. It is not recommended to predict z_{gl} when $f_{1,HVSR}$ is < 1 Hz (grey dashed line).

Table 3-1**. Peak frequency-sediment thickness relationships derived from MHVSRs in different parts of the world.**

Author	Region	a	b	R^2	N	Peak frequency range (Hz)	Sediment Thickness (m)	Sediment Type
Ibs-von Seht and Wohlenberg (1999)	Western Lower-Rhine, Germany	96	1.388	0.98	34	0.14-4.64	15-1600	Quaternary-Tertiary
Delgado et al. (2000)	Segura River Valley, Spain	55.11	1.256	0.97	27	1.16-8.3	4.1-44.7	Late Pleistocene-Holocene
Parolai et al. (2002)	Cologne, Germany	108	1.551	-	32	~0.4-15	0.5-402	Quaternary and Tertiary
Hinzen et al. (2004)	East Lower-Rhine, Germany	137	1.19	0.96	50	~0.2-2.5	~100-1250	Quaternary and Tertiary
D'Amico et al. (2008)	Florence, Italy	140	1.172	0.9	23	1.03-7.47	9-115	Plio-Quaternary
Gosar and Lenart (2010)	Ljubljana Moor, Slovenia	105.53	1.25	0.58	53	0.8-9	5-168	Lacustrine and fluvial Quaternary
Tun et al. (2016)	Eskisehir Basin, Turkey	136	1.36	0.98	30	~0.3-11	~0-500	Quaternary-Tertiary (Vs <800 m/s)
Molnar et al. (2018), Motazedian et al. (2011)	Ottawa, Canada	64.98	1.198	0.95	89	~0.6-6	~5-130	Soft glaciomarine sediments
Moon et al. (2019)	Bukit Timah, Singapore	92.5	1.06	0.94	14	~2-9	10-45.5	Quaternary and sedimentary (Jurong) rocks
This Study	Fraser River Delta, Canada	54.72	1.34	0.88	14	1-3.347	10.7-56	Holocene deltaic sediments
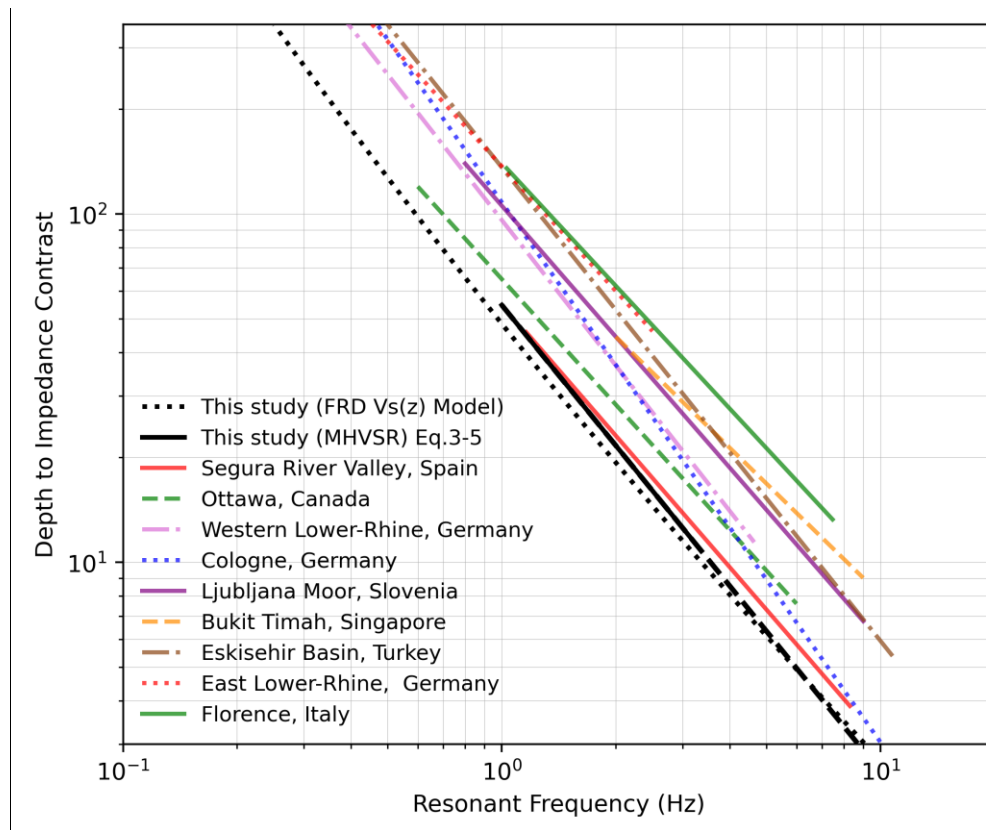
Figure 3-5: The relationships between the thickness of sediments and resonant frequencies for the FRD in this study compared to similar relationships in regions of the world (Table 3-1).

3.4 Vs Profiling from Non-Invasive Microtremor and Surface Wave Testing

In this section, active-source MASW and passive-source MAM measurements performed at 16 FRD sites (Fig. 3-1) of the Metro Vancouver project are analyzed to determine the fundamental-mode Rayleigh wave dispersion curve for each site. Joint inversion of the combined dispersion curve with MHVSR peak frequencies is performed to obtain 16 new FRD Vs profiles. We note that none of the existing Vs profiles of FRD sites (e.g., Hunter et al. 2016, Molnar et al. 2012) were obtained using multiple non-invasive *in situ* testing (MHVSR, MAM and MASW) as is done here.

The locations of the 16 array sites are chosen to provide good spatial coverage across the FRD. Eight of the array sites are targeted near (within 300 m) strong-motion stations that have recorded a few weak motion earthquakes (Molnar et al. 2020) and lack subsurface characterization. The mapped surficial geology unit at all 16 sites is soft post-glacial FR or Salish sediments, except DEPH01 (Fig. 3-1) which is located on Point Roberts peninsula, an upland and former island underlain by Pleistocene sediments (Clague 1998) and thus mapped as the Vashon Drift and Capilano Sediments unit.

3.4.1   Microtremor and Surface Wave Arrays Testing

Table 3-2 reports the location coordinates and details of the array measurements conducted at the 16 non-invasive array sites on the FRD, site locations are shown in Fig. 3-1. The nearby strong motions stations with the distances to the array edge are also reported in Table 3-2. Active-source MASW measurements are conducted using 24 4.5-Hz vertical-component geophones in a linear array. Multiple spacings between geophones (0.5, 1, and 3 m, sometimes 5 m) are used for each array based on the available open space at the site. A 5 kg hammer is vertically impacted on a steel plate to create the seismic source. For smaller spacings (0.5 and 1 m), a source offset distance of 5 m is used, while for larger spacings (3 and 5 m), an offset of 10 m is used with an additional source location at mid-length of the array. Synchronized recordings of the 24 geophones (shot gathers) are triggered by the seismic source and obtained using a sampling rate of 500 Hz for a 2 second duration.

Example MAM array geometries are shown in Figure 3-6. Circular arrays with radii of 5, 10, 15 and 30 m are used at most sites; 6 Tromino seismometers are symmetrically placed around a central 7th seismometer. At some locations where space is limited, the largest array radius is reduced to 15 or 20 m. In few cases, larger radii arrays are used: 40 m at DE043 and DE068 sites, and 45 m at RI097. A single 'Big Array' is performed with radii spanning 15 to 380 m in the deepest area of the FRD to attempt retrieval of dispersion estimates at lower frequencies. The BigArray is conducted with a total of 11 Tromino seismometers, a double ring of 5 seismometers spaced equidistantly at two different radii around the central

11th seismometer. Three sets of simultaneous array recordings are collected for the following double ring radii: 15 and 45 m, 45 and 145 m, and 270 and 380 m. At RI035 and RI036, an equilateral triangle array configuration with 3 seismometers at each apex and a 4th central seismometer is used, with side lengths of 5, 10, 15 and 30 m. Accurate seismometer positioning is determined using measuring tapes for smaller arrays ($\leq$ 45 m), and Global Positioning System (GPS) coordinates for the larger arrays ($\geq$ 145 m) at the BigArray site. The field logistics of the BigArray involved 11 personnel (one per seismometer) locating where to deploy the seismometer using tape measures (15 and 45 m radii) or according to pre-planned coordinates using the MapsMe App (145 to 380 m radii) and was accomplished over a 6 hour time period.

For each MAM array, ambient vibrations are recorded simultaneously by all array seismometers with a 15-minute duration for smaller arrays and between 30-minute and 2-hour duration for larger arrays ($\geq$ 30 m radius). The recordings at all sites are synchronized using GPS timing by the Tromino's proprietary software, Grilla. A cross-correlation analysis is performed within Geopsy (v. 2.9.1, Wathelet et al. 2020) to ensure proper synchronization between recorded time series when not visually apparent, i.e., for larger sized array recordings.
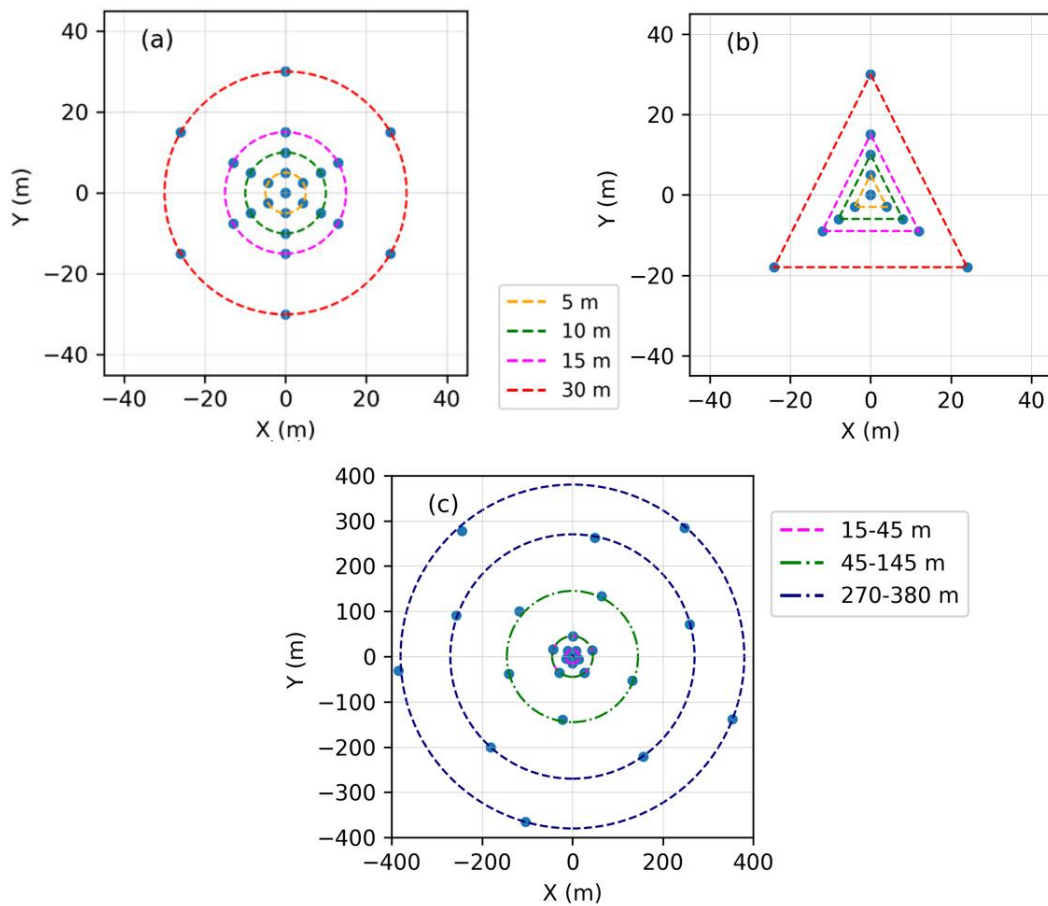
Fig. 3-6. MAM array geometries used in the field setup at the 16 sites. (a) Circular arrays of 6 equidistant seismometers with a central 7th seismometer. (b) Triangular arrays with 3 seismometers at each apex with a central 4th seismometer (RI035 and RI036 sites). (c) BigArray site of double circular arrays with 11 total seismometers recording simultaneously.

Table 3-2. Locations and details of array testing at 16 FRD sites. Strong-motion stations located close to array sites are reported by their station code.

Site	Latitude (°)	Longitude (°)	MAM array size (m)	MASW geophone spacing (m)	SM station[*]	Distance to SM station[**] (m)
BigArray	49.08696	-123.06169	15-45, 45-145, 270-380	0.5, 1, 3		
BU060	49.19397	-123.00012	5, 10, 15, 20	0.5, 1, 3		
DE043	49.08024	-123.08612	5,10,15,30, 40	0.5, 1, 3, 5		
DE050	49.03616	-123.05795	5, 10, 15	0.5, 1, 3		
DE059	49.08819	-123.06393	5, 10, 15, 30	0.5, 1, 3		
DE068	49.09684	-123.07056	5, 10, 15, 30, 40	0.5, 1, 3, 5		
DEPH01	49.00849	-123.08100	5, 10, 15, 30	0.5, 1, 3		
PC065	49.19901	-122.97341	5, 10, 15, 30	0.5, 1, 3		
RI015	49.17074	-123.18842	5, 10, 15, 30	0.5, 1, 3	RMD15	221
RI032	49.18603	-123.08759	5, 10, 15, 30	0.5, 1, 3	RMD03	180
RI035	49.16621	-123.14424	5, 10, 15, 30	0.5, 1, 3	RMD06	182
RI036	49.15393	-123.15189	5, 10, 15, 30	0.5, 1, 3		
RI038	49.13118	-123.18262	5, 10, 15, 30	0.5, 1, 3	RMD14	4
RI055	49.16553	-123.12877	5, 10, 15, 30	0.5, 1, 3	RMD04	183
RI091	49.1969	-123.11192	5, 10, 15, 30	0.5, 1, 3	KID[+], RMD01	257, 325
RI095	49.18375	-123.11619	5, 10, 15, 30	0.5, 1, 3	RMD02	54
RI097	49.18967	-123.15179	5, 10, 15, 30, 45	0.5, 1, 3	VNC09	152

[*]BCSIMS strong motion station (http://www.bcsims.ca/); [**]Distance between station and edge of the array.[+] BC Hydro station.

3.4.2   Dispersion and MHVSR Processing

The synchronized vertical-component recordings of the MASW and MAM arrays are imported into Geopsy software (v. 2.9.1, Wathelet et al. 2020) to perform the dispersion analysis. Use of vertical-component recordings is most suitable to obtain fundamental-mode Rayleigh wave dispersion estimates. Frequency wavenumber (fk) (Lacoss et al. 1969) dispersion analysis with maximum beam power normalization is performed for all MASW shots gathered with different shot offsets and receiver spacings per site. Consistent

dispersion estimates for multiple shots at the same offset distance are stacked, and the fundamental mode dispersion curve is picked from the stacked dispersion image for each array. Dispersion estimates of each array are combined into a single plot and edited manually, keeping in mind that larger spacings provide better resolution at lower frequencies and vice versa, to obtain the MASW fundamental-mode dispersion curve with its associated standard deviation. The standard deviation of the picked dispersion curve is manually assigned based on the observed variability of each array's reliable dispersion estimates.

MAM dispersion estimates are produced for each array using the Modified Spatial Auto Correlation (MSPAC) method (Bettig et al. 2001) and the High Resolution Frequency Wavenumber (HRFK) method (Capon 1969). The SPAC dispersion curve with the standard deviation are manually picked for each array spacing based on the generated autocorrelation curves (Foti et al. 2018). For HRFK, the mean and standard deviation dispersion curves for each array are computed. Phase velocities of HRFK-derived dispersion estimates are slightly higher than SPAC-derived estimates with higher uncertainty. Redundancy in the HRFK and SPAC dispersion estimates verifies reliable dispersion estimates, typically within the recommended minimum resolution and aliasing limits of the largest and smallest arrays respectively (Wathelet 2008). For example, dispersion estimates beyond the largest array's theoretical resolution limit ($k_{min}/2$) (Wathelet 2008) may be retained after confirming estimates from smaller arrays generally gave reasonable estimates beyond the relevant $k_{min}/2$ limit. In addition, SPAC-based dispersion analysis is capable of measuring wavelengths up to 5 times larger than those predicted by the theoretical array resolution limit (Foti et al. 2018). Thus, the $k_{min}/2$ limit was not strictly adopted to permit retrieval of the deepest measured velocities, however, dispersion estimates beyond $k_{min}/2$ limits are the least constrained (largest standard deviation). The MAM fundamental-mode dispersion curve with uncertainty is manually picked from larger spacings reliable SPAC picks at lower frequencies and smaller spacings SPAC reliable picks at higher frequencies.

The final dispersion curve for the site is built by combining the lower-frequency MAM and higher-frequency MASW dispersion curves. Array sizes were selected to improve frequency bandwidth overlap between MAM and MASW dispersion curves to again confirm reliable dispersion estimates by data redundancy. The final composite dispersion curve to be used for inversion is the combination of MASW and MAM dispersion estimates with their uncertainties. An example of the MAM, MASW and final composite dispersion curves for the BigArray site is shown in Fig.3-7. The dispersion estimates beyond the 45-m array resolution limit are consistent (redundant) with dispersion estimates from the largest 380-m array as mentioned previously. Since $f_{1,HVSR}$ typically occurs between 0.6-5 Hz in the FRD (see Section 3.3), Rayleigh wave dispersion estimates are typically not retrieved below this frequency range, i.e., $f_{1, HVSR}$ controls the low-frequency limit of the dispersion curve and therefore the depth of an inverted Vs profile. Only at the BigArray site where a maximum array radii of 380 m is used are phase velocities at frequencies lower than $f_{1,HVSR}$ retrievable. The BigArray dispersion curve spans 0.57 to 60 Hz and is the widest frequency bandwidth dispersion curve ever obtained for a FRD site. The coefficient of variation (COV) of the final dispersion estimates at each site are generally less than 5%; consistent with the COV value observed in Garofalo et al. (2016b).
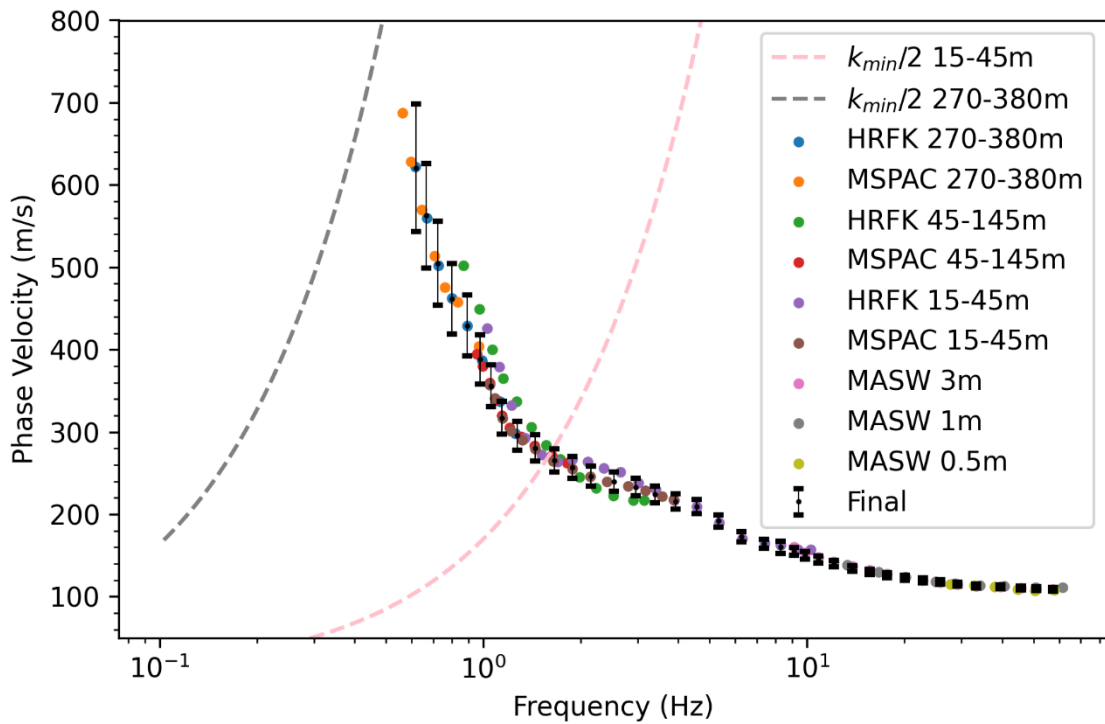
Fig. 3-7. Fundamental Rayleigh wave dispersion estimates from active-MASW and passive-MAM (MSPAC and HRFK processing techniques) array measurements at the BigArray site. The final composite dispersion curve (black circles) and its one standard deviation (black error bars) is shown. The theoretical array resolution limits ($k_{min}/2$) for the 15-45 m and 270-380 m arrays are shown.

A site average MHVSR is obtained from the three-component Tromino recordings of the MAM testing. For each Tromino recording, a time-averaged MHVSR is determined as described in section 3.3 after removal of time windows that produce anomalous MHVSR spectra. The average of these individual MHVSRs for all arrays provides the site or spatial average MHVSR with one standard deviation. The $f_{0,HVSR}$ is obtained according to SESAME clarity criteria from the site average MHVSR. At BigArray and RI015 sites, additional ambient vibration measurements are performed with a Guralp 40T broadband seismometer to validate the low $f_{0,HVSR}$ in the FRD; at RI015, the broadband measurement was about ~40 m away from the edge of the array, while at BigArray the broadband

measurement was ~1 m away from the central seismometer. Consistency in the MHVSR determined from Tromino and broad-band seismometers at these two sites confirms the shorter-period Tromino seismometer provides a reliable MHVSR even for thick FRD sediment sites. Most FRD sites exhibit two or more peaks in their MHVSR (Molnar et al. 2020). As discussed in Section 3.3, $f_{0,HVSR}$ is related to the deeper glaciated sediments-bedrock impedance contrast, while the $f_{1,HVSR}$ is related to the shallower post-glacial/glacial impedance boundary. At most FRD sites including those considered in this study, $f_{0,HVSR}$ is a clear or well defined peak within a range of 0.2 to ~0.55 Hz while higher frequency peaks are broader and not as clear. Consequently, only $f_{0,HVSR}$ is considered for inversions as it conforms with the SESAME criteria for a clear peak (Bard et al. 2004), except at DEPH01, DE043, RI032 and RI036 sites. At DEPH01 and RI032 sites, the $f_{0,HVSR}$ is broad and close to $f_{1,HVSR}$, while at DE043 and RI036 low frequency noise masks the clarity of the $f_{0,HVSR}$. Comparing $f_{0,HVSR}$ at these four array sites with $f_{0,HVSR}$ obtained from nearby MHVSR measurements (Molnar et al. 2020), it was found that both measurements provide similar $f_{0,HVSR}$ values. Thus, although not fully satisfying SESAME clarity criteria, $f_{0,HVSR}$ at these 4 sites were considered as reliable geologic-based peaks and subsequently included in the inversion.

3.4.3   Joint Inversion

Inversion of the experimental dispersion curve and/or MHVSR peak(s) aims at finding layered earth models consisting of elastic media parameters (Vp, Vs, density, and layer thickness) whose theoretical (forward) dispersion and Rayleigh ellipticity estimates adequately predict or fit the experimental input data. Joint inversion of surface wave dispersion curves and $f_{0,HVSR}$ results in constrained Vs estimates over the sediment depth profile as the dispersion curve constrains the near-surface velocities and $f_{0,HVSR}$ constrains depth to and Vs of the half-space. *A priori* information on the geologic stratigraphy (soil layering) and its elastic media parameter ranges help to pre-determine the model parameterization and parameter search space, thereby preventing unrealistic earth models. In this study, joint inversion of the dispersion curve and $f_{0,HVSR}$ is performed at all sites using the Dinver package within the Geopsy software suite. A modified version of the

global-search neighborhood inversion algorithm (Wathelet 2008) is used to determine theoretical layered earth models whose forward modelled fundamental-mode Rayleigh wave dispersion and ellipticity solutions minimize misfit with the site's experimental dispersion curve and $f_{0,HVSR}$, respectively. It is generally acceptable to assume that ambient vibrations are dominated by surface waves, thereby $f_{0,HVSR}$ can be modelled by Rayleigh wave ellipticity functions (Arai and Tokimatsu 2005, Rosenblad and Goetz 2010, Teague et al. 2018). Details on the forward calculations of the dispersion and ellipticity curves within Geopsy are provided in Wathelet et al. (2004). Model misfits are calculated based on summation of the weighted misfits of the dispersion curve and the ellipticity peak frequency over all input frequencies. Weighting of the dispersion curve and ellipticity misfit calculation are assigned values of 0.7 and 0.3, respectively. The choice of these weights is driven by the fact that $f_{0,HVSR}$ provides information at a single frequency while the dispersion curve provides data over a wider frequency band. This rationale was initially presented in Teague et al. (2018) where weights of 0.8 and 0.2, respectively, were used.

The model parameters defined for each layer are thickness (H), compressional wave velocity (Vp), Vs, and density (ρ) as well as Poisson's ratio (v) with the theoretical dispersion and ellipticity functions most sensitive to Vs and H. The parameter space should be constrained enough to avoid geologically unrealistic models, but loose enough to avoid over-constraining the problem. The model parameters ranges used in inversions are listed in Table 3-3. These ranges are determined based on available measurements in the FRD of these soil media parameters. The Vs ranges are chosen based on *in situ* Vs profiling (Hunter et al. 1999). For saturated post-glacial and glacial sediments, the maximum Vp is determined via the FRD sediment's Vs-Vp relationship of Hunter et al. (2016), while the minimum Vp is set to 1400 m/s as a lower bound for saturated sediments. For all sites except DEPH01, saturated conditions are assumed as the water table is located in the top few meters consistent with flat delta topography. DEPH01 site is located on relatively higher land and nearby water well observations (BC Groundwater Wells database 2021) indicate the water table may be over 10 m deep, thus dry conditions are assumed for this site. Poisson's ratio calculated from limited Vp and Vs measurements within the same FRD

borehole (Dallimore et al. 1995, Dallimore et al. 1996) are consistent with Poisson's ratio obtained from Vp-Vs ranges developed here, thus a Poisson's ratio range of 0.4 to 0.5 is assigned for saturated post-glacial and glacial sediments. For unsaturated (dry) sediments at DEPH01, a Poisson's ratio range from 0.15 to 0.35 (Foti et al. 2018) is used; Vp ranges are derived from Vs ranges as Vp measurements for dry sediments are not available. For the elastic half-space, the empirical Vs range of bedrock (Hunter et al. 2016) is used with typical Poisson's ratios to develop the Vp ranges. All available laboratory density measurements of FRD sediments are compiled (Dallimore et al. 1995, Dallimore et al. 1996) to determine average density values for both wet and dry post-glacial and glacial sediments. While the set of parameter ranges are developed for inversion application in this study, the reported ranges in Table 3-3 can be used in wider geotechnical applications as they are derived from available *in situ* measurements.

The post-glacial sediment layers were modelled using multiple uniform velocity layers, constrained to increase in velocity with depth, and the number of layers is increased progressively to obtain the minimum misfit. For PC065 site, Vs reversals are allowed, consistent with the velocity reversal observed in the dispersion curve. For all sites, the number of possible post-glacial layers ranges between 1 and 6 (Table 3-3). For glacial sediments, 1 to 3 uniform velocity layers are used and sufficient to provide an acceptable fit with the experimental data. To account for the epistemic uncertainty in the "true" model parameterization, three different model parametrizations of varying post-glacial sediment layering are considered for each site, following similar approaches by Farrugia et al. (2017) and Hollender et al. (2018). For example, the three different post-glacial (PG) layered models at the BigArray site includes 4, 5, and 6 PG layers over the single glacial layer. At DEPH01, post-glacial sediments are very shallow and thus the number of glacial layers is varied.

In the case of inversion of the dispersion curve alone, a misfit value of 1 indicates that the theoretical dispersion curve lies within one standard deviation of the experimental curve. However, for the joint inversion of the experimental dispersion curve and $f_{0,HVSR}$ considered

in this study (with different misfit weights), the number of models for each parameterization to achieve the minimum misfit varies for each site based on the dispersion curve and $f_{0,HVSR}$ characteristics. In general, tens of thousands to hundreds of thousands of models for a parameterization initiated with different seeds are sufficient to ensure a minimum misfit is reached. It is assumed that the resolvable model depth is one-half of the maximum retrieved wavelength from the experimental dispersion curve ($\lambda_{res}/2$), noting it might be less than this when a strong impedance contrast exists (Foti et al. 2018). Beyond the assumed resolvable depth ($\lambda_{res}/2$), the Vs profile is determined solely by $f_{0,HVSR}$ and exhibits a much higher uncertainty as it is not constrained by the experimental dispersion curves. *A priori* information in addition to Table 3-3 is not used to further constrain the inversions at most sites and thus inversions can be generally considered as blind inversions.

Table 3-3. Model parameter ranges used in the joint inversion.

Geologic unit	Vs (m/s)	Poisson's ratio	Vp (m/s)	Density (kg/m^3)	Maximum Depth (m)	Number of layers
Post-glacial	50 - 500	0.4 - 0.5[+] 0.15 - 0.35	1400 – 2000[+] 80 - 1050[&]	1884[+] 1438[&]	350	1 - 6
Glacial	400 -1100	0.4 - 0.5[+] 0.15 -0.35[&]	1400 – 2800[+] 625 - 2300[&]	2162[+] 1750[&]	1000	1 - 3
Bedrock	1000 - 2500	0.2 - 0.3	1600 - 4700	2500		

[+]Saturated sediments; [&]Dry sediments

3.4.4   Vs profiles from Joint Inversion

For each of the three selected layering model parameterizations, the 333 lowest misfit models are selected to generate a total of 999 lowest misfit models per site (Fig. 3-8). Selecting multiple subset populations of lowest misfit models accounts for uncertainty in the Vs profile rather than selecting the single lowest misfit model. The 999 models are discretized at 0.25 m depth intervals and the median values of Vp, Vs, and density are calculated along with minimum and maximum Vs envelopes and the logarithmic standard deviation in Vs (σ_{lnVs}) with depth. Figure 3-8 shows the 999 lowest misfit Vs profiles for the 16 FRD sites with the calculated median Vs and its minimum and maximum limits as well as the assumed resolution depth limit ($\lambda_{res}/2$). Fig. 3-9 is the same as Fig. 3-8, zoomed to the upper 150 m at each site. At depths $> \lambda_{res}/2$, the profiles are shaded with light red to

point out the high uncertainty associated with Vs values. The forward dispersion and ellipticity curves are calculated using the obtained median model (Vp, Vs and density) and plotted along with the 999 forward dispersion and ellipticity curves in Fig. 3-10 and Fig. 3-11, respectively. The experimental dispersion curves and $f_{0,HVSR}$ are judged to be adequately fit by the forward dispersion curves and ellipticity functions, respectively, at all sites based on the misfit values of the three different parametrization models and visual inspection (see Fig. 3-10 and Fig. 3-11).
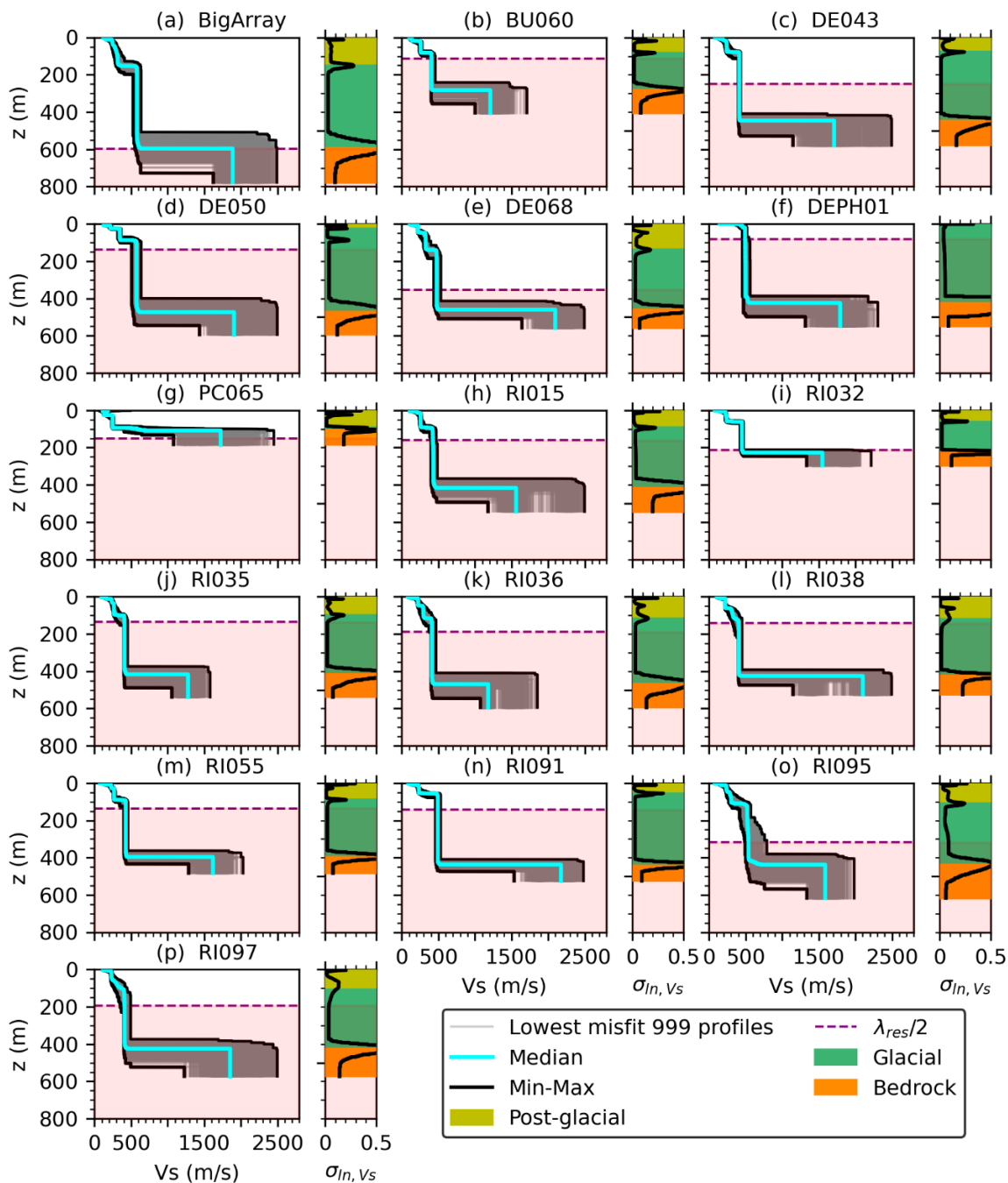
Fig. 3-8. Inverted Vs profiles for the 16 FRD sites; the assumed resolution or maximum depth limit ($\lambda_{res}/2$) of the site's dispersion data is shown by a dashed line below which the profiles are light red shaded to convey large uncertainty. The logarithmic standard deviation of Vs (σ_{lnVs}) with depth is shown by a solid black line

with inferred stratigraphic layering from the median density profiles (coloured shading).
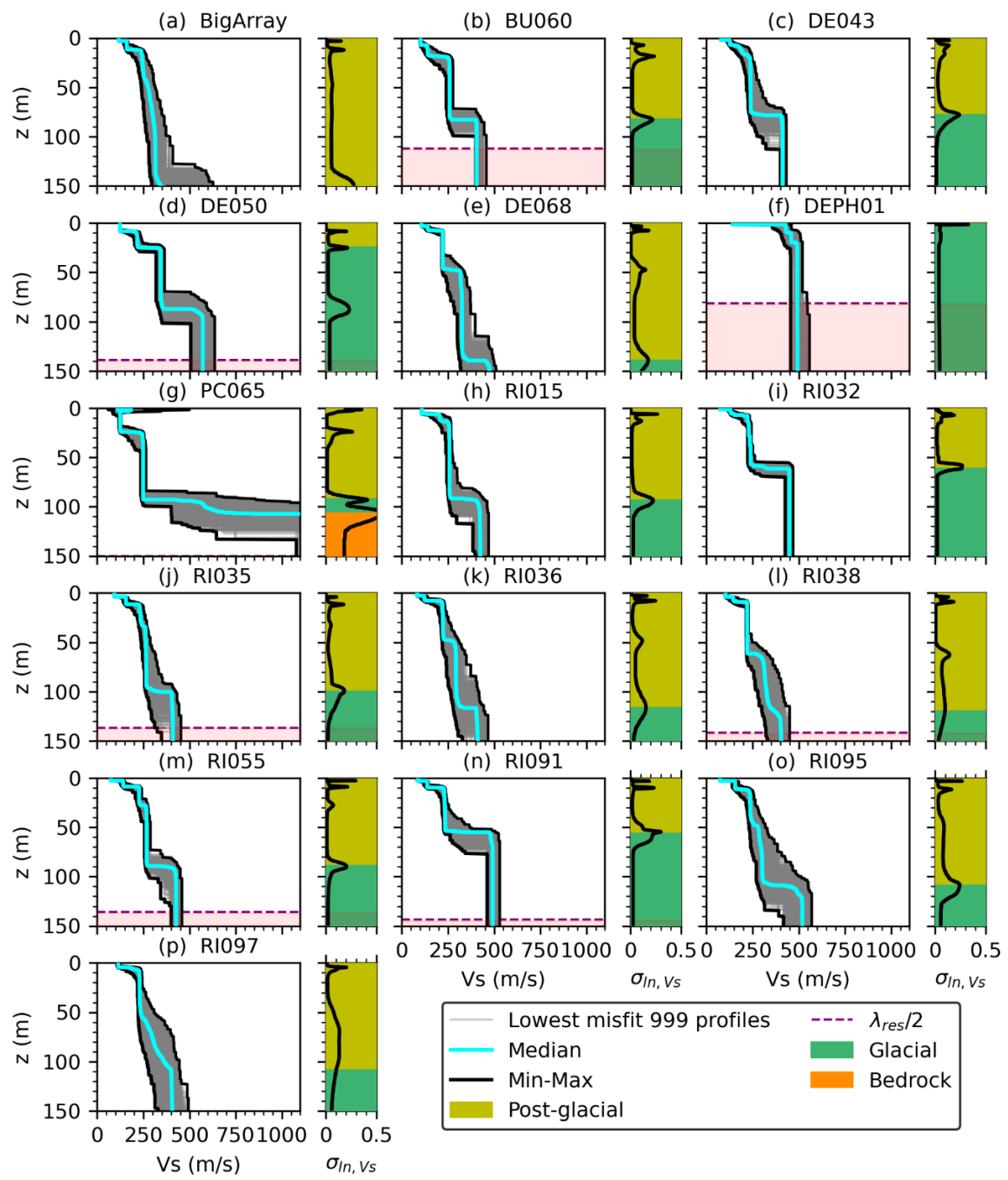
Fig. 3-9. Inverted Vs profiles to a depth of 150 m for the 16 FRD sites; the assumed resolution or maximum depth limit ($\lambda res/2$) of the site's dispersion data is shown by

a dashed line below which the profiles are shaded to convey large uncertainty. The logarithmic standard deviation of Vs (σlnVs) with depth is shown by a solid black line with inferred stratigraphic layering from the median density profiles (coloured shading).

In Fig. 3-8 and 3-9, the logarithmic standard deviation in Vs (σ_{lnVs}) with depth is plotted beside the inverted Vs profiles for each site atop of inferred stratigraphic layering. The σ_{lnVs} range at all sites is generally less than 0.25 log units at most depths with expected high Vs variance at model layer interfaces. These σ_{lnVs} values are generally higher than those obtained from inversions using a single model parametrization which neglects the inter-parametrization uncertainty. The inferred stratigraphic layering (z_{gl} and bedrock/resonator depth) is assigned based on the calculated median density profile (not shown) of the 999 models according to post-glacial, glacial, and bedrock units (Table 3-3). These stratigraphic boundaries based on median density are thus representative of the proportion of the 999 models that predict a certain stratigraphy layer at a certain depth. These stratigraphic (median density) interfaces are generally consistent with significant increases in Vs, i.e., the major seismic impedances (product of Vs and ρ) are identified. At RI015, RI038, RI055, and RI095 sites, the post-glacial/glacial interface obtained from the median density profile is a few meters deeper than the increase occurring in the median Vs profile, and thus the post-glacial/glacial interface is adjusted to the depth where the Vs increase occurs in median Vs (see Fig. 3-9).

At DE050, knowledge of geologic conditions allowed to further constrain the inversion. The glacial sediments Vs is allowed to be as low as 300 m/s (instead of 400 m/s) as the initial range predicted a very large z_{gl} inconsistent with the dispersion curvature at low frequencies and geologic evidence of z_{gl} (Fig. 3-1). The rapid increase in phase velocities at DE050 occurs at higher frequencies compared to other sites indicating a shallower impedance contrast. This is also confirmed with geologic evidence as the site is located at the top of the Point Roberts peninsula or the edge of the former island where glaciated sediments were eroded leading to the topographic low at DE050.

The median Vs profiles at all sites (except at PC065) increase with depth as expected in the FRD setting and consistent with the normally dispersive picked fundamental Rayleigh wave dispersion curves (i.e., phase velocity increases as frequency decreases) (see Fig. 3-10). At PC065, the dispersion curve shows a decrease in phase velocity between 22 and 4 Hz and thus a Vs reversal is allowed in the inversion model parametrization leading to a better fit of the dispersion curve. This Vs reversal is consistent with field observation where hard soils with pebbles and cobblestones, overlying softer clay soils as indicated from surficial geology, were identified at the surface.

The inverted Vs profiles in Fig. 3-8 reach to the site's resonator depth ($f_{0,HVSR}$) which can be significant (up to 800 m) beneath the FRD. The set of 16 inverted Vs profiles in Fig. 3-8 are the deepest available Vs profiles from surface for the FRD. However, it should be noted that the deeper portions of the inverted Vs profiles at depths $> \lambda_{res}/2$ (mainly glacial sediments Vs) are solely constrained by $f_{0,HVSR}$ and not the experimental dispersion curves typically limited to frequencies $> f_{1,HVSR}$ (see Fig. 3-10 and Fig. 3-11), and thus exhibit larger uncertainty. Similarly, no experimental constraint is used for the half-space bedrock Vs at the sites; a typical Vs range for bedrock in the FRD (Table 3-3) was assigned during inversion. Dispersion estimates down to a frequency of 0.57 Hz were retrieved only at the BigArray site where a large radius of 380 m was used, corresponding to a resolvable depth ($\lambda_{res}/2$) of around 600 m. To evaluate the glacial Vs of the inverted profiles at the 16 sites, we compare them to available invasive glacial sediments Vs in the FRD to a depth of 445 m (Hunter et al. 2016). The glacial sediment's Vs obtained from our inversions at the 16 sites (average of 463 m/s with a σ_{lnVs} of 0.135) are comparable with the glacial sediment's invasive Vs (average 480 m/s with a σ_{lnVs} of 0.227). Despite this consistency with glacial sediment's invasive Vs, the uncertainty of the inverted Vs profiles at depths $> \lambda_{res}/2$ should be included when used in any application.

The inferred z_{gl} from inverted Vs profiles at all 16 FRD sites ranges between 1.5 and 153 m, while the depth to bedrock ranges between 107 and 596 m. These ranges are reasonable when compared to previously reported thickness ranges of post-glacial and glacial deposits

in the FRD (Luternauer and Hunter 1996, Britton et al. 1995). The inferred z_{gl} values from the median Vs profiles at 3 sites are less than 60 m (DEPH01, 1.5 m; DE050, 25 m; and RI091, 55 m). To test the predictive z_{gl} model proposed in Section 3.3, the MHVSRs and their $f_{1,HVSR}$ are further examined at these sites. The MHVSR for DEPH01 (Fig. 3-11f) shows a second broad peak at about 40 Hz which is not clear enough to identify as $f_{1,HVSR}$ to test the predictive z_{gl} model. At such high frequencies and very shallow depths, it is not expected that the developed model will work well as lateral variability in surficial sediments can be significant. The MHVSR for DE050 (Fig. 3-11d) shows a second broad peak between 1 and 2 Hz but the peak is also not clear enough to identify as $f_{1,HVSR}$. Assuming z_{gl} as 25 m inferred from the inversion results (Fig. 3-9d), $f_{1,HVSR}$ predicted via Eq. 3-5 is 1.79 Hz, which may be the actual geologic-based $f_{1,HVSR}$ at DE050, however, masked within a broader peak (Fig. 3-11d). For RI091, using $f_{1,HVSR}$ of 1.048 Hz (Fig. 3-11n) in Eq. 3-5, a z_{gl} of 51.4 m is obtained which agrees with z_{gl} of 55 m inferred from the inversion. In addition, for RI032, a z_{gl} value of 61.5 m is inferred from the inversion, consistent with the location of this site close to the boundary of the area where z_{gl} is less than 50 m as shown in Fig. 3-1. The $f_{1,HVSR}$ at RI032 is 0.92 Hz (Fig. 3-11i) and predicts a similar z_{gl} value of 61.2 m using Eq. 3-5. This agreement between z_{gl} predicted from $f_{1,HVSR}$ (Eq. 3-5) and obtained from inverted Vs and density profiles given dispersion and $f_{0,HVSR}$ data at RI032 is perhaps due to the fact that the $f_{1,HVSR}$ is of geologic origin even though Eq. 3-5 was not developed, and not recommended to be used, for frequencies less than 1 Hz. While these few sites are not enough to test and verify the developed z_{gl} model in Section 3.3, the model works well at one site (RI091) when the $f_{1,HVSR}$ is a clear peak. Examining the MHVSRs at the 13 remaining sites (Fig. 3-11) and their locations in Fig. 3-1, it can be seen that the $f_{1,HVSR}$, if present, is generally less than 1 Hz. This conforms to observations made in Section 3.3, that the presence of a 2nd peak above 1 Hz in the MHVSR is generally associated with a z_{gl} value of less than 50 to 60 m.

Eight of the 16 developed Vs profiles from joint inversions of dispersion and $f_{0,HVSR}$ data are located near strong-motion stations (Table 3-2) that recorded weak shaking ($\leq 5.5\%$ g) of past earthquakes (Cassidy and Rogers 2004). The 1D site amplification (SH transfer

function) and seismic site parameters (Vs, Vs_z, Vs_{30}, $f_{0,HVSR}$, $f_{1,HVSR}$) at these station sites can be used to better understand recorded and future ground motions. The minimum, median, and maximum Vs profiles with the inferred stratigraphic boundaries and $\lambda_{res}/2$ depth for all 16 sites are provided in the electronic supplement of Assaf et al. (2022).
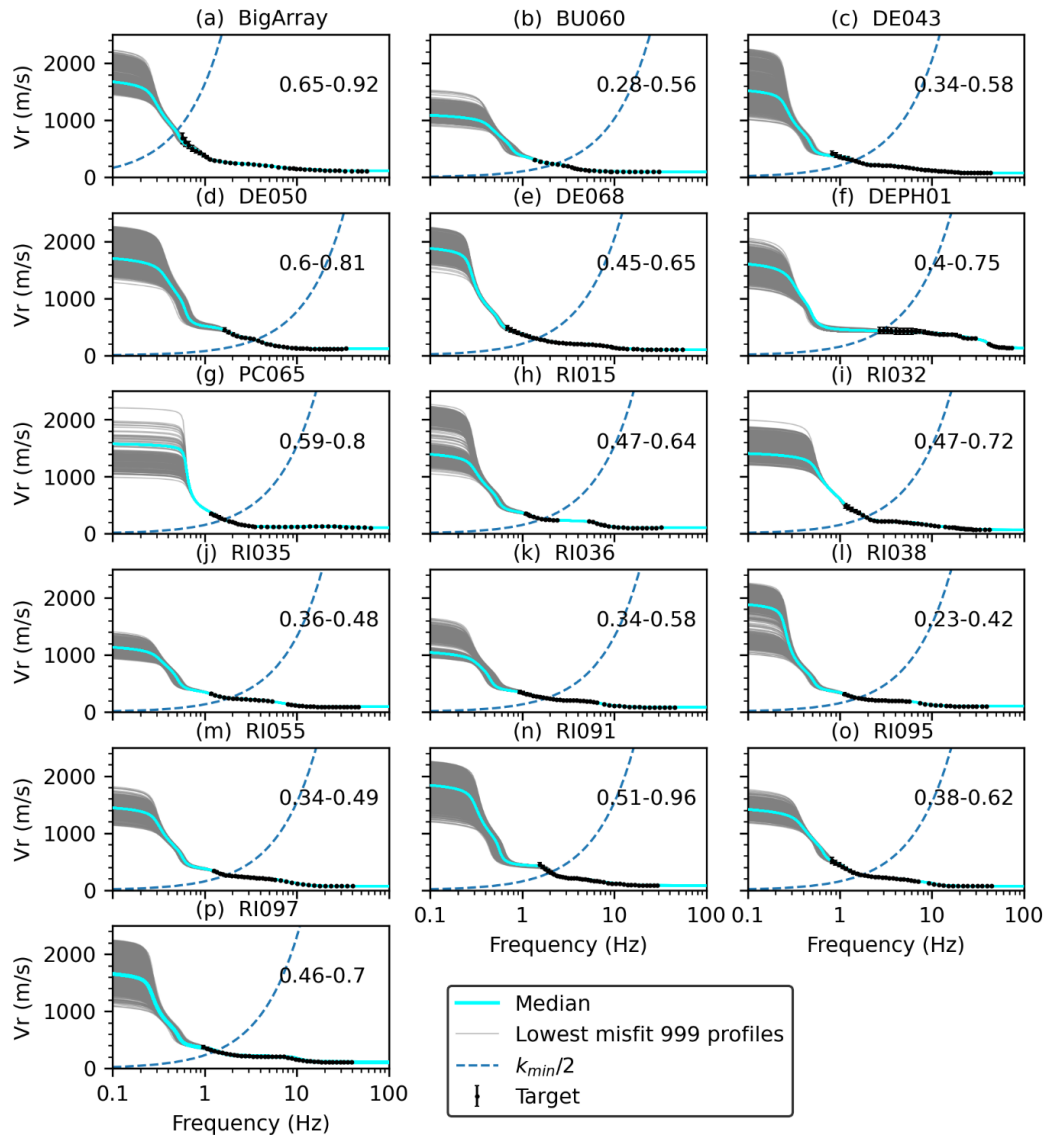
Fig. 3-10. Theoretical (forward modelled) dispersion curves of the 999 lowest misfit models are shown with the target dispersion data for the 16 FRD sites. The theoretical dispersion curve of the median model is also shown with the largest

array's resolution limit (kmin/2). Values reported in each plot is the minimum and maximum misfit range from all 999 profiles.
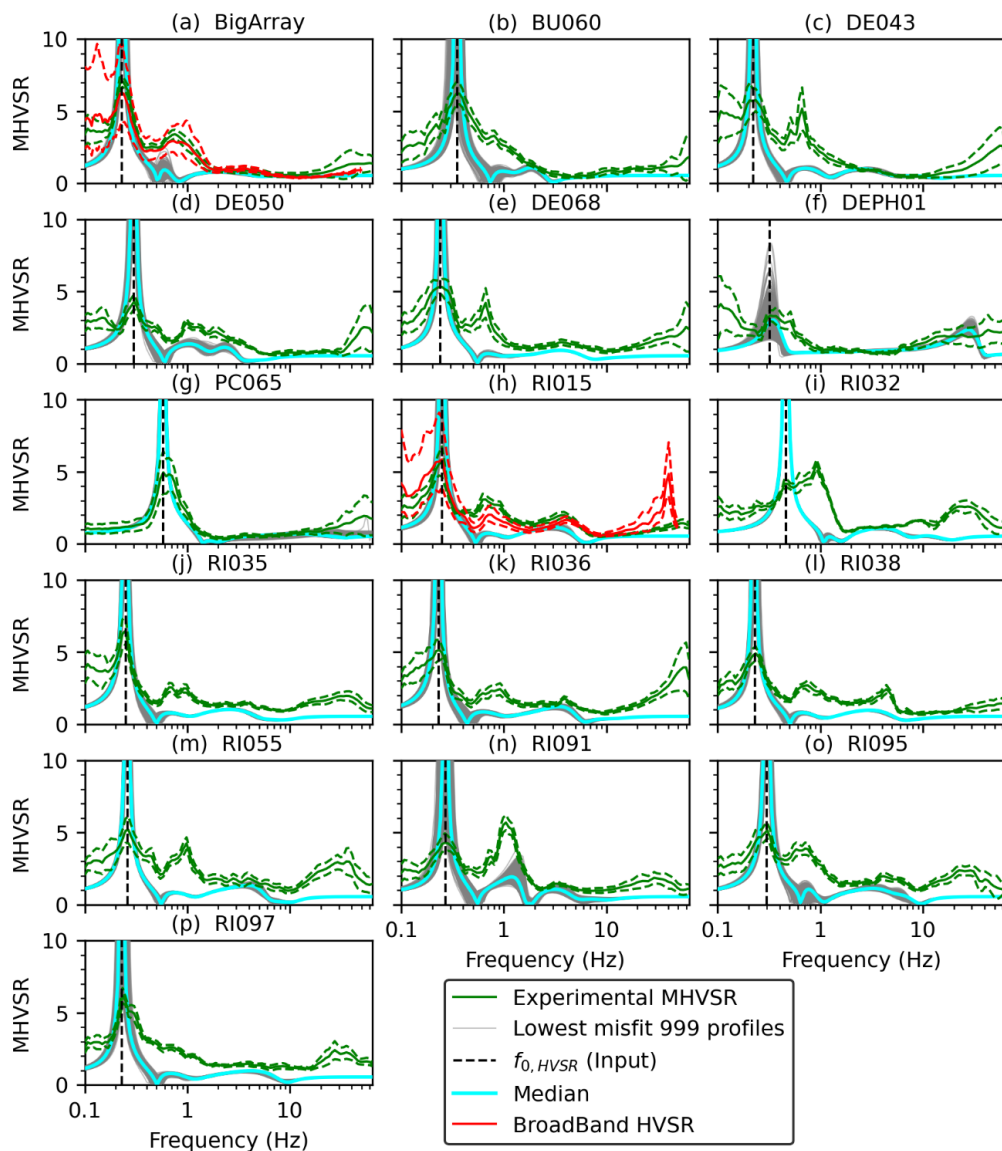
Fig. 3-11. Site-average MHVSR spectrum including one standard deviation (dashed lines) is shown with the theoretical Rayleigh wave ellipticity curves determined from the 999 lowest misfit models for the 16 FRD sites. $f_{0,HVSR}$ used to constrain inversions is shown by the vertical black dashed lines. At (a) BigArray and (h) RI015 sites, a

broadband seismometer is used to obtain a time-averaged MHVSR spectrum (solid red line) and its one standard deviation (red dashed lines).

3.5 Comparison of Inverted Vs Profiles with Existing Vs Measurements

The inverted Vs profiles from joint inversion of dispersion estimates and $f_{0,\text{HVSR}}$ at most sites are considered blind inversions. The model parameter ranges are informed by the general stratigraphy or Vs knowledge of the FRD, but not constrained by the nearest stratigraphic or Vs data. Only at DE050 was more local *a priori* information used to guide the inversion process and ensure the results are not inconsistent with the known geology. We now seek to evaluate the inverted Vs profile results at 10 array sites in comparison to the nearest existing Vs profiles from downhole, SCPTs and S-wave refraction measurements (Hunter et al. 2016). The comparison is presented for Vs and the time-averaged shear wave to a depth z (Vs_z) as well as Vs_{30}. The distances between the existing Vs measurements and the largest sized array range between a few meters and 485 m (Table 3-4); for example, SCPT93-11 lies within the BigArray configuration. The rate of change in site conditions across the FRD is not uniform; more rapid changes are expected at sites close to the edge of the delta compared to sites in the middle of the delta where similar site conditions may extend over a larger distances.

The median, minimum and maximum Vs from the joint inversions of Section 3.4 and their Vs_z profiles are compared to relevant nearby existing Vs and their Vs_z profiles in Fig. 3-12. Overall, the existing Vs and Vs_z profiles lie within the minimum and maximum ranges of the inverted Vs and Vs_z profiles, respectively, indicating good agreement between nearby Vs profiles obtained by various *in situ* methods. A total of 6 existing Vs profiles penetrate to 50 m depth or more (Fig. 3-12) whereas all inverted Vs profiles resolve Vs to resonator depth (see Fig. 3-8).

The absolute relative difference in Vs (as a percentage) between the inverted median Vs profile and each existing Vs profile (Fig. 3-12) is calculated at 1 m depth increments then

averaged for all depths. The absolute relative difference at each depth is calculated as follows:

$$\text{Absolute relative difference (percentage)} = 100 \, \frac{|Vs \; existing - Vs \; inverted|}{Vs \; existing} \qquad \textbf{Eq. 3-6}$$

The limited number of Vs profiles from different *in situ* methods at each site is not enough to provide statistically reliable COV estimates. The depth-averaged absolute relative differences in Vs are generally less than 20% indicating good agreement, except at a few sites where there is a difference in z_{gl} (e.g., DE050 and RI032) or large differences among the existing Vs profiles (e.g., BU060). The depth-averaged absolute relative difference in Vs amongst all 10 sites is an average of 18.2% (range of 9.1 to 41%), and for Vs_z is 7.5% (range of 1.6 to 15.2%). The observed differences in Vs within the top few meters at some sites is attributed to variation in near-surface materials. Surface wave methods presented here are mostly conducted at parks or school fields where artificial fills are often present atop of native soils and do not necessarily apply to the other Vs profiling methods. While the resolution of surface wave methods Vs profiles is known to decrease with depth, the agreement in Vs between FD96-1 and RI035 profiles (9.1% calculated to a depth of 220 m; Fig. 3-12j) is noteworthy considering the 4 nearby existing Vs profiles are not used to constrain the inversion at this site.

Considering that the array sites and the existing Vs profiles are up to few hundreds of meters apart, the comparison of z_{gl} obtained from both types of profiles may be significantly biased due to lateral variability. However, the agreement between z_{gl} at/around shallow array site R091 from three different methods is noteworthy. The Vs profile of downhole FD96-2, located 199 m west of array site RI091, indicates a z_{gl} of 53 m and is consistent with z_{gl} obtained from the RI091's median inverted Vs profile (55 m; Fig. 3-12j) and predicted by the $f_{1,HVSR}$ model (51.4 m) derived in Section 3.3. This agreement obtained from three independent methods of downhole Vs profiling, joint inversion of dispersion and $f_{0,HVSR}$, and a predictive z_{gl}-$f_{1,HVSR}$ model highlights the robustness of non-invasive methods (the

latter two methods) in retrieving important seismic site parameters such as z_{gl} for shallow sites in the FRD.

Table 3-4 reports minimum, median and maximum Vs_{30} at the 16 sites from the inverted Vs profiles with the median Vs_{30} determined from the existing nearby Vs profile(s) shown in Fig. 3-12. The difference in Vs_{30} between the median inverted and existing Vs profiles is an average of 7.7% (range of 3 to 12.2%). Considering the geologies of the array sites, the DEPH01 array site located on stiff Vashon drift and Capilano sediments in the Tsawwassen uplands corresponds to Canadian building code seismic site class C ($360 < Vs_{30} < 760$ m/s; NRC 2015) with median Vs_{30} of 415 m/s. Median inverted Vs_{30} ranges between 138 and 197 m/s at the 15 other sites located in FR sediments and Salish sediments surficial geology units. Array sites BU060 and PC065 exhibit the lowest Vs_{30} of all the sites, corresponding to site class E ($Vs_{30} < 180$ m/s; NRC 2015), related to the presence of soft peats in the northeastern FRD (Fig. 3-1). The Vs_{30} from the remaining 13 sites in FR sediments and Salish sediments surficial geology units are mainly at the boundary of seismic site classes D and E.
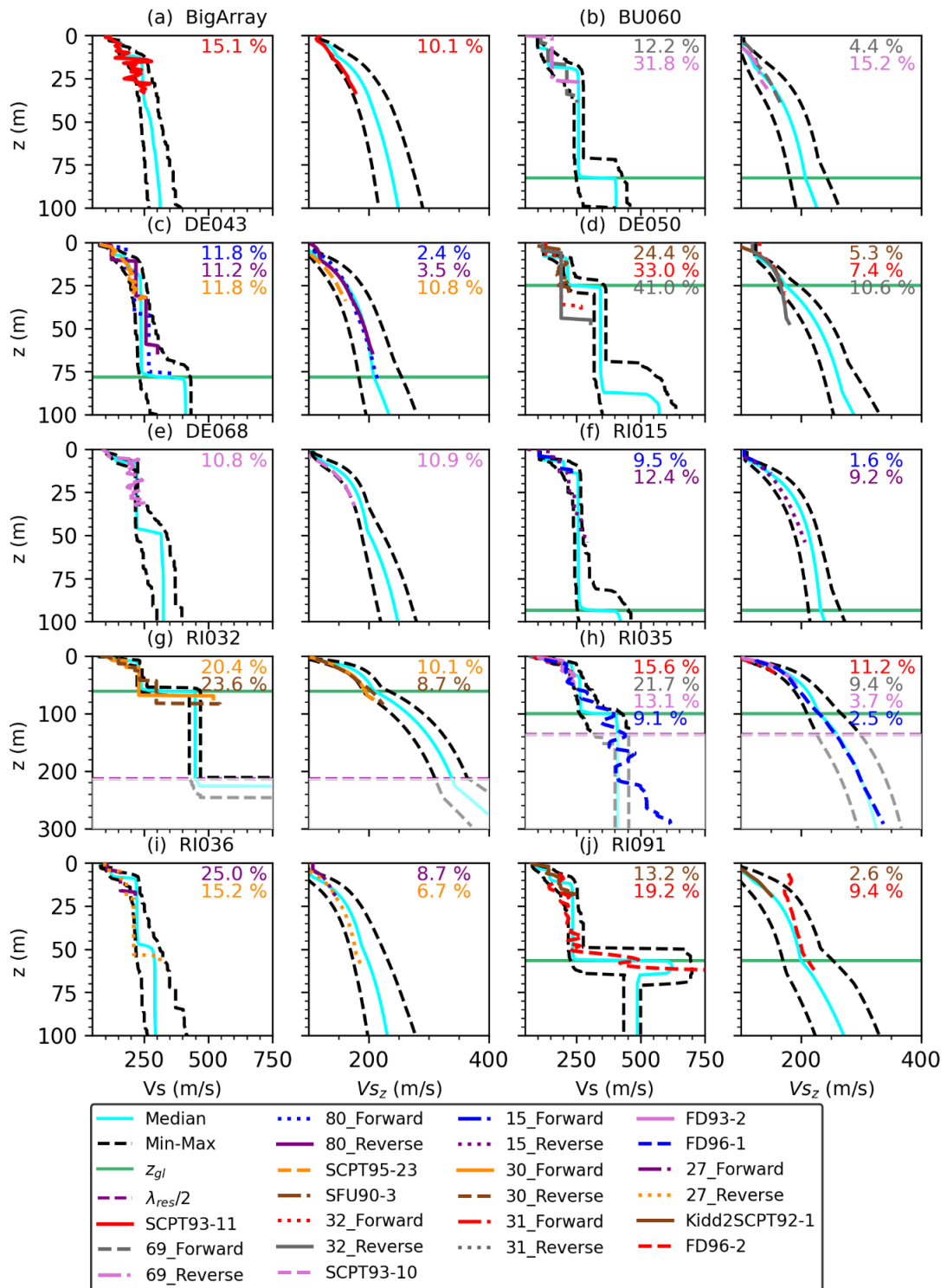
Fig. 3-12. Comparison between the inverted minimum, median and maximum Vs profiles with nearby existing Vs (label names correspond to Vs database of Hunter et al. 2016) for 10 FRD array sites; comparison is repeated per site in terms of Vsz. Values in each plot are the depth-averaged relative difference in Vs as a percentage between the existing Vs (Vsz) profile and the median Vs (Vsz) profile from joint inversion. zgl inferred from inversions are shown in green lines.

Table 3-4. Median and minimum (min) and maximum (max) Vs_{30} ranges determined from inverted and the nearby existing Vs profiles of Fig. 3-12. The geology unit at each array site is reported.

Array site	Median inverted Vs_{30} (m/s)	Inverted min and max Vs_{30} (m/s)	Median existing Vs_{30}	% absolute difference in median Vs_{30}	Distance ranges of existing Vs profiles to the edge of the array (m)	Geology Unit
BigArray	193	169-221	172	12.2	16*	Fraser River Sediments
BU060	153	127-183	146	4.8	53	Fraser River Sediments
DE043	172	145-198	167	3	82-96	Fraser River Sediments
DE050	189	169-212	170	11.2	287-319	Salish Sediments
DE068	186	173-197	171	8.8	86	Fraser River Sediments
DEPH01	415	367-447				Vashon Drift and Capilano Sediments
PC065	138	112-173				Salish Sediments
RI015	191	167-208	176	8.5	237	Fraser River Sediments
RI032	185	166-201	165	12.1	235	Fraser River Sediments
RI035	176	157-195	170	3.5	30-485	Fraser River Sediments
RI036	172	148-196	160	7.5	114	Fraser River Sediments
RI038	179	162-195				Fraser River Sediments
RI055	174	156-195				Fraser River Sediments
RI091	175	141-211	185	5.4	199-209	Salish Sediments
RI095	172	150-195				Salish Sediments

RI097	197	173-219	Fraser River Sediments

*: within array aperture

3.6 Conclusions

In this study, seismic site characteristics, specifically z_{gl} and Vs profiles, of the FRD in southern Metro Vancouver, Canada are determined from *in situ* non-invasive seismic measurements and compared with existing Vs measurements compiled as part of a comprehensive geodatabase for the ongoing Metro Vancouver seismic microzonation mapping project (Molnar et al. 2020). A predictive z_{gl} model based on $f_{1,HVSR}$ is developed in this study for shallow conditions ($z_{gl} \leq 56$ m) found at the edges of the FRD. This $f_{1,HVSR}$-z_{gl} relationship demonstrates the greatest agreement with a similar relationship developed to estimate the thickness of soft deltaic sediments in the Segura River valley in Spain, highlighting the similarities in material properties (Vs with depth) of deltaic sediments. This finding promotes the adoption of MHVSR peak frequency-sediment thickness models in regions with a similar Vs-depth relationship. Our developed z_{gl} model can be used with inexpensive MHVSR measurements to map out the depth to glaciated sediments around the edges of the FRD and constrain the geometry for 1D and 2D site response analyses in future.

Active-source MASW and passive-source MAM surface wave dispersion methods are conducted at 16 sites in the FRD. The extracted fundamental-mode Rayleigh wave dispersion estimates from both *in situ* dispersion methods are jointly inverted with the $f_{0,HVSR}$ with limited *a priori* information considering 3 different layered parametrization models. The resulting inverted Vs profiles with their uncertainties are compared to nearby existing Vs profiles from other *in situ* Vs profiling methods. The depth-averaged absolute relative difference (%) in Vs between the inverted and the existing Vs profiles to a maximum depth of 220 m is 18.2 % (range of 9.1 to 41%). This is comparable to the 8-26 % depth-averaged absolute relative difference in Vs between inverted MASW dispersion estimates and invasive Vs profiling methods to a maximum depth of only 30 m determined

for other FRD sites (Xia et al. 2000; Molnar et al. 2010). The agreement within 10 % between inverted Vs from three non-invasive methods and invasive downhole Vs to a depth of 220 m, deeper than most available Vs profiles in the FRD, is notable. Previously a 5% depth-averaged relative difference in Vs was determined between inverted dispersion estimates and invasive methods but only to 120 m depth (Molnar et al. 2010). While the inverted Vs profiles extend to significant depths, it should be noted that beyond the maximum resolution of the experimental dispersion ($\lambda_{res}/2$), the profiles exhibit higher uncertainty as they are solely constrained by $f_{0,HVSR}$. This higher uncertainty in the Vs profile with/at depth should be included when using the inverted Vs profiles. The average relative difference in Vs_z and specifically Vs_{30} amongst all 10 FRD sites is 6.9% (standard deviation of 3.1%) and 7.7% (3.4%) respectively, consistent with the 4% variation in Vs_{30} determined between non-invasive and invasive methods by the InterPacific project (Garofalo et al. 2016a). For 8 array sites co-located with strong-motion stations, the MHVSR and inverted Vs profiles will enable correlation of seismic site parameters (Vs, Vs_{30}, Vs_z, amplification spectrum, $f_{0,HVSR}$, $f_{1,HVSR}$) with recorded ground motions in future. The presented predictive z_{g1} model and Vs profiles provide important tools for site effect quantification and mapping in the FRD.

3.7   References

Adams, J. (2007). Soil amplification in Ottawa from urban strong ground motion records. In: Proceedings of the 9th Canadian Conference on Earthquake Engineering. Ottawa, ON, Canada. Paper (No. 1162)

Adams, J., Halchuk, S. (2002). Knowledge of in-slab earthquakes needed to improve seismic hazard estimates for southwestern British Columbia. In The Cascadia Subduction Zone and Related Subduction Systems-Seismic Structure, Intraslab Earthquakes and Processes, and Earthquake Hazards (Kirby, S, Wang, K, and Dunlop, S, eds): US Geological Survey Open-File Report 02-328 1–6

Adams, J., Halchuk, S., Allen, T., Rogers, G. (2015). Canada's 5th Generation Seismic

Hazard Model, As Prepared For the 2015 National Building Code of Canada. In Proceedings of the 11th Canadian Conference on Earthquake En- gineering, Victoria, Canada 1–11

Adhikari, S.R., Molnar, S. (2021). Significance of geodatabase development for seismic microzonation in Metropolitan Vancouver. In: 17th World Conference on Earthquake Engineering, 27 Sept. – 2 Oct. 2021, Sendai, Japan, Paper 4521.

Albarello, D., Lunedei, E. (2011). Structure of an ambient vibration wavefield in the frequency range of engineering interest ([0.5, 20] Hz): insights from numerical modelling. Near Surface Geophysics **9**:543–559. doi: 10.3997/1873-0604.2011017

Arai, H., Tokimatsu, K. (2005). S-Wave Velocity Profiling by Joint Inversion of Microtremor Dispersion Curve and Horizontal-to-Vertical (H/V) Spectrum. Bulletin of the Seismological Society of America **95**:1766–1778. doi: 10.1785/0120040243

Armstrong, E. (1990). Vancouver Geology. Geological Association of Canada Edited by Chad Roots and Chris Staargaard

Armstrong, JE. (1984). Environmental and Engineering Applications of the Surficial Geology of the Fraser Lowland, British Columbia. Geological Survey of Canada Paper 83-23. doi: 10.4095/119727

Atkinson, G.M., Cassidy, J.F. (2000). Integrated use of seismograph and strong-motion data to determine soil amplification: Response of the Fraser River Delta to the Duvall and Georgia Strait earthquakes. Bulletin of the Seismological Society of America **90**:1028–1040. doi: 10.1785/0119990098

Bard, P., Duval, A., Koehler, A., Rao, S. (2004). Guidelines for the Implementation of the H / V Spectral Ratio Technique on Ambient Vibrations Measurements , Processing and Interpretation, SESAME European research project WP12 – Deliverable D23.12

Bettig, B., Bard, P.Y., Scherbaum, F., Riepl, J., Cotton, F., Cornou, C., Hatzfeld, D. (2001).

Analysis of dense array noise measurements using the modified spatial auto-correlation method (SPAC): application to the Grenoble area

Bilson, Darko. A., Molnar, S., Sadrekarimi, A. (2020). Blind comparison of non-invasive shear wave velocity profiling with invasive methods at bridge sites in Windsor, Ontario. Soil Dynamics and Earthquake Engineering **129**:105906. doi: https://doi.org/10.1016/j.soildyn.2019.105906

Bodin, P., Smith, K., Horton, S., Hwang, H. (2001). Microtremor observations of deep sediment resonance in metropolitan Memphis, Tennessee. Engineering Geology **62**:159–168. doi: https://doi.org/10.1016/S0013-7952(01)00058-8

Borcherdt, R.D. (1994). Estimates of Site-Dependent Response Spectra for Design (Methodology and Justification). Earthquake Spectra 10:617–653

Borcherdt, R.D. (1970). Effects of Local Geology on Ground Motion Near San Francisco Rbay. Bulletin of the Seismological Society of America **60**:29–61

Braganza, S., Atkinson, G.M., Molnar, S. (2017). Assessment of the Spatial Variability of Site Response in Southern Ontario. Seismological Research Letters **88**:1415–1426. doi: 10.1785/0220170042

Britton, J.R., Harris, J.B., Hunter, J.A., Luternauer, J.L. (1995). The bedrock surface beneath the Fraser River delta in British Columbia based on seismic measurements. In: Current Research 1995-E. Geological Survey of Canada, pages 83–89

Capon, J. (1969). High-Resolution Frequency-Wavenumber Spectrum Analysis. In: Proceedings of the IEEE. pp 1408–1418

Cassidy, J.F., Rogers GC (1999). Seismic site response in the greater Vancouver, British Columbia, area: Spectral ratios from moderate earthquakes. Canadian Geotechnical Journal **36**:195–209. doi: 10.1139/cgj-36-2-195

Cassidy, J.F., Rogers, G.C. (2004). Variation in ground shaking on the Fraser River delta (Greater Vancouver , Canada) from analysis of moderate earthquakes. 13th World Conference on Earthquake Engineering Vancouver, BC, Canada August 1-6, 2004 Paper No 1010 7

Cassidy, J.F., Rogers, G.C., Weichert, D.H. (1997). Soil response on the Fraser delta to the Mw = 5.1 Duvall, Washington, earthquake. Bulletin of the Seismological Society of America **87**:1354–1361

Castellaro, S. (2016). The complementarity of H/V and dispersion curves. Geophysics **81**:T323–T338. doi: 10.1190/GEO2015-0399.1

Clague, J.J. (1998). Geological setting of the Fraser River delta; in Geology and Natural Hazards of the Fraser River Delta, British Columbia, (ed.) J.J. Clague, J.L. Luternauer, and D.C. M os her; Geological Survey of Canada, Bulletin 525, p. 7-16.

Clague J.J., Luternauer, J.L., Monahan, P.A., Edwardson, K.A., Dallimore, S.R., Hunter, J.A. (1998). Quaternary stratigraphy and evolution of the Fraser delta. In: Geology and the natural hazards of the Fraser River Delta, British Columbia; by Clague, J J (ed.); Luternauer, J L (ed.); Mosher, D C (ed.); Geological Survey of Canada, Bulletin 525. pp 57–90

D'Amico, V., Picozzi, M., Baliva, F., Albarello, D. (2008). Ambient noise measurements for preliminary site-effects characterization in the Urban area of Florence, Italy. Bulletin of the Seismological Society of America **98**:1373–1388. doi: 10.1785/0120070231

Dallimore, S., Edwarsdon, K.A., Hunter, J.A., Meldrum, J.L., Luternauer, J.L., Clague, J.J. (1996). Lithologie, geotechnical and geophysical logs for a deep borehole at Rchmond City Hall, British Columbia. Geological Survey of Canada, Open File Report 3356

Dallimore, S.R., Edwarsdon, K.A., Hunter, J.A., Clague, J.J., Luternauer, J.L. (1995). Composite geotechnical logs for two deep boreholes in the Fraser R ver delta, British

Columbia. Geological Survey o f Canada, Open File 3018

Delgado, J., López, Casado, C., Estévez, A., Giner, J., Cuenca, A., Molina, S. (2000). Mapping soft soils in the Segura river valley (SE Spain): A case study of microtremors as an exploration tool. Journal of Applied Geophysics **45**:19–32. doi: 10.1016/S0926-9851(00)00016-1

Deschenes, M.R., Wood, C.M., Wotherspoon, L.M., Bradley, B.A., Thomson, E. (2018). Development of Deep Shear Wave Velocity Profiles in the Canterbury Plains, New Zealand. Earthquake Spectra **34**:1065–1089. doi: 10.1193/122717EQS267M

Di Alessandro, C., Bonilla, L.F., Boore, D.M., Rovelli, A., Scotti, O. (2012). Predominant-Period Site Classification for Response Spectra Prediction Equations in Italy. Bulletin of the Seismological Society of America **102**:680–695. doi: 10.1785/0120110084

Dunn, D., Ricketts, B. (1994). Surficial Geology of Fraser Lowlands Digitized From GSC Maps 1484A, 1485A, 1486A, and 1487A. Geologic Survey of Canada Open File 2894

Farrugia, J. J., Atkinson, G. M., & Molnar, S. (2018). Validation of 1D earthquake site characterization methods with observed earthquake site amplification in Alberta, Canada Validation of 1D earthquake site characterization methods with observed earthquake site amplification. Bulletin of the Seismological Society of America, 108(1), 291-308.

Farrugia, J. J., Molnar, S., & Atkinson, G. M. (2017). Noninvasive Techniques for Site Characterization of Alberta Seismic Stations Based on Shear-Wave Velocity Noninvasive Techniques for Site Characterization of Alberta Seismic Stations Based on Shear-Wave Velocity. Bulletin of the Seismological Society of America, 107(6), 2885-2902.

Field, E., Jacob,. K (1993). The theoretical response of sedimentary layers to ambient seismic noise. Geophysical Research Letters **20**:2925–2928. doi: 10.1029/93GL03054

Finn, W.D.L., Zhai, E., Thavaraj, T., Hao, X-S., Ventura, C. (2003). 1-D and 2-D analyses of weak motion data in Fraser Delta from 1966 Duvall earthquake. Soil Dynamics and Earthquake Engineering **23**:323–329. doi: 10.1016/S0267-7261(02)00207-5

Foti, S., Hollender, F., Garofalo, F., Albarello, D., Asten, M., Bard, P. Y., Comina, C., Cornou, C., Cox, B., di Giulio, G., Forbriger, T., Hayashi, K., Lunedei, E., Martin, A., Mercerat, D., Ohrnberger, M., Poggi, V., Renalier, F., Sicilia, D., & Socco, V. (2018). Guidelines for the good practice of surface wave analysis: a product of the InterPACIFIC project. Bulletin of Earthquake Engineering, 16(6). https://doi.org/10.1007/s10518-017-0206-7

García-Fernández M, Jiménez MJ (2012). Site characterization in the Vega Baja, SE Spain, using ambient-noise H/V analysis. Bulletin of Earthquake Engineering **10**:1163–1191. doi: 10.1007/s10518-012-9351-1

Garofalo, F., Foti, S., Hollender, F., Bard, P. Y., Cornou, C., Cox, B. R., Ohrnberger, M., Sicilia, D., Asten, M., di Giulio, G., Forbriger, T., Guillier, B., Hayashi, K., Martin, A., Matsushima, S., Mercerat, D., Poggi, V., & Yamanaka, H. (2016a). InterPACIFIC project: Comparison of invasive and non-invasive methods for seismic site characterization. Part I: Intra-comparison of surface wave methods. Soil Dynamics and Earthquake Engineering, 82. https://doi.org/10.1016/j.soildyn.2015.12.010

Garofalo, F., Foti, S., Hollender, F., Bard, P. Y., Cornou, C., Cox, B. R., Dechamp, A., Ohrnberger, M., Perron, V., Sicilia, D., Teague, D., & Vergniault, C. (2016b). InterPACIFIC project: Comparison of invasive and non-invasive methods for seismic site characterization. Part II: Inter-comparison between surface-wave and borehole methods. Soil Dynamics and Earthquake Engineering, 82. https://doi.org/10.1016/j.soildyn.2015.12.009

Ghofrani, H., Atkinson, G.M. (2014). Site condition evaluation using horizontal-to-vertical response spectral ratios of earthquakes in the NGA-West 2 and Japanese databases. Soil Dynamics and Earthquake Engineering **67**:30–43. doi:

10.1016/J.SOILDYN.2014.08.015

Di Giulio, G., Savvaidis, A., Ohrnberger, M., Wathelet, M., Cornou, C., Knapmeyer-Endrun, B., Renalier, F., Theodoulidis, N., & Bard, P. Y. (2012). Exploring the model space and ranking a best class of models in surface-wave dispersion inversion: Application at European strong-motion sites. Geophysics, 77(3). https://doi.org/10.1190/geo2011-0116.1

Goetz (2009). Study of the horizontal-to-vertical spectral ratio (HVSR) method for characterization of deep soils in the Mississippi Embayment, MS Thesis, University of Missouri-Columbia, Columbia

Gosar, A., Lenart, A. (2010). Mapping the thickness of sediments in the Ljubljana Moor basin (Slovenia) using microtremors. Bulletin of Earthquake Engineering **8**:501–518. doi: 10.1007/s10518-009-9115-8

Griffiths, S.C., Cox, B.R., Rathje, E.M., Teague, D.P. (2016). Mapping dispersion misfit and uncertainty in Vs profiles to variability in site response estimates. Journal of Geotechnical and Geoenvironmental Engineering **142**:. doi: 10.1061/(ASCE)GT.1943-5606.0001553

Guéguen, P., Chatelain, J.L., Guillier, B., Yepes, H. (2000). An indication of the soil topmost layer response in Quito (Ecuador) using noise H/V spectral ratio. Soil Dynamics and Earthquake Engineering **19**:127–133. doi: 10.1016/S0267-7261(99)00035-4

Harris, J.B., Hunter, J.A., Luternauer, J.L., Finn, W. (1998). Site amplification modelling in the Fraser Delta, British Columbia; in Geology and Natural Hazards of the Fraser River Delta, British Columbia. In: Clague JJ, Luternauer JL, Mosher and DC (eds) Bulletin 525. Geological Survey of Canada, pp 211–216

Hashash, Y. M. A., Ilhan, O., Hassani, B., Atkinson, G. M., Harmon, J., & Shao, H. (2020). Significance of site natural period effects for linear site amplification in central and

eastern North America: Empirical and simulation-based models. Earthquake Spectra, 36(1). https://doi.org/10.1177/8755293019878198

Hassani, B., Atkinson, G.M. (2016). Site-effects model for central and eastern North America based on peak frequency. Bulletin of the Seismological Society of America **106**:2197–2213. doi: 10.1785/0120160049

Hinzen, K.G., Weber, B, Scherbaum, F. (2004). On the resolution of h/v measurements to determine sediment thickness, a case study across a normal fault in the lower rhine embayment, Germany. Journal of Earthquake Engineering **8**:909–926. doi: 10.1080/13632460409350514

Hollender, F., Cornou, C., Dechamp, A., Oghalaei, K., Renalier, F., Maufroy, E., Burnouf, C., Thomassin, S., Wathelet, M., Bard, P. Y., Boutin, V., Desbordes, C., Douste-Bacqué, I., Foundotos, L., Guyonnet-Benaize, C., Perron, V., Régnier, J., Roullé, A., Langlais, M., & Sicilia, D. (2018). Characterization of site conditions (soil class, VS30, velocity profiles) for 33 stations from the French permanent accelerometric network (RAP) using surface-wave methods. Bulletin of Earthquake Engineering, 16(6). https://doi.org/10.1007/s10518-017-0135-5

Hunter, J.A., Christian, H., Harris, J.R., Britton, J.L., Luternauer, J. (1999). Mapping shear wave velocity structure beneath the Fraser River delta sediments - Preliminary results. In: 8th Canadian Conference on Earthquake Engineering. Vancouver, BC

Hunter, J. A., Burns, R. A., Good, R. L., & Pelletier, C. F. (2016). Fraser River Delta–A compilation of shear wave velocities and borehole geophysics logs in unconsolidated sediments of the Fraser River Delta, British Columbia. Geological Survey of Canada Open File, 1-112.

Hunter, J.A., Christian HA (2001). Use of Shear Wave Velocities to Estimate Thick Soil Amplification Effects in the Fraser River Delta, British Columbia. In: Symposium on the Application of Geophysics to Engineering and Environmental Problems

(SAGEEP), Match 4-7, 2001, Denver, Colorado. Environment and Engineering Geophysical Society

Hunter, J.A., Crow, H.L. (2015). Shear wave velocity measurement guidelines for Canadian seismic site characterization in soil and rock. Natural Resources Canada. doi: 10.4095/297314

Jackson, F., Molnar, S., Ghofrani, H., Atkinson, G.M., Cassidy, J.F., Assatourians, K. (2017). Ground Motions of the December 2015 M 4.7 Vancouver Island Earthquake: Attenuation and Site Response. Bulletin of the Seismological Society of America 107:2903–2916

Banab, K. K., Kolaj, M., Motazedian, D., Sivathayalan, S., Hunter, J. A., Crow, H. L., Pugin, A. J. M., Brooks, G. R., & Pyne, M. (2012). Seismic site response analysis for Ottawa, Canada: A comprehensive study using measurements and numerical simulations. Bulletin of the Seismological Society of America, 102(5). https://doi.org/10.1785/0120110248

Lachet, C., & Bard, P. Y. (1994). Numerical and Theoretical Investigations on the Possibilities and Limitations of Nakamura's Technique. Journal of Physics of the Earth, 42(5). https://doi.org/10.4294/jpe1952.42.377

Lacoss, R. T., Kelly, E. J., & Toksöz, M. N. (1969). Estimation of seismic noise structure using arrays. Geophysics, 34(1), 21-38.

Luternauer, J.L., Hunter, J.A. (1996). Mapping Pleistocene deposits beneath the Fraser River delta: Preliminary geological and geophysical results. In Current Research 1996-E, Geological Survey of Canada 41–48

Macau, A., Benjumea, B., Gabàs, A., Figueras, S., Vilà, M. (2015). The Effect of Shallow Quaternary Deposits on the Shape of the H/V Spectral Ratio. Surveys in Geophysics 36:185–208

Molnar, S., Assaf, J., Sirohey, A., & Adhikari, S. R. (2020). Overview of local site effects and seismic microzonation mapping in Metropolitan Vancouver, British Columbia, Canada. Engineering Geology, 270, 105568. https://doi.org/https://doi.org/10.1016/j.enggeo.2020.105568

Molnar, S., Cassidy, J.F. (2006). A comparison of site response techniques using weak-motion earthquakes and microtremors. Earthquake Spectra **22**:169–188. doi: 10.1193/1.2160525

Molnar, S., Cassidy, J. F., Castellaro, S., Cornou, C., Crow, H., Hunter, J. A., Matsushima, S., Sánchez-Sesma, F. J., & Yong, A. (2018). Application of Microtremor Horizontal-to-Vertical Spectral Ratio (MHVSR) Analysis for Site Characterization: State of the Art. In Surveys in Geophysics (Vol. 39, Issue 4). https://doi.org/10.1007/s10712-018-9464-4

Molnar, S., Dosso, S.E., Cassidy, J.F. (2010). Bayesian inversion of microtremor array dispersion data in southwestern British Columbia. Geophysical Journal International **183**:923–940. doi: 10.1111/j.1365-246X.2010.04761.x

Molnar, S., Dosso, S.E., Cassidy, J.F. (2013). Uncertainty of linear earthquake site amplification via Bayesian inversion of surface seismic data. Geophysics **78**:WB37–WB48. doi: 10.1190/geo2012-0345.1

Molnar, S., Sirohey, A., Assaf, J., Bard, P.-Y., Castellaro, S., Cornou, C., Cox, B., Guillier, B., Hassani, B., Kawase, H., Matsushima, S., Sánchez-Sesma, F. J., & Yong, A. (2022). A review of the microtremor horizontal-to-vertical spectral ratio (MHVSR) method. Journal of Seismology, 26(4), 653–685. https://doi.org/10.1007/s10950-021-10062-9

Molnar, S., Ventura, C., Finn, W., Taiebat, M., Dosso, S., Cassidy, J. (2012). Evaluation of shear-wave velocity profiles from ambient vibration array recordings in SW British Columbia, Canada. In: Proceedings of the fifteenth world conference on earthquake

engineering, Lisbon, Portugal, Paper 3175, 2012

Monahan, P.A. (2005). Soil hazard map of the Lower Mainland of British Columbia for assessing the earthquake hazard due to lateral ground shaking. in Seismic Retrofit Guidelines (3rd edition), APEGBC, UBC, BC Ministry of Education, June 2017, Volume 9, Part III, 1p

Moon, S.W., Subramaniam, P., Zhang, Y., Vinoth, G., Ku, T. (2019). Bedrock depth evaluation using microtremor measurement: empirical guidelines at weathered granite formation in Singapore. Journal of Applied Geophysics **171**:103866. doi: 10.1016/j.jappgeo.2019.103866

Motazedian, D., Khaheshi Banab, K., Hunter, J. A., Sivathayalan, S., Crow, H., & Brooks, G. (2011). Comparison of site periods derived from different evaluation methods. Bulletin of the Seismological Society of America, 101(6). https://doi.org/10.1785/0120100344

Mustard, P., Roddick, J.A. (1992). Vancouver Subsurface Infromation Data Bank For the period 1913 to 1972. Geologic Survery of Canada. Open File 2532

Onur, T., Molnar, S., Cassidy, J., Venture, C.E., Hao, K.X.S (2004). Estimating site periods in Vancouver and Victoria, British Columbia using microtremor measurements and SHAKE analyses. In: 57th Canadian Geotechnical Conference. Quebec City, Canada

Oubaiche, E. H., Chatelain, J. L., Bouguern, A., Bensalem, R., Machane, D., Hellel, M., Khaldaoui, F., & Guillier, B. (2012). Experimental relationship between ambient vibration H/V peak amplitude and shear-wave velocity contrast. Seismological Research Letters, 83(6). https://doi.org/10.1785/0220120004

Oubaiche, E. H., Chatelain, J. L., Hellel, M., Wathelet, M., MacHane, D., Bensalem, R., & Bouguern, A. (2016). The relationship between ambient vibration H/V and SH transfer function: Some experimental results. Seismological Research Letters, 87(5). https://doi.org/10.1785/0220160113

Parolai, S., Bormann, P., Milkereit, C. (2002). New Relationships between V s , Thickness of Sediments, and Resonance Frequency Calculated by the H/V Ratio of Seismic Noise for the Cologne Area (Germany). Bulletin of the Seismological Society of America **92**:. doi: 10.1785/0120010248

Poggi, V., Fäh, D. (2010). Estimating Rayleigh wave particle motion from three-component array analysis of ambient vibrations. Geophysical Journal International **180**:251–267. doi: 10.1111/j.1365-246X.2009.04402.x

Pratt, T.L. (2018). Characterizing and Imaging Sedimentary Strata Using Depth-Converted Spectral Ratios: An Example from the Atlantic Coastal Plain of the Eastern United States. Bulletin of the Seismological Society of America **108**:2801–2815. doi: 10.1785/0120180046

Rahimi, S., Kamal Himel, A., Wood, C. M., & Asce, M. (n.d.). Application of Microtremor Horizontal to Vertical Spectra Ratio (MHVSR) and Multichannel Analysis of Surface Wave (MASW) for Shallow Bedrock Mapping for Transportation Projects. https://doi.org/10.1061/9780784482803.066

Rogers, G.C., Cassidy, J.F., Weichert, D.H. (1998). Variation in earthquake ground motion on the Fraser delta from strong-motion seismograph records. In: Clague JJ, Luternauer JL, Mosher and DC (eds) Bulletin 525. Geological Survey of Canada, pp 195–210

Rohmer, O., Bertrand, E., Mercerat, E.D., Régnier, J., Pernoud, M., Langlaude, P., Alvarez, M. (2020). Combining borehole log-stratigraphies and ambient vibration data to build a 3D Model of the Lower Var Valley, Nice (France). Engineering Geology **270**:105588. doi: 10.1016/j.enggeo.2020.105588

Rosenblad, B.L., Goetz, R. (2010). Study of the H/V spectral ratio method for determining average shear wave velocities in the Mississippi embayment. Engineering Geology **112**:13–20. doi: 10.1016/j.enggeo.2010.01.006

Seht, M. I. von, & Wohlenberg, J. (1999). Microtremor Measurements Used to Map Thickness of Soft Sediments. Bulletin of the Seismological Society of America, 89(1). https://doi.org/10.1785/bssa0890010250

Sirohey, A., Molnar, S. (2021). MHVSR 'Big Data' to outline standard procedures for Data Acquisition, Processing, Interpretation and Presentation. SSA annual meeting, 19-23 April 2021, virtual poster presentation

Teague, D., Cox, B., Bradley, B., Wotherspoon, L. (2018). Development of deep shear wave velocity profiles with estimates of uncertainty in the complex interbedded geology of christchurch, New Zealand. Earthquake Spectra **34**:639–672. doi: 10.1193/041117EQS069M

Teague, D.P., Cox, B.R. (2016). Site response implications associated with using non-unique Vs profiles from surface wave inversion in comparison with other commonly used methods of accounting for Vs uncertainty. Soil Dynamics and Earthquake Engineering **91**:87–103. doi: https://doi.org/10.1016/j.soildyn.2016.07.028

Tün, M., Pekkan, E., Özel, O., Guney, Y. (2016). An investigation into the bedrock depth in the Eskisehir Quaternary Basin (Turkey) using the microtremor method. Geophysical Journal International **207**:589–607. doi: 10.1093/gji/ggw294

Vantassel, J.P., Cox, B.R. (2021). A procedure for developing uncertainty-consistent Vs profiles from inversion of surface wave dispersion data. Soil Dynamics and Earthquake Engineering **145**:106622. doi: https://doi.org/10.1016/j.soildyn.2021.106622

Ventura, C. E., Onur, T., & X-s Hao, K. (2004). SITE PERIOD ESTIMATIONS IN THE FRASER RIVER DELTA USING MICROTREMOR MEASUREMENTS - EXPERIMENTAL AND ANALYTICAL STUDIES. 13th World Conference on Earthquake Engineering Vancouver, B.C., Canada. Paper No. 1075.

Wathelet, M., Jongmans, D., & Ohrnberger, M. (2004). Surface-wave inversion using a direct search algorithm and its application to ambient vibration measurements. *Near surface geophysics*, *2*(4), 211-221.

Wathelet, M. (2008). An improved neighborhood algorithm: Parameter conditions and dynamic scaling. Geophysical Research Letters **35**:L09301. doi: 10.1029/2008GL033256

Wathelet, M., Chatelain, J, Cornou, C., Giulio, G. Di., Guillier, B., Ohrnberger, M., Savvaidis, A. (2020). Geopsy: A User-Friendly Open-Source Tool Set for Ambient Vibration Processing. Seismological Research Letters **91**:1878–1889. doi: 10.1785/0220190360

Woeller, D.J., Hunter, J.A., Luternauer, J.L. (1993). Results of SCPT and SASW testing of the Fraser River delta sediments, British Columbia. Geological Survey of Canada, Open File 2714. doi: 10.4095/184215

Wotherspoon, L.M., Munro, J., Bradley, B.A., Wood, C., Thomson, E., Deschenes, M., Cox, B.R. (2018). Site Period Characteristics across the Canterbury Region of New Zealand. American Society of Civil Engineers (ASCE), pp 599–607

Xia, J., Miller, R.D., Park, C.B., Hunter, J.A., Harris, J.B. (2000). Comparing Shear-Wave Velocity Profiles from MASW with Borehole Measurements in Unconsolidated Sediments, Fraser River Delta, B.C., Canada. Journal of Environmental and Engineering Geophysics **5**:1–13. doi: 10.4133/JEEG5.3.1

<div align="center">

Chapter 4

</div>

4   CPT-Vs Correlations for Post-glacial Sediments in Metropolitan Vancouver

A comprehensive Seismic Cone Penetration Test (SCPT) database for post-glacial sediments is compiled to assess and establish relationships between CPT parameters and shear-wave velocity (Vs) in this chapter. Five world-wide and one existing FRD-specific empirical CPT-Vs correlations are examined and found to have limited applicability in predicting Vs from the SCPT database. Region-specific CPT-V_S models are then developed using multiple CPT parameter combinations and multiple regression approaches. The models' performances are compared, and a final model is selected and applied to 59 CPTs in the region for validation with existing Vs profiles from *in situ* Vs measurements.

4.1   Introduction

The intensity of earthquake shaking at the ground surface is greatly influenced by site effects, which are mainly attributed to the variability of soil stiffness, characterized by soil shear wave velocity (Vs), near the ground surface (Borcherdt 1970). Gradual reduction in Vs, or seismic impedance (product of soil density and Vs) towards the ground surface leads to a broadband amplification, while a sharp decrease (impedance contrast) produces resonance amplification of seismic waves (Shearer and Orcutt 1987; Hunter et al. 2010). Seismic amplification may also be affected by other factors such as topography, subsurface geometry, depth to impedance contrasts and strain-dependent soil behavior (Bard and Bouchon 1985; Athanasopoulos and Zervas 1993; Seed and Idriss 1970). Borcherdt (1994) proposed employing the time-averaged Vs in the top 30 m, Vs_{30}, as a simple and quantitative measure of local site conditions, and Vs_{30} has since been used for seismic site categorization in many seismic design building codes (e.g., National Building Code of Canada, NBCC 2015). The Vs depth (z) profile, Vs(z), and its corresponding Vs_{30} are required inputs in most seismic hazard analyses that involve site effects quantification such as development of ground motion models (GMMs), seismic hazard mapping, and site- and region-specific ground response analyses.

Vs(z) is directly measured using *in situ* methods including invasive Vs(z) methods (e.g., crosshole, downhole, P-S suspension, and Seismic Cone Penetration Test, SCPT), and non-invasive Vs(z) methods (e.g., refraction, various surface wave dispersion methods including Spectral Analysis of Surface Waves (SASW), active-source Multi-channel Surface Wave Analysis (MASW) or the microtremor array method (MAM)) (Hunter and Crow 2015). Each method has inherent uncertainty associated with its Vs measurement and interpretation (e.g., user-involved picking of wave arrival times or dispersion curve modes). Several studies have shown that Vs(z) profile and its Vs_{30} are similar within and between invasive and non-invasive methods (e.g., Garofalo et al. 2016a; Garofalo et al. 2016b; Bilson Darko et al. 2020). The most recent international blind-test comparison (Garofalo et al. 2016b) demonstrated that Vs variability from invasive and non-invasive methods is generally less than or equal to a coefficient of variation of 0.2 at most depths for 3 sites representing soft, stiff, and rock site conditions. For Vs_{30}, the difference is even smaller (~4%) and thus within the measurable error between methodologies (Garofalo et al. 2014b), i.e., the selected Vs(z) method does not impact Vs_{30}. Assaf et al. (2022) showed the depth-averaged absolute relative difference in Vs and absolute relative difference in Vs_{30} from non-invasive (MAM& MASW) inverted Vs profiles and nearby existing downhole, SCPT, and refraction profiling in the Fraser River Delta (FRD) of Metropolitan (Metro) Vancouver are on average about 18 % and 7.7 %, respectively.

Because of the prevalent use of Vs_{30} worldwide, many prediction models have been developed to estimate Vs from more readily available *in situ* invasive testing parameters or proxies. These parameters include the number of blow counts (N) obtained from Standard Penetration Test (SPT) and undrained shear strength (s_u) obtained from testing laboratory samples or field-vane measurements (e.g., Seed et al. 1986, Dickenson 1994, Wair et al. 2012). Several building code site classification schemes permit use of N or s_u, in lack of direct Vs measurements, to infer seismic site class at a site (e.g. NBCC 2015). Although CPT measurements are continuous with depth and thereby have the highest depth resolution of all mentioned *in situ* methods, it is not until recently that the ASCE 7-22 introduced use of CPT to Vs (CPT-Vs) correlations to determine site class. A significant number of

empirical CPT-Vs correlation models exist in literature (e.g., Andrus et al. 2007, McGann et al. 2015b, McGann et al. 2018,Tong et al. 2018, Kruiver et al. 2021a, Salsabili et al. 2022, Yang et al. 2022), and are developed for local regions and/or particular material types (e.g., all soils, sands, clays). These empirical models are generally derived using multi-linear or non-linear regression from region-specific and/or international databases of measured CPT parameters and Vs. Recently, Entezari et al. (2022) implemented machine learning Random Forest regression to develop a CPT-Vs model from a large SCPT database mainly in North America. The SCPT databases and hence the developed CPT-Vs models generally exhibit strong regional dependency due to the natural variability of sediments in regions with different geologic processes and depositional environments. Thus, CPT-Vs models are best represented using region-specific data if available, otherwise empirical correlations developed based on measurements from other regions should be evaluated prior to their application in an alternate region.

The Metro Vancouver seismic microzonation project (https://metrovanmicromap.ca, Molnar et al. 2020, Adhikari and Molnar 2021) developed a comprehensive geodatabase of S/CPT profiles from various open and proprietary sources. This study uses the compiled Metro Vancouver SCPT database to improve CPT and Vs correlations for post-glacial sediments in the region. 91 SCPT soundings are compiled and used to first evaluate the performance of 5 empirical CPT-Vs models from different regions and one FRD specific empirical CPT-Vs model for post-glacial sand soil in Metro Vancouver. The applicability of these models to the Metro Vancouver SCPT data is evaluated by their ability to predict measured Vs. Region-specific CPT-Vs prediction models are then developed using four regression approaches and six different CPT parameters combinations. The performance of all models and parameter combinations is assessed using a testing dataset of 11 SCPTs. A final preferred model is chosen and applied to 59 CPT soundings in Metro Vancouver to estimate Vs(z). The predicted CPT-based Vs profiles are compared to invasive measured Vs profiles within the same geology unit to assess the model's applicability from an independent dataset. The developed models are important tools for seismic site

characterization and thereby future non-ergodic seismic hazard analyses for Metro Vancouver.

4.2   Geologic Setting and S/CPT Database

The FRD, south of Metro Vancouver, is a lowland region (Figure 4-1) with post-glacial Holocene-aged fluvial and deltaic sediments (Salish and Fraser River sediments) that can extend to more than 300 m below ground surface (Hunter et al. 1998). The FRD post-glacial deposits comprise topset, foreset, and bottomset units (Clague et al. 1998). The topset consists of a few meters of intertidal and floodplain silts and peat, underlain by 10 to 30 m thick distributary-channel sands. These channel sands pose a serious geotechnical hazard in the FRD due to their liquefaction susceptibility during earthquakes (Clague et al. 1992, Javanbakht et al. 2021). Below the channel sands, up to 165 m thick foreset interbedded silts and sands overlie the bottomset fine-grained clayey silt. The post-glacial sediments are underlain by stiff Pleistocene and older-aged glacial and interglacial sediments (up to 500 m thick below the central FRD, Britton et al. 1995) which are underlain by Tertiary sedimentary rocks. The thickness of Quaternary sediments (depth to rock) in FRD ranges between about 200 and 800 m below ground surface. The post-glacial FRD sediments have a relatively well-resolved power-law Vs gradient (Hunter et al. 1999; Molnar et al. 2010), Vs is generally < 200 m/s within the top 20 m. Although the FRD dominates post-glacial sediments in Metro Vancouver, post-glacial sediments can also be found north and east of the FRD (grey and yellow areas outside the FRD boundaries in Figure 4-1). The seismic site characteristics (e.g., soil thickness, Vs(z), Vs_{30}) of post-glacial sediments in Metro Vancouver are important as they impact period-dependent earthquake shaking amplitudes and amplification.

Extensive invasive and non-invasive Vs profiling, involving more than 500 Vs(z) profiles, was conducted throughout the 1980's and 1990's by the Geologic Survey of Canada (GSC) in an effort to characterize the geophysical properties of the deep stratigraphy below the FRD (Hunter et al. 1998; Hunter et al. 2016). The Hunter et al. (2016) Vs dataset includes invasive downhole and SCPT testing, and non-invasive seismic refraction depth profiles

and reflection cross-sections. Recently, the Metro Vancouver microzonation project has conducted multi-method non-invasive seismic testing, including combined MASW & MAM array testing at 120 sites and microtremor horizontal-to-vertical spectral ratio (MHVSR) testing at over 2000 locations, across the region to assess earthquake amplification, liquefaction and landslide hazards (Molnar et al. 2020, Assaf et al. 2022, Sirohey 2022). The project further compiled existing Vs(z) and SCPT profiles as part of a regional geodatabase from various public (online) and private agencies (Adhikari and Molnar 2021, Molnar et al. 2020). SCPT profiles are primarily accomplished in post-glacial sediments (mainly constrained to southern Metro Vancouver) as CPT refusal occurs when the cone tip penetrates stiff glaciated till or till-like sediments with Vs $\geq$ 400 m/s (Monahan and Levson 2001, Assaf et al. 2022).

As the quality of the SCPT database impacts the accuracy of any potential CPT-Vs relationships, data screening was required for quality control to only select reliable Vs and CPT measurements. A total of 91 SCPT soundings are collected for this study, i.e., SCPT sites that include dual CPT and Vs profiling, which included 46 SCPTs from previous GSC testing and 45 SCPTs compiled from various geotechnical reports within the Metro Vancouver microzonation project's geodatabase (Hunter et al. 2016, P. Monahan, pers. comm., 2020, Monahan 1999) as well as from another provincially-funded regional seismic dike assessment project. The locations of the 91 SCPTs used in this study are shown in Figure 4-1, 80 SCPTs will be designated to a training dataset for CPT-Vs model development and the remaining 11 SCPTs will comprise a testing dataset to evaluate prediction accuracy of the developed CPT-Vs models. A regional surficial Quaternary geology map is shown in the background of Figure 4-1 (Dunn and Ricketts 1994, Armstrong and Hicock 1979). The 91 SCPTs occur in four major geologic units: Fraser River (67 SCPTs), Salish (22), Capilano, Ce (1), and Fort Langley FLd (1) sediments. Ce and FLd units are primarily silt and clay facies of Pleistocene age located in eastern Metro Vancouver (Clague et al. 1998; Monahan and Levson 2001). Although of Pleistocene age, these sediments were not ridden by glaciers and thus are also characterized as post-glacial sediments here.

In addition, 59 selected CPT soundings of the Metro Vancouver project geodatabase were conducted in Fraser River, Salish sediments, and Ce geology units (Figure 4-1). These 59 CPTs will be used to test the developed CPT-Vs model in section 4.5.
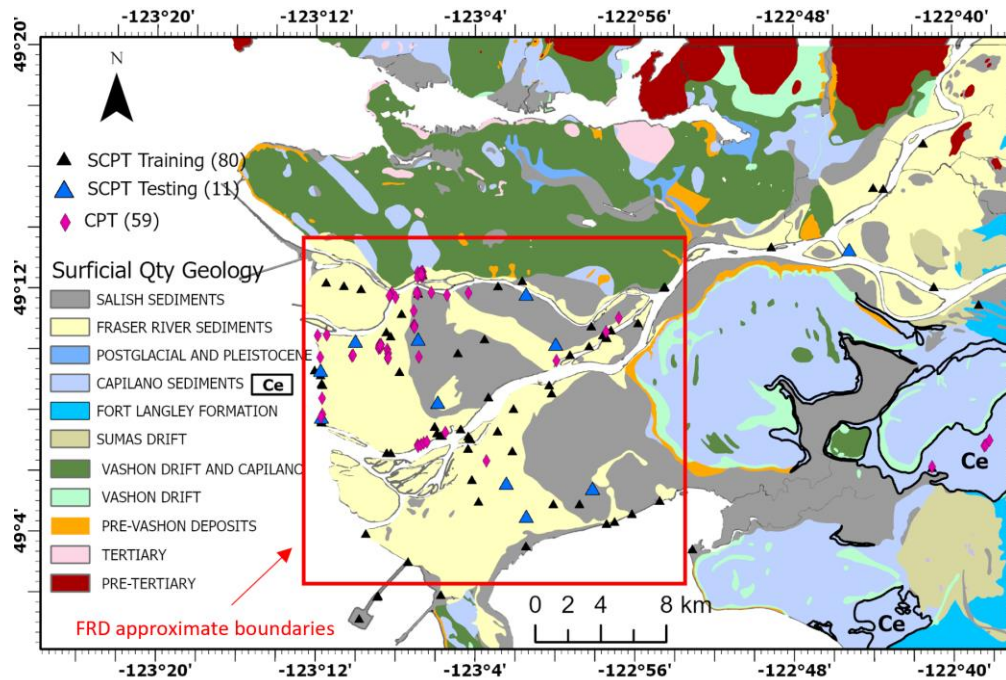
Figure 4-1. Locations of 91 SCPT sites and 59 selected CPT profiles used in this study. Background map is the regional surficial Quaternary (Qty) geology map of Dunn and Ricketts (1994) and Armstrong (1979, 1980).

Measurements obtained during CPT profiling (referred to herein as basic CPT parameters) include: depth (z), cone tip resistance (q_c), sleeve friction (f_s), and pore water pressure behind the cone (u_2). These basic parameters are used with CPeT-IT software (GeoLogismiki Geotechnical Software 2014, ver. 3.0.3.2) to obtain processed CPT parameters including the corrected cone tip resistance (q_t) and normalized soil behaviour type index (I_c), which differentiates soil behavior types into sand, silt and clay (Robertson and Wride 1998; Robertson 2009). The empirical soil unit weight model of Robertson and Cabal (2010) as a function of q_t and f_s is used to estimate effective stress.

The direct *in situ* Vs measurements obtained during SCPT profiling consist of downhole interval Vs measured typically at 1 m z intervals. The reported interval Vs values in SCPT logs are used verbatim; we do not re-interpret arrival time picks as the shear waveforms are typically not available. The z sampling of basic CPT parameters (q_c, f_s, u_2) is much finer than Vs sampling, typically every 5 cm. To reconcile the different measured z intervals of Vs and CPT parameters, the higher-resolution CPT parameters are averaged within the lower-resolution Vs profile z intervals at each site. Averaging CPT parameters within Vs intervals essentially smooths the original CPT data and the high z resolution (layers thinner than 1 m) is lost. The z of each CPT-Vs data pair is taken as the midpoint of each z interval. As our focus is on the native ground conditions, all high Vs values of compacted engineered fill near the ground surface at dike sites are removed from our analyses. It should also be noted that accuracy of Vs measurement in the top few meters by *in situ* invasive Vs(z) methods is generally reduced or poor near the surface due to the non-verticality of the travel path of the source shear waves. However, we retain all near surface CPT-Vs data pairs from non-dike sites as they did not show any significant bias compared to pairs at larger z.

A total of 2728 CPT-Vs processed data pairs are extracted from the 91 SCPTs and are used to first evaluate existing CPT-Vs relationships. Figure 4-2 displays a scatter plot matrix of the four basic SCPT parameters (z, q_c, f_s, Vs) as well as the processed soil behaviour type index, I_c (Robertson and Wride, 1998), using all 2728 CPT-Vs data pairs, single parameter histograms are plotted along the main diagonal. Colour shading in Figure 4-2 is based on I_c value; an $I_c \leq 2.6$ corresponds to coarse-grained soils or sands and $I_c > 2.6$ corresponds to fine-grained soils or silts and clays. Table 4-1 reports the minimum, mean, and maximum values of the 2728 CPT-Vs data for the five selected SCPT parameters. SCPT profiles reach z of about 80 m but are dominantly 50 m or less. Measured Vs ranges between 60 and 317 m/s, and I_c indicates good coverage of all soil behavior types with a slight over presence of coarse-grained sand behaviour ($I_c \leq 2.6$). The distribution of I_c with z is representative of the general FRD soil lithology where topset channel sand layers are limited to z = 40 m and are underlain by foreset silty soils (Clague et al. 1998). The correlations between Vs with z, q_c and f_s can be observed in Figure 4-2. The correlation between Vs and I_c is not

immediately clear as it does not account for differences of I_c with z. However, at a specific z (e.g., 20 m), Vs of coarse-grained soils is generally higher than that of fine-grained soils base on I_c colouring in the Vs-z correlation scatter plot in Figure 4-2. Overall, Figure 4-2 confirms correlations between measured Vs and four common CPT parameters for post-glacial soils in Metro Vancouver.
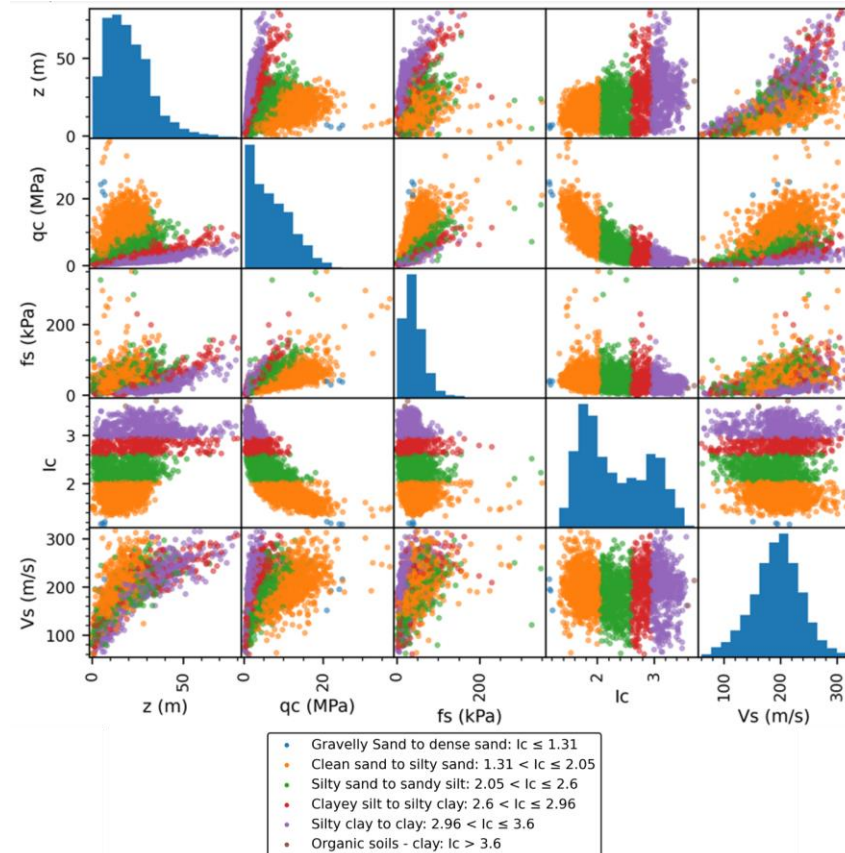
Figure 4-2. Correlation matrix of the 2728 CPT-Vs data pairs from the 91 SCPTs in Metro Vancouver post-glacial soils, coloured by I_c.

Table 4-1. Statistics of the 2728 CPT-Vs data pairs obtained from 91 SCPTs in Metro Vancouver post-glacial soils.

CPT parameter	z (m)	q_c (MPa)	f_s (kPa)	Vs (m/s)	I_c^+
Mean	16.08	9.5	48.19	191.43	≤ 2.6
	28.67	2.49	34.08	198.02	> 2.6
Minimum	0.35	0.46	1.91	61.8	≤ 2.6

	0.58	0.19	1.07	60.33	> 2.6
Maximum	64.65	37.05	350.4	317.12	≤ 2.6
	80.02	11.34	229.28	315.1	> 2.6

[+]: 1781 CPT-Vs pairs with $I_c \leq 2.6$, and 947 CPT-Vs pairs with $I_c > 2.6$

4.3 Evaluation of Existing CPT-Vs Models

The compiled SCPT database for post-glacial soils in Metro Vancouver allows evaluating existing CPT-Vs relationships developed from different region-specific or international datasets to verify their applicability to Vs prediction from CPT measurements in Metro Vancouver. Some existing CPT-Vs prediction models are specific to certain soil types (i.e., sand soils or clay/silt soils); however, general relationships applicable to all types of soils are more practical for design problems. Robertson et al. (1992; hereafter R92) proposed a relation between the effective stress normalized Vs (V_{S1}) and q_c (q_{c1}) for clean uncemented sands from a limited ~70 CPT-Vs data pairs in the FRD. For our application, the R92 V_{S1}-q_{c1} equation was converted to Vs-q_c (Table 4-2) using the normalization equations provided in R92. Testing the R92 relationship is of particular interest as it is the only existing region-specific CPT-Vs model within Metro Vancouver. In addition, 5 other existing general CPT-Vs models that use common CPT parameter combinations are selected for evaluation using the SCPT database of this study. The 5 other considered models (Table 4-2) are: Andrus et al. (2007; A07) for Holocene sediments in California, South Carolina, and Japan, Robertson (2009; R09) for Holocene and Pleistocene sediments in California and other non-specified regions, Hegazy and Mayne (2006; HM06) for soft and stiff sediments from a USA, Japan, and Italy, Salsabili et al. (2022; S22) for general soil-type post-glacial sediments in Southern Quebec, Canada, and McGann et al. (2015b; MG15) for non-gravelly soils in Christchurch.

Table 4-2. Selected existing CPT-Vs relationships evaluated using the Metro Vancouver SCPT database.

Source	Vs (m/s)	Notes	Sediment Type; Vs range	Number of pairs[!]

R92	$102\, q_c^{\,0.23}\,(\frac{Pa}{\sigma_v'})^{-0.135}$	q_c in MPa	FRD clean sand; not reported	~70
A07	$2.27\, q_t^{\,0.412}\, I_c^{\,0.989}\, z^{0.033}$	q_t in kPa	Holocene; ~70-250 m/s	72
R09	$[\,10^{1.68\,+\,0.55 I_c}\,\left(\frac{q_t-\sigma_v}{P_a}\right)]^{0.5}$	q_t and σ_v in kPa	Holocene and Pleistocene; not reported	1035
HM06	$0.0831\, q_{c1N}\mathrm{e}^{1.786\, I_c}(\frac{\sigma_v'}{P_a})^{0.25}$	σ_v' in kPa	Sand, clay, intermediate soils, and mine tailings; ~15-700 m/s	558
S22	$3.868 q_t^{0.386} I_c^{0.881} z^{0.048}(1+B_q)^{\,0.225}$	q_t in kPa	General soil-type post-glacial sediments in Southern Quebec, Canada; 90-340 m/s	991
MG15_qc	$18.4\, q_c^{\,0.144} f_s^{\,0.0832} z^{0.278}$	q_c and f_s in kPa	Christchurch non-gravel soils; 50-~300 m/s	513

σ_v, total vertical stress; σ_v', effective vertical stress; q_{c1N}, normalized cone tip resistance; Pa, atmospheric pressure (100 kPa), B_q: normalized excess pore pressure. [†]Number of CPT-Vs data pairs.

The performance of the six selected models is assessed by comparing their predicted Vs from each of the 2728 CPT values with the measured Vs. The coefficient of determination (R^2) and the root-mean-square error (RMSE) between measured and predicted Vs are calculated to evaluate the performance of each model. R^2 is a measure of the degree of correlation between measured and predicted Vs, ranging between 0 (i.e., no statistical correlation) and 1 (i.e., perfect correlation). RMSE in m/s units represents the variance of the errors between measured and predicted Vs, a perfect relationship has a RMSE of 0.

Figure 4-3 shows plots comparing the measured and predicted Vs with reported R^2 and RMSE values for the six models. Based on the R^2 and RMSE values in Figure 4-3, it is clear that the A07 (lowest RMSE) and MG15_q_c (highest R^2) models provide the closest prediction to measured Vs, whereas the HM06 and S22 models are the least applicable to Metro Vancouver soils. The HM06 model shows strong bias especially at higher Vs values while the S22 model overestimates measured Vs for all soil types in Metro Vancouver. The Metro Vancouver region-specific R92 model developed only for clean sands of the FRD slightly under predicts Vs for coarse-grained soils ($I_c \leq 2.6$) and significantly underestimates Vs for fine-grained soils ($I_c > 2.6$). The limited CPT-Vs pairs used in developing the R92 model may be the reason for its inability to robustly predict measured

Vs for coarse-grained soils in Metro Vancouver, while its bias in estimating fine-grained soil Vs is expected. The databases used to develop the HM06 and R09 models include older soils with higher Vs than the post-glacial sediments present in Metro Vancouver (Table 4-1) which may explain their poor performance. Moreover, the HM06 model was developed using Vs profiles obtained from a variety of methods (SCPT, downhole, cross hole and SASW, i.e., Vs profiles nearby or co-located with CPT profiles), while the current study only uses SCPT measurements. Although S22 is developed from SCPT measurements in post-glacial sediments in southern Quebec, Canada with a similar Vs range, its limited applicability to Metro Vancouver CPT-Vs data may be attributed to the strong regional dependency of CPT-Vs relationships.

Of the 6 selected models, A07 and MG15_q_c developed from SCPT measurements in Holocene sediments are generally the most applicable to predicting Vs from CPT parameters in Metro Vancouver post-glacial soils. However, by examining I_c trends in Figure 4-3a and 3d, both A07 and MG15_q_c models underestimate Vs of fine-grained soils. To confirm this, the average measured-to-predicted Vs ratio is calculated for both models for coarse- and fine-grained soils. The average measured-to-predicted Vs ratio from A07 and MG15_q_c models are 1.12 and 1.13 for fine-grained soils and 0.98 and 1 for coarse-grained soils, respectively. This indicates that on average both models underestimate fine-grained Vs by about 12 to 13 %.

The reasons A07 and MG15 models underpredict Vs for fine-grained soils in Metro Vancouver is due to the data used to derive the models. The A07 model was developed from only 72 CPT-Vs pairs with z < 10 m and only 32 pairs with I_c > 3. The MG15_q_c model used 513 CPT-Vs pairs from Christchurch, New Zealand with the majority of pairs with I_c < 2.05 and z < 16 m (McGann et al. 2015a). In contrast, our Metro Vancouver CPT-Vs database consists of 1574 pairs (58 %) at z > 16 m and ~47 % of these pairs have I_c > 2.6. In other words, most of the 91 SCPTs in Metro Vancouver are relatively deep and associated with silty soil behavior. The underrepresentation of fine-grained soils and different depth ranges in the A07 and MG15_q_c model databases explains why both models

are biased in predicting Vs of post-glacial soils in Metro Vancouver. Additional sources of bias may be attributed to the geologic processes that lead to region-specific soil composition and properties (e.g., aging effects, cementation, consolidation ratio, material fabric) of Holocene soils elsewhere compared to post-glacial sediments in Metro Vancouver. Thus, development of an unbiased improved region-specific CPT-Vs relationship for all post-glacial soil types in Metro Vancouver is a logical next step.
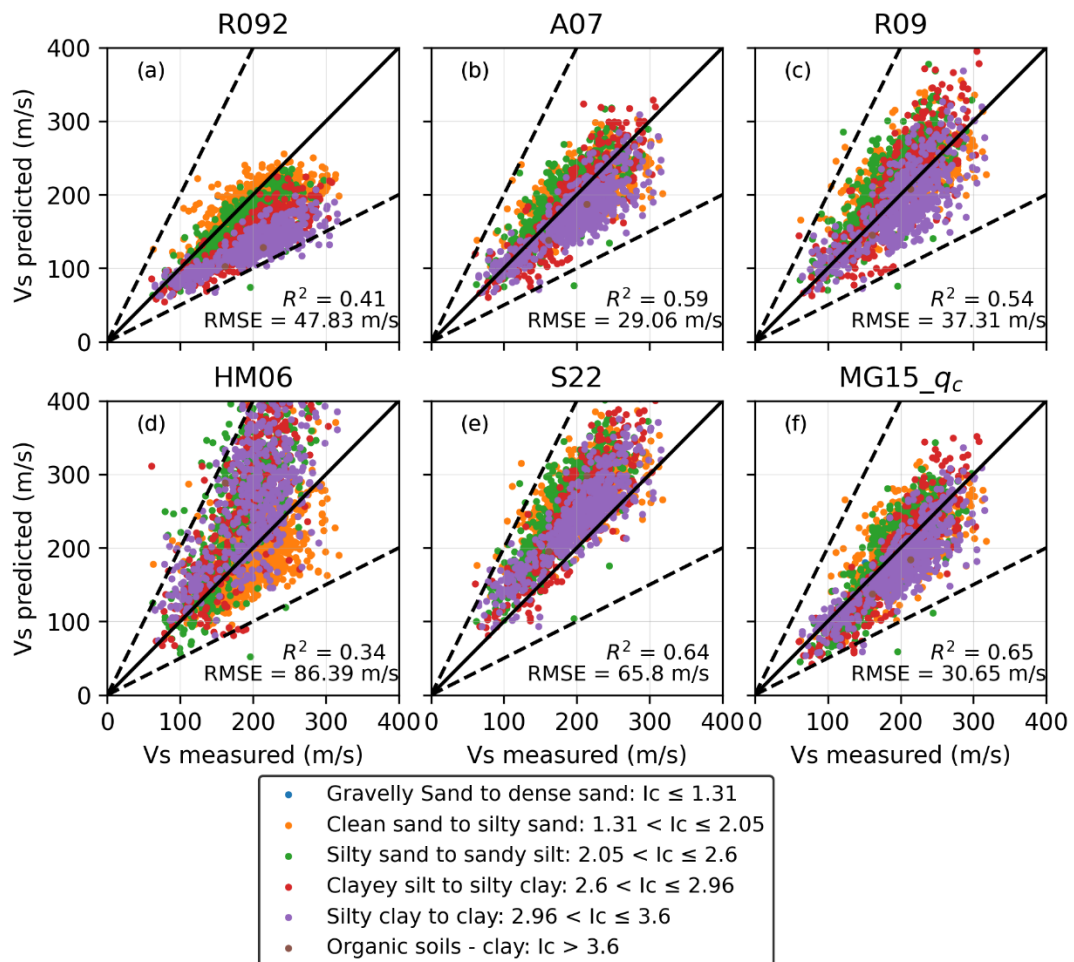
Figure 4-3. Comparison of measured Vs with predicted Vs from the 6 selected existing CPT-Vs models. Solid black line shows 1:1 correlation, dashed black lines show a factor of 2 deviation. Colour shading is based on I_c as in Figure 4-2.

4.4 Development of CPT-Vs Models for Post-glacial Sediments in Metro Vancouver

To develop CPT-Vs models specific to post-glacial soils in Metro Vancouver, six different CPT parameter combinations and four different regression approaches are considered. The regression approaches include multi-linear and non-linear least-squares regressions, as well as supervised machine learning ensemble methods, Random Forest and Extreme Gradient Boosting regressions. Traditional multi-linear and non-linear regressions utilize a pre-defined functional form of predictor variables and model coefficients, while Random Forest and Extreme Gradient Boosting regressions are ensemble methods that use predictions of many combined decision trees built on a set of predictor variables to provide an average prediction. Instead of using a functional form, tree-based ensemble methods are defined with parameters that include the number of trees and maximum depth of a tree to predict the response.

The variety of regression models and CPT parameters combinations provides insights on the optimal model to predict Vs from CPT data of post-glacial soils in Metro Vancouver. To develop and assess the performance of all models consistently, the CPT-Vs database is divided into a training dataset consisting of 80 SCPTs with 2399 CPT-Vs pairs, and a testing dataset consisting of 11 SCPTs with 329 CPT-Vs pairs, about 12 % of the total database (locations shown in Figure 4-1). The training dataset is first used to develop CPT-Vs models, and the models' performances are then evaluated using the testing dataset. The testing dataset is chosen to provide adequate spatial coverage of the post-glacial sediments in Metro Vancouver as well as include adequate representation of different soil types with 104 pairs (32 %) having $I_c > 2.6$.

Table 4-3 lists the six selected CPT-Vs models and their CPT parameters combinations. CPT parameters combinations have been used previously in other CPT-Vs models. Table 4-3 references the associated existing model forms in Table 4-2, which are justified for use here since common CPT parameters were found to be correlated with Vs for post-glacial soils in Metro Vancouver as shown in Figure 4-2. The selected CPT parameters

combinations are based on directly measured CPT parameters such as q_c, f_s, and z (e.g., MG15_q_c), and post-processed CPT parameters such as q_t, I_c, and σ'_v (e.g., A07 or W12_q_t) that are determined considering water table depth and soil unit weight. The last four models listed in Table 4-3 are included to evaluate model performance based on the selected CPT parameters, i.e., either q_c or q_t and either z or σ'_v. For example, in sandy soils, q_c is almost the same as q_t since little to no excess pore pressure develops; however, in clayey soils, q_t might better correlate with Vs than q_c as it is corrected for pore pressure. Similarly, σ'_v is theoretically better correlated to Vs than z. CPT-Vs models that require only basic CPT parameters can be directly applied to measured CPT profiles. The prediction benefit of including post-processed CPT parameters should therefore outweigh the extra step and its associated uncertainty in assuming a unit weight involved in computing the post-processed parameters.

To develop CPT-Vs models specific to post-glacial soils in Metro Vancouver, each of the six selected CPT parameters combinations listed in Table 4-3 is fitted to the 2399 CPT-Vs training data pairs using four different regression approaches. Fig. 4-4 shows the model development procedure for the MG15_q_c model example. The performance of each of the 24 models will be evaluated in terms of Vs prediction compared to measured using the 329 CPT-Vs testing dataset.

Table 4-3. Six selected CPT-Vs model forms and their associated CPT parameter combinations.

Associated existing model	Model form	Total required model parameters
Based on A07	$Vs = a\ q_t^b\ I_c^c\ z^d$	7: q_c, f_s, z, u_2, water table depth, a, unit weight
Based on R09	$Vs = [10^{\ a+b\ Ic}\ (\frac{q_t-\sigma_v}{p_a})]^{0.5}$	7: q_c, f_s, z, u_2, water table depth, a, unit weight
Based on MG15_q_t	$Vs = a\ q_t^b\ f_s^c\ z^d$	5: q_c, f_s, z, u_2, a
Based on MG15_q_c	$Vs = a\ q_c^b\ f_s^c\ z^d$	3: q_c, f_s, z
Based on W12_q_t	$Vs = a\ q_t^b\ f_s^c\ \sigma'_v{}^d$	7: q_c, f_s, z, u_2, water table depth, a, unit weight
Based on W12_q_c	$Vs = a\ q_c^b\ f_s^c\ \sigma'_v{}^d$	5: q_c, f_s, z, water table depth, unit weight

Note: a = Cone net area ratio. Vs in m/s; z in meters; q_c, q_t, f_s σ_v and σ_v' in kPa.
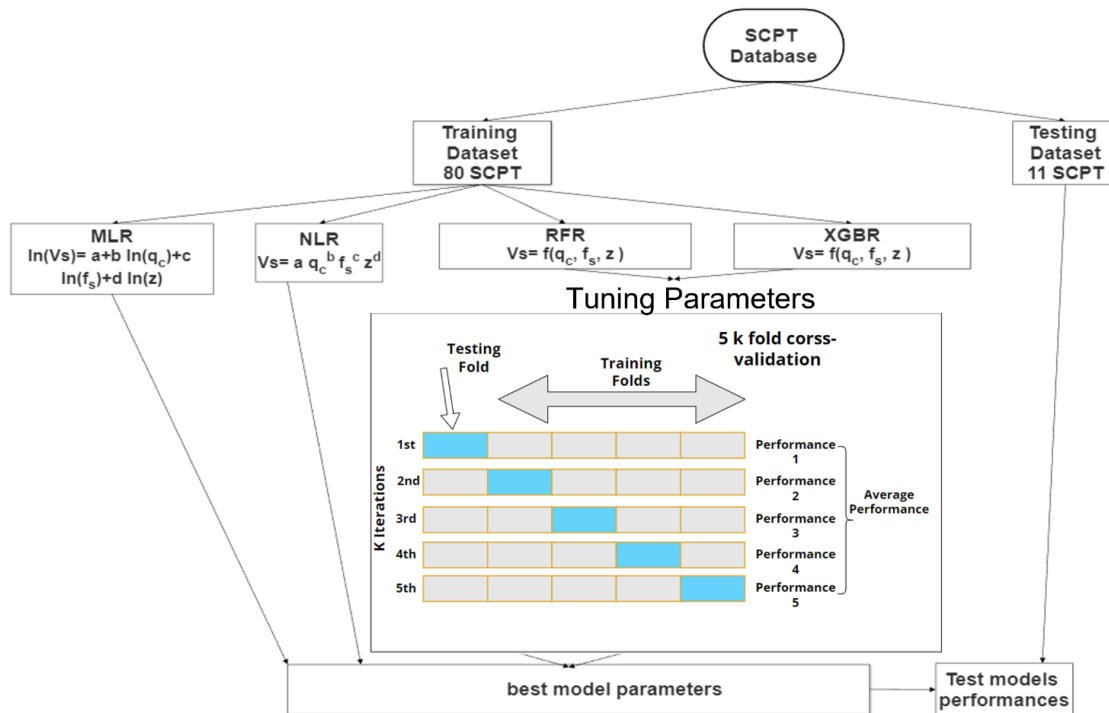
Figure 4-4. Flow chart depicting application of 4 regression approaches (multi-linear, MLR, non-linear, NLR, Random Forest, RFR, and Extreme Gradient Boosting, XGBR) given a selected CPT parameters combination; the MG15_q_c model form is shown here as an example.

4.4.1   Multi-linear and Non-linear Regressions

To conduct multi-linear regression (MLR), a natural logarithmic (ln) transformation of Vs and CPT parameters is used, i.e., the regression is performed on ln(Vs) and ln(CPT) parameters. For non-linear least-squares regression (NLR), several iterations are used to find the optimal model coefficients that minimize the sum of squares between observed and predicted Vs. NLR has advantages of capturing non-linear relationships in the data and can be directly applied without the need for transformation of Vs or CPT parameters. NLR, however, requires defining reasonable initial model coefficients to allow the algorithm to converge. These initial coefficient values are set based on typical existing CPT-Vs models

(e.g., Table 4-2). The obtained regressed model coefficients from each MLR and NLR model are reported in Tables B-1 and B-2, respectively in Appendix B.

4.4.2   Random Forest and Extreme Gradient Boosting regressions

Machine learning algorithms have been emerging in many geotechnical applications (e.g., Zhou et al. 2016, Zhang et al. 2021a, Zhang et al. 2021b, Baghbani et al. 2022) due to advancements in their implementation tools, their improved predictive power, and the growing availability of large datasets. In particular, machine learning models have been successfully applied to CPT data for soil behavior classification (e.g., Reale et al. 2018, Erharter et al. 2021, Wu et al. 2021, Pippi et al. 2022) and prediction of soil density (Entezari et al. 2021) and Vs (Entezari et al. 2022). To make use of our large compiled SCPT database specific to Metro Vancouver post-glacial soils, two different ensemble learning algorithms, Random Forest regression (RFR) (Breiman 2001) and Extreme Gradient Boosting regression (XGBR) (Chen and Guestrin 2016) are implemented here.

Ensemble learning is a class of supervised machine learning algorithms and combines predictions from multiple models and averages them to obtain an enhanced prediction (Dietterich 2000). A RFR is a combination of many decision trees built on independently sampled subsets (bootstrap aggregation) of the original training dataset (Breiman 2001). The predictions from all the trees in the forest are then averaged to provide a final prediction. RFR uses only a subset of the predictor variables (typically referred to as features) to build less correlated (unique) trees and hence improve the prediction accuracy (Breiman 2001). XGBR, proposed by Chen and Guestrin (2016) to address shortcomings of gradient boosting decision trees, is a similar tree-based ensemble learning method but differs from RFR in the sampling strategy. Unlike bootstrap sampling used in RFR where an instance has the same chance of being selected and the trees are built independently, XGBR boosting uses residuals from the previous sampling to make a better-informed decision on subsequent sampling (Zhang and Ma 2012). Boosting therefore iteratively enhances the performance by learning from previous decisions (Friedman 2001). XGBR has recently gained significant popularity in different fields due to its speed and precision

in regression problems; however, its application in geotechnical engineering is relatively novel and evolving (e.g., Wang et al. 2020, Zhang et al. 2021b, Zhang et al. 2021c, Zhou et al. 2021, Amjad et al. 2022).

RFR models can be defined using several user-selected tuning parameters. Most important parameters are the number of trees, the maximum depth of a tree, the number of predictor variables used in each node split, and the bootstrap sample size on which a tree is built. The number of predictor variables for each node split is typically chosen as a random subset of the total number of variables used in the model. Similarly, bootstrap sample size for building a single tree is chosen as a random subset of the full training dataset. The introduction of randomness in these two parameters leads to less correlated trees and provide a better averaged prediction (Breiman 2001).

 XGBR models utilize the same parameters as RFR as well as tuning parameters such as the minimum child weight and learning rate (eta) (Chen and Guestrin 2016). Choosing the tuning parameters appropriately is an essential step in developing robust machine learning models. To select the optimal set or combination of the tuning parameters values that improve prediction of sub-datasets and thereby leads to improved model performance, a range of each tuning parameter is defined and a hyper-parameter tuning procedure is followed. The hyper-parameter tuning procedure can be conducted via a grid or a random search over each defined parameter range and each model is then scored in a k fold cross-validation method. The k fold cross-validation method splits the training dataset into k different folds (subsets); and for each fold, the model is trained using data of the other remaining k-1 folds and is tested on the selected fold via a performance score. This process is repeated for each of the k folds and the final model score is calculated as the average of the k test scores. The set of tuning parameters that yield the highest average test score is chosen as the optimal set. The hyper-parameter tuning procedure is important to ensure the model performs relatively well on new unseen data (still part of the training dataset).

RFR and XGBR approaches are applied to the Metro Vancouver SCPT training datasets for each of the six selected CPT parameters combinations listed in Table 4-3. The number

of predictor variables for each node split is taken as 2 out of the 3 predictor variables of each model and the sample size is set to 67 % of the training dataset. For each model, the number of trees and the maximum depth of a tree (in addition to minimum child weight and the learning rate eta for XGBR models) are tuned in a grid search and with a 5 k fold cross-validation (Figure 4-4). The optimal set of tuning parameters for each RFR and XGBR model are reported in Tables B-3 and B-4, respectively, in Appendix B.

4.4.3   Performance of developed CPT-Vs models

Performance of the 24 developed CPT-Vs models is evaluated by comparing predicted Vs with measured Vs. The prediction accuracy of the models is evaluated in terms of R^2 and RMSE. Figure 4-5 (Table 4-4) summarizes R^2 and RMSE of all 24 developed CPT-Vs models for the training and testing datasets. The testing dataset R^2 and RMSE indicate the performance of the models on new unseen data, while the training dataset R^2 and RMSE show how much of the input data can be explained by the developed model. Comparing the performance of traditional regression approaches MLR and NLR, all NLR models show slight improvement in Vs prediction compared to MLR models in both testing and training datasets. This highlights the relationship between Vs and CPT parameters is better captured with non-linear models. Both machine learning XGBR and RFR approaches have similar R^2 and RMSE for the training dataset. It is expected that machine learning regression approaches outperform traditional regression approaches for the training dataset. RFR and XGBR better capture non-linearities in the CPT-Vs training data due to their ensemble nature without being constrained to a specific functional form. Although XGBR uses gradient boosting which allows learning from previous residuals, its predictive power is not effectively improved when compared to RFR. XGBR provides slightly improved predictions compared to RFR for all CPT parameters combinations, except for W12 models. For the testing data, the machine learning regression approaches continue to slightly outperform the traditional regression approach models for all six CPT parameters combinations. Generally, the testing dataset's RMSE is reduced 7.33 % when using XGBR instead of NLR. The best performing model among the 24 models is RFR_W12_q_t which uses q_t and σ'_v with $R^2 = 0.76$ and RMSE = 19.82 m/s. The machine learning algorithms in

this study provided slightly better Vs prediction capabilities (~ 1 to 3 m/s reduction in RMSE for training and testing data sets) compared to traditional linear regressions mainly due to the availability of a large SCPT database. This emphasizes the importance of large databases that allow developing machine learning models with improved prediction capabilities.

Considering 6 parameters combinations allows understanding the predictive power of individual parameters separately, within a regression approach from the testing and training datasets. For example, it would be interesting to see if the model performance improves when employing only basic CPT parameter vs. post-processed parameters (e.g., z vs. σ'_v, q_c vs. q_t and f_s vs. I_c). Theoretically, processed parameters such as q_t, σ'_v, and I_c hold additional information/parameters on the soils such as the unit weight, u_2, and water table depth compared to q_c, z, and f_s, respectively. It can be expected that processed parameters correlate better with Vs.

Among MLR models, R09 exhibits the poorest performance, and the 5 remaining models exhibit fairly similar R^2 and RMSE, while the W12_q_t model produces the lowest RMSE. R09 poor performance could be due to its different functional form compared to the other 5 models (Table 4-3). All XGBR and RFR models have fairly similar R^2 and RMSE with XGBR_W12_q_t also having lowest RMSE. To compare the predictive powers of q_c and q_t, we examine the performance of similar models in Table 4-3 (i.e., MG15_q_t vs MG15_q_c and W12_q_t vs W12_q_c). MG15_q_t and W12_q_t provide similar R^2 and RMSE as MG15_q_c and W12_q_c, which indicates that there is no effective improvement in model performance when q_c is replaced with q_t. Similarly, the predictive power of σ'_v and z is compared using similar models (i.e., W12_q_t vs MG15_q_t and W12_q_c vs MG15_q_c). Both W12_q_t and W12_q_c lead to slightly improved predictions in the testing dataset compared to MG15_q_t and MG15_q_c, indicating a better prediction power of σ'_v. A07 and MG15_q_t models allow exploring the effect of replacing f_s by I_c on the model's prediction as they share the two other parameters (q_t and z). For MLR and NLR, I_c in A07 model seems to have better

predictive strength than f_s in MG15_q_t. Conversely, f_s has slightly better prediction than I_c for RFR and XGBR models.

The observed overall prediction improvement of the post-processed parameters is not large. For example, RMSE in the testing dataset ranges between 20.06 and 20.25 m/s for all 6 XGBR models and between 20.63 and 21.13 m/s for the 5 NLR models (excluding R09). All MLR and NLR coefficients of the developed CPT-Vs models are provided in the Appendix B; coefficients for R09 MLR and NLR models are not provided due to their low performance.
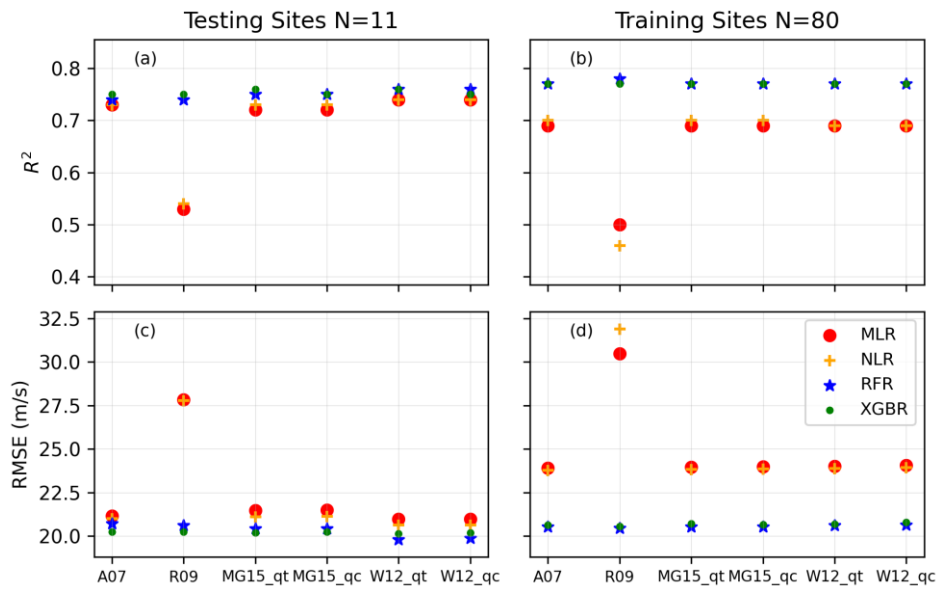
Figure 4-5. Comparison of R^2 and RMSE model performance measures of the 24 developed CPT-Vs models, six CPT parameters combinations and four regression approaches, for the training and testing datasets.

Table 4-4. R^2 and RMSE for all considered models (Figure 5) for the training and testing datasets.

Model	Regression Approach	Training Dataset N=2399		Testing Dataset N=329	
		R^2	RMSE (m/s)	R^2	RMSE (m/s)
A07	MLR	0.69	23.92	0.73	21.17

R09	MLR	0.5	30.49	0.53	27.83
MG15_q_t	MLR	0.69	23.95	0.72	21.48
MG15_q_c	MLR	0.69	23.99	0.72	21.49
W12_q_t	MLR	0.69	24.02	0.74	20.97
W12_q_c	MLR	0.69	24.06	0.74	20.98
A07	NLR	0.7	23.78	0.73	21.01
R09	NLR	0.46	31.88	0.54	27.79
MG15_q_t	NLR	0.7	23.82	0.73	21.11
MG15_q_c	NLR	0.7	23.86	0.73	21.13
W12_q_t	NLR	0.69	23.89	0.74	20.63
W12_q_c	NLR	0.69	23.94	0.74	20.65
A07	RFR	0.77	20.52	0.74	20.71
R09	RFR	0.78	20.46	0.74	20.61
MG15_q_t	RFR	0.77	20.54	0.75	20.42
MG15_q_c	RFR	0.77	20.54	0.75	20.44
W12_q_t	RFR	0.77	20.62	0.76	19.81
W12_q_c	RFR	0.77	20.64	0.76	19.88
A07	XGBR	0.77	20.63	0.75	20.25
R09	XGBR	0.77	20.56	0.75	20.25
MG15_q_t	XGBR	0.77	20.71	0.76	20.18
MG15_q_c (AMEN)	**XGBR**	**0.77**	**20.66**	**0.75**	**20.25**
W12_q_t	XGBR	0.77	20.69	0.76	20.13
W12_q_c	XGBR	0.77	20.8	0.75	20.19

4.5 Preferred CPT-Vs model for Post-glacial Sediments in Metro Vancouver

Practical aspects are considered to select one of the 24 developed CPT-Vs models to predict Vs throughout Metro Vancouver from only CPT (not SCPT) data. The models' accuracy does not effectively increase when q_t is used instead of q_c. Thus, our preference is to use the directly measured q_c. The prediction in the testing dataset is slightly improved when σ'_v is used instead of z. However, the calculation of σ'_v requires the water table depth as well as the unit weight of the soil. Water table depth may not be available for many CPT data in Metro Vancouver, and thus further assumptions that add to the model's uncertainty are needed. The unit weight of the soil may be assumed or calculated from CPT data using other empirical models that have their own uncertainty. The potential biases in the model will also increase when additional assumptions and less certain (non-measured) parameters are included. Therefore, we select a model that optimizes reducing uncertainty of the

available input parameters (i.e., basic vs. post-processed CPT parameters) and the model's prediction performance. This model can be simply and accurately applied to predict Vs from a large CPT database across Metro Vancouver. From this perspective, the MG15_q_c model with the three basic CPT measurements (q_c, f_s, z) is the most appealing CPT parameter combination model and has been shown to provide a good prediction performance based on Metro Vancouver SCPT data compared to the best models. The XGBR MG15_q_c model is selected as the preferred model as it provides the lowest RMSE (0.2 to 1.25 m/s reduction in RMSE; Table 4-4) compared to MLR, NLR, and RFR MG15_q_c for the testing dataset. For reference, the absolute difference in m/s between predicted Vs from the XGBR MG15_q_c model and the RFR_W12_q_t model, which has the lowest RMSE (i.e., best performing model), is calculated for all 2728 CPT-Vs pairs (both training and testing datasets). The maximum absolute difference is 33.83 m/s and the absolute difference average and standard deviation are 4.0 m/s and 3.64 m/s, respectively. Therefore, the XGBR MG15_q_c model, hereafter Assaf, Molnar, El Naggar (AMEN) model, is selected for Vs prediction from CPT (q_c, f_s, z) profiles across Metro Vancouver in this study.

Figure 6 compares the predicted Vs from the AMEN model with the measured Vs for both the testing and training datasets. Although the results are shown coloured by I_c, it is not a parameter in the AMEN model. The comparison demonstrates that the AMEN model does not have any systematic bias in predicting Vs for soils with different I_c categories. The measured-to-predicted Vs ratio for the training dataset is unity for both coarse- and fine-grained soils, which confirms no bias exists. For the testing dataset, the measured-to-predicted Vs ratio is 0.97 and 1 for coarse- and fine-grained soils, respectively. This confirms the robustness of the AMEN model in predicting Vs from CPT measurements for different soils in post-glacial sediments in Metro Vancouver. Although developed for 60 < Vs < 320 m/s, the AMEN model is mainly applicable for Vs < ~285 m/s due to limited samples above this value.

While the machine learning models in this study have enhanced predictions compared to traditional regression approaches, the overall improvement is not large for all the models (~ 1 to 3 m/s reduction in RMSE for training and testing data sets, Table 4-4). This may be expected given the limited number of available CPT predictor variables (3 considered variables in this study). Machine learning algorithms' full potential may be better explored when many predictor variables are involved. In this regard, the inclusion of additional basic and post-processed CPT predictor variables can achieve higher prediction accuracy. To explore this, a regression using XGBR model with a total of 7 predictor variables (q_c, f_s, z, I_c, σ'_v, σ_v, u_2) is performed following the procedure outlined in Figure 4-4. Compared to the AMEN model, the XGBR model with 7 predictor variables leads to an increase of 0.01 in R^2 for both the training and testing dataset, and a decrease of 0.56 m/s and 0.45 m/s in RMSE of the training and testing datasets, respectively. Although the improvement is only marginal, it is expected as additional parameters can better capture the nonlinear relationship between CPT and Vs. Practically, the AMEN model with only basic parameters is still preferred.

One limitation of machine learning models in this study is their inability to extrapolate beyond the parameter ranges the models were trained on (Table 4-1) unlike MLR and NLR approaches. Although Vs < 80 m/s and Vs > 320 m/s from SCPT are rare in Metro Vancouver, MLR and NLR models might be more applicable in those ranges. Moreover, MLR and NLR models provide uncertainty of the predicted Vs, while the machine learning models used in this study do not include uncertainty quantification. In cases where MLR or NLR models are to be used, the A07 model is recommended; while MLR and NLR W12_q_t models provided slightly better predictions than A07 on the testing dataset, however, f_s in W12_q_t model is statistically not significant (Tables B-1 and B-2).
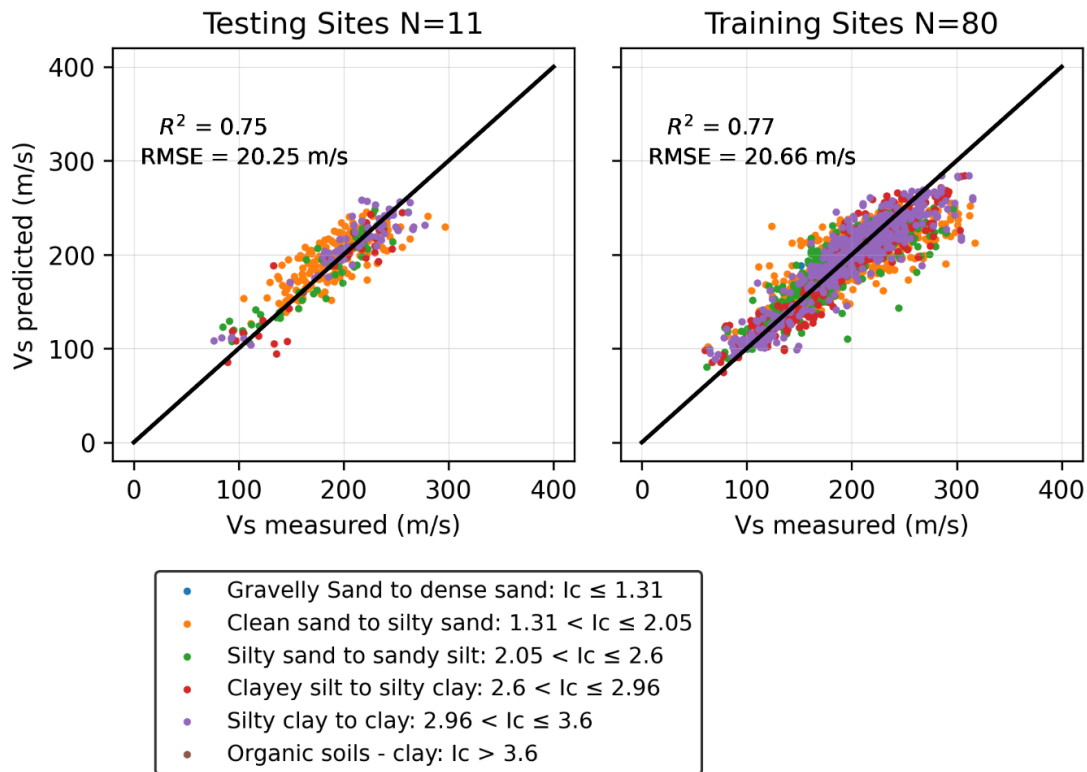
Figure 4-6. Comparison of measured and predicted Vs from the AMEN model for post-glacial sediments in Metro Vancouver coloured by I$_c$ for the testing and training datasets.

We further investigate the AMEN model's performance in terms Vs(z). For selected SCPTs of the training and testing datasets, the AMEN model is used to predict Vs for the given CPT measurements (q$_c$, f$_s$ at 5 cm sampling with depth); since the SCPT's measured Vs has a 1 m sampling with depth, predicted Vs is averaged within the measured Vs depth intervals for comparison. We calculate the depth averaged absolute error (ε̂) in Vs as a percentage (%) for SCPT as follows:

$$\hat{\varepsilon} = 100 \; \frac{1}{n}\sum \frac{|Vs_{measured} - Vs_{predicted}|}{Vs_{measured}} \qquad \textbf{Eq. 4-1}$$

where n is the number of measured Vs samples.

The measured and predicted Vs are first compared for 5 SCPTs selected randomly from the training dataset. Figure 4-7 shows the measured SCPT profiles (q_c, f_s, Vs) as well as I_c profile for the 5 selected sites. Measured interval Vs are plotted as data points at the midpoint of each 1-m sampling interval. The predicted Vs(z) is displayed as a continuous function or line, same as for the CPT profiles. It is obvious that using CPT profiles to predict Vs is conducted at a finer depth sampling than measured in reality during SCPT testing. A relatively small error between measured and predicted Vs values is obtained for the 5 SCPTs; $\hat{\varepsilon}$ ranges between 5.2 % and 11.9 %. Predicted Vs is consistent with measured Vs regardless of I_c, indicating that the AMEN model is capable of predicting Vs in coarse- or fine-grained behaviour soil. The largest deviations in measured and predicted Vs occurs when measured Vs fluctuates and the corresponding CPT data is relatively smooth (e.g., Figure 4-8d). Interestingly, the largest deviations in measured and predicted Vs occur towards the base of the profiles, but is not at a constant depth, rather at points with Vs values greater than 285 m/s. As mentioned previously, this is due to the limited number of data points with Vs > 285 m/s.

Figure 4-8 compares measured and predicted Vs for all 11 SCPTs of the testing dataset that were not included in the AMEN model development. The measured and predicted Vs(z) agree well with $\hat{\varepsilon}$ ranging between 6.8 % and 13.9 % for the 11 testing SCPTs. The largest variations in measured and predicted Vs occur over particular depth intervals at shallow or mid-depths of the SCPT profiles (see Figure 4-8b, d, and g).

$\hat{\varepsilon}$ is a measure of the prediction error that can be anticipated when applying the AMEN model to a CPT measured data. The average $\hat{\varepsilon}$ at all 91 SCPT in Metro Vancouver is 8.8 % and ranges between 4.1 and 19.6 % indicating that the AMEN model is capable of predicting measured Vs with a maximum error < 20 %. Assaf et al. (2022) showed that $\hat{\varepsilon}$ between inverted Vs profiles from non-invasive array measurements and nearby existing downhole, refraction, and SCPT Vs profiles in the FRD is around 18 %. Hence, the

developed AMEN model provides Vs predictions from CPT data with an acceptable error range that is within the expected variability from inter-method *in situ* Vs measurements in post-glacial sediments. For reference, $\hat{\varepsilon}$ for the 91 SCPTs in Metro Vancouver for NLR A07 ranges between 4.3 and 22.3 % with an average of 9.6 %.
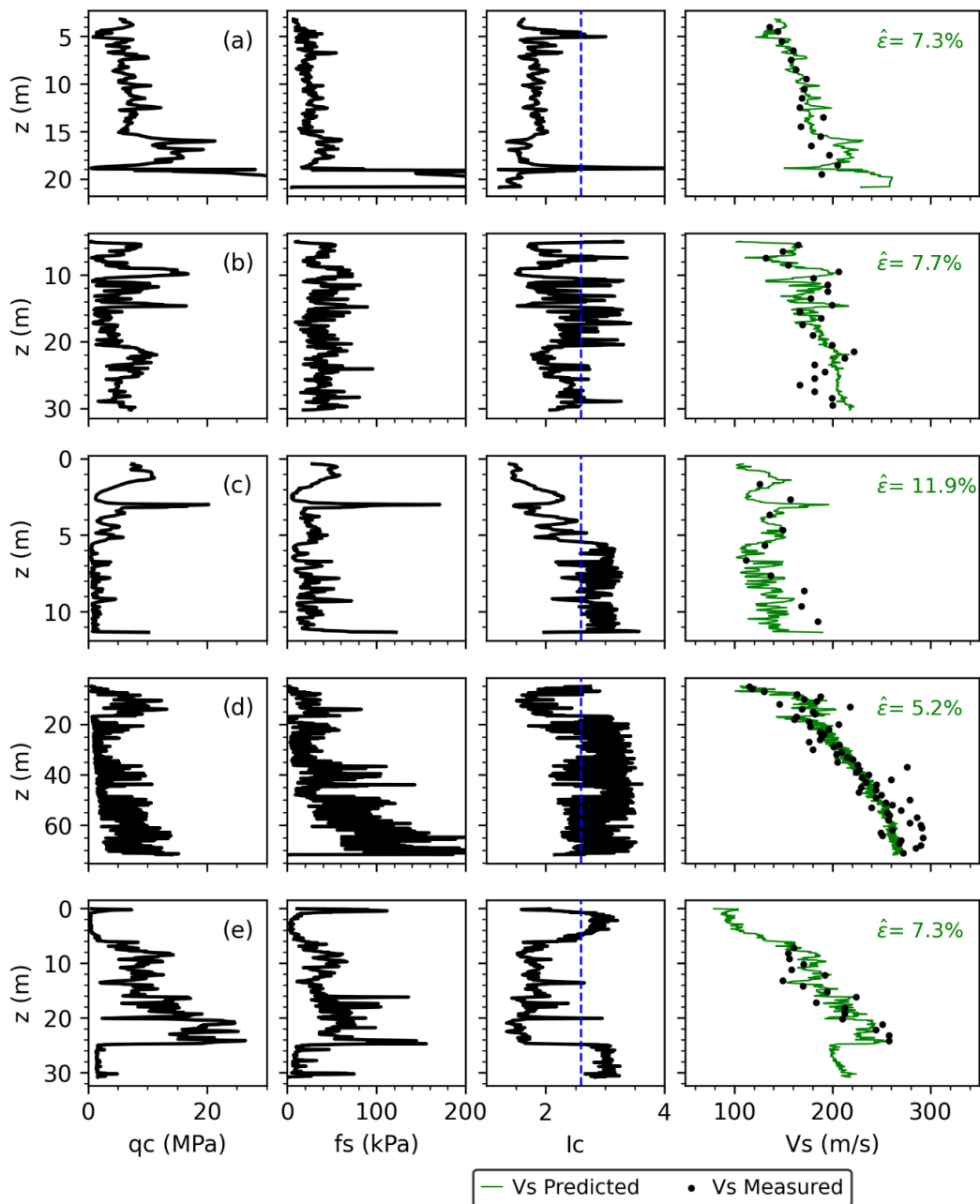
Figure 4-7. Depth profiles of *in situ* SCPT measurements (q_c, f_s, Vs) as well as processed I_c for 5 SCPT sites of the training dataset. Predicted Vs is calculated from q_c and f_s using our developed AMEN model. An I_c value of 2.6 is shown by the dashed blue line; sandy soil behaviour corresponds to $I_c \leq 2.6$ and silt/clay soil behaviour corresponds to $I_c > 2.6$.
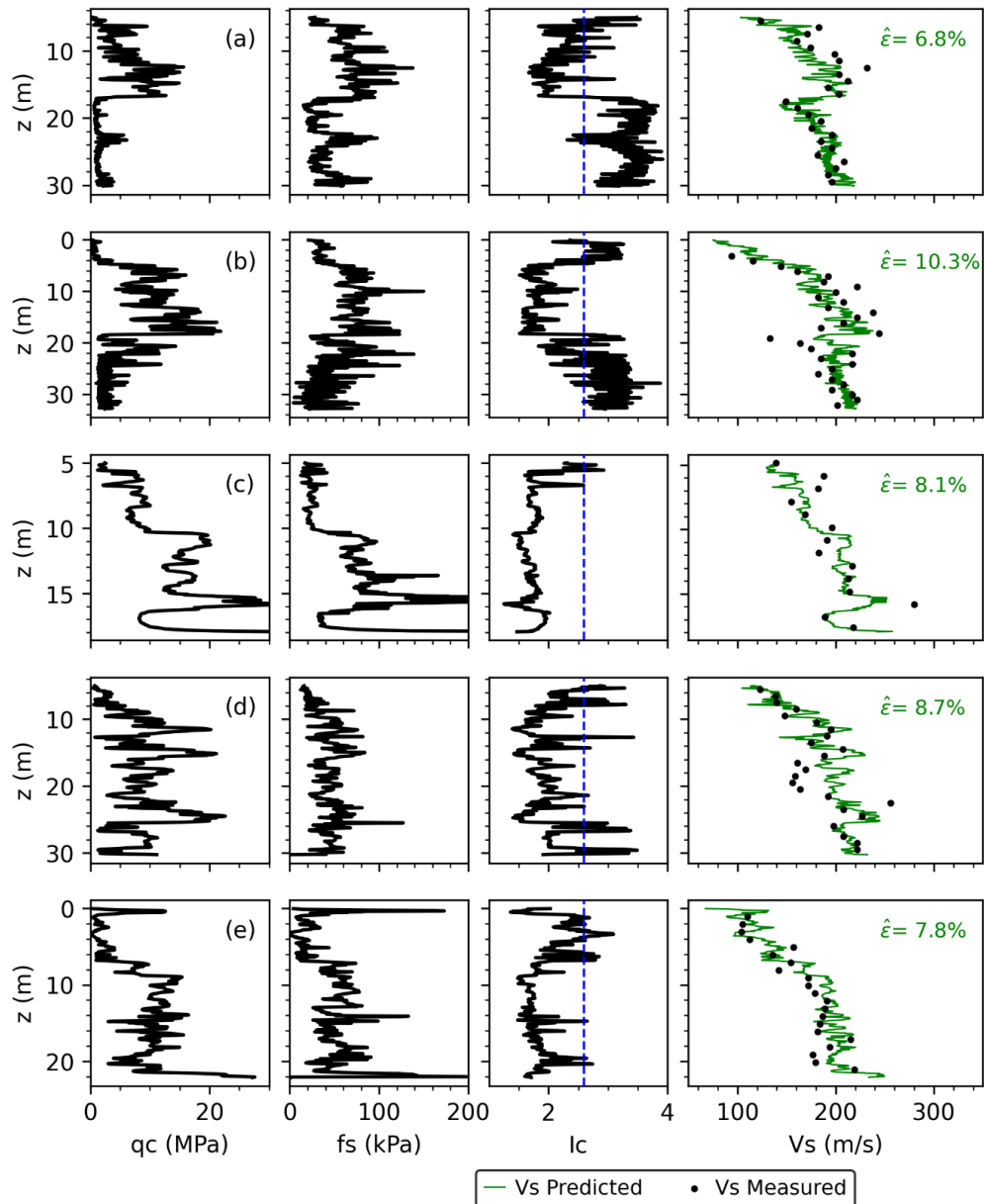
Figure 4-8. Depth profiles of *in situ* SCPT measurements (q$_c$, f$_s$, Vs) as well as I$_c$ for all 11 SCPT sites (see Figure 1) of the testing dataset. Predicted Vs is calculated from q$_c$ and f$_s$ using our developed AMEN model. An I$_c$ value of 2.6 is shown by the dashed blue line; sandy soil behaviour corresponds to I$_c$ ≤ 2.6 and silt/clay soil behaviour corresponds to I$_c$ > 2.6.
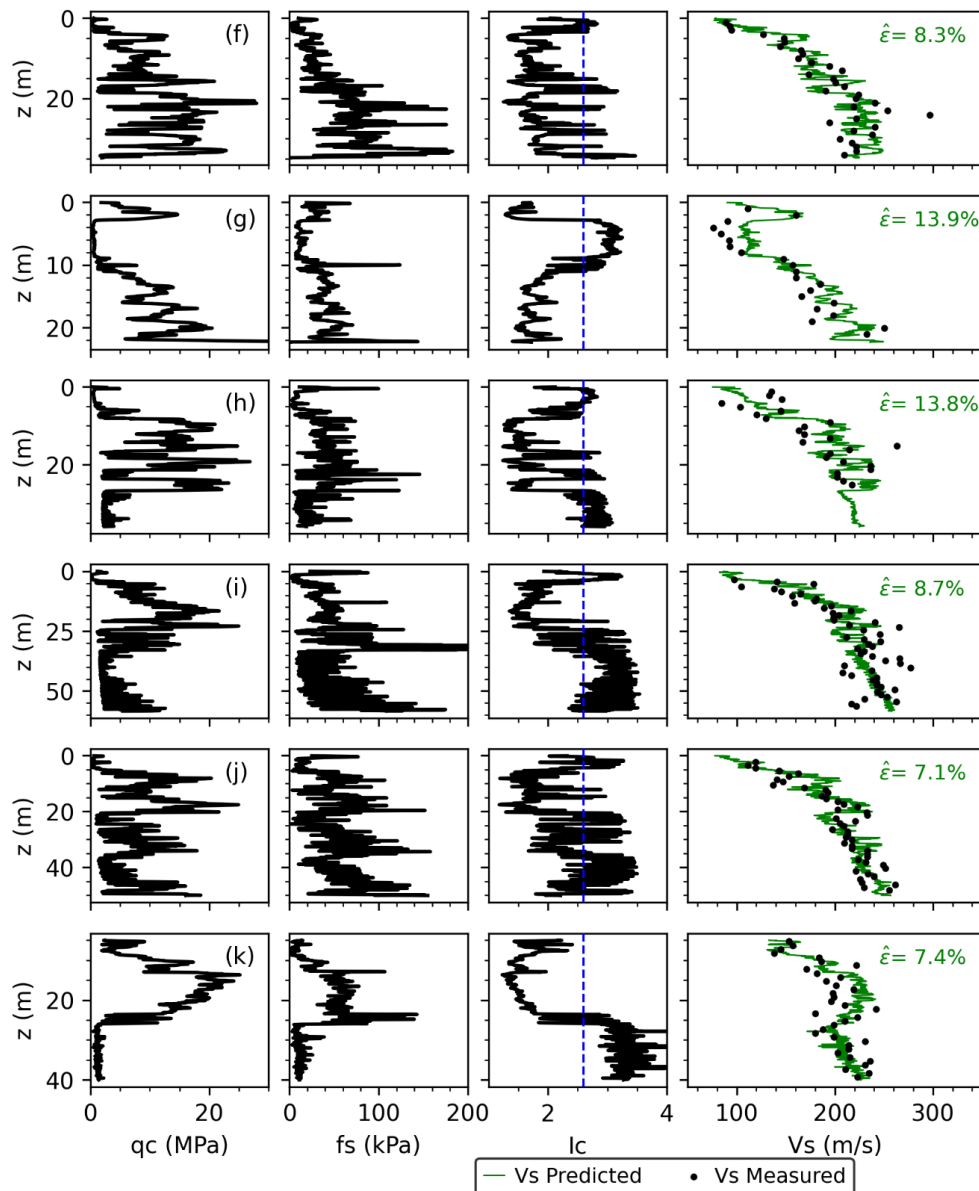
Figure 4-8. Continued.

4.6   AMEN Model Application to CPTs in Metro Vancouver

This section demonstrates the applicability of AMEN model to predicting Vs(z) for post-glacial sediments in Metro Vancouver using only *in situ* CPT measurements. The AMEN model is applied to predict Vs(z) for 59 CPTs compiled from various sources. Figure 4-1 shows that the 59 CPTs are located in mapped geologic units of the Fraser River (41 CPTs), Salish (14), and Capilano (Ce; 4) sediments. Predicted Vs profiles are compared to directly measured Vs(z), obtained from various *in situ* Vs(z) methods, within the same mapped geology units to further assess the performance of AMEN model applied to independent Vs datasets. The direct Vs(z) measurements include 176 Vs profiles from SCPT testing present in the Metro Vancouver project's Vs database of which 90 had available CPT profiles and were used in developing the AMEN model in section 4.3; 1 SCPT profile in FLd unit is not included. For the Fraser River and Salish sediments units, Vs(z) is predicted from 55 CPTs and *in situ* Vs is available from 170 SCPTs. For the Ce unit, Vs(z) is predicted from 4 CPTs and *in situ* Vs is available from 6 SCPTs. Comparison of predicted and measured Vs(z) is accomplished in terms of the average Vs at a 1 m depth sampling. In addition, the predicted and measured Vs(z) are compared to predictions of a published Vs-depth relationship for FRD sediments (Hunter et al. 1999; Hunter et al. 2016) and the average Vs of Capilano sediments (Monahan and Levson 2001). The former is a well-known Vs-z relationship for the FRD developed from downhole, SCPT, and refraction Vs (Hunter et al. 2016), given by:

$$\text{Vs(z)} \ = \ 71.22 \ + \ 35.26z^{0.4362} \pm 2\sigma_{\text{Vs}} \qquad \text{for z} \ \leq 90 \text{ m} \qquad \textbf{Eq. 4-2}$$

where z is the depth in meters and σ_{Vs} is one standard deviation (19.4 m/s). It should be noted that Eq. 4-2 is mistakenly reported in Figure 5 in Hunter and Christian (2001), and the correct equation is found in Figure 2 in Hunter et al. (1999). Vs-z relationships have not been developed for other geologic units; Monahan and Levson (2001) determined the average Vs (and standard deviation) of geologic units but not as a function with depth. At a glaciomarine Capilano sediments site in Langley (included in this study), the average SCPT V_S of over consolidated clays in the shallow desiccated crust and of underlying

normally consolidated clays in the top 30 m are 147 ± 15 m/s and 160 ± 32 m/s, respectively (Monahan and Levson, 2001; hereafter M&L01). Our study is the first to present Vs(z) specific to Ce sediments.

Figure 4-9a compares predicted and measured Vs corresponding to mapped Fraser River and Salish sediments units. CPT profiles and thereby predicted Vs penetrate a maximum of 78 m but are mainly limited to the top 30 m. The scatter of the 55 predicted Vs(z) is expectedly less than that of the 170 SCPTs, especially at z > 30 m due to limited data. Figure 4-9b shows the averaged interval Vs (calculated every 1 m depth increment) of the predicted and measured Vs datasets. The close agreement observed in Figure 4-9b demonstrates that Vs(z) profiles within the Fraser River and Salish sediments can be predicted reliably from independent CPT data using the AMEN model. The averaged predicted and measured Vs(z) are in excellent agreement with each other and also the average FRD Vs(z) from Eq. 4-2 over the upper 22 m. Below 22 m, the averaged predicted Vs(z) is in closer agreement to the averaged measured Vs(z), but both are slightly lower than the average FRD Vs(z). The deviation between predicted and measured Vs(z) at z > 65 m is due to the under-representation of Vs > 280 m/s in CPT-Vs database used for developing the AMEN model. The deviation between measured Vs(z) and the FRD V(z) could be attributed to two reasons: the data reduction in the measured Vs data from SCPT with depth; and the average FRD Vs(z)'s powerlaw gradient functional form is controlled by varying types of *in situ* Vs data (refraction, SCPT, and downhole). The match between Vs_{30} calculated from averaged predicted Vs(z) (167 m/s) and that calculated from averaged measured and averaged FRD Vs(z) (172 m/s for both) confirms the applicability of the AMEN model to predict Vs_{30} for FRD sediments.

Figure 4-10a shows measured and predicted Vs(z) in Ce unit, and Figure 4-10b shows their average along with the M&L01 average Vs(z) of the crust and the underlying normally consolidated clays and the average FRD Vs(z) from Eq. 4-2. Although only one SCPT in Ce geology unit was included in the development of the AMEN model, the averaged predicted and measured Vs(z) are in good agreement to a z of 30 m. M&L01 is obtained

from one measured Vs(z) at a site composed of clays to a depth of 52 m. This profile is one of the 6 measured SCPTs included in this study. The remaining 5 measured Vs(z) as well as the 4 predicted Vs(z) are lower than M&L01 in the upper 14 m as shown in Figure 4-10b. Vs_{30} of 135 m/s and 136 m/s are calculated from predicted and measured averaged Vs(z), respectively; both are lower than the 160 m/s average Vs in top 30 from M&L01. The predicted and measured Vs(z) are new information on the Vs(z) of Ce units in in Metro Vancouver. Average FRD Vs(z) expectedly overestimates both measured and predicted Vs(z) in Ce unit at z < 30 m and slightly overestimate measured Vs(z) from one site at z > 30 m. This overestimation is attributed to the presence of thick, soft silts and clays in Ce unit, unlike FRD sediments where topset channel sands prevail between few meters from the surface and z up to 40 m. Predicted Vs(z) from AMEN model point out the inapplicability of the average FRD Vs(z), as confirmed by measured SCPT profiles, and presents new information on Vs(z) of Ce unit.

The proposed AMEN model is validated by demonstrating its ability to accurately predict the Vs(z) profiles from independent CPT profiles in the FRD and in Ce geology unit east of Metro Vancouver. The developed CPT-Vs models in this study are important tools for microzonation mapping and site effect estimation. Additional applications of these models include comparing site-specific liquefaction CPT- and Vs-based methods and mapping Vs_{30} across the region.
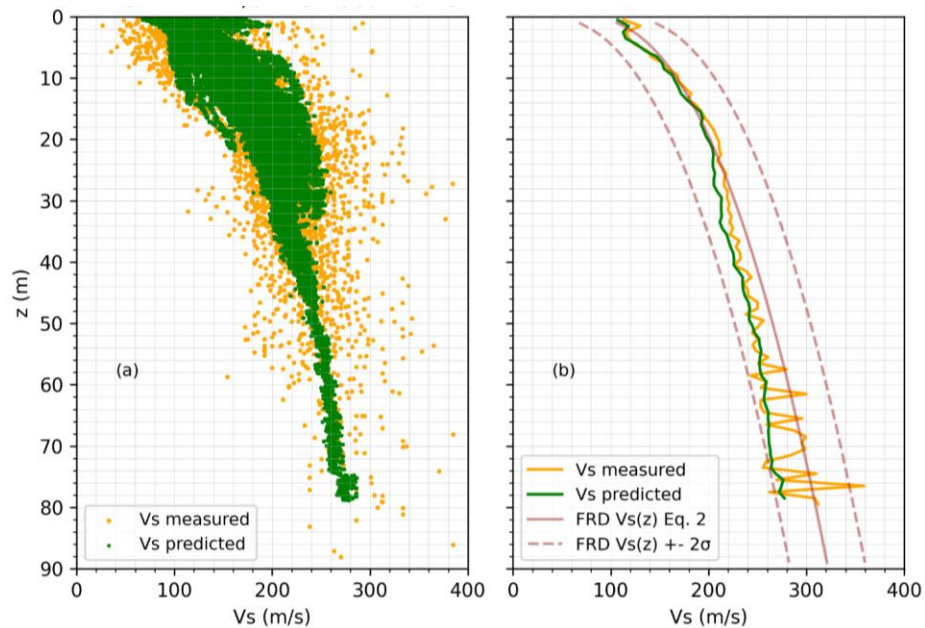
Figure 4-9. (a) AMEN model predicted Vs compared to measured SCPT Vs specific to Fraser River and Salish sediments. The Vs values in (a) are averaged at each 1 m depth increment and plotted as continuous Vs(z) in (b) in comparison to the average FRD Vs(z) of Hunter et al. (1999).
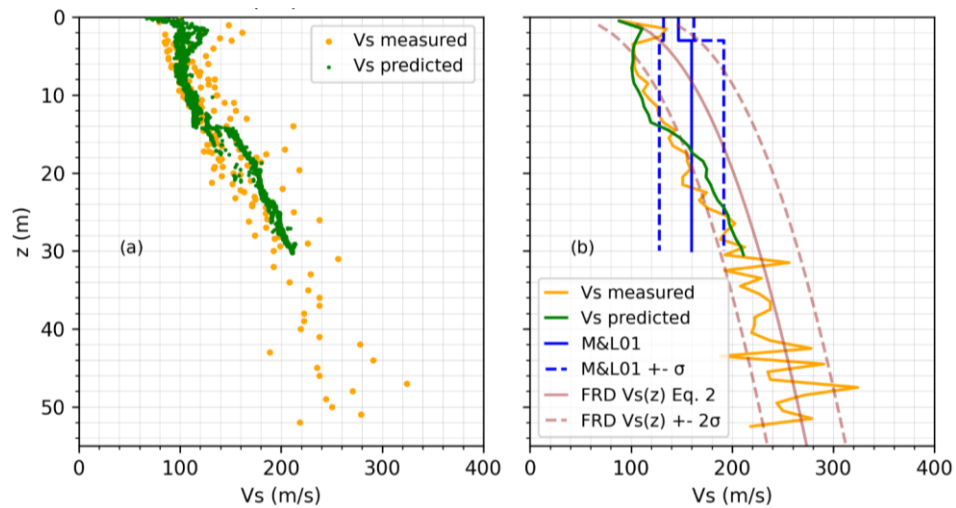
Figure 4-10. Vs profiles in Capilano Ce geology unit (a) AMEN model predicted Vs with measured Vs from SCPT, (b) predicted and measured average Vs(z) in comparison to average M&L01 and FRD Vs(z).

4.7   Conclusions

A comprehensive SCPT database for post-glacial sediments in Metro Vancouver is compiled to understand region-specific correlations between CPT parameters and Vs. 6 existing CPT-Vs models with various CPT parameters combinations were evaluated in terms of their predicted Vs with the measured Vs of the compiled SCPT database. Existing CPT-Vs models are found to be biased in predicting Vs in Metro Vancouver. Development of region-specific CPT-Vs models is therefore necessary. A total of 24 CPT-Vs models are developed from a training SCPT dataset using four regression approaches and six CPT parameters combinations. The regression approaches include traditional multi-linear and non-linear regressions, and supervised machine learning ensemble regressions, Random Forest and Extreme Gradient Boosting. The machine learning models slightly outperform the multi-linear and nonlinear regressions in a fair comparison using a testing SCPT dataset not included in development of the models. The performance of the models within a regression approach doesn't significantly improve when processed CPT parameters are used instead of basic parameters. For practicality reasons, one of the 24 developed CPT-Vs models, the AMEN model, based on Extreme Gradient Boosting regression and basic CPT parameters (q_c, f_s, z) is selected as the preferred CPT-Vs model for regional application in this study. The AMEN model reliably predicts coarse- and fine-grained soil Vs with a maximum depth-averaged absolute error of 19.6 %, consistent with the ~ 18% Vs variability from various *in situ* Vs(z) methods in the FRD (Assaf et al. 2022). Application of the AMEN model is demonstrated by predicting Vs(z) given 59 CPT profiles within Metro Vancouver. Comparison of the average predicted Vs(z) with the average measured Vs(z) from SCPTs as well as previous average Vs(z) profiling in similar geologic units generally agrees for FRD & Salish sediments and is relatively new information for Ce units. The CPT-Vs prediction models developed in this study offer useful tools for seismic site characterization in Metro Vancouver and can be employed to: (1) develop Vs profiles for 1D and 2D site response analysis, (2) compare CPT- and Vs-based liquefaction evaluation methods, and (3) map Vs_{30}.

4.8   Data & Resources

The CPT digital data within the compiled Metro Vancouver seismic microzonation database used in this study is provided by Patrick Monahan and from geotechnical reports provided by GeoPacific Consultants Ltd, and City of Vancouver. Vs profiles from SCPT testing within the compiled Metro Vancouver project database are obtained from Hunter et al. (2016), GeoPacific Consultants Ltd, City of Vancouver, City of Delta, and Patrick Monahan. SCPT digital data are provided by Golder Associates Ltd. from the Seismic Assessment and Geotechnical Investigation of Lower Mainland Dikes project. The majority of SCPT testing in the described data sources was performed by ConeTec.

MLR and RFR models are developed using Scikit-learn (Sklearn) Python package (v 1.1.1). XGBR is conducted in XGBoost Python package (v 1.6.1). NLR is conducted using lmfit Python package (v.1.0.3). The hyper-parameter tuning procedure for RFR and XGBR models is implemented in Sklearn Python package (v 1.1.1).

4.9   Acknowledgements

4.10 References

Adhikari, S.R., Molnar, S. (2021). Significance of geodatabase development for seismic microzonation in Metropolitan Vancouver. In: 17th World Conference on Earthquake Engineering, 27 Sept. – 2 Oct. 2021, Sendai, Japan, Paper 4521.

Amjad, M., Ahmad, I., Ahmad, M., Wróblewski, P., Kamiński, P., & Amjad, U. (2022). Prediction of pile bearing capacity using XGBoost algorithm: modeling and performance evaluation. Applied Sciences, 12(4), 2126.

Andrus, R. D., Mohanan, N. P., Piratheepan, P., Ellis, B. S., & Holzer, T. L. (2007). Predicting shear-wave velocity from cone penetration resistance. Proceedings of the 4th International Conference on Earthquake Geotechnical Engineering, 1454.

Armstrong, J.E., Hicock, S.R. (1979). Geological Survey of Canada, "A" Series Map 1486A, 1979, 1 sheet,. https://doi.org/https://doi.org/10.4095/108876

Assaf, J., Molnar, S., El Naggar, M. H., & Sirohey, A. (2022). Seismic site characterization in Fraser River Delta in Metropolitan Vancouver. Soil Dynamics and Earthquake Engineering, 161, 107384. https://doi.org/https://doi.org/10.1016/j.soildyn.2022.107384

Athanasopoulos, G.A., Zervas, C.S. (1993). Effects Of Ridge-like Surface Topography On Seismic Site Response. In: Carmak AS, Brebbia CA, editors. Proceedings of 6th international conference on soil dynamics and earthquake engineering, Computational Mechanics Publications, Southampton, pages 16.

Baghbani, A., Choudhury, T., Costa, S., Reiner, J. (2022). Application of artificial intelligence in geotechnical engineering: A state-of-the-art review. Earth-Science Reviews 228:103991. https://doi.org/https://doi.org/10.1016/j.earscirev.2022.103991

Bard, P.Y., Bouchon, M. (1985). The two-Dimensional Resonance of Seidments-Filled Valleys. Bulletin of the Seismological Society of Americ 75:519–54

Bilson Darko, A., Molnar, S., & Sadrekarimi, A. (2020). Blind comparison of non-invasive shear wave velocity profiling with invasive methods at bridge sites in Windsor, Ontario. Soil Dynamics and Earthquake Engineering, 129. https://doi.org/10.1016/j.soildyn.2019.105906

Borcherdt, R.D. (1970). Effects of Local Geology on Ground Motion Near San Francisco Rbay. Bulletin of the Seismological Society of America 60:29–61

Borcherdt, R.D. (1994). Estimates of Site-Dependent Response Spectra for Design (Methodology and Justification). Earthquake Spectra 10:617–653

Breiman, L. (2001). Random Forests. Machine Learning 45:5–32. https://doi.org/10.1023/A:1010933404324

Britton J.R., Harris J.B., Hunter J.A., Luternauer J.L. The bedrock surface beneath the Fraser River delta in British Columbia based on seismic measurements. Current Research 1995;83–89.

Chen, T., Guestrin, C. (2016). Xgboost: a scalable tree boosting system. In: Proceedings of the 22nd Acm Sigkdd International Conference on Knowledge Discovery and Data Mining, ACM (2016), pp. 785-794

Clague, J. K., Naesgaard, E., and Sy, A. (1992). Liquefaction features on the Fraser delta: evidence for prehistoric earthquakes?, Canadian Journal of Earth Science, v. 29, p. 1734-1745

Clague, J.J., Luternauer, J.L., Monahan, P.A., Edwardson, K.A., Dallimore, S.R., and Hunter, J.A., (1998). Quaternary stratigraphy and evolution of the Fraser delta; in Geology and Natural Hazards of the Fraser River Delta, British Columbia, (ed.) J.J. Clague, J.L. Luternauer, and D .C. Mosher; Geological Survey of Canada, Bulletin 525, p. 57-90.

Dickenson, S. (1994). Dynamic Response of Soft and Deep Cohesive Soils during the Loma Prieta Earthquake of October 17, 1989. PhD, University of California

Dietterich, T.G. (2000). Ensemble Methods in Machine Learning BT - Multiple Classifier Systems. Springer Berlin Heidelberg, Berlin, Heidelberg, pp 1–15

Dikmen, Ü. (2009). Statistical correlations of shear wave velocity and penetration resistance for soils. Journal of Geophysics and Engineering 6:61–72. https://doi.org/10.1088/1742-2132/6/1/007

Dunn, D., Ricketts, B. (1994). Surficial Geology of Fraser Lowlands Digitized From GSC Maps 1484A, 1485A, 1486A, and 1487A. Geologic Survey of Canada Open File 2894

Entezari, I., Sharp, J., Mayne, P.W. (2022). A data-driven approach to predict shear wave velocity from CPTu measurements. In: GeoCalgary 2022. 6 pages

Entezari, I., Sharp, J., Mayne, P.W. (2021). Soil unit weight estimation using the cone penetration test and machine learning. In: Proc. GeoNiagara 2021, Niagara Falls, Canada. 8 pages

Erharter, G. H., Oberhollenzer, S., Fankhauser, A., Marte, R., & Marcher, T. (2021). Learning decision boundaries for cone penetration test classification. Computer-Aided Civil and Infrastructure Engineering, 36(4). https://doi.org/10.1111/mice.12662

Friedman, J.H. (2001). Greedy function approximation: A gradient boosting machine. The Annals of Statistics 29:1189–1232. https://doi.org/10.1214/aos/1013203451

Garofalo, F., Foti, S., Hollender, F., Bard, P. Y., Cornou, C., Cox, B. R., Ohrnberger, M., Sicilia, D., Asten, M., di Giulio, G., Forbriger, T., Guillier, B., Hayashi, K., Martin, A., Matsushima, S., Mercerat, D., Poggi, V., & Yamanaka, H. (2016a). InterPACIFIC project: Comparison of invasive and non-invasive methods for seismic site characterization. Part I: Intra-comparison of surface wave methods. Soil Dynamics and Earthquake Engineering, 82. https://doi.org/10.1016/j.soildyn.2015.12.010

Garofalo, F., Foti, S., Hollender, F., Bard, P. Y., Cornou, C., Cox, B. R., Dechamp, A., Ohrnberger, M., Perron, V., Sicilia, D., Teague, D., & Vergniault, C. (2016b). InterPACIFIC project: Comparison of invasive and non-invasive methods for seismic site characterization. Part II: Inter-comparison between surface-wave and borehole methods. Soil Dynamics and Earthquake Engineering, 82. https://doi.org/10.1016/j.soildyn.2015.12.009

GEOLOGISMIKI Geotechnical Software (2014). CPeT-IT User's Manual v.1.4

Hegazy, Y., Mayne, P. (2006). A Global Statistical Correlation between Shear Wave Velocity and Cone Penetration Data. Proceedings of the GeoShanghai, site and geomaterial characterization (GSP 149). Reston, VA: ASCE; 243–8

Hunter, J.A., Christian, H.A., Harris, J.B., Britton, J.R., Luternauer, J.L. (1999). Mapping shear-wave velocity structure beneath the Fraser River delta sediments–Preliminary results. InProceedings 8th Canadian Conference on Earthquake Engineering (pp. 13-16).

Hunter, J.A., Christian, H.A. (2001). Use of Shear Wave Velocities to Estimate Thick Soil Amplification Effects in the Fraser River Delta, British Columbia. In: Symposium on the Application of Geophysics to Engineering and Environmental Problems (SAGEEP), Match 4-7, 2001, Denver, Colorado. Environment and Engineering Geophysical Society

Hunter, J.A., Crow, H.L. (2015). Shear wave velocity measurement guidelines for Canadian seismic site characterization in soil and rock. Natural Resources Canada. https://doi.org/10.4095/297314

Hunter, J.A., Crow, H.L., Brooks, G.R., Pyne, M., Lamontagne, M., Pugin, A.J.M., Pullan, S.E., Cartwright, T., Douma, M., Burns, R.A. and Good, R.L. (2010). Seismic Site Classification and Site Period Mapping in the Ottawa Area Using Geophysical Methods. Geological Survey of Canada Open File 6273.

Hunter, J. A., Burns, R. A., Good, R. L., & Pelletier, C. F. (2016). Fraser River Delta–A compilation of shear wave velocities and borehole geophysics logs in unconsolidated sediments of the Fraser River Delta, British Columbia. Geological Survey of Canada Open File, 1-112.

Javanbakht, A., Molnar, S., Sadrekarimi, S. (2021). Liquefaction hazard mapping using geostatistical method in Richmond, British Columbia, Canada. 17th World Conference on Earthquake Engineering, 27 Sept. – 2 Oct. 2021, Sendai, Japan, Paper 4625.

Kruiver, P. P., de Lange, G., Kloosterman, F., Korff, M., van Elk, J., & Doornhof, D. (2021). Rigorous test of the performance of shear-wave velocity correlations derived from CPT soundings: A case study for Groningen, the Netherlands. Soil Dynamics and Earthquake Engineering, 140, 106471. https://doi.org/https://doi.org/10.1016/j.soildyn.2020.106471

McGann, C. R., Bradley, B. A., & Jeong, S. (2018). Empirical correlation for estimating shear-wave velocity from cone penetration test data for Banks Peninsula loess soils in Canterbury, New Zealand. Journal of Geotechnical and Geoenvironmental Engineering, 144(9), 04018054.

McGann, C. R., Bradley, B. A., Taylor, M. L., Wotherspoon, L. M., & Cubrinovski, M. (2015). Development of an empirical correlation for predicting shear wave velocity of Christchurch soils from cone penetration test data. Soil Dynamics and Earthquake Engineering, 75. https://doi.org/10.1016/j.soildyn.2015.03.023

Molnar, S., Assaf, J., Sirohey, A., & Adhikari, S. R. (2020). Overview of local site effects and seismic microzonation mapping in Metropolitan Vancouver, British Columbia, Canada. Engineering Geology, 270, 105568. https://doi.org/https://doi.org/10.1016/j.enggeo.2020.105568

Molnar S., Dosso S.E., Cassidy J.F. Bayesian inversion of microtremor array dispersion data in southwestern British Columbia. Geophys J Int 2010;183(2):923–940.

Monahan, P. (1999). The Application of Cone Penetration Test Data to Facies Analysis of the Fraser River Delta, British Columbia; PhD Dissertation, University of Victoria.

Monahan. P., Levson, V. (2001). Development of a shear-wave velocity model of the near-surface deposits of southwestern British Columbia, Canada. in Proceedings: Fourth International Conference on Recent Advances in Geotechnical Earthquake Engineering and Soil Dynamics, San Diego, California, March 26–31, 2001, Paper 11-16, 12 p

NBCC2015. (2015). National Building Code of Canada 2015. National Research Council of Canada, Ottawa, NRCC 56190 Vol 1 & 2.

Newville, M., Otten, R., Nelson, A., Ingargiola, A., Stensitzki, T., Allan, D., Fox, A., Carter, F., Michał, Osborn, R., Pustakhod, D., lneuhaus, Weigand, S., Glenn, Deil, C., Mark, Hansen, A. L. R., Pasquevich, G., Foks, L., … Persaud, A. (2021). lmfit/lmfit-py: 1.0.3. https://doi.org/10.5281/ZENODO.5570790

Pippi, M., Vink, R., Haasnoot, J., & Bersan, S. (2022). Automated CPT interpretation with a Convolutional Neural Network. In Cone Penetration Testing 2022 (pp. 646-650). CRC Press.

Reale, C., Gavin, K., Librić, L., & Jurić-Kaćunić, D. (2018). Automatic classification of fine-grained soils using CPT measurements and Artificial Neural Networks. Advanced Engineering Informatics, 36, 207-215.

Robertson, P.K. (2009). Interpretation of cone penetration tests — a unified approach. Canadian Geotechnical Journal 46:1337–1355. https://doi.org/10.1139/T09-065

Robertson, P.K., Cabal, K.L. (2010). Estimating soil unit weight from CPT. In: 2nd International Symposium on Cone Penetration Testing, Huntington Beach, CA, USA. Volume 2&3: Technical Papers, Session 2: Interpretation, Paper No. 40

Robertson, P.K., Woeller, D.J., Hunter, J., Luternauer, J. (1992). Seismic Techniques to Evaluate Liquefaction Potential. In: 45th Canadian Geotechnical Conference, Toronto, October, 10 pages

Robertson, P.K., Wride CE (1998). Evaluating cyclic liquefaction potential using the cone penetration test. Canadian Geotechnical Journal 35:442–459. https://doi.org/10.1139/t98-017

Sirohey, A. (2022). Soil amplification and peak frequencies from thousands of passive seismic measurements across metro Vancouver, British Columbia, Canada. London, Ontario: The University of Western University.

Salsabili, M., Saeidi, A., Rouleau, A., Nastev, M. (2022). Development of empirical CPTu-Vs correlations for post-glacial sediments in Southern Quebec, Canada, in consideration of soil type and geological setting. Soil Dynamics and Earthquake Engineering 154:107131. https://doi.org/https://doi.org/10.1016/j.soildyn.2021.107131

Seed, B.H., Wong, T.R., Idriss, I.M., Tokimatsu, K. (1986). Moduli and Damping Factors for Dynamic Analyses of Cohesionless Soils. Journal of Geotechnical Engineering 112:1016–1032. https://doi.org/10.1061/(ASCE)0733-9410(1986)112:11(1016)

Seed, H., Idriss, I.M. (1970). Soil moduli and damping factors for dynamic response analyses. TechnicalReport EERRC-70-10, University of California, Berkeley

Shearer, P.M., Orcutt, J.A. (1987). SURFACE AND NEAR-SURFACE EFFECTS ON SEISMIC WAVES-- THEORY AND BOREHOLE SEISMOMETER RESULTS. Bulletin of the Seismological Society of America 77:1168–1196

Tong, L.Y., Che, H.B., Zhang, M.F., Pan, H.S. (2018). Determination of shear wave velocity of Yangtze Delta sediments using seismic piezocone tests. Transportation Geotechnics 14:29–40. https://doi.org/https://doi.org/10.1016/j.trgeo.2017.09.005

Wang, M. X., Huang, D., Wang, G., & Li, D. Q. (2020). SS-XGBoost: a machine learning framework for predicting newmark sliding displacements of slopes. *J Geotech Geoenviron Eng*, *146*(9), 04020074.

Wair, B., DeJong, J., Shantz, T. (2012). Guidelines for estimation of shear wave velocity profiles. Berkeley: Pacific Earthquake Engineering Research Center, University of California PEER report no 2012/08;

Wu, S., Zhang, J-M., Wang, R. (2021). Machine learning method for CPTu based 3D stratification of New Zealand geotechnical database sites. Advanced Engineering Informatics 50:101397. https://doi.org/https://doi.org/10.1016/j.aei.2021.101397

Yang, Z., Cui, Y., Guo, L., Liu, X., Jia, C., Shi, W., & Ling, X. (2022). Semi-empirical correlation of shear wave velocity prediction in the Yellow River Delta based on CPT. Marine Georesources & Geotechnology, 40(4), 487–499. https://doi.org/10.1080/1064119X.2021.1913458

Zhang C., Ma Y., editors Ensemble Machine Learning: Methods and Applications. Springer Science & Business Media; 2012

Zhang, R., Wu, C., Goh, A. T. C., Böhlke, T., & Zhang, W. (2021). Estimation of diaphragm wall deflections for deep braced excavation in anisotropic clays using ensemble learning. Geoscience Frontiers, 12(1). https://doi.org/10.1016/j.gsf.2020.03.003

Zhang, W., Wu, C., Zhong, H., Li, Y., & Wang, L. (2021). Prediction of undrained shear strength using extreme gradient boosting and random forest based on Bayesian optimization. Geoscience Frontiers, 12(1). https://doi.org/10.1016/j.gsf.2020.03.007

Zhang, W. G., Li, H. R., Wu, C. Z., Li, Y. Q., Liu, Z. Q., & Liu, H. L. (2021). Soft computing approach for prediction of surface settlement induced by earth pressure balance shield tunneling. Underground Space (China), 6(4). https://doi.org/10.1016/j.undsp.2019.12.003

Zhou, J., Shi, X., Du, K., Qiu, X., Li, X., and Mitri, H.S. (2016). Feasibility of random-forest approach for prediction of ground settlements induced by the construction of a shield-driven tunnel, International Journal of Geomechanics, 17(6): 04016129

Zhou, J., Qiu, Y., Armaghani, D. J., Zhang, W., Li, C., Zhu, S., & Tarinejad, R. (2021). Predicting TBM penetration rate in hard rock condition: A comparative study among six XGB-based metaheuristic techniques. Geoscience Frontiers, 12(3). https://doi.org/10.1016/j.gsf.2020.09.020

Chapter 5

5   Development of Average Vs(z) for Different Sediment Types and Proxy-based Vs_{30} Prediction Models for Metro Vancouver

In this chapter, a comprehensive shear-wave velocity (Vs) database for Metro Vancouver is compiled from various *in situ* invasive and non-invasive Vs(z) measurements. Invasive Vs(z) measurements are used to develop average Vs(z) relationships for major sediment types in the region. Further, a Vs_{30} database is established from the Vs(z) database and used to calibrate an extrapolation model to calculate Vs_{30} from Vs_{zp}, where zp is the maximum profile depth < 30 m. Available *in situ* Cone Penetration Test (CPT) data and surface wave dispersion curves from non-invasive seismic testing are converted to Vs_{30} using region-specific correlations. The compiled Vs_{30} database from direct Vs and other *in situ* measurements is used to develop region-specific Vs_{30} prediction models based on Vs_{30} proxies: geology, topographic slope, and depth to glacial till (z_{gl}). Two hybrid proxy-based Vs_{30} prediction models based on geology and slope (geology-slope), and geology and z_{gl} (geology-z_{gl}) are developed for the Metro Vancouver region. Final recommendations on Vs_{30} mapping using the recommended models are provided.

5.1   Introduction

Seismic site effects describe the effect of local near surface geologic conditions on the propagating seismic waves. Site amplification, the increase in surface ground motion amplitude at a site relative to shaking amplitude at the base of the soil due to reduction in seismic impedance (product of velocity and density) towards surface and soil resonance when impedance contrast(s) are large, is a 1D seismic site effect most commonly identified by seismic site characterization studies. Site characteristics include the variability of soil stiffness with depth (z), characterized by shear wave velocity profile Vs(z) (Borcherdt 1970) and the subsurface geometry and depth to impedance boundaries (Shearer and Orcutt 1987, Bard and Bouchon 1985). Borcherdt (1994) proposed employing the time-averaged Vs in the top 30 m, Vs_{30}, as a simple and quantitative measure to categorize seismic site

conditions. Other site characteristic quantities (e.g., site period, T_0) have recently been shown to correlate, equally or even better than Vs_{30}, with observed site amplification in specific cases (Zhao and Xu, 2013, Hassani et al. 2018; Zhu et al. 2022). However, Vs_{30} remains the most widely used site characteristic quantity to incorporate 1D site amplification in seismic hazard assessment and seismic design applications.

The Canadian seismic site characterization guideline (Hunter and Crow, 2015) describes various *in situ* methods to measure $Vs(z)$, including invasive methods (crosshole, downhole, P-S suspension, and Seismic Cone Penetration Test, SCPT) and non-invasive methods (seismic refraction and various surface wave dispersion methods such as Spectral Analysis of Surface Waves (SASW), active-source Multi-channel Surface Wave Analysis (MASW) and microtremor array method (MAM). Several studies have shown that the differences in $Vs(z)$ and Vs_{30} between different invasive and non-invasive measurement methods are insignificant (e.g., Garofalo et al. 2016; Assaf et al. 2022, Bilson Darko et al. 2020). Assaf et al. (2022) showed that the absolute relative difference in the average $Vs(z)$ and Vs_{30} between non-invasive surface wave and nearby existing invasive and non-invasive measurements in the Fraser River Delta (FRD) of Metropolitan (Metro) Vancouver are on average about 18 % and 7.7 %, respectively. It is common that measured $Vs(z)$ may not extend to 30 m depth, and thus several extrapolation methods to obtain Vs_{30} from Vs_{zp} and/or $Vs(zp)$, where zp is the maximum available profile depth, have been proposed (e.g., Boore 2004; Boore et al. 2011; Dai et al. 2013; Wang and Wang 2015).

Many other *in situ* methods exist and empirical relationships to convert their measures to $Vs(z)$ or Vs_{30} are very common (Wair et al. 2012), such as Standard Penetration Test (SPT) (e.g., Seed et al. 1986), CPT (e.g., McGann et al. 2015; Assaf et al. 2023), and field shear-vane measurements (e.g., Dickenson 1994). These empirical relationships were originally developed for geotechnical site-specific design applications; however, due to the availability of large database of *in situ* measurements from regional studies (e.g., McGann et al. 2017; Adhikari 2021; Assaf et al. 2023), their use in regional $Vs(z)$ mapping have become popular. Additionally, obtaining Vs_{30} directly from surface wave dispersion curves

from multi-method non-invasive testing, without the need for inversion, have been explored (e.g., Martin & Diehl 2004; Lin 2021; Comina et al. 2022).When *in situ* measurements are not available, regional average (generic) Vs(z) distributions determined for similar soil types (e.g., same stratigraphy or mapped geologic unit) may be used with borehole lithology or a three-dimensional (3D) geological model to predict Vs(z), Vs_z, or Vs_{30} at a specific site or for a region (e.g., Motazedian et al. 2011; Rosset et al. 2015; Nastev et al. 2016; Foulon et al. 2018; Salsibili et al. 2021). In Metro Vancouver, Hunter et al. (1999) (Hunter99) derived a power law Vs(z) relationship for combined FRD post-glacial sediments from Geologic Survey of Canada (GSC) testing (Hunter et al. 1998, 2016). Additionally, Monahan and Levson (2001) (M&L01) developed Vs_z model for different sediments in southwestern BC (not z dependent). Glacial and Tertiary rock sediments Vs in the M&L01 model were assigned based on Hunter et al. (1999) recommendations from the GSC testing in the FRD.

The need for Vs_{30} maps for regional quantification of seismic hazard and risk (e.g., ShakeMaps, loss maps) motivated development of time- and cost-efficient proxy-based Vs_{30} prediction models. These models are based on widely available proxies/predictors such as mapped surficial geology (e.g., Wills and Clahan 2006), topographic slope (e.g., Allen and Wald 2007), and terrain classification (e.g., Iwahashi and Pike 2007; Yong et al. 2012; Iwahashi et al. 2018) or a combination of them (e.g., Thompson et al. 2014; Wills et al. 2015; Parker et al. 2017; Ahdi et al. 2017; Foster et al. 2019). Proxy-based Vs_{30} prediction methods are generally anchored on *in situ* Vs_{30} measurements and geostatistical frameworks to establish correlations between Vs_{30} and the selected readily available proxies. Such Vs_{30} prediction models typically exhibit strong regional dependency due to the unique geologic processes and depositional environments prevalent in a specific region. Vs_{30} variability is best captured using region-specific measurements if available, otherwise models developed for other regions should be evaluated prior to their application in an alternate region. Ahdi et al. (2017) developed a hybrid Vs_{30} model based on categories of geology and topographic slope for the Pacific Northwest (PNW) region of North America from Vs_{30} measurements in Washington, Oregon, Alaska, and Metro Vancouver.

The Metro Vancouver seismic microzonation project (Molnar et al. 2020, Adhikari and Molnar 2021) has developed the most comprehensive geodatabase (Borehole lithology, Vs, CPT, SPT, etc.) from open and proprietary sources for the region to date. This study compiles the Metro Vancouver seismic microzonation project's comprehensive Vs(z) database to develop generic average Vs(z) relationships for the major sediment types in the region. Although M&L01 published average Vs_z of major geologic units, a Vs(z) relationship has only been developed for the FRD post-glacial sediments (Hunter99; Hunter et al. 1999). Additionally, a Vs_{30} database is compiled from available Vs(z) that extend to $zp \geq 30$ m, and further used to calibrate a Vs_{zp}-to-Vs_{30} model to calculate Vs_{30} when $zp <$ 30 m. Additional *in situ* CPT profiles and dispersion curves from combined active-and passive-source surface wave testing are compiled from the project's geodatabase and converted to Vs_{30} using Metro Vancouver specific correlations. The comprehensive Vs_{30} database from various *in situ* measurements in the region is utilized to derive regional Vs_{30} prediction models based on proxy measures of geology, topographic slope, and depth to glacial till (z_{gl}). Two hybrid geology-slope and geology-z_{gl} Vs_{30} prediction models are developed for Metro Vancouver and evaluated to the Ahdi et al. (2017) geology-based model (PNWA17) via residual analysis. Final recommendations to achieve regional Vs_{30} mapping using the recommended Vs_{30} prediction models for Metro Vancouver are provided.

5.2 Metro Vancouver Vs(z) database

The Vs(z) database compiled in this study consists of 762 Vs(z) in Metro Vancouver, which is assembled from various public (online) and private agencies involved in major engineering projects in the region (Molnar et al. 2020, Adhikari and Molnar 2021). A total of 522 Vs profiles from a variety of *in situ* methods collected within the Fraser River Delta (FRD) by the GSC are documented in multiple open file reports (compilations of Hunter et al. 1998, Crow et al. 2015, Hunter et al. 2016). A total of 165 Vs(z) are collected or acquired by the Metro Vancouver seismic microzonation project from proprietary sources, primarily as site-specific geotechnical investigation reports. In addition, the project performed multi-method non-invasive seismic testing at 123 sites for Vs(z); 75 Vs(z) are included in this

study's Vs(z) database and the remaining 49 site's dispersion curves are used to obtain Vs_{30} (section 5.4.4). The project enabled compilation of 240 Vs(z) that constitute a relatively small proportion (31%) of the compiled Vs(z) database but are a vital addition since many are located outside of the FRD and measure Vs in other geologic units. The Vs(z) database includes the georeferenced latitude and longitude coordinates (WGS84 Datum) for each Vs(z) location, the Vs values with depth, and associated site metadata including mapped geologic unit (discussed at section end), geologic stratigraphy (when nearby borehole data is available), water table depth, depth to glacial till (z_{gl}) or depth to bedrock (z_{brk}), when available. When fill sediments are identified at the surface of a Vs(z) corresponding to another mapped geology unit (e.g., Tertiary rock sediments), these layers were removed from Vs(z) to represent native ground conditions. The described Vs(z) database is used in this study to develop: (1) average Vs(z) for different geologic units (Section 5.3); and (2) proxy-based Vs_{30} prediction models for Metro Vancouver (Sections 5.5 and 5.6).

The 522 GSC Vs(z) are obtained from 1 crosshole Vs(z), 43 downhole Vs(z), 87 SCPT Vs(z), 209 refraction Vs(z), and 182 reflection Vs(z) (converted from Vp) measurements (Hunter et al. 2016, Crow 2015). The shear-wave refraction measurements were completed at 111 unique locations, and at most sites two Vs(z) are provided corresponding to forward and reverse shot gathers along the same refraction survey line (Hunter et al. 2016). 14 refraction Vs(z) exhibited much higher Vs values than other nearby Vs(z) from higher resolution invasive methods and were judged to be unreliable and removed from the database. The 182 Vp(z) are provided by the GSC from approximately 126 kms of multichannel Vp reflection surveys in the FRD. The GSC used a FRD-specific Vp-to-Vs relationship (Britton et al. 1995, Hunter et al. 1998) to convert the Vp(z) to Vs(z). The 182 Vs(z) were originally produced to map the depth to bedrock on the order of hundreds of meters beneath the FRD (Britton el al. 1995), and thus have low resolution near the surface where the first model layer thickness can be > 100 m.

The 165 Vs(z) compiled by the project from open/public and proprietary sources (Adhikari et al. 2021) were also obtained from a variety of *in situ* methods: crosshole (2), downhole

(53), Spectral Analysis of Surface Waves (SASW) (3), and SCPT (107). Many of these Vs(z) log into stiff glaciated sediments and Tertiary sedimentary rock and thus provide new and valuable information on the Vs of these geologies. The acquisition date of these 165 Vs(z) spans from the 1990s to the present, with varying levels of documentation quality. In some cases, the numeric Vs values, site location and lithology information were well-documented, and in other cases only a copy of the Vs log report (image of the Vs(z) with a map of the site) were available. Two generic Vs(z) with one standard deviation representative of weathered and competent Pre-Tertiary Coast Mountain plutonic rocks of the North Shore are provided by S. Molnar (pers. comm., 2021).

In addition, the project accomplished multi-method non-invasive seismic testing for Vs(z) at 123 sites. This study includes 75 Vs(z) obtained from inversion of the dispersion curve alone or joint inversion of the dispersion curve with the Microtremor Horizontal-to-Vertical Spectral Ratio (MHVSR) peak frequency(ies) (Ladak 2020, Assaf et al. 2022, Boucher 2022). For 4 sites, two V(z) are provided per site which captures the site's lateral Vs(z) variability (Boucher, 2022).

The locations of the 762 compiled Vs(z) are shown in Figure 5-1 differentiated by the type of measurement and overlaid on a consolidated regional Quaternary geology map. The regional Quaternary geology map is consolidated from three GSC maps: a 1:50,000 scale map for Metro Vancouver (Dunn and Ricketts 1994), a 1:20,000 scale map for North Vancouver (Bednarski 2014), and a 1:50,000 scale map for West Vancouver (Blais-Stevens 2008). Geologic units are consolidated to the Metro Vancouver geology mapping by Adhikari et al. (unpublished).
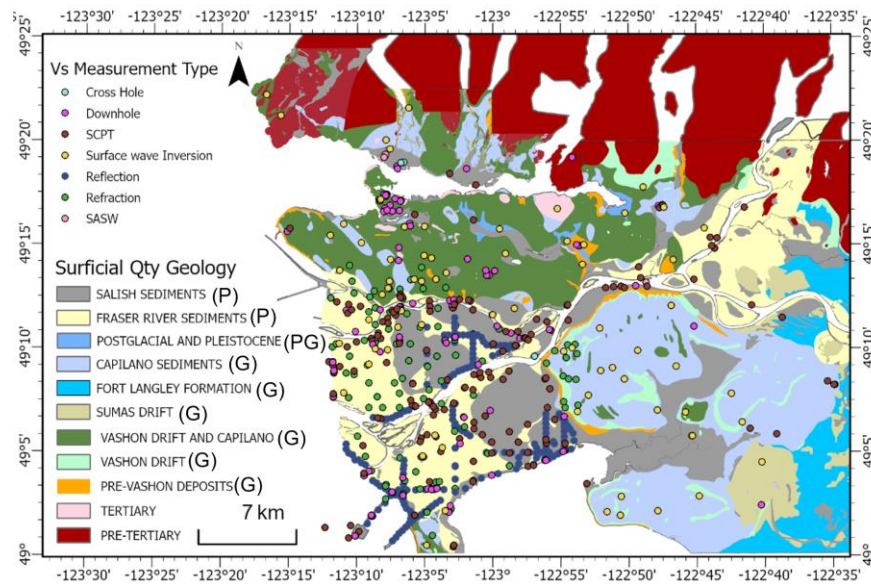
Figure 5-1. Locations of 762 collected Vs(z) in Metro Vancouver from various *in situ* measurements overlaid on the consolidated regional Quaternary geology map. The post-glacial (P) and Glacial (G) geologies are shown in between parenthesis.

5.3   Average Vs(z) of Different Sediment Types in Metro Vancouver

The Vs database in this study provides the first measured Tertiary sedimentary and Pre-Tertiary igneous rock Vs along with newly acquired measurements outside FRD and not covered by previous GSC testing. Metro Vancouver geology is divided into four main geologic groups based on the their age and glacial history: Pleistocene and younger post-glacial sediments, Pleistocene and older interglacial and glaciated sediments (simplified as 'glacial'), Tertiary sedimentary rocks, and Pre-Tertiary volcanic and granitic rocks (Armstrong 1984). Figure 5-1 shows the post-glacial (P), glacial (G), Tertiary, and Pre-Tertiary rock sediments locations.

The extracted metadata from invasive Vs measurements (borehole lithology descriptions or CPT soil behaviour type), in combination with the geology map, allows identifying sediment types along each Vs(z). A total of 293 Vs(z) from invasive measurements with sediment types identified are used to derive generic Vs(z) distributions. Vs(z) of the major

geologic units (Figure 5-1) are grouped together and further sub-grouped based on soil type or location. A total of 11 generic Vs(z) distributions are compiled: 4 post-glacial groupings based on soil type (Figure 5-2), 4 glacial groupings based on soil type or location (Figure 5-3), 2 Tertiary groupings based on location and 1 Pre-Tertiary grouping (Figure 5-4). Uniform, linear or powerlaw Vs(z) relationships are fit to the Vs(z) distributions. Table 5-1 reports details of the best fit generic Vs(z) relationships shown in Figure 5-2 to 5-4 including its z range, coefficient of determination (R^2), and one standard deviation (σ_{Vs}). The number of Vs(z) observations (N) for each group are reported in Figure 5-2 to 5-4. For Tertiary and Pre-Tertiary rock groups, no relationship is derived as the data is limited; depths and Vs ranges are reported in Table 5-1.

Table 5-1. Generic Vs(z) relationships from invasive Vs(z) measurements for Metro Vancouver sediments.

Major grouping	Subgrouping	Vs(z) relationship (m/s)	z range (m)	R^2	σ_{Vs} (m/s)
Post-Glacial sediments (Pleistocene and younger)	Peat & Organic Silt	$71.4 + 3.09z$	0-17	0.31	19
	Capilano & Fort Langley Clay & Silt	$88.8 + 3.67z$	0-52	0.81	21
	Clay & Silt & Mixed soils	$78.9 + 21.4z^{0.541}$	0-200	-	25
	Sand	$56 + 56z^{0.339}$	0-40	-	28
Glacial sediments (Pleistocene and older)	Capilano (Silt & Clay)	$178 + 3.43z$	9-42	0.2	65
	Capilano (Sand & Gravel)	265	0-39	-	62
	Beneath the FRD	$375 + 0.875z$; for $z \leq 200$ m 550 ; for $z > 200$ m	0-443	0.49	76
	Uplands	$481 + 6.49z$	0-43	0.12	164
Tertiary sedimentary rock	Beneath the FRD	576 - 1524	445-605	-	-
	Uplands	$572 + 16.1z$	0-43	0.28	211
Pre-Tertiary igneous rock	North Shore	343 - 2350	0-80	-	-

In Figure 5-2, Vs(z) of post-glacial sediments in Metro Vancouver are grouped into 4 categories based on soil type. Capilano and Fort Langley marine clays and silts are Pleistocene age sediments that were not ridden by glaciers and are thus applicable as post-

glacial sediments here. Although Vs(z) measurements from outside the FRD are included in the silts and clays with mixed soils group, the majority of the data is from measurements within the FRD. The sand group is the signature of the FRD topset (distributary channel sand) and sand dominated parts of the FRD foreset. Not surprisingly, the previous FRD powerlaw Vs(z) relationship Hunter99 (Hunter et al. 1999) is the average of the two sub-groupings of post-glacial FRD sediments (sand and mixed soils groups) because it did not distinguish between these soil types. These powerlaw Vs(z) relationships for FRD silts and sands are distinct from the Vs(z) relationships for lower velocity peat and organic soils and Capilano & Fort Langley clays (outside of the FRD).
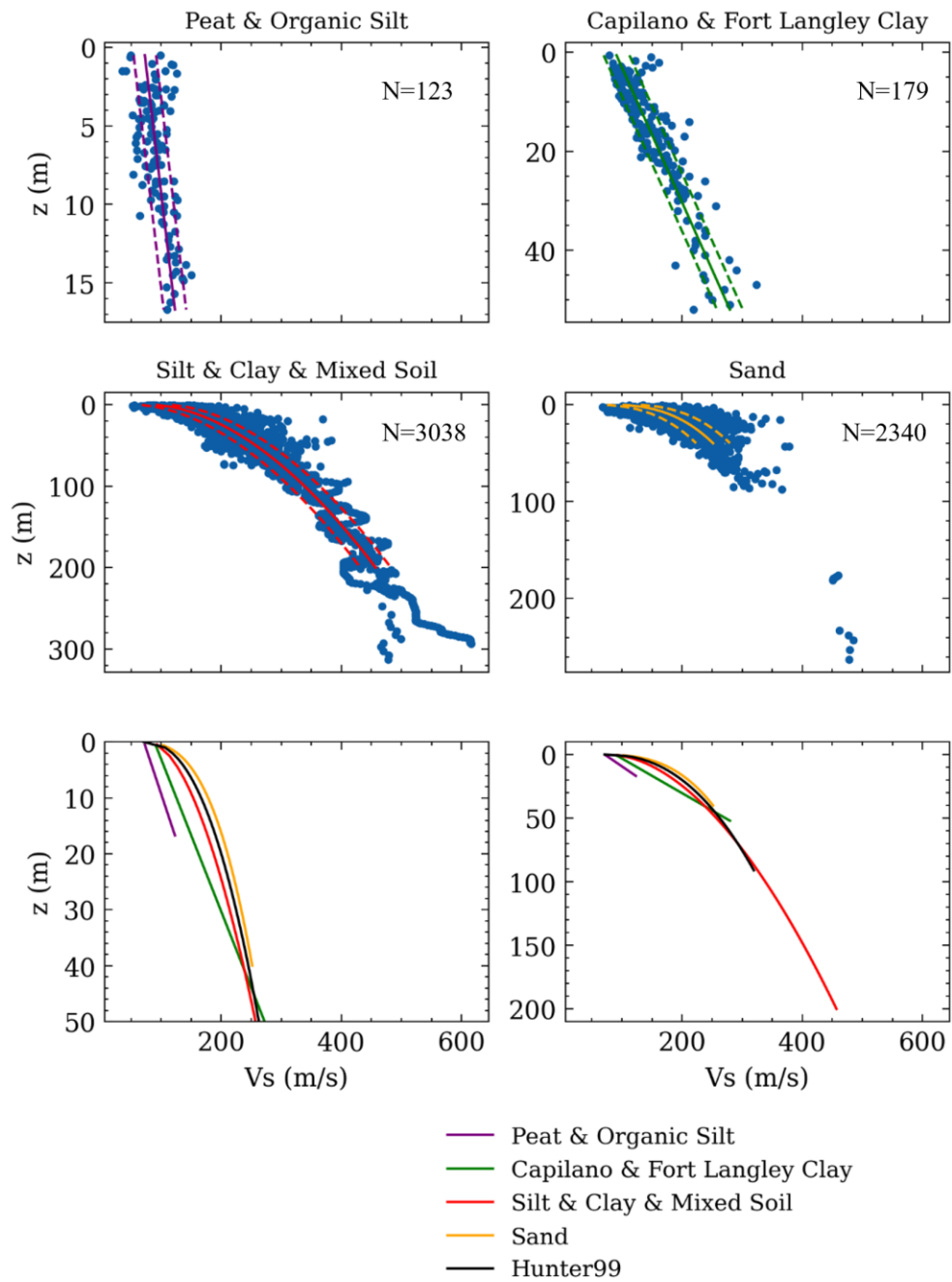
Figure 5-2. Vs(z) distributions and generic Vs(z) relationships for post-glacial sediment groups in Metro Vancouver.

In Figure 5-3, Vs(z) of the glaciated Capilano sediments could be sub-grouped based on material type (silt & clay, sand & gravel) whereas Vs(z) of glacial sediments are sub-divided based on location: glacial sediments present to significant depth (500 m) beneath post-glacial FRD sediments, and glacial sediments present at 0-50 m in the Metro Vancouver Uplands (Vancouver, Surrey, Burnaby, Tsawwassen). As mentioned previously, the amount of Vs(z) data outside of the FRD is limited and apparent in Figure 5-3. In addition, Vs variability of stiffer glacial sediments (Figure 5-3) is larger than low velocity post-glacial sediments (Figure 5-2). Figure 5-3 confirms Vs(z) of Uplands glacial sediments is generally higher than that of glacial sediments beneath the FRD. Despite the limited and highly variable Vs(z) data of glacial sediments in Metro Vancouver, Figure 5-3 presents Vs(z) relationships for these geologic units for the first time, superseding their uniform average Vs reported by Monahan and Levson (2001).
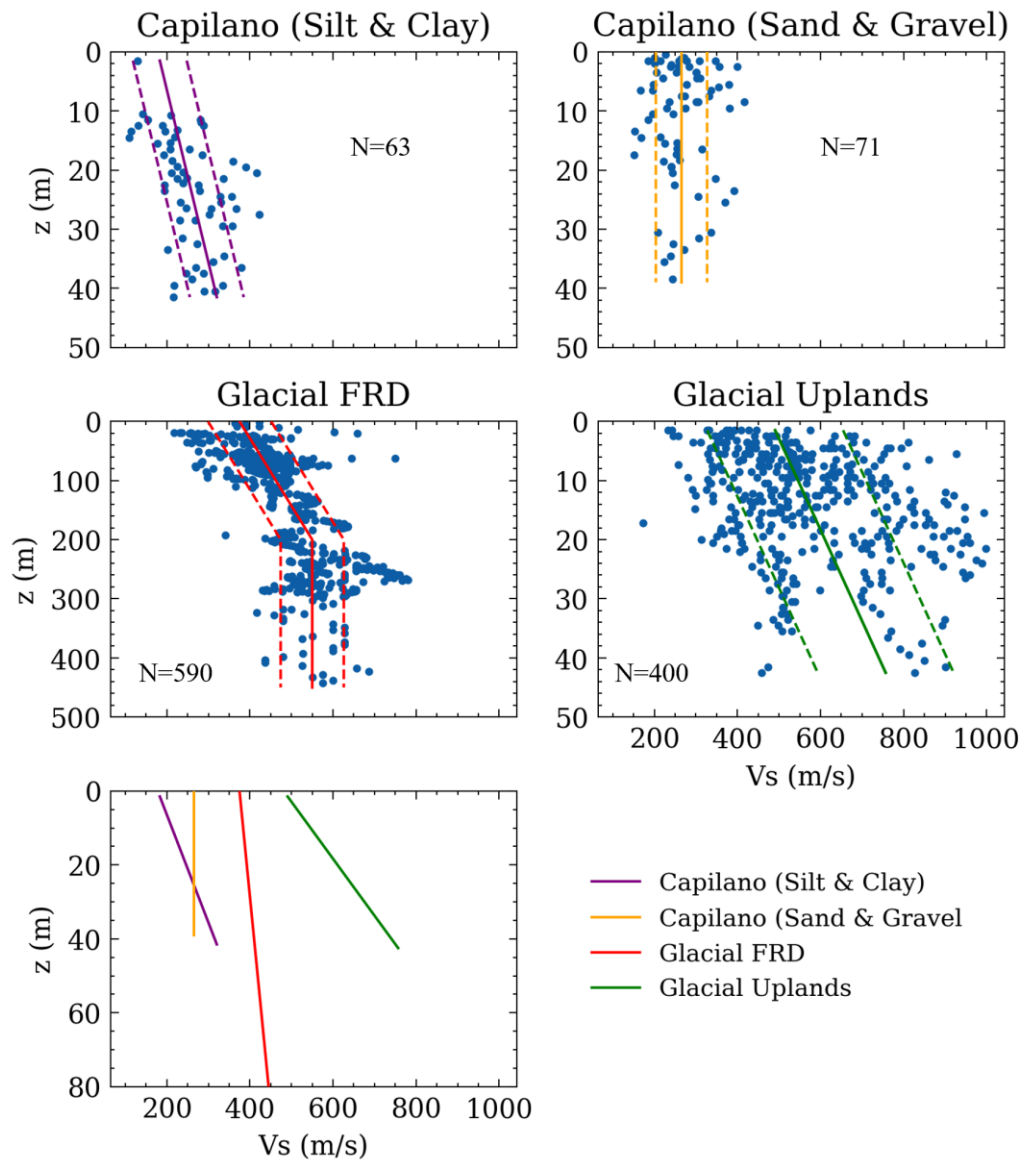
Figure 5-3. Vs(z) distributions and generic Vs(z) relationships for glacial sediments groups in Metro Vancouver.

In Figure 5-4, Vs(z) of Tertiary sedimentary rocks are sub-grouped based on location: at significant depth (> 450 m) beneath the southern FRD, and at 0-50 m beneath the Vancouver Uplands. Only one invasive method Vs(z) profile is available in Tertiary sedimentary rock beneath the FRD, converted by the GSC from the original downhole Vp(z) measurements along the Conoco-Dynamic Mud Bay d-95-D borehole; weathering

of the rock is noted over its upper 10 m. The Vs(z) distribution of Tertiary sedimentary rocks beneath the FRD is re-visited in section 6.2 including non-invasive method Vs(z) data, converted by the GSC from reflection Vp surveying. Vs(z) of Tertiary rock in the Uplands shows Vs as low as 200 m/s at surface that increases to around 1000 m/s at 40 m with a σ_{Vs} of 211 m/s. Descriptions from borehole logs and core samples comment on strong weathering of Tertiary rocks near surface. For Pre-Tertiary rocks, a generic Vs(z) with one standard deviation is available for both weathered and competent Coast Mountain granitic rocks of the North Shore (averaged from proprietary invasive method velocity profiling at 3 rock sites), and one downhole Vs(z) acquired by the project in a 80-m deep water well (OW349) in Belcarra of which the first layer corresponds to weathered rock. Vs(z) of Pre-Tertiary plutonic granitic rocks of the North Shore are clearly higher than that of Tertiary sedimentary rocks found beneath the Uplands and FRD.
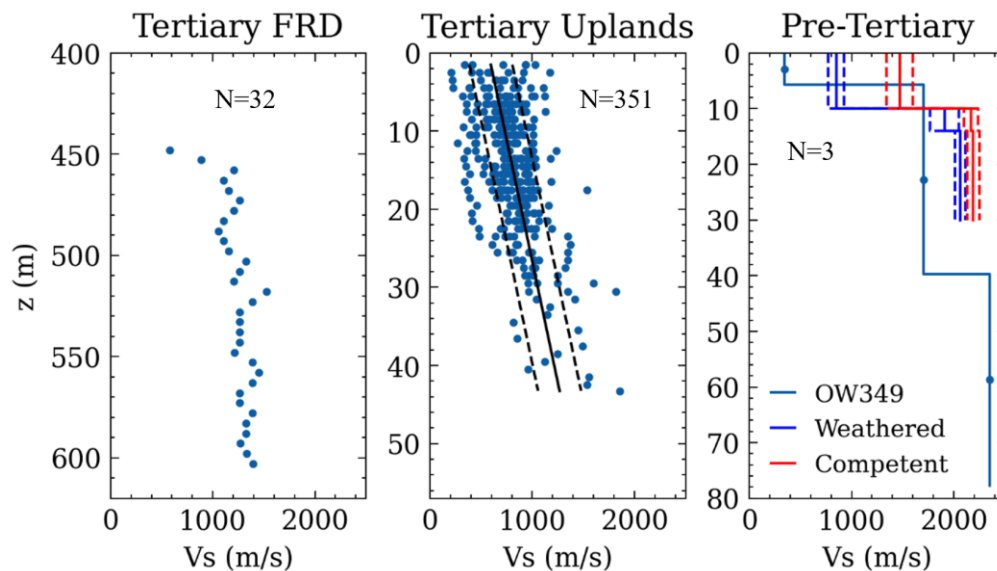
Figure 5-4. Available Vs(z) for Tertiary and Pre-Tertiary rock sediments in Metro Vancouver. Coefficients of the fitted model are listed in Table 5-1.

5.4   Vs$_{30}$ from *in situ* Measurements in Metro Vancouver

The widespread use of Vs$_{30}$ for evaluating seismic site effects in our regional application motivates the development of an *in situ* Vs$_{30}$ database in which all Vs$_{30}$ values are calculated from *in situ* Vs(z) or proxy-Vs (CPT, dispersion data) measures. Standard Penetration testing (SPT) can also be used to obtain Vs(z) and Vs$_{30}$, however, the project's regional SPT database is still under development and not available at this time. Vs$_{30}$ is calculated according to

$$Vs_{30} = \frac{30}{\sum \frac{h_i}{Vs_i}}$$
$$\textbf{Eq. 5-1}$$

where h_i and Vs_i are the thickness and Vs or layer i when zp ≥ 30. Only Vs(≥ 5) will be used to avoid adding considerable bias to the Vs$_{30}$ database. When zp < 30 m, extension is required either by extrapolating Vs$_{zp}$ to Vs$_{30}$ or assignment of reasonable Vs to 30 m. The former will require assessment and/or development of a region applicable Vs$_{zp}$-to-Vs$_{30}$ extrapolation model calibrated by Metro Vancouver's *in situ* Vs(z) data in section 5.4.2. The latter can be achieved using generic Vs(z) relationships developed in section 5.3. To further populate the Vs$_{30}$ database using *in situ* measurements and increase density and spatial coverage of Vs$_{30}$ measurements across Metro Vancouver, other *in situ* measures of CPT(z) and experimental dispersion curves from multi-method non-invasive seismic testing are utilized in section 5.4.3 to predict Vs$_{30}$.

5.4.1   Vs$_{30}$ from *in situ* Vs(z) Data

The Vs(z) database from invasive and non-invasive measurements in Metro Vancouver is used to calculate Vs$_{30}$. A total of 360 Vs(z) with zp ≥ 30 m are used to calculate Vs$_{30}$. A total of 180 Vs(z) with zp < 30 m will require extrapolation to calculate Vs$_{30}$ or relationships to predict Vs$_{30}$ from other Vs$_z$. The 182 GSC Vs(z) converted from Vp reflection measurements have low resolution near surface (1st layer is up to 100 m thick) and provide higher Vs$_{30}$ than that obtained from nearby higher resolution methods (downhole, SCPT) and are therefore not included in the Vs$_{30}$ database. Seven Vs$_{30}$ values for which the

corresponding *in situ* Vs(z) is not available to the authors are included (Jackson et al. 2017; S. Molnar, pers. comm., 2017).

Figure 5-5 presents the statistical distribution of the compiled empirical *in situ* Vs_{30} data for Metro Vancouver, binned into 100 m/s intervals. The majority of Vs(z) deeper than 30 m are concentrated in soft and thick post-glacial Holocene sediments of the FRD (Hunter et al. 1998; 2016). Higher Vs_{30} values (up to 971 m/s in Pre-Tertiary rocks) are compiled from unpublished sources and provide new and important insights on Vs_{30} of stiffer site conditions in the region, even if limited in number. A log-normal distribution is assumed for Vs_{30} in this study in accordance with previous similar studies (e.g., Wills and Clahan 2006; Parker et al. 2017; Ahdi et al. 2017); for a distribution of positive (Vs_{30}) values, both reciprocal normal and log-normal distributions may be used (Mital et al. 2021). Figure 5-5 shows the exponent of natural log mean of Vs_{30} (μ_{lnVs30}) in m/s and the log standard deviation (σ_{lnVs30}) for the empirical Vs_{30} dataset.
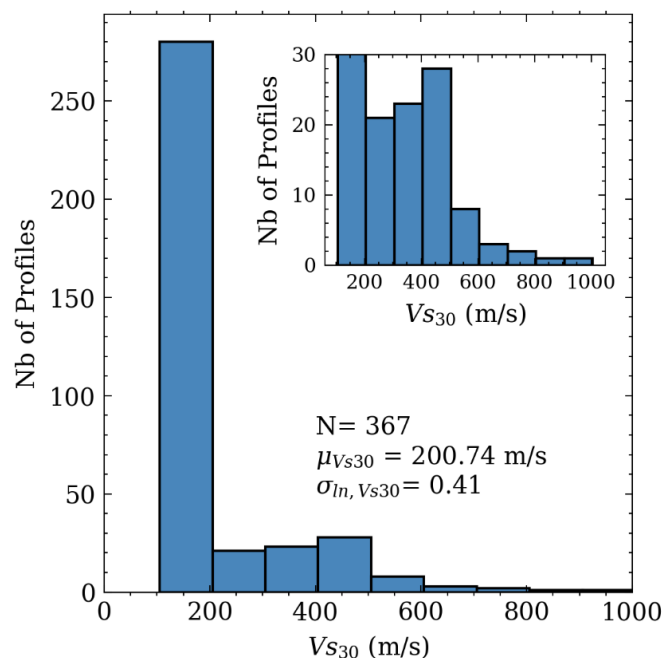
Figure 5-5. Distribution of Vs$_{30}$ from *in situ* Vs($\geq$ 30) in Metro Vancouver. Inset shows a zoomed Nb of Profiles.

5.4.2 Development and Application of a Vs_{zp}-to-Vs_{30} Relationship for Metro Vancouver

To develop an empirical Vs_{zp}-to-Vs_{30} model where zp is < 30 m, Vs_z is calculated at 1 m increments from 5 to 29 m (Vs_5 to Vs_{29}) for all $Vs (\geq 30)$. Four Vs_{zp}-to-Vs_{30} functional forms proposed in the literature (Table 5-2) are selected for regression analysis using the Metro Vancouver Vs_{5-29} data set. In addition to the regressions, two existing Vs_{zp}-to-Vs_{30} models presented by Wang and Wang (2015; WW15) and Ahdi et al. (2017) are tested (Table 5-2). The WW15 model is based on linear extrapolation in log space of Vs_{zp} to 30 m based on 2 depths, z_1 and z_2; we select z_2 = zp and z_1 = zp -5 in this study. Ahdi et al. (2017) developed a Vs_{zp}-to-Vs_{30} model (DEA_A17) based on Dai et al.'s (2013) functional form for Pacific North America using a compiled Vs data set from Washington, Oregon, Alaska, as well Metro Vancouver, primarily from Hunter et al. (1998; 2016). It is thus of interest to test the performance of the DEA_A17 model when applied to our more extensive Metro Vancouver's Vs data set.

Table 5-2. The 5 selected functional forms for Vs_{zp}-to-Vs_{30} regression analysis (solving for model coefficients c_0-c_2). The last two listed Vs_{zp}-to-Vs_{30} models are tested here using the Vs_{zp} Metro Vancouver data set.

Reference	Model	Equation
Boore (2004)	B04	$\ln(Vs_{30}) = c_0 + c_1 \ln(Vs_{zp})$
Boore et al. (2011)	B011	$\ln(Vs_{30}) = c_0 + c_1 \ln(Vs_{zp}) + c_2 [\ln(Vs_{zp})]^2$
Midorikawa and Nogi (2015)	MN15	$\ln(Vs_{30}) = c_0 + c_1 \ln(Vs_{zp}) + c_2 \ln(Vs(zp))$
Dai et al. (2013)	DEA13	$\ln(Vs_{zp-30}) = c_0 + c_1 \ln(Vs(zp)); \; Vs_{30} = \dfrac{30}{ttzp + \frac{30-zp}{Vs_{zp-30}}}$
Wang and Wang (2015)	WW15	$\ln(Vs_{30}) = \ln(Vs_{z2}) \dfrac{\ln 30 - \ln z_2}{\ln z_2 - \ln z_1} [\ln(Vs_{z2}) - \ln(Vs_{z1})]$

Ahdi et al. (2017)	DEA13_ A17	$\ln(Vs_{zp-30}) = c_0 + c_1 \ln(Vs_{zp})$; $Vs_{30} = \dfrac{30}{ttzp + \frac{30-zp}{Vs_{zp-30}}}$; $c_0 = 3.892 - 1.451\ln(zp)^{0.777}$ $c_1 = 0.228 + 0.394\ln(zp)^{0.524}$

Notes: zp is depth in meters; Vs_{zp} is time-averaged Vs to zp. Vs(zp) is Vs at zp. Vs_{zp-30} is time-averaged Vs between zp and 30 m; $ttzp$ is shear wave travel time between surface and zp; For the WW15 model, $z_2 = zp$ and $z_1 = zp -5$.

The obtained coefficients for the selected 6 models and at each zp between Vs_5 and Vs_{29} (Table 5-2) are used to predict Vs_{30}. In addition, Vs_{30} is predicted using the DEA13_A17 and WW15 models at 1 m increments between Vs_6 and Vs_{29}. Figure 5-6 shows the mean (μ_{Res}) and standard deviation (σ_{Res}) of $\ln(Vs_{30})$ model residuals for all 6 selected Vs_{zp}-to-Vs_{30} models. μ_{Res} of the four regressed models are near zero at all zp values, while μ_{Res} for the WW15 and DEA_A17 models approaches zero only at $zp \geq 15$ m. The WW15 model shows the largest residual dispersion at $zp < 17$ m, while B04 and B11 models show the highest residuals dispersion at $zp > 17$ m. The MN15, DEA13 and DEA_A17 models show similar lower σ_{Res} at all zp compared to the other models. The tested DEA_A17 model, which was developed with some of the presented Metro Vancouver Vs(z), tends to overestimate measured Vs_{30} (negative μ_{Res}) especially at shallow zp. This overestimation might be attributed to the inclusion of Vs profiles from Washington, Alaska, and Oregon that are not present in our Vs database. Hence, the preferred Vs_{zp}-to-Vs_{30} model for use in Metro Vancouver is the DEA13 model with similar prediction accuracy (residual trends) as MN15 but with fewer model coefficients. Instead of using the regressed model coefficients (c_0 and c_1) at each depth, powerlaw relationships are developed to capture the DEA13 model's $c_0(zp)$ and $c_1(zp)$ coefficients (Figure 5-7, Table 5-3). Similarly, σ_{Res} is fit using a linear model based on zp.

The developed DEA13 model (Tables 5-2 and 5-3) is used to predict Vs_{30} at the 180 *in situ* Vs(z) with $zp < 30$ m. The quality of predicted Vs_{30} is checked against nearby measured Vs_{30} to confirm their adequacy for regional Vs_{30} mapping. In cases where a strong impedance contrast occurs below zp, the DEA13 extrapolation model does not predict this

increase in Vs and thereby will lead to underestimated V_{S30}. This V_{S30} underprediction may occur for Vs(z) when z_{gl} is < 30 m. Several V_{S30} from shallow Vs(z) were identified as underpredicted for this reason and removed from the V_{S30} database.
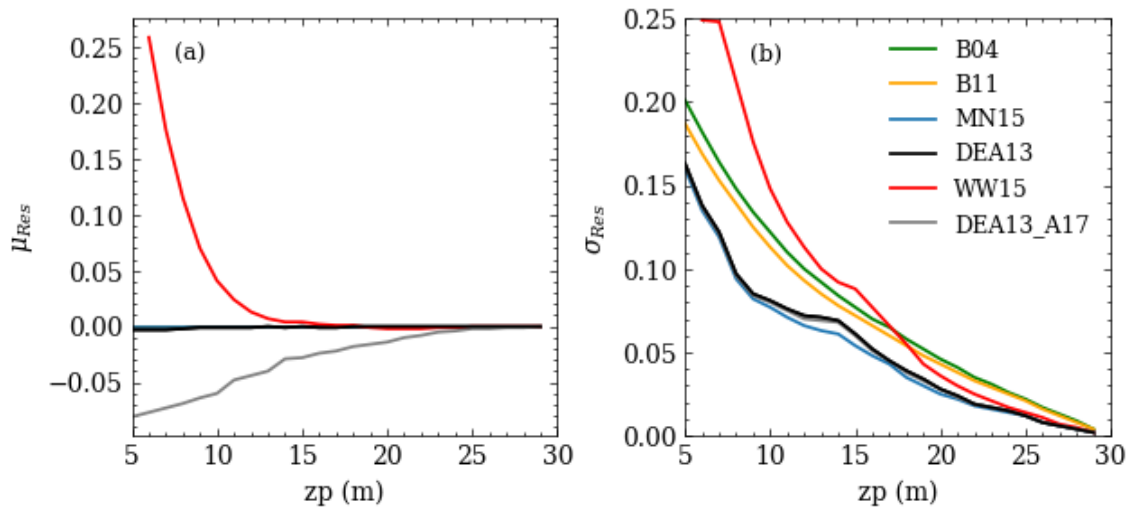
Figure 5-6. (a) Mean (μ_{Res}) and (b) standard deviation (σ_{Res}) of ln(V_{S30}) residuals calculated from ln($V_{s<30}$) for the 6 tested models in Metro Vancouver.
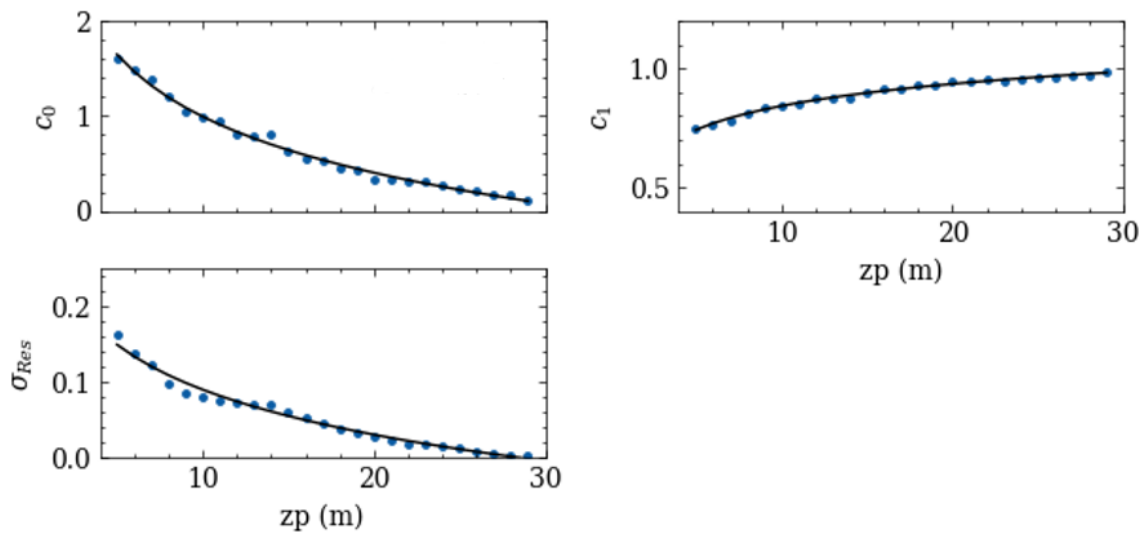
Figure 5-7. Regressed c₀ and c₁ coefficients and σRes with zp from DEA13 model (blue dots). The best fit models equations based on zp (powerlaw for c₀ and c₁ and linear for σRes) shown in solid lines are reported in Table 5-3.

Table 5-3. DEA13 model coefficients and standard deviation to be used with Table 5-2 for calculating Vs₃₀ from Vszp in Metro Vancouver.

Parameter	Equation
c_0	$3.406 - 1.191\ [\ln(zp)]^{0.839}$
c_1	$0.507 + 0.153\ [\ln(zp)]^{0.937}$
σ_{Res}	$0.288 - 0.0866\ \ln(zp)$

5.4.3   Vs₃₀ from *in situ* CPT(z) Data

A large S/CPT database has been compiled from open and proprietary sources in Metro Vancouver. Assaf et al. (2023) developed a machine learning CPT-to-Vs (AMEN) model from 80 SCPT measurements and validated it at 11 SCPT sites in Metro Vancouver. The model's depth-averaged Vs prediction error is ≤ 20 %, similar to the Vs variability amongst different nearby direct Vs measurements in the FRD (Assaf et al. 2022). The AMEN model can be applied to available CPT profiles to obtain Vs(z) and consequently Vs₃₀.

More than 1100 CPT measurements are identified in the geodatabase primarily from the FR and Serpentine-Nicomekl Lowlands, and limited areas in the Uplands and North Shore. The CPTs are primarily located in post-glacial sediments as cone refusal occurs when the cone tip penetrates stiff glaciated till or till-like sediments with Vs $\geq$ 400 m/s. To avoid adding nearby redundant or less accurate Vs₃₀ predictions to the Vs₃₀ database obtained from direct Vs measurements, 368 CPT profiles that are at least 500 m or further from the closest existing Vs₃₀ location are identified to provide Vs₃₀ at unique locations of benefit to regional mapping. At many sites, several nearby CPT profiles are collected and only one CPT profile (typically the deepest) is used as the site representative profile.

The AMEN model requires two basic CPT measures, cone tip resistance (q_c in kPa) and sleeve friction (f_s in kPa), with z (in m) for Vs(z) calculation. These measures are compiled in numerical format in the project's CPT database, i.e., digitized from geotechnical reports

when required. In some cases, the corrected cone tip resistance (q_t) is reported instead of q_c and thus the AMEN equivalent model based on q_t (XGBR MG15_q_t model, Table B-4) is used for Vs(z) calculation. Each CPT measure [q_c(z) or q_t(z) and f_s (z)] is averaged into 1 m z bins and the relevant CPT-Vs model (q_t or q_c based) is used to calculate Vs(z) and consequently Vs30. Figure 5-8 shows an example of using CPT q_t and fs digitized profiles from a site in the FRD to predict Vs(z). For Vs(< 30), Vs(zp) and Vs$_{zp}$ are calculated and the Vs$_{zp}$-to-Vs30 (developed DEA13 model Tables 5-2 and 5-3) is used to predict Vs30. As these extrapolated Vs30 are of higher uncertainty compared to Vs30 obtained from direct Vs measurements, a quality check is performed on the obtained Vs30 with surrounding nearby Vs30 values to exclude outliers. Generally in soft sediments where $z_{gl} > 30$ m, Vs30 predicted using the combination of CPT-to-Vs and Vs$_{zp}$-to-Vs30 models is consistent with Vs30 from direct Vs(z). However, when $zp < z_{gl} < 30$ m, the DEA13 model underestimates Vs30. Hence, several Vs30 predicted from the combination of CPT-to-Vs and Vs$_{zp}$-to-Vs30 models are disregarded. For two CPT(z) in the Uplands, the generic Vs(z) relationship for Uplands glacial sediments (Figure 5-3) is used to extrapolate Vs(z) and calculate Vs30. Use of the generic Vs(z) relationship provides more reasonable Vs30 values compared to underpredicted Vs30 by the DEA13 extrapolation model. In total, 52 Vs30 values are added to the *in situ* Vs30 database from CPT(z) data.
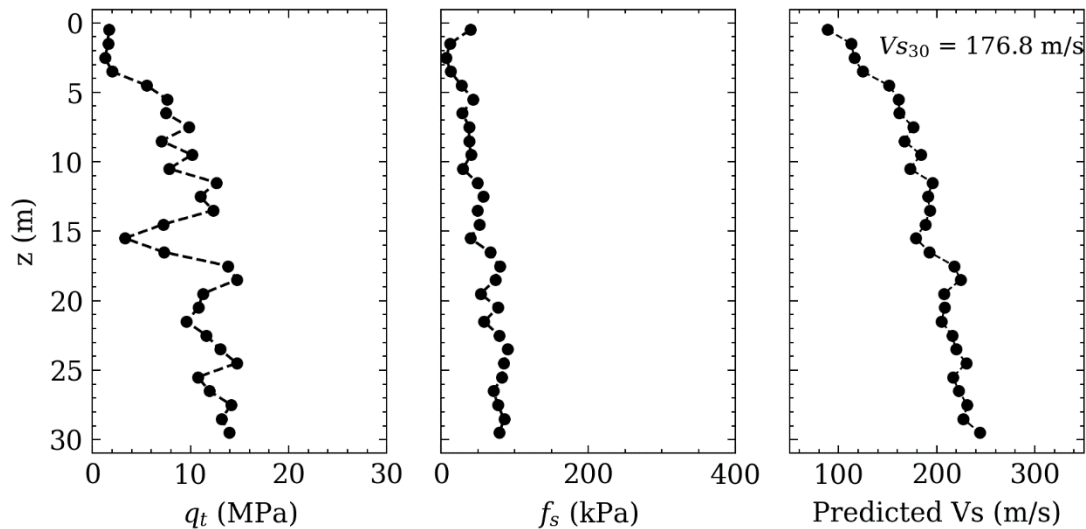
Figure 5-8. Digitized CPT q_t and f_s profiles at RAN2724 site in the FRD and corresponding predicted Vs(z) using the XGBR CPT-to-Vs model developed in Chapter 4.

5.4.4 Vs_{30} from *in situ* Surface Wave Dispersion Data

The Metro Vancouver project performed multi-method non-invasive seismic testing at 124 sites for Vs(z) during its 4 field campaigns. The sites were selected to fill in spatial gaps in Vs and to populate Vs measurements in specific geology units. Thus far, 75 Vs(z) have been determined from joint inversion of Rayleigh wave fundamental-mode dispersion estimates and MHVSR peak frequency(ies). Hence 75 Vs(z) are added to the Vs_{30} database. Dispersion estimates at many sites in the Uplands suffer from multi-mode contributions often attributable to velocity reversal(s) at depth in Pleistocene and older inter/glacial sediments (Molnar et al. 2020) that require advanced inversion approaches to obtain Vs(z) (Boucher 2022). To serve our regional Vs_{30} mapping application, the possibility of extracting reasonably accurate Vs_{30} directly from the remaining 49 sites with *in situ* surface wave dispersion data is explored in this section. Several methods to calculate Vs_{30} directly from *in situ* dispersion data have been investigated in literature. For example, Martin and Diehl (2004) proposed calculating Vs_{30} as

$$Vs_{30} = 1.045(Vr_{40}) \qquad \textbf{Eq. 5-2}$$

where Vr_{40} is the measured phase velocity of a 40-m wavelength Rayleigh wave. Furthermore, Comina et al. (2022) developed an empirical λ-z transformation from comparison of invasive and non-invasive seismic testing methods that converts the *in situ* dispersion data [Vr(λ)] to Vr(z) from which Vr_{39} is used to predict Vs_{30}. Lin (2021) proposed a method to calculate Vs_{30} from *in situ* dispersion data assuming that V_R at a given frequency (f) is proportional to the average shear-wave velocity of soils within 1/2λ.

The Martin and Diehl (2004) and Lin (2021) relationships are selected to test Vs_{30} prediction for the 75 sites with both pre-inversion dispersion data and post-inversion Vs(z). Additionally, 5 Vp(> 30) and Vs(> 30) from 3 downhole and 2 crosshole surveys available

from the geodatabase are used to calculate the theoretical fundamental Rayleigh dispersion curve. Using the experimental or theoretical dispersion curve at each site, the predicted Vs_{30} from each method is compared to measured Vs_{30} from the inverted or invasive $Vs(z)$. The comparison between measured and predicted Vs_{30} is shown in Figure 5-9 with the calculated R^2, μ_{Res}, and σ_{Res}. The Martin and Diehl (2004) relationship slightly overestimates Vs_{30}, while Lin (2021) method tends to underestimate higher Vs_{30} (> 300 m/s) s. The underestimation of higher Vs_{30} may be attributed to the discretization performed in the Lin (2021) method for Vs calculation; the top 30 m are discretized into 60 layers each with 0.5 m thickness. At stiff sites with a strong impedance contrast, the gradual increase of Vs in thin 0.5 m layers cannot predict the sharp Vs increase in the actual profile leading to underestimation of Vs_{30}.
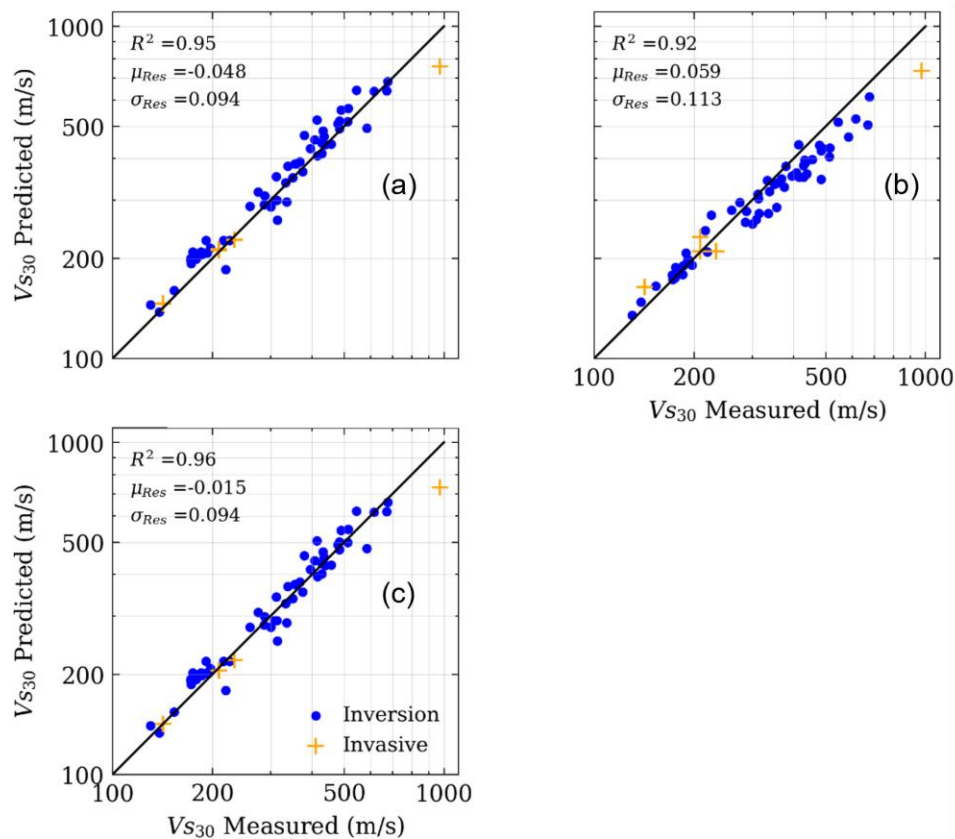
Figure 5-9. Comparison of measured Vs$_{30}$ (from inversion and invasive testing) and predicted Vs$_{30}$ from (a) Martin & Diehl (2004) method (Eq 5-2), (b) Lin (2021), and (c) the new regressed relation between Vs$_{30}$ and Vr$_{40}$ (Eq 5-3).

In addition to testing existing Vr$_\lambda$-to-Vs$_{30}$ methods, a regression analysis is performed between measured Vs$_{30}$ and Vr$_\lambda$ at λ between 35 and 45 m for the Metro Vancouver experimental and theoretical dispersion curves. The Metro Vancouver specific Vr$_\lambda$-to-Vs$_{30}$ relationship is

$$Vs_{30} = 1.011(Vr_{40}) \qquad\qquad \textbf{Eq. 5-3}$$

with a slightly lower multiplicative factor than Martin and Diehl (2004) (Eq 5-2). Equation 5-2 has minor prediction improvement compared to the other two non-region-specific methods over the whole Vs$_{30}$ range with slight overestimation of Vs$_{30}$ between 160-200 m/s (Figure 5-9). Thus, we use our region-specific Vr$_{40}$-to-Vs$_{30}$ relationship to calculate Vs$_{30}$ from the *in situ* dispersion data at the remaining 49 sites. Only sites with a wide dispersion frequency band (minimum $\lambda < 10$ m and maximum $\lambda > 50$ m) are selected to ensure reliable Vs$_{30}$ estimates. Sites with dispersion data showing multi-mode jumping or contributions are disregarded. Hence, 29 Vs$_{30}$ predicted from *in situ* dispersion data, in addition to the 75 Vs$_{30}$ calculated from the project's inverted Vs(z), are added to the Vs$_{30}$ database.

5.5   Metro Vancouver *in situ* Vs$_{30}$ Database

The compiled *in situ* Vs$_{30}$ database for Metro Vancouver includes 519 Vs$_{30}$ calculated from *in situ* Vs(z) and other Vs(z) proxy measures. The locations of the 519 Vs$_{30}$ sites are shown in Figure 5-10 and the $\mu_{\ln Vs30}$ and $\sigma_{\ln Vs30}$ of the region's Vs$_{30}$ distribution identified by the *in situ* measure are shown in Figure 5-11. For refraction surveys with two Vs$_{30}$ from forward and reverse surveys, average Vs$_{30}$ is considered to provide a single Vs$_{30}$ for each refraction site. The highest density of Vs$_{30}$ data occurs in the FRD primarily from the open-source GSC Vs(z) data. The Metro Vancouver project has achieved notable addition of Vs$_{30}$ data outside of the FRD from proprietary and project-performed *in situ* measures. The

spatial distribution of *in situ* methods used to determine Vs_{30} is not uniform; invasive methods are used primarily to measure $Vs(z)$ in post-glacial sediments and shallow Tertiary sedimentary rock compared to non-invasive seismic methods that are required to provide $Vs(z)$ measurements in stiffer and deeper sediments and rock. Predicted Vs_{30} from CPT data mainly fills in spatial gaps in soft post-glacial sediments, while predicted Vs_{30} from DEA13 model and dispersion data populate the Vs_{30} database for stiffer site conditions.
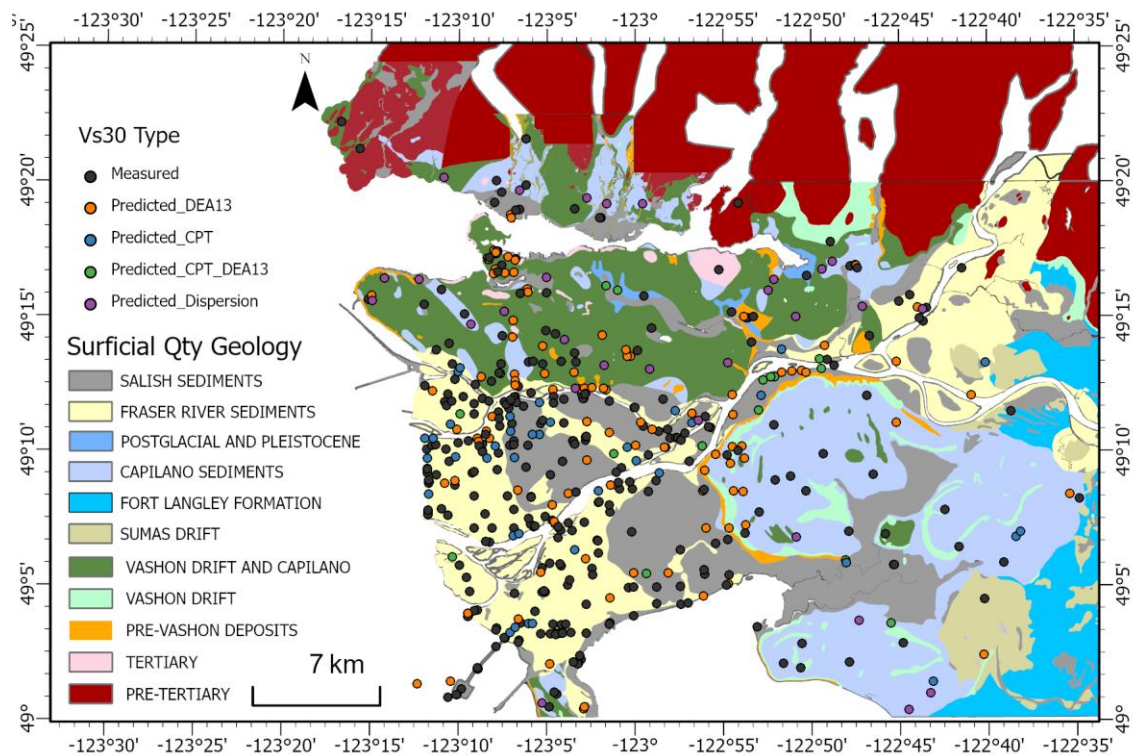
Figure 5-10. Metro Vancouver Vs_{30} database locations differentiated by the type of calculation used from direct Vs and other *in situ* measurements.
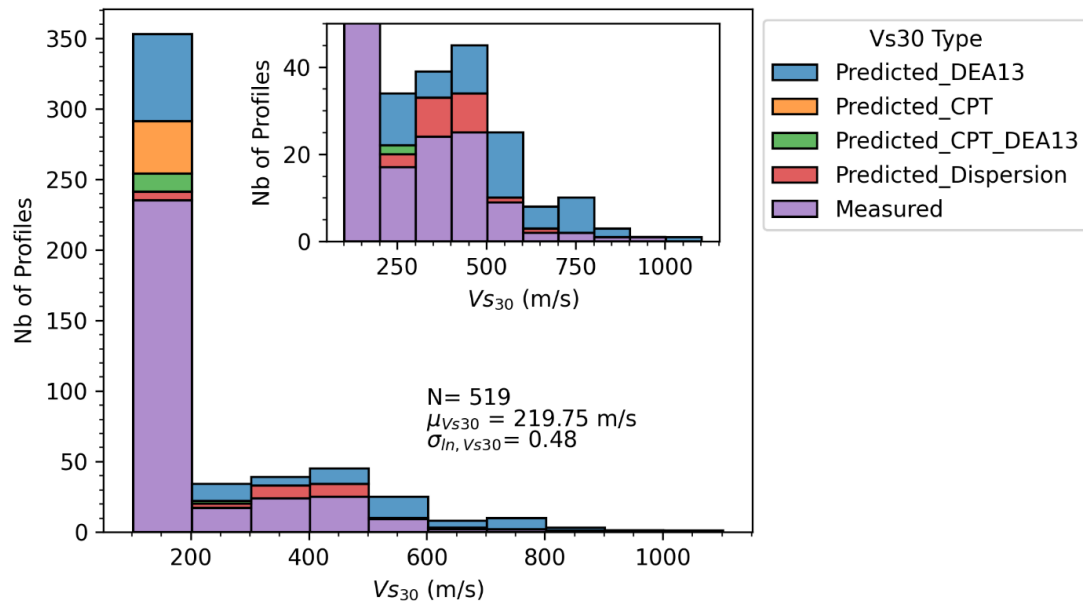
Figure 5-11. Metro Vancouver Vs30 database statistics differentiated by the type of calculation used from direct Vs and other *in situ* measurements.

Figure 5-10 shows the 519 locations with the lowest Vs30 uncertainty, determined from *in situ* Vs(z) measurements or estimates. There are multiple ways to further densify the Vs30 database utilizing other *in situ* measures of the Metro Vancouver geodatabase (e.g., borehole lithology in combination with generic Vs profiles in section 5.3, MHVSR peak frequencies); however, efficient approaches to achieve regional Vs30 mapping with low uncertainty are desired. This study targets use of additional seismic site characteristic (proxy Vs30) measures that are available (mapped) for the entire region (e.g., geology, topographic slope, z_{gl}) to verify their prediction accuracy to densify Vs30 data throughout the region to achieve high resolution Vs30 mapping.

5.6   Development of Hybrid Proxy-Based Vs30 Prediction Models

The first considered proxy for Vs30 prediction is the mapped Quaternary geology (Figure 5-1) described in Sections 5.2 and 5.3. A total of 515 Vs30 are assigned to 28 different geologic units. The Fraser River sediment geologic units are well populated with Vs30, while other units include only a few Vs30 (e.g., Tertiary and Pre-Tertiary rock units). The

Quaternary geologic unit associated with each Vs_{30} (database metadata described in Section 5.2) is reviewed based on nearby Vs_{30} and re-assigned when at/on a geologic boundary as required. Vs_{30} within each geology unit are then averaged and μ_{lnVs30} and σ_{lnVs30} are calculated. While some post-glacial units have different geology descriptions, μ_{lnVs30} and σ_{lnVs30} are not significantly different (not shown). The 28 different geologic units with Vs_{30} data are combined into 12 unique groupings (Table 5-4) based on several factors including geologic age, depositional environment, unit thickness, location, and the observed Vs_{30} variability. For example, Groups 8 and 10 correspond to the same Vashon drift and Capilano sediment types but Group 8 is thicker (> 10 m) than Group 10 (< 10 m; $z_{brk} < 10$ m). The μ_{lnVs30} and σ_{lnVs30} for each of the 12 groupings are shown in Figure 5-12. As expected, Vs_{30} increases with Group number (geologic age, material stiffness) with relatively consistent moderate Vs_{30} variability between groups; the very low Vs_{30} variability for rock Group 11 is a consequence of few Vs_{30} data. For Group 12 Pre-Tertiary rock, only one *in situ* Vs_{30} is available; Vs_{30} ranges of the two higher $Vs(z)$ for weathered and competent granitic rocks of the North Shore are also plotted in Figure 5-12 for comparison.

Table 5-4. Geologic groupings and associated Vs$_{30}$ statistics.

Group number	Geologic Age	Geologic description[*]	Geologic Label[*]	N	μ_{lnVs30} (m/s)	σ_{lnVs30}
1	Qty	Capilano & Fort Langley clays and silts	Ce, FLd	11	153	0.212
2	Holocene	Peat	SAb, SAc	69	153	0.165
3	Holocene	FRD sand, silt sediments	SAd, SAf, Fa, Fb, Fc	268	171	0.105
4	Holocene	Fills	SAa, H	24	215	0.319
5	Qty	Upland peat & fluvial sediments	SAe, SA-C	7	300	0.37
6	Qty	Sand & gravel	SAg, SAi, SAj,i, At	9	312	0.363
7	Pleistocene	Capilano sediments	Cb, Cc, Se, GFt	19	362	0.242
8	Pleistocene & older	Capilano & Vashon drift (> 10 m)	VC, VCb, Cd, Gmh, Tb	74	435	0.221
9	Pleistocene & older	Older Vashon and Pre-Vashon drift	Va, PVa,c PVa,c,b,f, Pva,d	13	463	0.363
10	Pleistocene & older	Capilano & Vashon drift (< 10 m)	VCa	17	651	0.296
11	Tertiary	Sedimentary rocks	T	3	783	0.052

| 12 | Pre-Tertiary | Igneous rocks | PT | 1 | 971 | - |

Qty = Quaternary. *from the consolidated Quaternary geologic map.
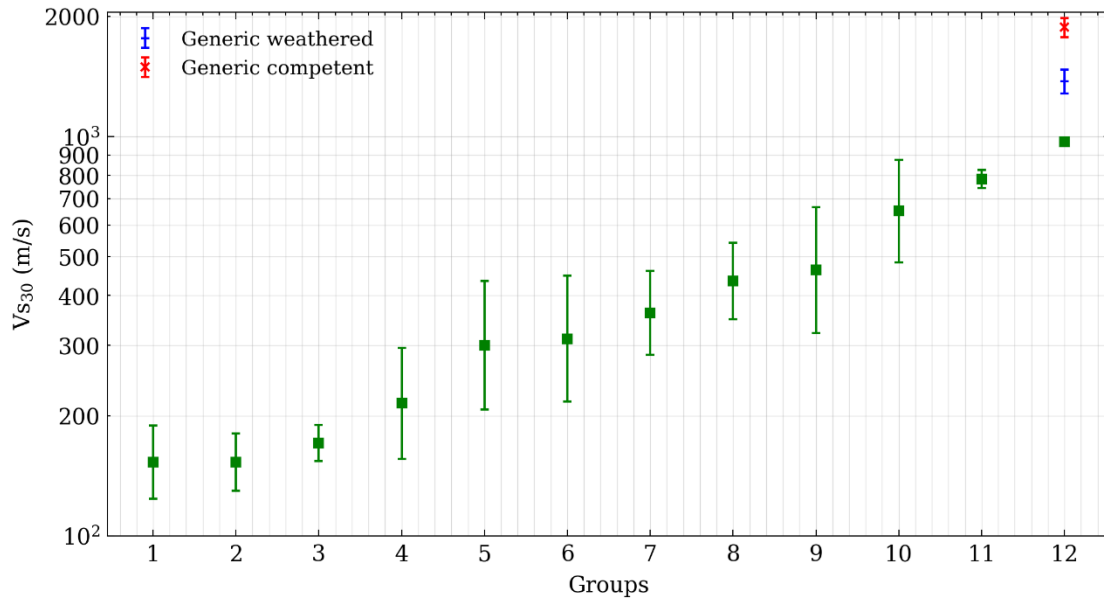
Figure 5-12. μ_{lnVs30} **and** σ_{lnVs30} **of the 12 unique geology groups for Metro Vancouver (Table 5-4). Pre-Tertiary weathered and competent generic Vs(z) Vs$_{30}$ ranges are plotted. The error bar represents ± one** σ_{Res}**.**

Figure 5-12 confirms mapped Quaternary geology in Metro Vancouver is a reasonable proxy of *in situ* Vs$_{30}$ but its use to predict Vs$_{30}$ would not be very accurate on its own. Additional proxies, in combination with geology, such as the topographic slope may improve Vs$_{30}$ prediction accuracy. Topographic slope has been proven to correlate well with Vs$_{30}$ (Allen & Wald 2007) in which softer and/or thicker sediments are typically located at lower elevation and vice versa. Alternatively, pairing z$_{gl}$ with mapped geology may have better predictive accuracy as it is a direct measure of post-glacial soil thickness. Two alternative regional Vs$_{30}$ prediction models based on hybrid combinations of Vs$_{30}$ proxies, geology & topographic slope (geology-slope) and geology & z$_{gl}$, are investigated next.

5.6.1   Geology-Slope model

To examine the correlation between topographic slope and *in situ* Vs_{30} in Metro Vancouver, the topographic slope (m/m) at each Vs_{30} site is extracted from the Canadian Digital Elevation Model (DEM; see Data and Resources) at varying resolutions (12, 6, 3, 1.5, and 0.75 arc seconds). The strongest correlations between *in situ* Vs_{30} and the various resolution DEMs (not shown) exist for the 6 arc seconds (200 m) and 12 arc seconds (400 m) maps. Generally, the correlation between topographic slope and Vs_{30} decreases with increasing resolution of the DEM (e.g., Allen & Wald 2009, Crespo et al. 2022). Topographic slope values from the 6 arc seconds DEM are selected for further analysis.

The correlation between *in situ* Vs_{30} and topographic slope is assessed for each of the 12 geologic groups (Table 5-4). The correlation is modelled using a log-linear model of the form

$$\ln(Vs_{30}) = d_0 + d_1(s) \qquad \textbf{Eq. 5-4}$$

where s is the 6 arc seconds topographic slope in m/m, and d_0 and d_1 are the regression coefficients. Figure 5-13 shows the variation of Vs_{30} with topographic slope and the best-fit Vs_{30} prediction model for the 12 geologic groups; the 95 % confidence interval (CI) is plotted for statistically significant correlations ($p < 0.05$) only. While slope correlates well with Vs_{30} for Groups 1 to 7 (softer, younger deposits), statistically significant correlations are determined for only 4 groups (1, 3, 4, and 7). For Groups 8 to 10, the Vs_{30} correlation with slope is weak. Thus, use of an extremely efficient open-source site characteristic (topographic slope) improves geology-based Vs_{30} predictions for 4 geologic groups. Table 5-5 reports details of the developed geology-slope models for the 4 groups with statistically significant Vs_{30} correlation. $\mu_{\ln Vs_{30}}$ is taken as the average of predicted Vs_{30} from Eq. 5-4 and $\sigma_{\ln Vs_{30}}$ is calculated from the residuals between measured and predicted Vs_{30} for Groups 1, 3, 4, and 7. For groups without a statistically significant dependence on the topographic slope, Vs_{30} prediction will be based on geology only. It should be noted that Groups 4 (Fills) and 7 (Capilano sediments) can be located in very steep regions in the North Shore.

The provided coefficients in Table 5-5 are limited to the topographic slope values found at available Vs_{30} locations and might lead to very high Vs_{30} when applied to much steeper areas not included in the model development. In case unrealistic Vs_{30} are obtained for these two groups, Vs_{30} predictions can be capped at a certain value selected in guidance from the geology model predictions.
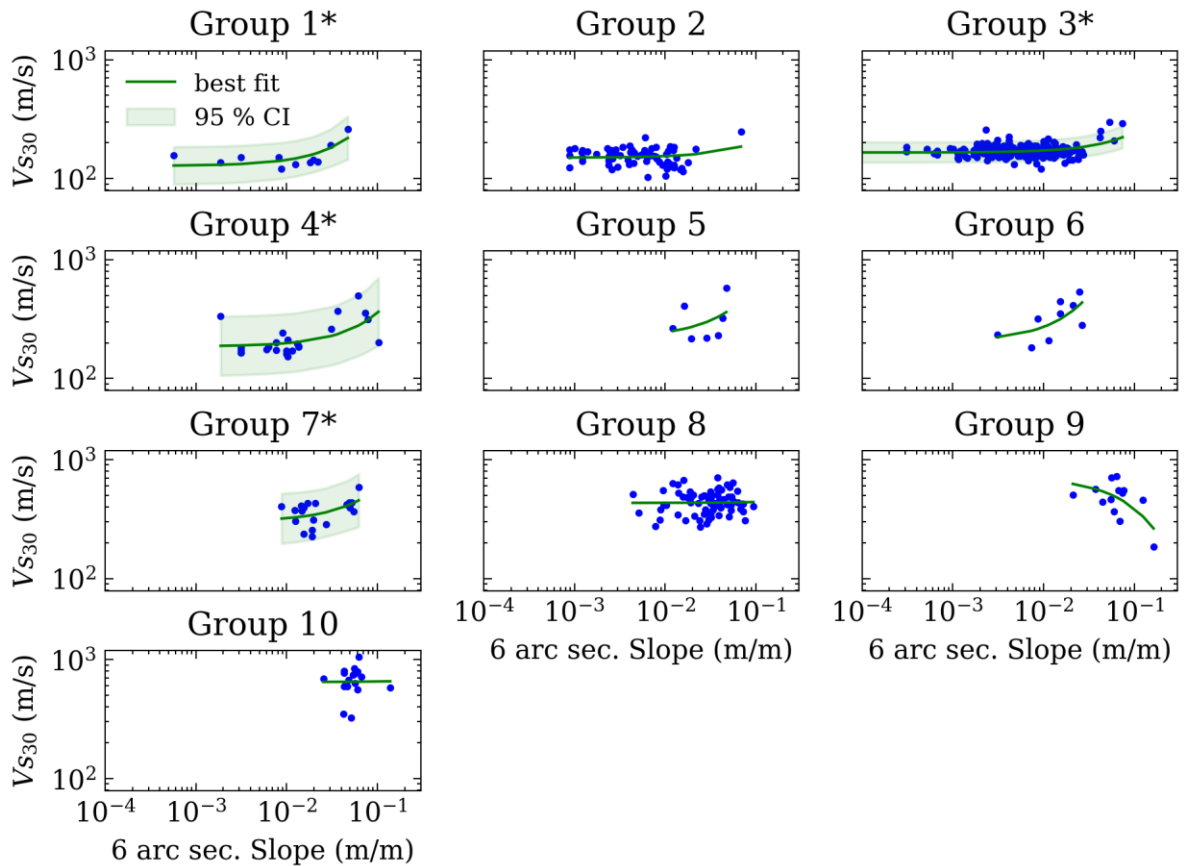
Figure 5-13. Vs_{30} correlation with the 6 arc sec. topographic slope (m/m) for different geology groups. The best fit line from Eq. 5-2 is shown with the 95 % confidence interval for groups with statistically significant correlations (Group 1, 3, 4, and 7).

5.6.2   Geology-z_{gl} Model

The depth of a significant impedance contrast in the upper 30 meters controls Vs_{30}. For Metro Vancouver, the most significant impedance contrast in the upper 30 meters is z_{gl}; only at steeper elevations in the North Shore would z_{brk} occur in the upper 30 m. Since z_{gl} is the more regionally applicable proxy Vs_{30} measure, we ignore z_{brk} in North Shore in this study. Within the same geology unit, sites with $z_{gl} < 30$ m are expected to have higher Vs_{30} than sites with $z_{gl} \geq 30$ m. Hence, sites within each of the 12 geology groups are classified into two z_{gl} subgroups based on whether z_{gl} is more or less than 30 m.

Regional mapping of z_{gl} and z_{bdrk} for Metro Vancouver are underway. In this study, z_{gl} is compiled from borehole descriptions of the project's geodatabase for each *in situ* Vs_{30} measure. When required, other information is used to define the z_{gl} subgroup (less or more than 30 m) including nearby boreholes or sharp increases in velocity along the $Vs(z)$ or in the dispersion data. The z_{gl} data permits further subdivision of Vs_{30} data for 6 geology-based groups (Figure 5-14, Table 5-5). Not surprising, it is the lower Vs_{30} values (lower number groups) that are impacted by use of z_{gl}; Vs_{30} is significantly lower when z_{gl} is > 30 m. For Groups 5 and 8-10, z_{gl} is always < 30 m. For Group 7 (Capilano sediments), the majority of Vs_{30} data have $z_{gl} < 30$ m; till corresponds to 43 m depth from nearby borehole descriptions for 3 Vs_{30} sites in Coquitlam (Cc geologic unit). Figure 5-14 shows there is a clear dependence of z_{gl} on Vs_{30}. It is also clear that Vs_{30} variability is reduced when z_{gl} is > 30 m. The high σ_{lnVs30} when z_{gl} is < 30 m further confirms the strong correlation between Vs_{30} and z_{gl}. The crude bi-categorial nature of the z_{gl} measure is not able to explain the high variability in subgroups with $z_{gl} < 30$ m. Overall, the addition of the z_{gl} measure, although not as efficient and readily-available as topographic slope, with regional geology mapping will improve lower Vs_{30} predictions in the Metro Vancouver region.
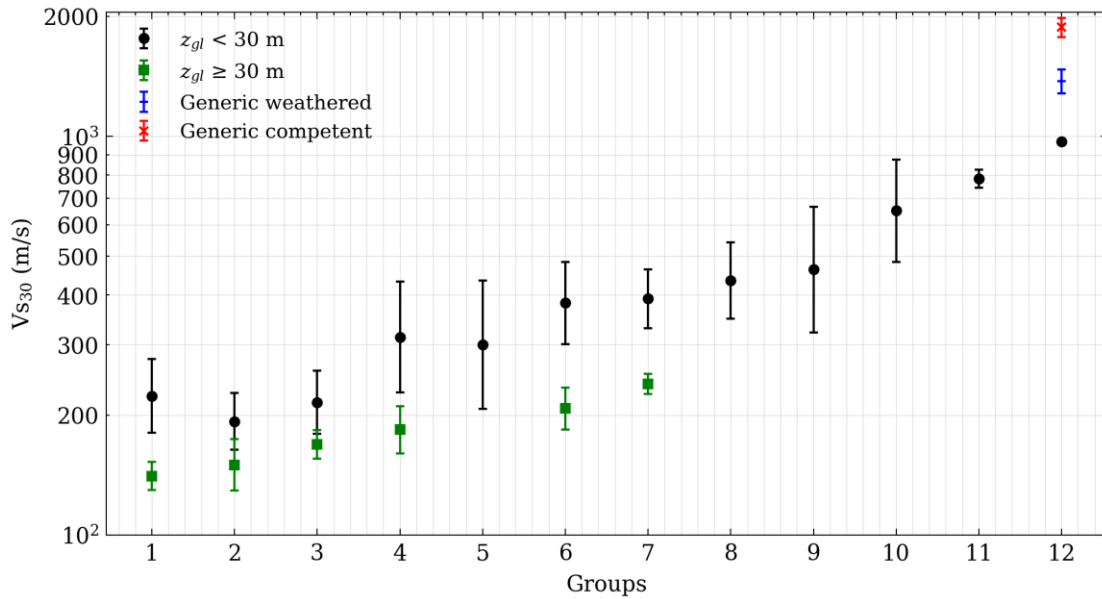
Figure 5-14. Measured and predicted Vs₃₀ statistics (μ_{lnV} and σ_{lnV}) from the developed models within surficial geology sub units in Metro Vancouver (Table 5-5).

Table 5-5. Hybrid geology-slope and geology-z_{gl} Vs₃₀ prediction models for Metro Vancouver.

Group number	Geology-Slope					Geology-z_{gl}					
	Geology			Slope coefficients		$z_{gl} \geq 30$ m			$z_{gl} < 30$ m		
	μ_{lnVs30} (m/s)	σ_{lnVs30}	N	d_0	d_1	μ_{lnVs30} (m/s)	σ_{lnVs30}	N	Mean Vs₃₀ (m/s)	σ_{lnVs30}	N
1	153	0.132	11	4.851	11.42	140	0.081	9	223	0.212	2
2	153	0.165	69	-	-	150	0.149	63	193	0.164	6
3	171	0.099	268	5.108	3.992	169	0.083	254	215*	0.181	14
4	215	0.256	24	5.226	6.537	184	0.137	17	314	0.32	7
5	300	0.37	7	-	-	-	-	-	300	0.37	7
6	312	0.363	9	-	-	208	0.121	3	382	0.238	6
7	362	0.206	19	5.707	6.608	239	0.057	3	391	0.17	16
8	435	0.221	74	-	-	-	-	-	435	0.221	74
9	463	0.363	13	-	-	-	-	-	463	0.363	13
10	651	0.296	17	-	-	-	-	-	651	0.296	17
11	783	0.052	3	-	-	-	-	-	783	0.052	3
12	971	-	1	-	-	-	-	-	971+	-	1

*Eq. 5-5 to be used if z_{gl} is known. + Vs₃₀ ranges between 1293 and 1981 m/s from the two generic Vs(z) with variability for weathered and competent granitic rocks of the North Shore.

The possibility of using z_{gl} as a continuous parameter in the hybrid geology-z_{gl} Vs_{30} prediction model to explored further. The z_{gl} is value is known at 13 of the 14 Vs_{30} observations in Group 3 with $z_{gl} < 30$ m. Figure 5-15 shows correlation between *in situ* Vs_{30} and z_{gl} for Group 3. The best-fit log-log model is statistically significant ($p < 0.05$) and described by

$$\ln(Vs_{30}) = 5.294 - 0.2124 \ln(z_{gl}), \quad \text{for Group 3 and } z_{gl} < 30 \text{ m.} \quad \textbf{Eq. 5-5}$$

Incorporating Eq. 5-5 in the geology-z_{gl} model can reduce Vs_{30} uncertainty when z_{gl} is $<$ 30 m. Direct use of z_{gl} would improve Vs_{30} predictions but requires available borehole data that log into glacial sediments to accurately determine z_{gl}. The attractiveness of the bi-categorical geology-z_{gl} model based on z_{gl} less or greater than 30 m is in its simpler application to a map as will be discussed in section 5.6.4.
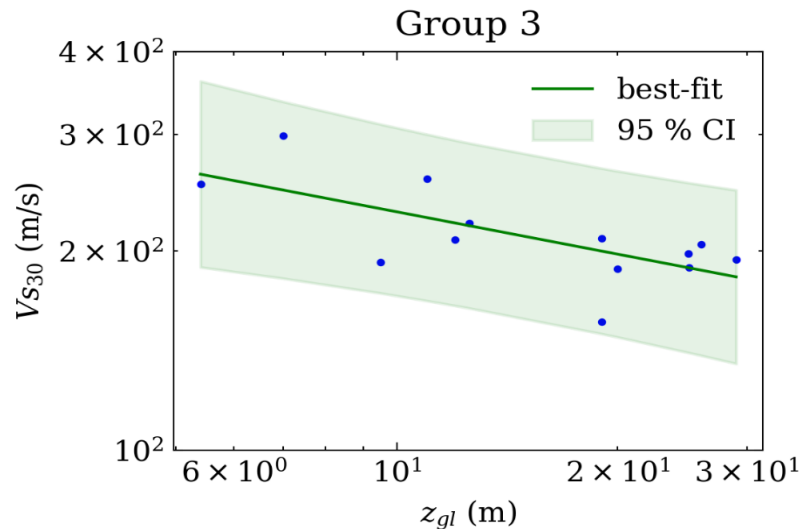
Figure 5-15. Vs₃₀ scaling with z_gl for the Group 3 and z_gl < 30 m. The best fit model (Eq. 5-5) is shown with the 95 % confidence interval (CI).

5.6.3 Performance of the Developed Hybrid Proxy-based Vs_{30} Prediction Models

To assess the performance of the two developed hybrid proxy-based (geology-slope and geology-z_{gl}) Vs_{30} prediction models, their Vs_{30} predictions at each *in situ* Vs_{30} are calculated using the site's mapped Quaternary geology, topographic slope, and z_{gl} category (Table 5-5). For sites in Group 3 with known $z_{gl} < 30$ m, Vs_{30} is predicted from z_{gl} using Eq. 5-5. The residuals (in natural log units) between measured and predicted Vs_{30} from each model are calculated. Groups 5, 8, 9, 10, 11, and 12 are based on geology only, the same Vs_{30} is predicted using either hybrid Vs_{30} prediction model. Comparison of model residuals for groups distinguished by both topographic slope and z_{gl} (Groups 1, 3, 4, and 7) enables comparing the Vs_{30} predictive power of the two different proxy Vs_{30} metrics.

The only other existing Vs_{30} prediction model that is specific to the Pacific Northwest is the PNWA17 (Adhi et al. 2017) geology-proxy model, which was developed using compiled Vs_{30} from Washington, Oregon, Alaska, and 320 Vs_{30} from British Columbia (315 Vs_{30} from Metro Vancouver mostly from GSC testing), is also used to predict Vs_{30}. The Metro Vancouver $Vs(z)$ data included in the PNWA17 model includes the 182 $Vs(z)$ converted from Vp reflection surveying by the GSC, which are not included in this study due to their low Vs_{30} resolution. For direct comparison, the geologic unit assigned by Ahdi et al. (2017) to each *in situ* Vs_{30} location is used. For sites located in geologic units not included in the development of the PNWA17 model, a Vs_{30} of the PNWA17 group with similar geology description to that of the site is assigned.

Figure 5-16 presents the residuals ($\mu_{Res} \pm \sigma_{Res}$) between *in situ* and predicted Vs_{30} for the three considered models. Both hybrid Vs_{30}-proxy models developed in this study have near zero μ_{Res} in all geologic groupings as the models are derived from the *in situ* Vs_{30} data. The PNWA17 model shows small μ_{Res} for Groups 2, 4, 7-9 indicating low bias. The 315 Metro Vancouver Vs_{30} included in PNWA17 are mainly limited to the FRD (Groups 2-4), and thus the largest μ_{Res} occur for non-FRD geologic groups (e.g., 1, 5, 6, 10). The PNWA17 model slightly overestimates Vs_{30} for Groups 2 and 3 possibly due to the inclusion of 182

converted-Vp reflection profiles in their model. Although Ahdi et al. (2017) applied a correction factor to reduce Vs_{30} from these converted-Vp profiles, the PNWA17 predicted Vs_{30} are higher (negative μ_{Res}) than Vs_{30} obtained in this study for Group 2 and 3 from higher resolution $Vs(z)$ measurements. Although only a few Vs_{30} are available in the two rock groups (Groups 11 and 12), the positive μ_{Res} from PNWA17 predictions in those groups are worth noting. PNWA17 predicts mean Vs_{30} of 455 m/s for undifferentiated sediments and sedimentary rocks (their Group 15) while the current study predicts mean Vs_{30} of 783 m/s (Group 11); the inclusion of softer sediments in their Group 15 explains the difference in predicted Vs_{30} between models. For Pre-Tertiary rocks, the PNWA17 model predicts a mean Vs_{30} of 750 m/s, their crystalline igneous and metamorphic rocks Group 18 (with 5 Vs_{30} observations, Table 4 in Ahdi et al. 2017), compared to a Vs_{30} range of 971-1981 m/s in this study (Table 5-5). One of the 5 Vs_{30} in the PNWA17 Group 18 came from a North Vancouver site ($Vs_{30} = 433$ m/s) that is assigned to Group 7 in this study (Gft outwash terrace deposits unit; Bednarski et al. 2014). By removing this site from PNWA17 Group 18, the mean Vs_{30} of the remaining 4 observations becomes 860 m/s, instead of 750 m/s, which is closer to this study's Group 12 Vs_{30} range. As mentioned previously in Section 5.2, Vs_{30} for Tertiary and Pre-Tertiary groups in this study are calculated from fill-corrected $Vs(z)$. This correction leads to higher Vs_{30} representative of the actual geology unit without including fill layers. Correcting $Vs(z)$ for fills is more adequate for developing models to be applied to more-detailed geology maps that accurately depict fill areas. The fill-corrected Tertiary and Pre-Tertiary rock Vs_{30} presented here are considered more representative of the actual geology in Metro Vancouver.

Comparing the two hybrid proxy-based Vs_{30} prediction models developed in this study, μ_{Res} and σ_{Res} of all 12 groups are respectively 4.04 x 10^{-4} and 0.157 for the geology-z_{gl} model and 1.07 x 10^{-4} and 0.173 for the geology-slope model. In comparison to the PNWA17 geology-proxy model, μ_{Res} and σ_{Res} are 0.0294 and 0.22. The two models developed in this study from the compiled comprehensive *in situ* Vs_{30} database expectedly outperform the PNWA17 model based on Vs_{30} data from mostly other regions. The geology-z_{gl} model provides lower σ_{Res} for all groups combined and for the 4 groups where

both topographic slope and z_{gl} correlations exist (1, 3, 4, and 7). This confirms that z_{gl}, in combination with geology, leads to more accurate Vs_{30} predictions than geology with topographic slope in Metro Vancouver. Figure 5-13 demonstrates that strong trends exist between Vs_{30} and the topographic slope even for groups that yielded statistically insignificant correlations (2, 5, and 6). It is believed that with the inclusion of more Vs_{30} data in those groups, a combined geology-z_{gl}-slope Vs_{30} prediction model can outperform the geology-z_{gl} model and overcome its z_{gl} bi-categorization. The hybrid geology-z_{gl} model is recommended for Vs_{30} prediction in Metro Vancouver until more Vs_{30} data is compiled to supersede it.
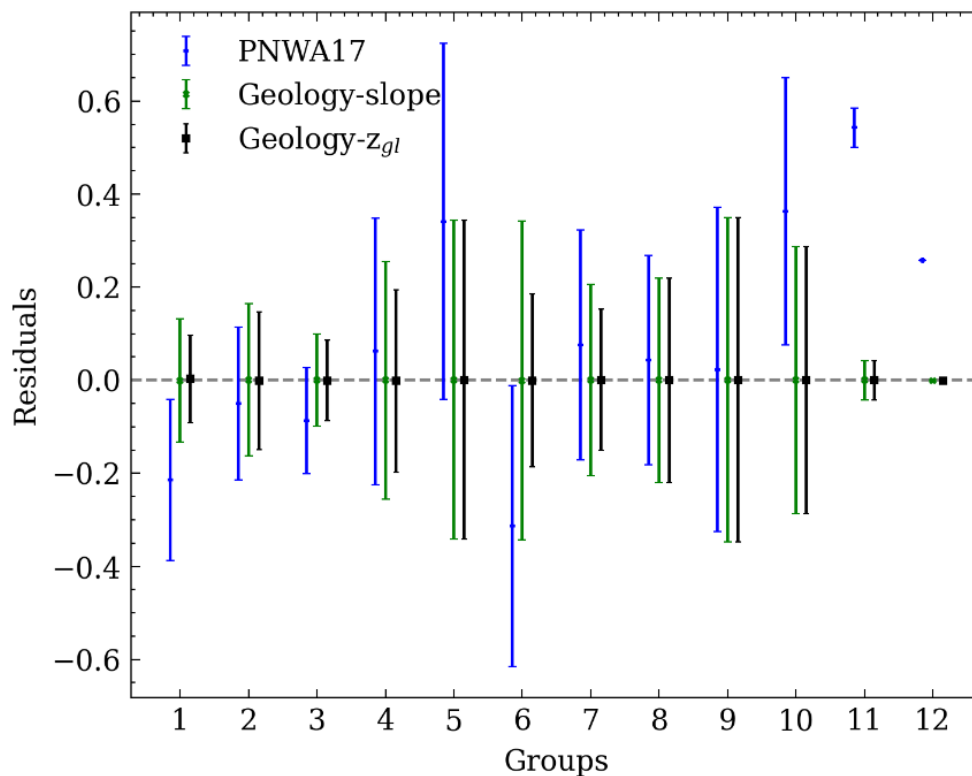
Figure 5-16. μRes and σRes of the geology-slope and geology-zgl Vs30 prediction models in this study in comparison to the PNWA17 model (Ahdi et al. 2017). The error bar represents ± one σRes.

5.6.4 Recommendations to Achieve Regional Vs$_{30}$ Mapping Geology-z$_{gl}$ Model

From a mapping perspective, the geology-slope model can be directly applied to available geology and topographic slope maps for the region. The application of the recommended geology-z$_{gl}$ model, however, requires 30-m-based z$_{gl}$ categorization that are currently not an available regional map product. Areas where z$_{gl}$ spans the 30 m threshold, include the edges of the FRD, Serpentine-Nicomekl valley, Capilano and Seymour deltas in the North Shore, and limited locations in the city of Coquitlam. Although incorporating z$_{gl}$ as a continuous parameter in a geology-z$_{gl}$ model can lead to improved Vs$_{30}$ predictions (Figure 5-15), substantial borehole information is required to regionally map z$_{gl}$ accurately. Using a simple 30-m threshold for z$_{gl}$ (bi-categorization) provides a practical solution for our regional application. Defining the 30-m threshold for z$_{gl}$ may be accomplished using available deep borehole information from the geodatabase where available and guided by alternative simplified methods. Assaf et al. (2022) developed a z$_{gl}$ predictive model (Eq. 3-5) based on the 2nd peak frequency from MHVSR measurements (f$_{1,HVSR}$) for shallow sites in the FRD; a z$_{gl} \geq 30$ m corresponds to a f$_{1,HVSR} \leq 1.55$ Hz. The 2000+ MHVSR measurements compiled during the project (Sirohey, 2022) can be used to define the 30-m threshold for z$_{gl}$ based on f$_{1,HVSR}$. Additionally, Monahan (2017) defined a 1-km wide zone around the FRD where z$_{gl}$ is ≤ 50 m; post-glacial FRD sediments are generally thicker than 50 m at distances greater than 1 km from the delta margins. This delta edge zone can be updated to reflect the 30 m z$_{gl}$ boundary instead of 50 m. Incorporating the geology-z$_{gl}$ model into regional Vs$_{30}$ mapping is simple and achievable using a combination of the suggested methods. The only currently existing form of a Vs$_{30}$ map for Metro Vancouver is a site class (categorized Vs$_{30}$) map developed by Monahan (2017). Thus, application of the developed hybrid geology-z$_{gl}$ model, adequate with the most recent and detailed geology maps, enables generation of the first refined Vs$_{30}$ map for Metro Vancouver.

5.7 Conclusions

A comprehensive Vs database from various *in situ* seismic site characteristic measurements is compiled for the Metro Vancouver region and used to establish generic Vs(z) relationships for various post-glacial, glacial, and rock geologies. The generic Vs(z) relationships for post-glacial sediments differentiate Vs(z) based on soil type and define Vs(z) of glacial and rock sediments for the first time. The generic Vs(z) relationships have direct use in many seismic hazard modelling applications (e.g., 3D geology modelling, site response analysis). The comprehensive Vs(z) database compiled for the Metro Vancouver region is used to develop a Vs_{30} database and calibrate a region-specific Vs_{zp}-to-Vs_{30} model for calculating Vs_{30} when $zp < 30$ m. Various additional *in situ* measurements (CPT and surface wave dispersion data) are converted to Vs(z) to calculate Vs_{30} and further populate an *in situ* Vs_{30} database. The compiled Vs_{30} database is used to develop two hybrid proxy-based Vs_{30} prediction models (geology-slope and geology-z_{gl}) for efficient regional mapping of Vs_{30} with reduced uncertainty. The inclusion of topographic slope and z_{gl} improves Vs_{30} prediction for 4 and 6 geologic groups, respectively, compared to geology-only Vs_{30} predictions. Using residual analysis, the performance of the two developed local Vs_{30} prediction models is compared to that of a PNWA17 geology-only model. The PNWA17 model generally overestimates Vs_{30} of softer post-glacial sediments and underestimates Vs_{30} of rock types in Metro Vancouver. The geology-z_{gl} model provides less variable residuals compared to the geology-slope model, indicating use of z_{gl} is a more powerful proxy for Vs_{30} prediction in Metro Vancouver. The geology-z_{gl} model can be easily implemented using simplified methods to produce the first Vs_{30} map for Metro Vancouver.

5.8 Data and Resources

The CPT digital data is obtained from the Metro Vancouver seismic microzonation database (Adhikari, PhD thesis, in progress).

Regressions are performed using statsmodels (Seabold et al. 2010, v.0.13.2), and lmfit (Newville et al. 2021, v.1.0.3) python packages. Topographic slope maps are obtained from the Canadian Digital Elevation model available at "Geospatial Extraction Tool" website (https://maps.canada.ca/czs/index-en.html, last accessed September 2022).

5.9   Acknowledgements

5.10 References

Adhikari, S.R., Molnar, S. (2021). Significance of geodatabase development for seismic microzonation in Metropolitan Vancouver. In: 17th World Conference on Earthquake Engineering, 27 Sept. – 2 Oct. 2021, Sendai, Japan, Paper 4521.

Ahdi, S. K., Stewart, J. P., Ancheta, T. D., Kwak, D. Y., & Mitra, D. (2017). Development of VS profile database and proxy-based models for VS30 prediction in the Pacific Northwest region of North America. Bulletin of the Seismological Society of America, 107(4), 1781-1801.https://doi.org/10.1785/0120160335

Allen, T. I., & Wald, D. J. (2009). On the use of high-resolution topographic data as a proxy for seismic site conditions (VS30). Bulletin of the Seismological Society of America, 99(2A), 935-943.

Armstrong, J.E., Hicock, S.R. (1979). Geological Survey of Canada, "A" Series Map 1486A, 1979, 1 sheet,. https://doi.org/10.4095/108876

Armstrong, J.E., Hicock, S.R. (1980). Surficial geology of New Westminster, Map 1484A, Geological Survey of Canada, "A" Series Map 1484A, 1980, 1 sheet, https://doi.org/10.4095/108874

Armstrong, J.E. (1984). Environmental and engineering applications of the surficial geology of the Fraser Lowlands, British Columbia; Geological Survey of Canada, Paper 83-23, 54 pages.

Assaf, J., Molnar, S., El Naggar, M. H., & Sirohey, A. (2022). Seismic site characterization in Fraser River Delta in Metropolitan Vancouver. Soil Dynamics and Earthquake Engineering, 161, 107384. https://doi.org/https://doi.org/10.1016/j.soildyn.2022.107384

Assaf, J., Molnar, S., & El Naggar, M. H. (2023). CPT-Vs correlations for post-glacial sediments in Metropolitan Vancouver. Soil Dynamics and Earthquake Engineering, 165, 107693. https://doi.org/10.1016/j.soildyn.2022.107693

Blais-Stevens, A. (2008). Surficial geology and landslide inventory of the lower Sea to Sky corridor, British Columbia: Geological Survey of Canada, Open File 5324, 2008, 1 sheet; 1 CD-ROM, https://doi.org/10.4095/224964

Bednarski, J. M. (2014). Surficial geology, District of North Vancouver, British Columbia, Geological Survey of Canada, Canadian Geoscience Map 203, 2014, 1 sheet, https://doi.org/10.4095/295128

Bard, P-Y., Bouchon, M. (1985). THE TWO-DIMENSIONAL RESONANCE OF SEDIMENT-FILLED VALLEYS. Bulletin of the Seismological Society of Americ 75:519–54

Bilson Darko, A., Molnar, S., & Sadrekarimi, A. (2020). Blind comparison of non-invasive shear wave velocity profiling with invasive methods at bridge sites in Windsor, Ontario. Soil Dynamics and Earthquake Engineering, 129. https://doi.org/10.1016/j.soildyn.2019.105906

Boore, D.M. (2004). Estimating $\bar{V}s(30)$ (or NEHRP Site Classes) from Shallow Velocity Models (Depths < 30 m). Bulletin of the Seismological Society of America 94:591–597. https://doi.org/10.1785/0120030105

Boore, D.M., Thompson, E.M., Cadet, H. (2011). Regional Correlations of VS30 and Velocities Averaged Over Depths Less Than and Greater Than 30 Meters. Bulletin of the Seismological Society of America 101:3046–3059. https://doi.org/10.1785/0120110071

Boucher, C. (2022). Approaches to model non-uniquness and site complexity for non-invasive shear-wave depth profiling. London, Ontario: The University of Western University.

Borcherdt, R.D. (1994). Estimates of Site-Dependent Response Spectra for Design (Methodology and Justification). Earthquake Spectra 10:617–653

Borcherdt, R.D. (1970). Effects of Local Geology on Ground Motion Near San Francisco Rbay. Bulletin of the Seismological Society of America 60:29–61

Britton, J.R., Harris, J.B., Hunter, J.A., Luternauer, J.L. (1995). The bedrock surface beneath the Fraser River delta in British Columbia based on seismic measurements. In: Current Research 1995-E. Geological Survey of Canada, pages 83–89

Clague, J.J., Luternauer, J.L., Monahan, P.A., Edwardson, K.A., Dallimore, S.R., and Hunter, J.A., (1998): Quaternary stratigraphy and evolution of the Fraser delta; in Geology and Natural Hazards of the Fraser River Delta, British Columbia, (ed.) J.J. Clague, J.L. Luternauer, and D .C. Mosher; Geological Survey of Canada, Bulletin 525, pages 57-90.

Comina, C., Foti, S., Passeri, F., & Socco, L. V. (2022). Time-weighted average shear wave velocity profiles from surface wave tests through a wavelength-depth transformation. Soil Dynamics and Earthquake Engineering, 158, 107262.

Crespo, M. J., Benjumea, B., Moratalla, J. M., Lacoma, L., Macau, A., González, Á., ... & Stafford, P. J. (2022). A proxy-based model for estimating VS30 in the Iberian Peninsula. Soil Dynamics and Earthquake Engineering, 155, 107165.

Crow, H. L., Good, R. L., Hunter, J. A., Burns, R. A., Reman, A., & Russell, H. A. J. (2015). Borehole geophysical logs in unconsolidated sediments across Canada. Geological Survey of Canada, Open File 7591.

Dai, Z., Li, X., Hou, C. (2013). A Shear-Wave Velocity Model for VS30 Estimation Based on a Conditional Independence Property. Bulletin of the Seismological Society of America 103:3354–3361. https://doi.org/10.1785/0120130025

Dallimore, S.R., Edwardson, K.A., Hunter, J.A., Meldrum, J.L., Luternauer, J.L., & Clague, J.J. (1996). Lithologic, geotechnical and geophysical logs for a deep borehole at Richmond City Hall, British Columbia. Geological Survey of Canada Open File, 3356, 16.

Dickenson, S. (1994). Dynamic Response of Soft and Deep Cohesive Soils during the Loma Prieta Earthquake of October 17, 1989. PhD, University of California

Dunn, D., Ricketts, B. (1994). Surficial Geology of Fraser Lowlands Digitized From GSC Maps 1484A, 1485A, 1486A, and 1487A. Geologic Survey of Canada Open File 2894

Foulon, T., Saeidi, A., Chesnaux, R., Nastev, M., & Rouleau, A. (2018). Spatial distribution of soil shear-wave velocity and the fundamental period of vibration–a case study of the Saguenay region, Canada. Georisk: Assessment and Management of Risk for Engineered Systems and Geohazards, 12(1), 74-86.

Foster, K.M., Bradley, B.A., McGann, C.R., Wotherspoon, L.M. (2019). A VS30 Map for New Zealand Based on Geologic and Terrain Proxy Variables and Field Measurements. Earthquake Spectra 35:1865–1897. https://doi.org/10.1193/121118EQS281M

Garofalo, F., Foti, S., Hollender, F., Bard, P. Y., Cornou, C., Cox, B. R., Ohrnberger, M., Sicilia, D., Asten, M., di Giulio, G., Forbriger, T., Guillier, B., Hayashi, K., Martin,

A., Matsushima, S., Mercerat, D., Poggi, V., & Yamanaka, H. (2016). InterPACIFIC project: Comparison of invasive and non-invasive methods for seismic site characterization. Part I: Intra-comparison of surface wave methods. Soil Dynamics and Earthquake Engineering, 82. https://doi.org/10.1016/j.soildyn.2015.12.010

Hassani, B., and G. M. Atkinson (2018). Site-effects model for central and eastern North America based on peak frequency and average shear-wave velocity, Bull. Seismol. Soc. Am. 107, 338-350.

Hunter, J. A., Burns, R. A., Good, R. L., & Pelletier, C. F. (2016). Fraser River Delta–A compilation of shear wave velocities and borehole geophysics logs in unconsolidated sediments of the Fraser River Delta, British Columbia. Geological Survey of Canada Open File, 1-112.

Hunter, J. A., Burns, R. A., Good, R. L., & Pelletier, C. F (1998). A compilation of shear wave velocities and geophysical logs in unconsolidated sediments of the Fraser River delta.

Iwahashi, J., Pike, R.J. (2007). Automated classifications of topography from DEMs by an unsupervised nested-means algorithm and a three-part geometric signature. Geomorphology 86:409–440. https://doi.org/10.1016/j.geomorph.2006.09.012

Iwahashi, J., Kamiya, I., Matsuoka, M., & Yamazaki, D. (2018). Global terrain classification using 280 m DEMs: segmentation, clustering, and reclassification. Progress in Earth and Planetary Science, 5(1), 1-31.

Ladak, S. (2020). "Earthquake site characterization of rock sites in Eastern Canada and stiff ground sites in Vancouver, British Columbia". Electronic Thesis and Dissertation Repository. 6972. https://ir.lib.uwo.ca/etd/6972

Lin, S., Gucunski, N., Shams, S., & Wang, Y. (2021). Seismic Site Classification from Surface Wave Data to Vs,30 without inversion. Journal of Geotechnical and Geoenvironmental Engineering, 147(6), 04021029.

Martin, A.J., Diehl, J.G. (2004). Practical experience using a simplified procedure to measure average shear-wave velocity to a depth of 30 meters (VS30). In13th World Conf. on Earthquake Engineering 2004 Aug 1. Tokyo: International Association for Earthquake Engineering. 8 pages.

McGann, C. R., Bradley, B. A., Taylor, M. L., Wotherspoon, L. M., & Cubrinovski, M. (2015). Development of an empirical correlation for predicting shear wave velocity of Christchurch soils from cone penetration test data. Soil Dynamics and Earthquake Engineering, 75. https://doi.org/10.1016/j.soildyn.2015.03.023

McGann, C.R., Bradley, B.A., Cubrinovski, M., (2017). Development of a regional VS30 model and typical VS profiles for Christchurch, New Zealand from CPT data and region-specific CPT-VS correlation. Soil Dyn. Earthq. Eng. 95 (2017), 48–60. https://doi.org/10.1016/j.soildyn.2017.01.032.

Midorikawa S., Nogi Y., (2015). Estimation of V_{S30} from Shallow Velocity Profile. Journal of JAEE 15:2_91-2_96. https://doi.org/10.5610/jaee.15.2_91

Mital, U., Ahdi, S., Herrick, J., Iwahashi, J., Savvaidis, A., & Yong, A. (2021). A probabilistic framework to model distributions of Vs30. *Bulletin of the Seismological Society of America*, *111*(4). https://doi.org/10.1785/0120200281

Molnar, S., Assaf, J., Sirohey, A., & Adhikari, S. R. (2020). Overview of local site effects and seismic microzonation mapping in Metropolitan Vancouver, British Columbia, Canada. Engineering Geology, 270, 105568. https://doi.org/https://doi.org/10.1016/j.enggeo.2020.105568

Monahan. P., Levson, V. (2001). Development of a shear-wave velocity model of the near-surface deposits of southwestern British Columbia, Canada. in Proceedings: Fourth International Conference on Recent Advances in Geotechnical Earthquake Engineering and Soil Dynamics, San Diego, California, March 26–31, 2001, Paper 11-16, 12 p

Monahan, P.A. (2017). Soil hazard map of the Lower Mainland of British Columbia for assessing the earthquake hazard due to lateral ground shaking. APEGBC, UBC, BC ministry of education, June 2017. In: Seismic retrofit guidelines. third ed. volume 9; 2005. Part III, 1pp.

Motazedian, D., Hunter, J.A., Pugin, A., Crow, H. (2011). Development of a Vs30 (NEHRP) map for the city of Ottawa, Ontario, Canada. Canadian Geotechnical Journal 48:458–472. https://doi.org/10.1139/T10-081

Nastev, M., Parent, M., Ross, M., Howlett, D., & Benoit, N. (2016). Geospatial modelling of shear-wave velocity and fundamental site period of Quaternary marine and glacial sediments in the Ottawa and St. Lawrence Valleys, Canada. Soil Dynamics and Earthquake Engineering, 85, 103-116.

Newville, M., Otten, R., Nelson, A., Ingargiola, A., Stensitzki, T., Allan, D., Fox, A., Carter, F., Michał, Osborn, R., Pustakhod, D., lneuhaus, Weigand, S., Glenn, Deil, C., Mark, Hansen, A. L. R., Pasquevich, G., Foks, L., … Persaud, A. (2021). lmfit/lmfit-py: 1.0.3. https://doi.org/10.5281/ZENODO.5570790

Parker, G. A., Harmon, J. A., Stewart, J. P., Hashash, Y. M. A., Kottke, A. R., Rathje, E. M., Silva, W. J., & Campbell, K. W. (2017). Proxy-based Vs30 estimation in central and Eastern North America. *Bulletin of the Seismological Society of America*, *107*(1). https://doi.org/10.1785/0120160101

Rosset P, Bour-Belvaux M, Chouinard L (2015). Microzonation models for Montreal with respect to Vs30. Bulletin of Earthquake Engineering 13:2225–2239. https://doi.org/10.1007/s10518-014-9716-8

Salsabili, M., Saeidi, A., Rouleau, A., & Nastev, M. (2021). Seismic microzonation of a region with complex surficial geology based on different site classification approaches. Geoenvironmental Disasters, 8(1), 1-13.

Shearer, P.M., Orcutt, J.A. (1987). SURFACE AND NEAR-SURFACE EFFECTS ON SEISMIC WAVES THEORY AND BOREHOLE SEISMOMETER RESULTS. Bulletin of the Seismological Society of America 77:1168–1196

Seabold, S., & Perktold, J. (2010). Statsmodels: Econometric and statistical modeling with python. In Proceedings of the 9th Python in Science Conference (Vol. 57, No. 61, pp. 10-25080).

Thompson, E.M., Wald, D.J., Worden, C.B. (2014). A VS30 Map for California with Geologic and Topographic ConstraintsA VS30 Map for California with Geologic and Topographic Constraints. Bulletin of the Seismological Society of America 104:2313–2321. https://doi.org/10.1785/0120130312

Wald, D. J., & Allen, T. I. (2007). Topographic slope as a proxy for seismic site conditions and amplification. Bulletin of the Seismological Society of America, 97(5), 1379-1395.

Wair, B., DeJong, J., Shantz, T. (2012). Guidelines for estimation of shear wave velocity profiles. Berkeley: Pacific Earthquake Engineering Research Center, University of California PEER report no 2012/08;

Wang, H., Wang, S. (2015). A New Method for Estimating VS(30) from a Shallow Shear-Wave Velocity Profile (Depth <30 m). Bulletin of the Seismological Society of America 105:1359–1370. https://doi.org/10.1785/0120140103

Wills, C.J., Clahan, K.B. (2006). Developing a Map of Geologically Defined Site-Condition Categories for California. Bulletin of the Seismological Society of America 96:1483–1501. https://doi.org/10.1785/0120050179

Wills, C. J., Gutierrez, C. I., Perez, F. G., & Branum, D. M. (2015). A next generation Vs30 map for California based on geology and topography. *Bulletin of the Seismological Society of America*, *105*(6). https://doi.org/10.1785/0120150105

Yong, A., Hough, S.E., Iwahashi, J., Braverman, A. (2012). A Terrain-Based Site-Conditions Map of California with Implications for the Contiguous United States. Bulletin of the Seismological Society of America 102:114–128. https://doi.org/10.1785/0120100262

Zhao, J. X., & Xu, H. (2013). A comparison of VS 30 and site period as site-effect parameters in response spectral ground-motion prediction equations. Bulletin of the Seismological Society of America, 103(1), 1-18.

Zhu, C., M. Pilz, and F. Cotton (2020b).Which is a better proxy, site period or depth to bedrock, in modelling linear site response in addition to the average shear-wave velocity? Bull. Earthq. Eng. 18, 797–820.

Chapter 6

6 Regional Site Response Analysis in Metro Vancouver Considering Different Earthquake Source Types

Due to the limited quantity of observed earthquake recordings in Metro Vancouver, one-dimensional (1D) site response analysis (SRA) is investigated in this chapter in an effort to develop a region-specific site effects (amplification) model for Metro Vancouver. The Vs(z) database presented in Chapter 5 is used to examine reference site conditions and recommend 51 sites for SRA. Based on the Vs(z) data, reference site conditions with Vs_{30} = 760 m/s for the Uplands and Fraser River Delta (FRD) and Vs_{30} = 1500 m/s for the North Shore are selected. Regional Probabilistic Seismic Hazard Analyses (PSHA) compatible with the 6th generation seismic hazard model of Canada (CanadaSHM6) are conducted to develop input time histories for crustal, intraslab, and interface earthquake types for regional SRA. For each earthquake source type, time histories are scaled to the 2 and 10 % probabilities of exceedance (POE) in 50 years ground motions. The linear and nonlinear SRA results at 8 selected sites are presented and compared to the BSSA14 (Boore et al., 2014) ground motion model (GMM) site amplification. Sensitivity analyses are performed to evaluate the effect to site amplifications due to Vs variability of the deeper glacial sediments in the FRD and inclusion of Vs reversals. Other uncertainties and limitations associated with 1D SRA for the Metro Vancouver region are discussed. Observations and recommendations for developing a regional site amplification model are presented.

6.1 Introduction

Site effects (amplification) models are developed to account for the effect of local site conditions on the seismic waves. These models are incorporated in most ground motion models (GMMs) that predict the surface ground motions given earthquake source, path, and site parameters. Site amplification models are typically derived from earthquake recordings and statistical regressions based on selected seismic site characteristic

measure(s). Vs_{30}, the time-averaged shear wave velocity in the top 30 m (Borcherdt 1994), is the most commonly used *in situ* site characteristic measure to account for site effects. Vs_{30} values in a GMM are generally associated with full implicit Vs profiles that represent an average of the profiles used in deriving that GMM. Additional site characteristics such as the depth to a Vs of 1.0, 1.5, and 2.5 km/s ($Z_{1.0}$, $Z_{1.5}$, and $Z_{2.5}$, respectively) are used in addition to Vs_{30} in GMM development to capture site amplification at long spectral periods resulting from deep sedimentary basins (e.g., Day 2008; Campbell and Bozorgnia, 2014). More recently, several studies highlighted the importance of f_0, the fundamental site frequency, $f_0 = 1/T_0$, as an important amplification metric when a significant impedance contrast are present (e.g., Di Alessandro et al. 2012; Ghofrani and Atkinson 2014; Hashash et al. 2020a; Zhu et al. 2020). Peak frequency has been incorporated as an additional site term to Vs_{30} in several Central and Eastern North America (CENA) GMMs (e.g., Hassani & Atkinson 2018, Harmon et al. 2019b). GMMs developed using numerous earthquake recordings from several similar seismotectonic settings (countries) are referred to as ergodic models. The applicability of these ergodic ground motion models to other regions is often assumed valid when the two regions share similar seismotectonic settings. Ground motion uncertainty can be reduced when the site amplification model is appropriate for the site of interest. Ergodic models predict ground motions via simple site characteristic metrics (e.g., Vs_{30}, peak frequency, $Z_{2.5}$). Non-ergodic models reduce ground motion uncertainty further by incorporating site amplification models appropriate to the site/region.

Numerical one-dimensional (1D) site response analyses (SRA) have been used to derive site amplification specific to the site of interest (e.g., high consequence infrastructure of dams, nuclear facilities) or regionally as a non-ergodic GMM (e.g., Walling et al. 2008, Kamai et al. 2014, Abrahamson et al. 2014; Campbell and Bozorgnia 2014). Seyhan and Stewart (2014) derived a semi-empirical nonlinear amplification model for western North America (WNA) based on shallow crustal NA earthquake data and nonlinear SRAs by Kamai et al. (2014). The Seyhan and Stewart (2014) amplification model is adopted in the Boore et al. (2014, hereafter BSSA14) GMM for WNA crustal earthquakes. The BSSA14 GMM is implemented as one of four WNA crustal GMMs in the 6th generation seismic

hazard model of Canada (CanadaSHM6) (Kolaj et al, 2019). Recently, Harmon et al. (2019a, 2019b) developed an amplification model for Central and Eastern North America (CENA) from over 1.5 million linear, equivalent linear, and nonlinear SRAs. The Harmon et al. (2019b) amplification model (Hashash et al. 2020) was adopted in CENA GMMs used in the most recent national seismic hazard models for both Canada (Kolaj et al. 2019) and the United States (Petersen et al., 2020). Falcone et al. (2021) produced amplification maps for Italy based on regional-scale equivalent linear SRAs.

In the Fraser River Delta (FRD) south of Vancouver, several earthquake site response modelling studies have been accomplished. Atkinson and Cassidy (2000) compared linear SRI amplification via the quarter-wavelength approach with SSRs from the 1996 Duvall, Washington, and 1997 Georgia Strait earthquakes. They found a broadband amplification in the FRD of at least 3 to 6 relative to a reference condition with a Vs of 3.7 km/s at seismogenic depths (8 km). Finn et al. (2003) showed that 2D modelled linear amplification, in comparison to 1D modelling, improved the prediction of low amplitude recorded ground motions specifically for sites with thin post-glacial sediment deposits. Molnar et al. (2014a, b) used a finite-difference code and a 3D velocity structure of the Georgia Basin with a minimum Vs of 625 m/s to examine 3D site amplifications for long-period ground motion for shallow crustal and deep intraslab scenario earthquakes. They found that long period amplification (> 2 s) is a factor of 3-4 in Metro Vancouver. Recently, Kim (2019) produced a site amplification map for the FRD from equivalent linear and nonlinear SRA using crustal earthquake recordings from the NGA-West2 database (Ancheta et al. 2014). Kim (2019) generated 21 1D models with the same soil layering and assigned Vs from the Hunter et al. (2016) database, and derived amplification functions based on PGA on rock (PGA_r) and T_0. Kim (2019) included 10 profiles with depth to bedrock between 50 and 200 m; however, the shallowest known depth to bedrock in the FRD is 200 m (Britton et al. 1995). For producing the site amplification map, Kim (2019) calculated the natural period (T_0) from the available Vs profiles. None of the used Vs profiles extends to the bedrock depth, and thus T_0 calculated from shallow Vs profiles underestimates the actual T_0 related to bedrock depth. All the mentioned SRA studies were

limited to the FRD area in Metro Vancouver and none considered the probabilistic seismic hazard (all three earthquake source types together) in the modeling.

In this study, the most comprehensive Vs(z) database compiled for Metro Vancouver is used to predict site-specific (non-ergodic) surface ground motions via 1D SRA for the Metro Vancouver region considering the probabilistic seismic hazard, i.e., input motions scaled to 2% and 10% POE in 50 years hazard levels. Selection of an appropriate site reference condition (amplification is relative to the chosen reference) is accomplished by comparing the Vs(z) for Metro Vancouver rocks with the implicit Vs(z) of the four WNA crustal GMMs used in CanadaSHM6. PSHA using CanadaSHM6 is accomplished to develop a suite of 66 input time histories appropriate to each of the three earthquake source types at 2% and 10% POE in 50 years hazard levels. Linear and nonlinear 1D SRAs are performed for 8 representative sites in Metro Vancouver to generate site-specific amplification for comparison with the CanadaSHM6 BSSA14 site amplification model. SRA sensitivity analyses are conducted to examine the influence of Vs variability of deeper glacial sediments in the FRD and inclusion of Vs reversals on the predicted site amplification. Uncertainties and limitations of this study's 1D SRA procedure to accomplishing regional site amplification mapping are discussed. This study identifies 51 sites at which 1D SRA can be accomplished to develop a robust regional site amplification model.

6.2   Reference Site Condition Selection

The compiled comprehensive Vs(z) database of Chapter 5 identifies over 500 locations with *in situ* site characteristic measures sufficient to determine Vs_{30}. Of these, 51 sites are identified (Figure 6-1) that have sufficient *in situ* site characteristic measures (e.g., Vs(z), borehole lithology, z_{gl}, geotechnical laboratory sample testing) to perform 1D SRA and are spatially distributed to provide a representative sample of site conditions across Metro Vancouver. The reference site condition at the base of these 51 sites is variable. In geotechnical engineering applications (e.g., liquefaction assessment), the reference site condition (half-space in the 1D SRA soil column model) is often assigned to the top of

glaciated sediments immediately beneath the base of the FRD post-glacial sediments. This common practice is driven primarily by the fact that Vs(z) that penetrate into stiff glacial sediments correspond to seismic site class C (Vs_{30} = 450 m/s) which was the standard reference condition in national seismic hazard models (e.g., Adams et al. 2015). However, in CanadaSHM6, the site classification approach and its corresponding need of a particular reference condition is abandoned; amplification depends directly on Vs_{30}, i.e., each GMM's inherent site amplification model determines the site-specific ground motions.
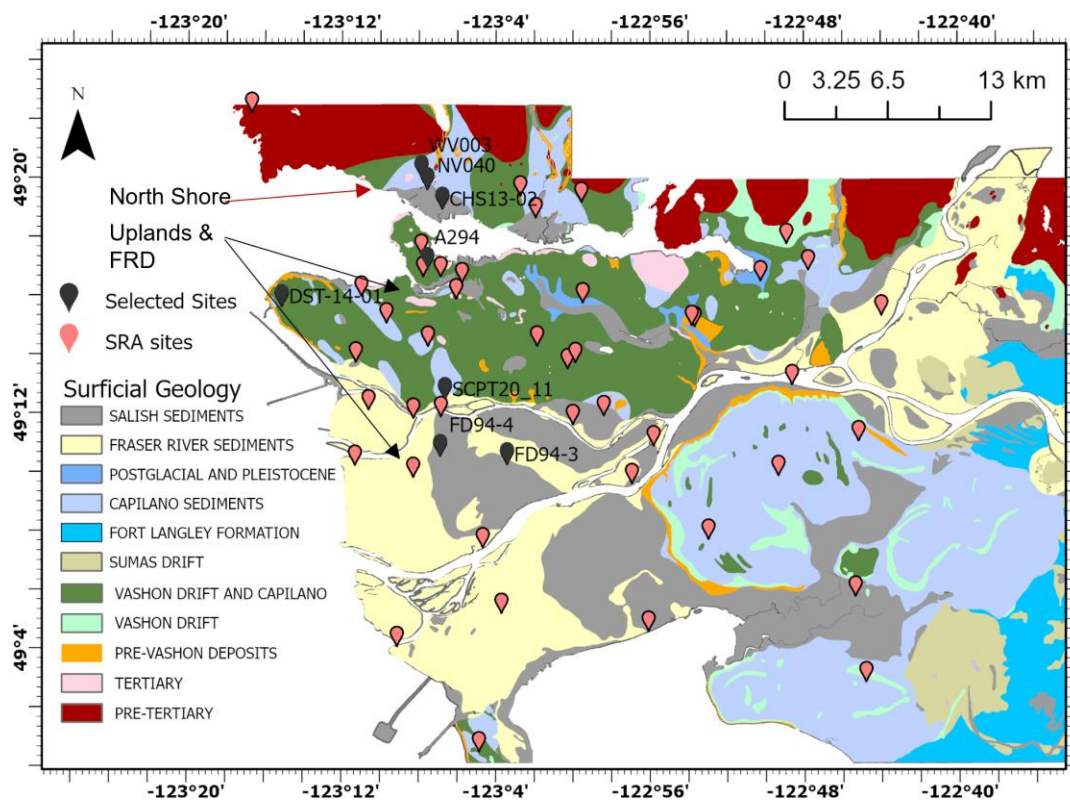
Figure 6-1. Locations of the 8 selected and 51 recommended sites for 1D SRAs overlaid on the compiled Quaternary geology map.

The appropriate reference condition to develop a regional site amplification model for Metro Vancouver is geologic bedrock (base of the full sediment column). The FRD and Uplands areas are underlain by Tertiary sedimentary rocks, while Pre-Tertiary plutonic

granitic rocks underlie the North Shore area, with some localized Tertiary rock outcrops (Figure 6-1). Hence the Vs(z) of these two different geologic rock types need to be compiled to select the appropriate reference site condition (Vs_{30}). As the reference Vs_{30} will be used in conjunction with the CanadaSHM6 hazard values to develop input time histories, it is important to ensure compatibility between the chosen reference Vs_{30} and the Vs_{30} used in CanadaSHM6 GMMs. Differences between the GMM implicit and the reference condition's Vs(z) should be corrected for. This approach is typically referred to as host-to-target corrections (e.g., Bard et al. 2019, Williams and Abrahamson 2021). However, implicit Vs(z) in GMMs are often not available or documented by GMM developers. Al Atik and Abrahamson (2021) proposed a method to derive implicit Vs(z) for the NGA-West2 GMMs associated with Vs_{30} of 620, 760 and 1100 m/s. As four NGA-West2 GMMs are equally weighted in calculating shallow crustal earthquake ground motions in the CanadaSHM6, the implicit Vs(z) of these GMMs are also compared to Vs(z) of Tertiary and Pre-Tertiary rocks in Metro Vancouver.

The Vs obtained from downhole measurements in Tertiary rock at shallow depths in Uplands is first compared to the implicit crustal GMMs Vs profiles for Vs_{30} of 620, 760 and 1100 m/s in Figure 6-2. It is obvious that GMMs implicit Vs profiles with Vs_{30} of 760 m/s (B/C site class boundary for soft rock in California) are the closest to Vs of Tertiary rock near the surface in the Uplands. For Tertiary rock beneath FRD, one Vs profile from downhole Vp measurement and 182 Vs profiles from Vp dynamic reflection measurements are available along with the depth to Tertiary bedrock from Hunter et al. (2016); 9 reflection Vs profiles were removed due to very low Vs from the presence of natural gas (Hunter et al. 2016). The remaining 173 Vs profiles separated by sediment type (above or below depth to bedrock) are shown in Figure 6-3a; the average +- one standard deviation (std) of soil and rock Vs are shown in Figure 6-3b. Tertiary rock average profile shows low Vs (<500 m/s) indicating weathering at shallow depths < 300 m and increase to around 1500 m/s at 800 m depth.

To compare these Tertiary Vs at depth with the implicit Vs profiles for crustal GMMs, the implicit profiles are plotted at the top of the Tertiary rock for each site following Williams and Abrahamson (2021). The comparison between the downhole profile and a selected reflection site Tertiary Vs profile with implicit GMM profiles for Vs_{30} of 760 and 1100 m/s (Figure 6-4a and b, respectively) shows that although the Vs_{30} of the FRD Tertiary rock at the two sites lies 760 and 1100 m/s (960 and 1018 m/s), the implicit Vs profiles for Vs_{30} of 760 m/s matches better with the Tertiary rock full Vs profile. The comparison for most of the remaining 172 reflection Vs profiles shows similar results. Thus, a reference condition Vs_{30} of 760 m/s is assigned to the FRD and Uplands areas.

For Pre-Tertiary rocks Vs in North Shore area, the comparison to the implicit Vs profiles with Vs_{30} of 1100 m/s in Figure 6-5. Vs_{30} ranges between 971 m/s and 1981 m/s for weathered and competent Pre-Tertiary rock in Metro Vancouver, respectively. Implicit Vs profiles with Vs_{30} of 1100 m/s underestimate the actual Vs profiles of Pre-Tertiary rock in North Shore, and thus a reference Vs_{30} of 1500 m/s is assumed.

Ideally, all CanadaSHM6 GMMs implicit Vs profiles should be compared to Metro Vancouver Vs reference conditions (i.e., Tertiary and Pre-Tertiary rock Vs). However, there are no publicly available implicit Vs profiles for the four intraslab and four interface GMMs in CanadaSHM6. Kolaj et al. (2019) applied correction factors to CanadaSHM6 interface and intraslab GMMs developed from Japan data to account for differences between site conditions in Cascadia and Japan following the method used for the 5th generation seismic hazard model (Adams et al., 2015; Atkinson & Adams, 2013). Thus, it is assumed that this correction factor is sufficient to ensure compatibility between intraslab and interface GMMs implicit profiles with Metro Vancouver reference site conditions.

The selected reference Vs_{30} values are representative of weathered rock conditions and eliminate the need to include weathered rock layers in SRA, thus removing additional uncertainties to the modeling. While selecting a higher reference condition in SRA includes more site-specific information, it should be noted that most GMMs are not well constrained above Vs_{30} of 1000-1500 m/s due to limited available earthquake recordings on hard rock.

The selected reference conditions provide a reasonable balance between including more region-specific information and providing well constrained seismic hazard estimates at the selected reference conditions. The reference conditions will be used to develop SRA input time histories.
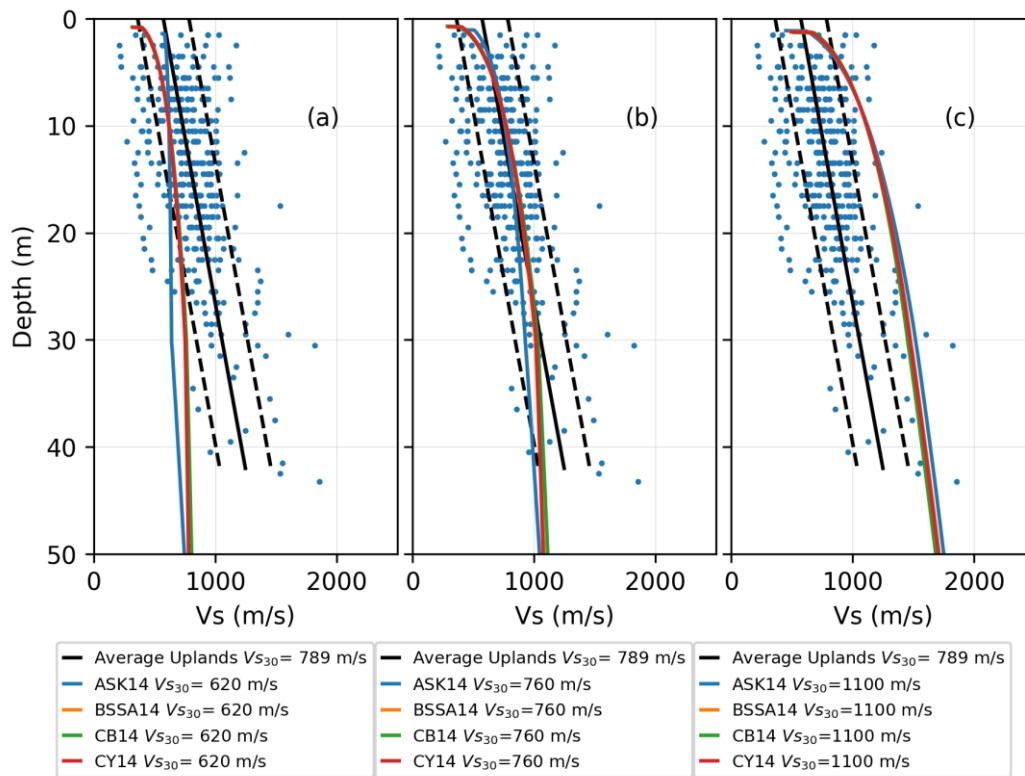
Figure 6-2. Comparison of the Vs(z) distribution of Tertiary sedimentary rocks (Table 5-1) in Uplands areas of Metro Vancouver and the four NGA-West2 GMM's implicit Vs(z) associated with Vs$_{30}$ of (a) 620, (b) 760 and (c) 1100 m/s.
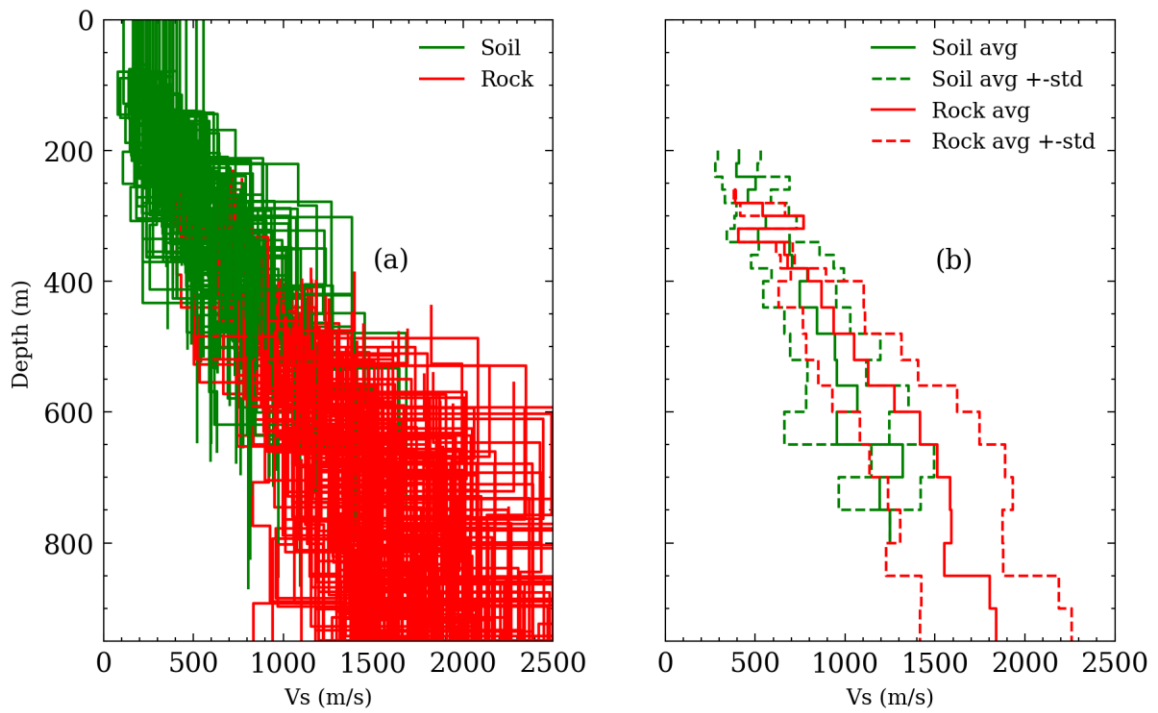
Figure 6-3. (a) Vs(z) distribution and (b) Vs(z) relationships for soil and Tertiary sedimentary rock beneath the FRD from 173 seismic reflection Vp(z) of Hunter et al. (2016).
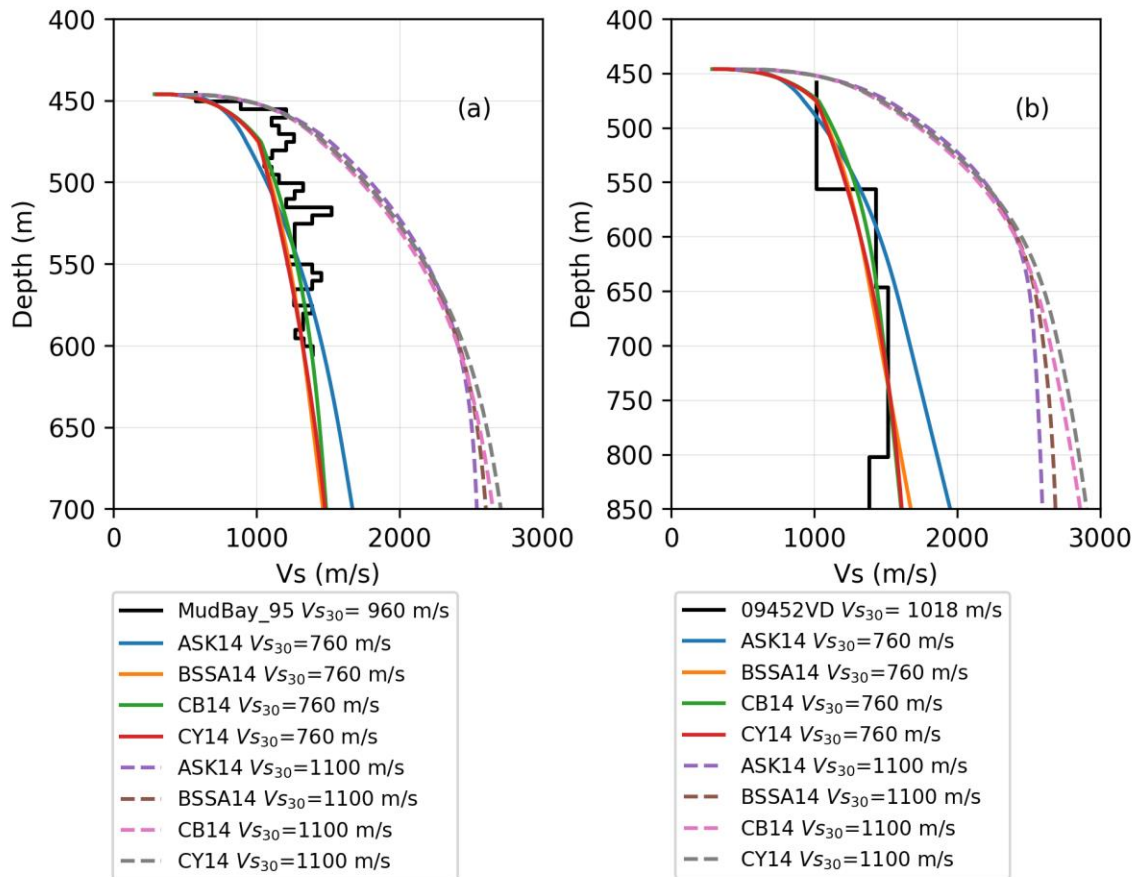
Figure 6-4. Vs(z) of FRD Tertiary rock from (a) an invasive Vs profile, and (b) an example reflection Vs profile compared to the four NGA-West2 GMM's implicit Vs profiles associated with Vs$_{30}$ of 760 and 1100 m/s.
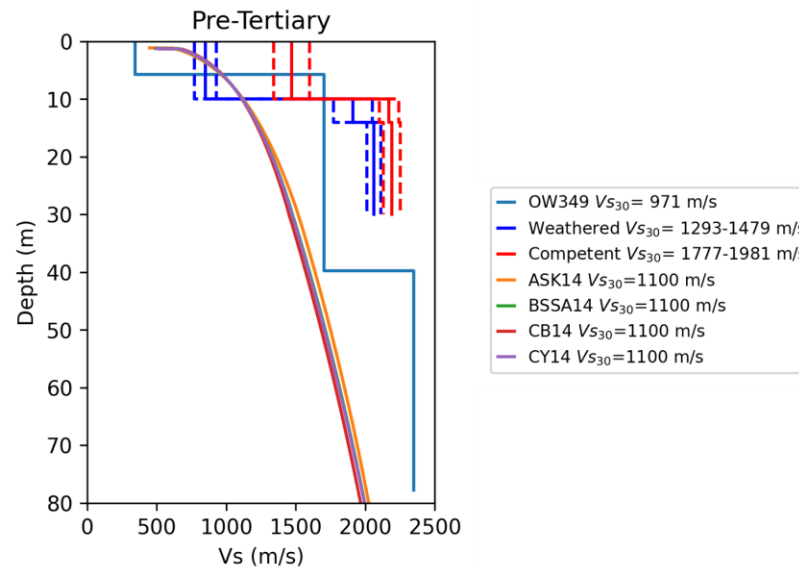
Figure 6-5. Vs(z) of Pre-Tertiary igneous beneath the North Shore compared to the four NGA-West2 GMM's implicit Vs profiles associated with a Vs_{30} of 1100 m/s.

6.3 Input Time Histories for Regional SRA

To develop input time histories representative of the local seismicity in Metro Vancouver for regional SRA, the 2 and 10 % in 50 years POE ground motions hazard levels for reference conditions Vs_{30} of 760 m/s and 1500 m/s are considered. PSHA using the CanadaSHM6 provides the total uniform hazard spectrum (UHS) for a specific Vs_{30}. In Metro Vancouver, this UHS is a combination of crustal, intraslab, and interface earthquake sources. However, the total UHS does not distinguish between contributions of different earthquake sources at different periods and cannot be directly used as a target spectrum for selecting input time histories for individual earthquakes. Individual UHS from single earthquake source types is a more representative target spectrum for developing input time histories. Ideally, the conditional mean spectrum (CMS) (Baker 2011) for each earthquake source type can better represent the spectral shape of earthquakes and may be a more realistic target spectrum than the individual UHS. However, due to the wide range of T_0 present in Metro Vancouver (very short T_0 in North Shore to very long T_0 in FRD), the CMS approach becomes unpractical for this regional study. Thus, the individual UHS for

each earthquake source at two hazard levels and at the two selected reference conditions is adopted as the target spectrum for time histories selection.

To generate the individual target UHS spectra, a suite of regional PSHAs are performed for each earthquake source type at the two selected hazard levels and reference site conditions. The CanadaSHM6 input model (M. Kolaj, pers. comm., 2022) is modified and implemented in the seismic hazard and risk modelling software OpenQuake (OQ) engine (v.3.2.2) (Pagani et al. 2014), which is the same OQ version used by NRCAN for generating CanadaSHM6 hazard values. The OQ model is first validated with NRCAN's CanadaSHM6 hazard values from the online NBCC 2020 Seismic Hazard Tool (https://www.seismescanada.rncan.gc.ca/hazard-alea/interpolat/nbc2020-cnb2020-en.php). For each earthquake source type, a series of PSHAs are performed at a grid of Metro Vancouver sites with 5 km spacing for the two selected POE levels and two reference site conditions (Vs_{30} of 760 m/s and 1500 m/s). In this way, target reference condition UHS spectra are produced specific to each earthquake source type (individual UHS). The individual target UHS spectra are determined as 5%-damped horizontal-component spectral acceleration (SA) at 9 spectral periods (0.05, 0.1, 0.2, 0.3, 0.5, 1.0, 2.0, 5.0, 10 seconds) in addition to Peak Ground Acceleration (PGA) taken as 0.01 s. Empirical recordings (time histories) of crustal, intraslab, and interface earthquakes will be selected and scaled to each of the applicable individual target UHS spectrum.

It is impractical to develop input time histories for each earthquake source and POE at many sites across Metro Vancouver. To overcome this challenge, time histories are selected and scaled to the individual target UHS to develop input time histories at 2 sites in the FRD and Uplands for reference condition of Vs_{30} = 760 m/s and one site in North Shore area for reference condition of Vs_{30} = 1500 m/s (see Figures C-1 and C-2 in Appendix C). Input time histories at other SRA sites can be obtained by scaling the scaled time histories at these three sites. To select earthquake time histories with characteristics applicable to the regional seismic hazard, the PSHAs at the three reference sites are disaggregated to identify the magnitude (M_w) and closest rupture-to-site distance (R_{rup}) that contribute the most to

the hazard (Table 6-1, Figure C-3). These M_w and R_{rup} are used to filter and select empirical earthquake recordings from the NGA-West2 database (Ancheta et al. 2013) for crustal earthquakes and the NGA-Subduction database (Mazzoni et al. 2021) for intraslab and interface earthquakes. For each earthquake source type, a suite of 11 horizontal time-histories with characteristics consistent with the regional seismic hazard are selected and scaled to the individual target UHS at each of the two POE levels for each of the three sites, i.e., (11 time histories x 2 POE x 3 earthquake sources x 3 sites = 198 scaled time histories total). For each reference site, the suite of 22 (crustal, inslab, or intraslab) time histories are scaled to the individual target UHS between 0.01 and 6.5 seconds such that their geometrical mean does not fall below 90 % of the target UHS. The final scaling factors for all the records at the 3 reference sites range between 0.44 and 4.38. Example acceleration, velocity, and displacement time series for reference site 35 in FRD (2 % in 50 yr POE) are shown in Figures C-4 to C-6 for crustal, intraslab, and interface earthquakes respectively. The time interval between 5 and 95 % of the arias intensity of the time series (Trifunac and Brady, 1975), or the significant duration (D5_95), is also shown as a blue shaded box in the displacement time series plot. An example of the suite of 11 crustal earthquake time histories scaled for the FRD site 35 at the 2 % in 50 yr POE is shown in Figure C-7 in log-log scale and in Figure C-8 in log-lin scale of Appendix C. The characteristics of all selected recordings for the three reference sites are listed in Tables C-1 to C-18. As seen in Figure C-2, the intraslab UHS has the highest spectral accelerations at shorter periods (< 1-2 sec for both POE), while interface UHS has the highest spectral acceleration at longer periods. As a result, intraslab input time histories have the highest PGA at the rock level (PGA_r) among the three earthquake source types.

Table 6-1. M_w and R_{rup} search criteria applied to select potential records for each earthquake type source at reference sites.

Earthquake Source Type	M_w	R_{rup} (km)
Crustal	6-7.4	10-110

Intraslab	6-7.5	50-120
Interface	>7.99	100-200

The time histories scaled to the three reference sites are then scaled with a constant factor to develop input time histories for each SRA site. The constant scaling factor is calculated as $UHS_{SRA}(T_s)/UHS_{ref}(T_s)$ where T_s is chosen as 1 s for crustal earthquakes and 2 s for intraslab and interface earthquakes. The choice of T_s is determined via iterative trial and error comparison of $UHS_{SRA}(T)$ and the adjusted $UHS_{ref}(T)$. The scaling factors for the 8 SRA sites range between 0.85 and 1.09 for the three earthquake types and 2 POEs. This methodology efficiently develops 66 input time histories at each of the 8 selected SRA sites in this study and at any SRA site (51 recommended) in future. The maximum error in UHS_{SRA} for the recommended 51 SRA sites is less than 5.7 % for all considered earthquake types, POE, and reference conditions.

6.4   SRA at 8 Selected Sites

The suite of SRAs performed at 8 selected sites in Metro Vancouver are presented here. The 8 sites are selected to represent a variety of subsurface conditions and locations across Metro Vancouver. The 8 sites span both shallow to deep glacial till and bedrock conditions (Table 6-2) and correspond to locations of *in situ* seismic measurements: 2 downhole Vs(z) sites (FD-94-4, FD94-3) and 1 SCPT site (SCPT20-11) in the FRD, 2 downhole Vs(z) sites (DST14-01, A294) in the Uplands, and 1 crosshole Vs(z) (CHS13-02) and 2 inverted Vs(z) (NV040, WV003) sites in the North shore. The inverted Vs(z) at NV040 and WV003 sites are obtained from joint inversion of multi-method non-invasive seismic testing performed by the Metro Vancouver microzonation project (Boucher 2022). Figure 6-6 depicts the 1D SRA models developed for the 8 sites in terms of Vs(z) and geology.

The soil layering at each site (Figure 6-6) is extracted from borehole or SCPT information. For NV040 and WV003, the soil layering is assigned from nearby boreholes. For SCPT20-11, the linear Vs (z) relationship for glacial sediments (Table 5-1) in the FRD is applied below the maximum available depth; for sites with glacial sediments at deeper depth

(FD94-4, FD94-3, DST14-01, CHS13-02), the last measured Vs value or a Vs of 550 m/s consistent with deeper glacial Vs (Table 5-1) are assigned as constant to bedrock depth (z_{brk}). The 1D soil model is developed to z_{brk} determined either from available z_{brk} data in the FRD (J. Hunter, pers. comm., 2016) or approximated based on $f_{0,HVSR}$ ($1/T_{0,HVSR}$) from nearby MHVSRs (Sirohey 2022) via equation

$$T_0 = 4 \ \sum \frac{h_i}{Vs_i} \qquad\qquad \textbf{Eq. 6-1}$$

where h_i and Vs_i are the thickness and Vs of layer i. For NV040 and WV003 sites, the half-space Vs from inversion is replaced with a Vs of 1500 m/s, the selected reference site condition for the North Shore.

Table 6-2. Site characteristics of the 8 selected sites.

Location	Site	Vs_{30} (m/s)	$T_0(s)^+$	z_{gl} (m)	z_{brk} (m)
FRD	FD94-4	140	5.2	235	526
FRD	FD94-3	206	3.77	19	464
FRD	SCPT20-11	195	2.06	22	200
Uplands	A294	427	0.21	1	16
Uplands	DST14-01	422	1.53	3	200
North Shore	CHS13-02	231	1.73	92	122
North Shore	NV040	489	0.36	3.4	49
North Shore	WV003	507	0.18	1	16

[+] $T_0(s)$ calculated using Eq. 6-1. z_{gl} = depth to glacial sediments. z_{brk} = depth to bedrock.
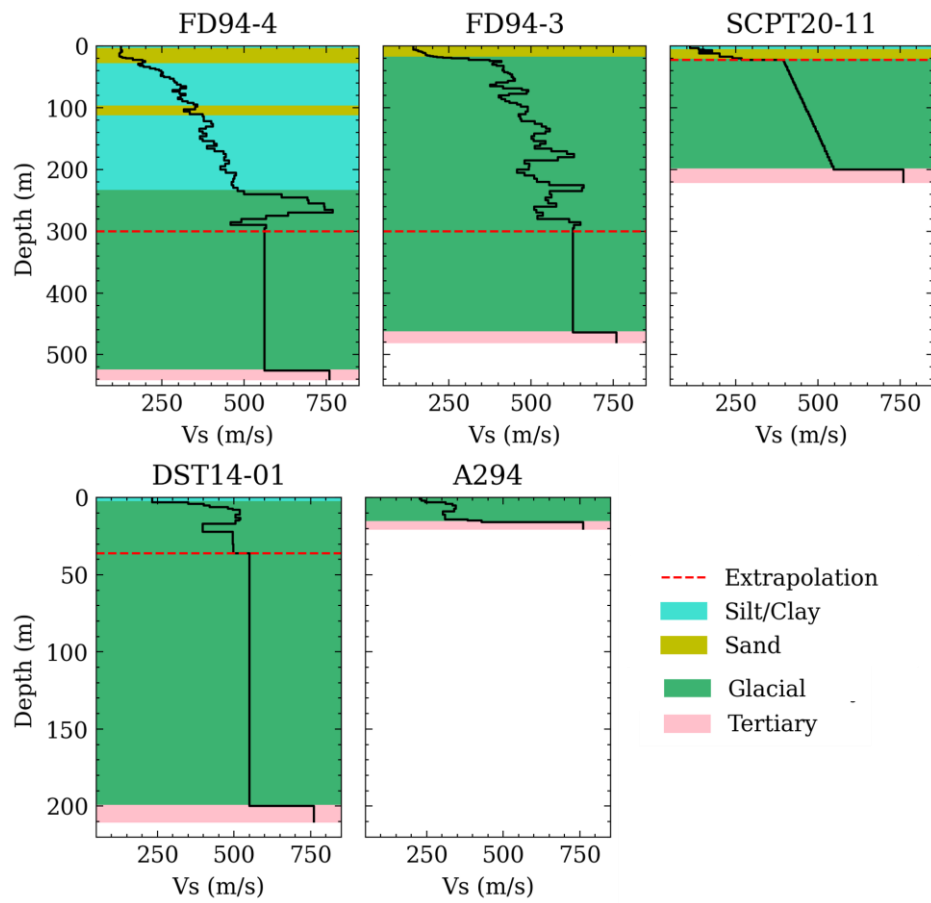
Figure 6-6. Depiction of the 1D soil models for the 3 North Shore sites.
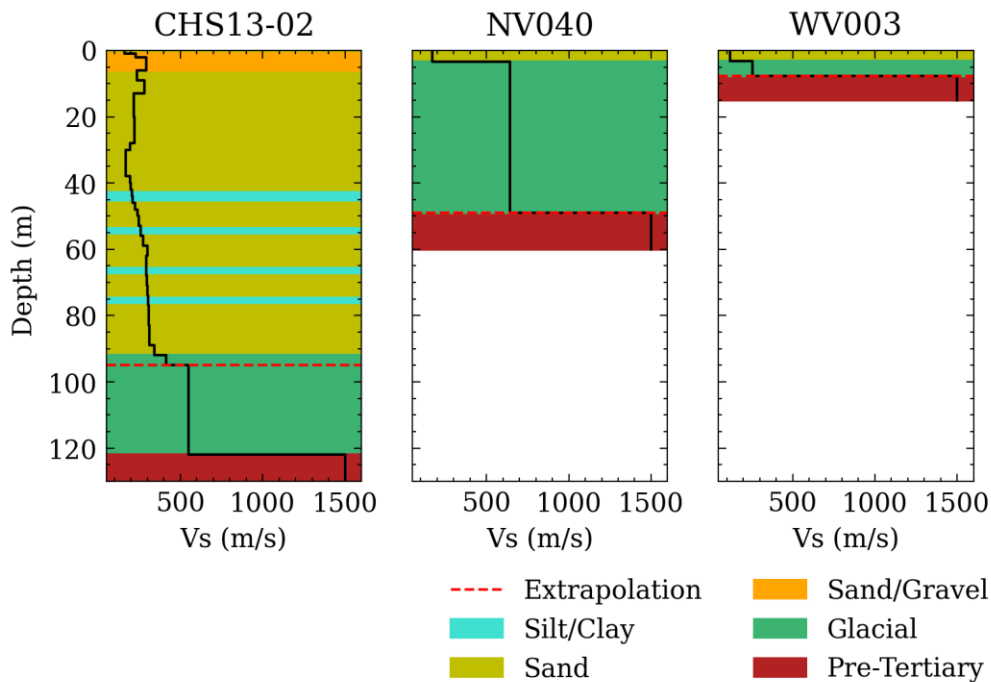
Figure 6-7. Depiction of the 1D soil models for the 3 North Shore sites.

Additional material properties required for the 1D soil models are reported in Table 6-3. Unit weights are calculated from soil densities available in the Metro Vancouver project's geodatabase (Adhikari and Molnar 2021). For Pre-Tertiary rock, the unit weight is assumed to be 24 kN/m^3. Nonlinear soil models in terms of dynamic modulus reduction and damping (MRD) curves are determined from a literature review of geotechnical reports in the Metro Vancouver project's geodatabase (e.g., Anderson et al. 2007). The MRD for glacial sediments are assigned a higher PI to consider the effect of depth (overconsolidation).

At total of 528 Linear (frequency domain) and 528 non-linear (time domain) SRA are performed using DEEPSOIL v7 software (Hashash et al. 2021) for the 8 sites. The modified Konder-Zolasko (MKZ) model (Matasovic 1993) is fit to the reference MRD curves using the non-Masing fitting tool (Phillips and Hashash, 2009). The small-strain damping (Dmin) obtained from the fitted MKZ model is also adopted for linear analysis. It should be noted that Dmin has influence on the results of linear amplification and some studies suggest the actual damping in the field is higher due to additional scattering effects not accounted for

in laboratory settings (e.g., Campbell 2009). The borehole array recordings of the 2015 earthquake (Molnar et al. 2020) are utilized to estimate Dmin of soils from the difference in spectral decay parameter (κ) at surface and at depth recordings; however, κ at depths was similar or sometimes higher than κ at surface depth leading to negative Dmin results. Future recordings by the borehole arrays can lead to better constraints on Dmin for SRA.

Table 6-3. Unit weight and MRD curves for different sediments used in SRA .

Soil Type	Unit Weight (kN/m³)	Modulus Reduction Curve	Damping Curve
Sand	18.3	Seed & Idriss (1970) Upper	Seed & Idriss (1970) Lower
Sand & Gravel	19.5	Seed & Idriss (1970) Upper	Seed & Idriss (1970) Lower
Silts and Clays	17.7	Vucetic & Dobry (1991) z < 150 m, PI = 15 z > 150 m, PI = 30	
Glacial sediments	21.2	Vucetic & Dobry (1991) z < 100 m; PI = 30 z > 100 m; PI = 50	
Half-space (Tertiary rock)	22.5	NA	NA
Half-space (Pre-Tertiary rock)	24	NA	NA

6.4.1   SRA Results and Comparison to BSSA14 GMM Site Amplification

For each of the 8 selected sites, linear and nonlinear site response analyses are conducted using the site-specific 66 scaled input time histories. Site amplification is defined as the ratio of the 5% damped surface acceleration response spectrum to the 5 % damped input acceleration spectrum. For sites in North Shore, the amplification is relative to reference condition of 1500 m/s while the amplification at sites in the FRD and Uplands is relative to reference condition of 760 m/s. To directly compare site amplification results, amplification values for North Shore sites are converted to the 760 m/s reference site condition (Stewart et al. 2017) as follows

$$Amp_{/760} = Amp_{/1500} \text{ x } \mu_{1500/760} \qquad \textbf{Eq. 6-2}$$

Where $Amp_{/760}$ is the converted SRA amplification relative to 760 m/s reference, $Amp_{/1500}$ is the SRA amplification in North Shore relative to 1500 m/s, and $\mu_{1500/760}$ is the ergodic mean amplification of Vs_{30} of 1500 m/s relative to 760 m/s from the four CanadaSHM6 GMMs adopted for each earthquake source type. The $\mu_{1500/760}$ amplification ratio for the three earthquake source types are shown in Figure 6-8.
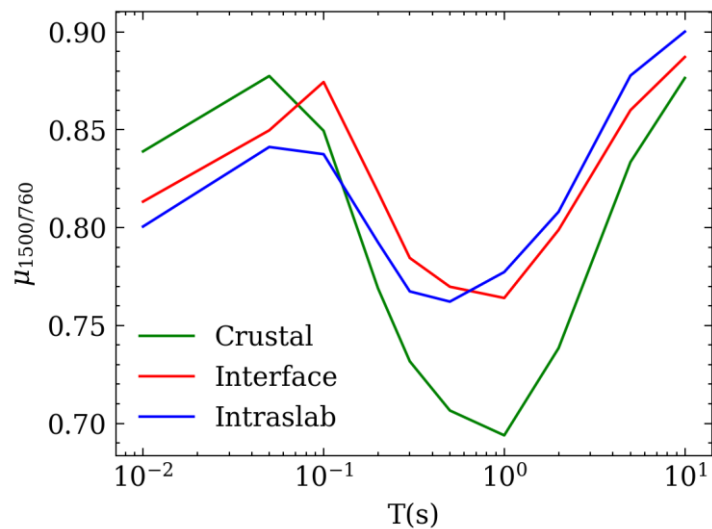
Figure 6-8. Mean amplification for a site with Vs_{30} = 1500 m/s relative to a reference of Vs_{30} = 760 m/s as calculated from the four GMMs used in CanadaSHM6 for each earthquake source type.

To understand the site-specific ground motions generated via 1D SRA in the context of the CanadaSHM6 seismic design motions, the SRA amplification spectra are compared to the BSSA14 WNA crustal GMM median site amplification implemented in CanadaSHM6. The BSSA14 site amplification model is developed for Vs_{30} ranging from 150 to 1500 m/s with a reference condition of 760 m/s and periods 0.01 to 10 s. Kolaj et al. (2019) also applied the BSSA14 amplification model in one intraslab and one interface GMM of CanadaSHM6 that lacked a native site amplification model assuming it is a reasonable estimate of WNA site amplification. Thus, all SRA site amplifications are compared to BSSA14 site

amplification for simplicity and to limit the number of GMM site amplification model comparisons.

The BSSA14 linear site amplification are calculated based on Vs_{30} at each site (Table 6-2). The mean linear amplification for each earthquake source (from 22 input time histories) at each site is calculated and compared to the BSSA14 linear amplification in Figure 6-9. The mean linear amplification values from different earthquake source types are generally similar at all sites. The interface-source linear amplification at short periods is slightly higher than crustal and intraslab sources for deep sites (long T_0, e.g., FD94-4), and lower for shallow sites with very short T_0 (e.g., A294 and WV003). Crustal and intraslab input motions are usually rich in shorter periods content that is amplified at shallow sites, while interface input motions carry significant long period content that is amplified at deeper sites. Not surprisingly, the site-specific SRA linear amplification displays more frequency dependence (site resonances) than the empirical broadband BSSA amplification model (ergodic GMM development leads to smoothed amplification models). For sites with deep bedrock (FD94-4, FD94-3, SCPT20-11), BSSA14 linear amplification is higher than SRA specifically at longer periods. For shallow sites, the SRA linear amplification exceeds that of BSSA14 at specific (resonance) periods. This is readily apparent for the two North Shore sites, NV040 and WV004, where the shallow strong impedance contrast leads to high linear amplification not accounted for in the ergodic Vs_{30}-based BSSA14 model.

The mean nonlinear SRA amplifications for the 2 % in 50 yr POE hazard level for each earthquake source type at the 8 sites are shown in Figure 6-10. The differences between mean amplifications of different earthquake sources are more obvious for sites with lower Vs_{30} due to strong nonlinearity (e.g., FD94-4 and CHS13-02). At the 2 % in 50 yr POE, PGA_r of intraslab input motions is the highest leading to stronger nonlinearity and deamplification. Although interface input motions are of lower PGA_r compared to crustal input motions, they induce more pronounced deamplification at deep soft sites (e.g., FD94-4 and CHS13-02) due to higher induced shear strains caused by longer shaking durations.

At stiffer sites (e.g., A294 and DST14-01), nonlinear SRA amplification from the three earthquake sources are similar as limited soil nonlinearity occurs for these stiffer soil sites.
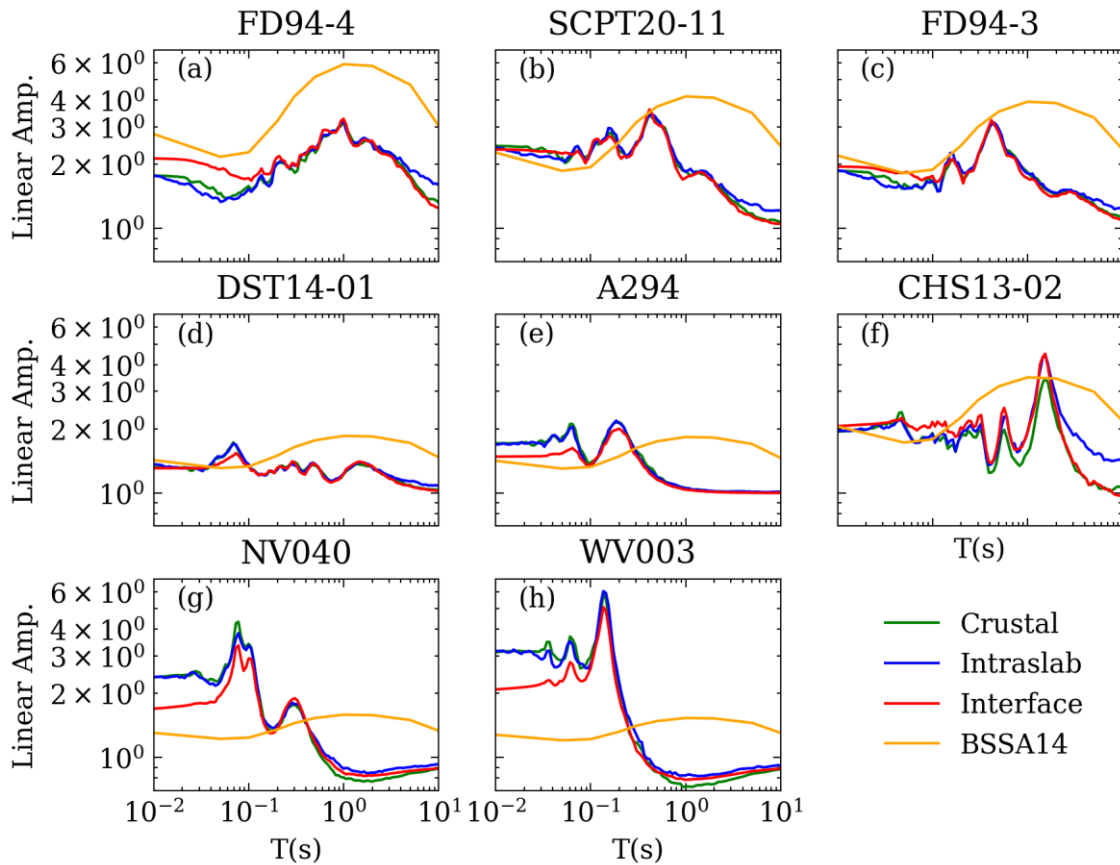
Figure 6-9. Mean linear amplification from 1D SRA for each earthquake source type at 8 sites in comparison to the BSSA14 GMM linear amplification.

To better evaluate the nonlinear behaviour, the amplification at the deep soft site FD94-4 is plotted with PGA_r at 8 spectral periods for both POE input ground motion levels in Figure 6-11; 10 % POE results plot at lower PGA_r than 2 % POE and linear SRA amplification from Figure 6-9 are plotted at a PGA_r of 0.001 g. The BSSA amplification for the same Vs_{30} of 140 m/s is also plotted for comparison. More prominent de-amplification occurs as PGA_r increases due to nonlinear soil behaviour. The strongest observed de-amplification occurs for intraslab input motions due to their higher PGA_r. The nonlinearity due to interface input motions is stronger than that of crustal motions with similar PGA_r for

periods up to 2 s. Compared to BSSA14, SRA results demonstrate stronger nonlinearity manifested as a steeper slope in amplification with PGA_r. This may be due to post-glacial sediments in the FRD ($z_{gl} = 235$ m at FD94-4) being thicker than most sites from which the BSSA14 model is derived. The same comparison is shown in Figure 6-12 for North Shore site CSH13-02 with z_{gl} of 92 m. Similar trends to FD94-4 are observed where deamplification in SRA is stronger than that of BSSA14. These observations of the non-ergodic site amplification at two sites in FRD and North Shore areas suggest that nonlinearity in Metro Vancouver can be stronger than that in BSSA14 due to the large thickness of soft post-glacial sediments. Figure 6-13 shows the nonlinear SRA amplification with PGA_r for SCPT20-11 site with z_{gl} of 22 m only. The nonlinearity at SCPT20-11 is less significant compared to FD94-4 and CHS13-02, and the amplification at shorter periods is more consistent with BSSA14 amplification. At periods longer than T_0 ~ 2.06 seconds, BSSA14 amplification is much higher.
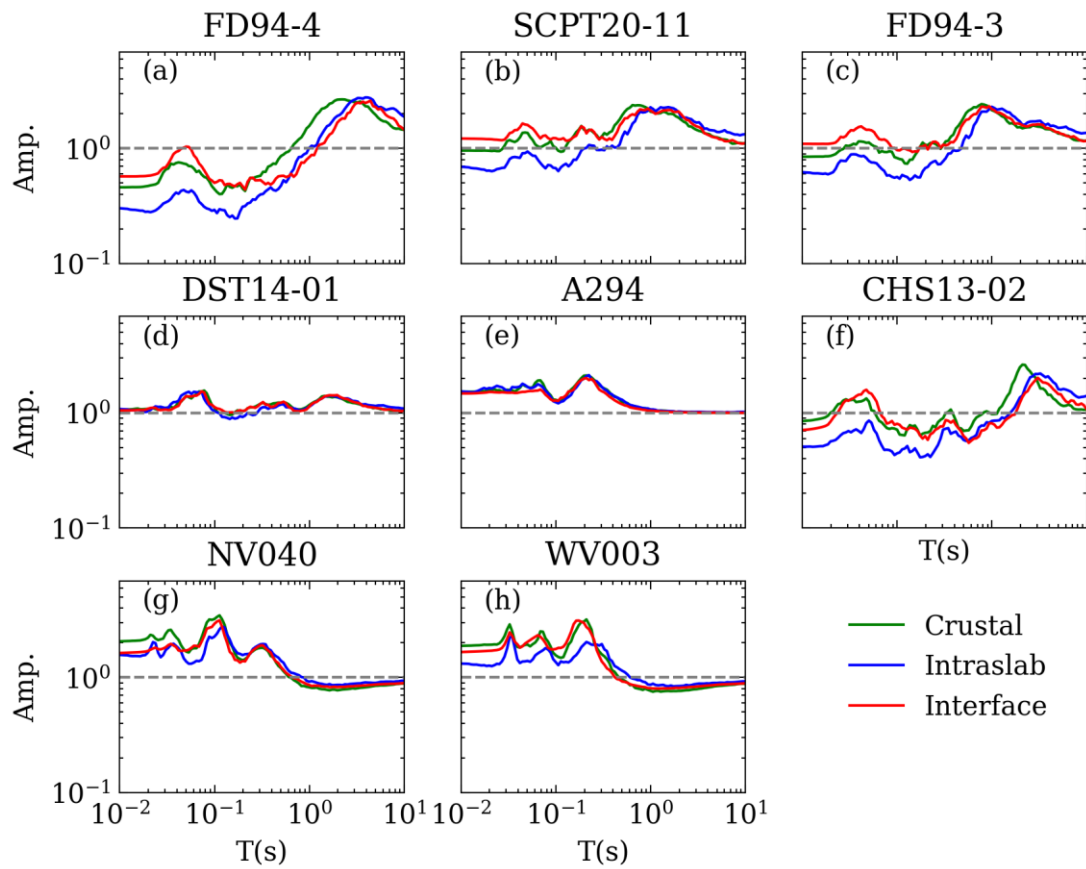
Figure 6-10. Mean nonlinear amplification (2 % in 50 yr) from 1D SRA for each earthquake source type at the 8 sites.
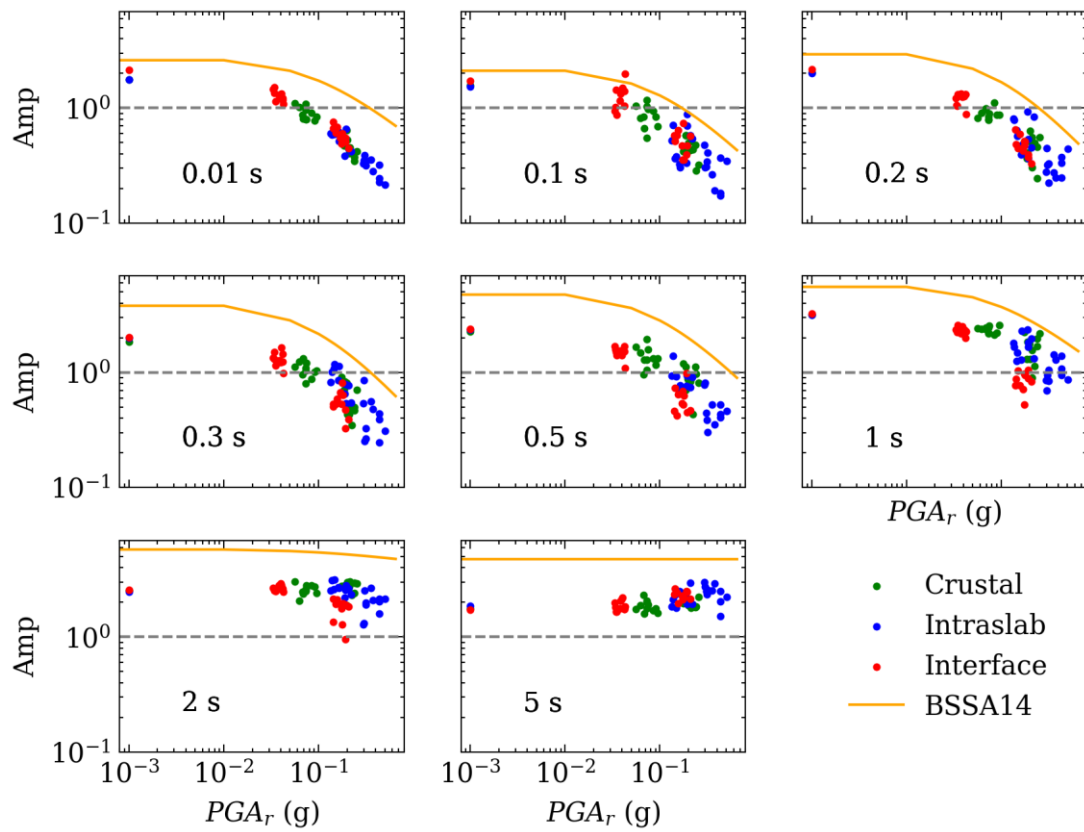
Figure 6-11. SRA linear and nonlinear amplification with PGA$_r$ in comparison to BSSA14 amplification at FRD site FD94-4 (z_{gl} = 235 m).
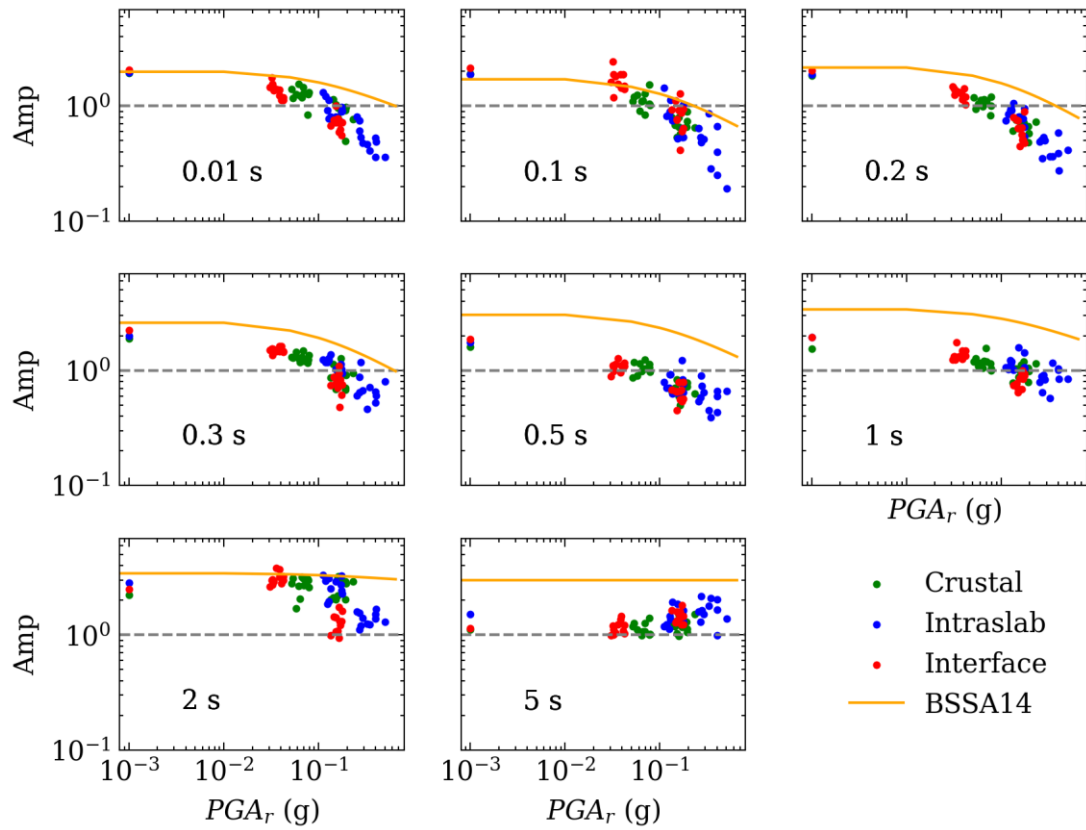
Figure 6-12. SRA linear and nonlinear amplification with PGA$_r$ in comparison to BSSA14 amplification at North Shore site CHS13-02 (z_{gl} = 92 m).
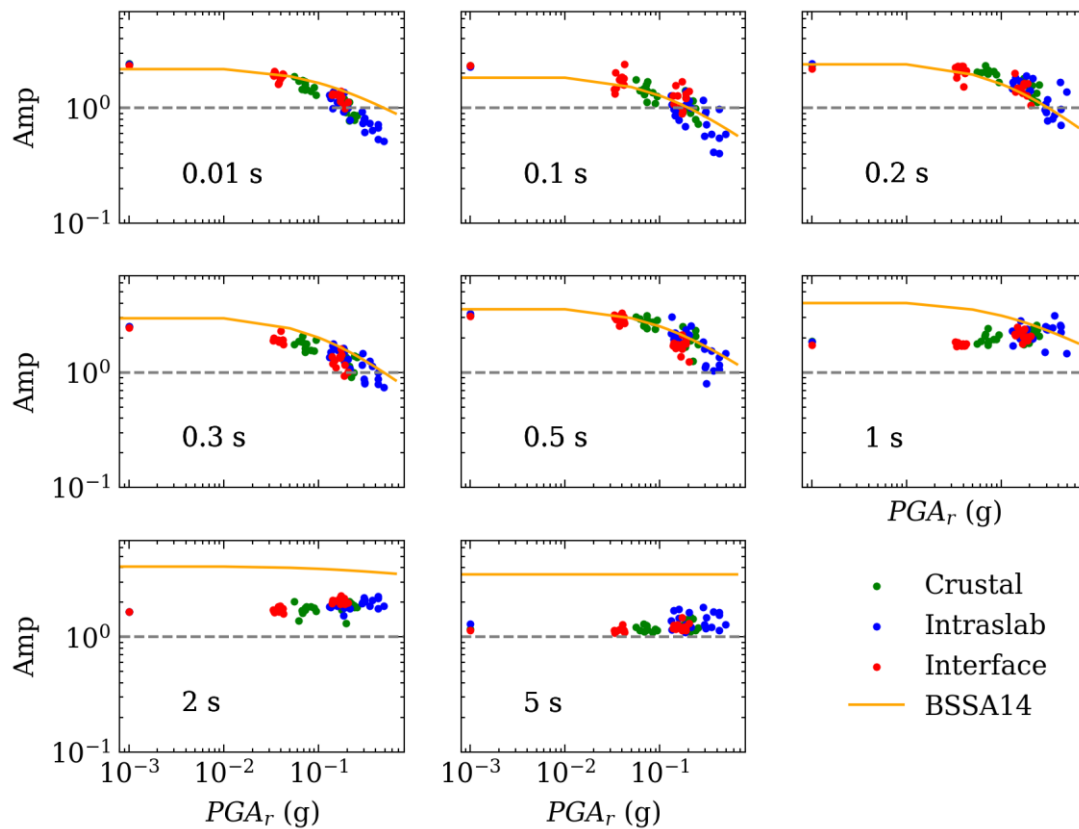
Figure 6-13. SRA linear and nonlinear amplification with PGA_r in comparison to BSSA14 amplification at FRD site SCPT20-11 (z_{gl} = 20 m).

Based on the presented results at 8 selected sites for different earthquake sources and different site conditions, site-specific amplification in Metro Vancouver is observed to differ from the ergodic amplification in BSSA14. The ergodic amplification predicts weaker nonlinearity than that observed from SRA at sites with thick, soft post-glacial sediments in Metro Vancouver and underestimates the amplification at shallow sites with strong impedance contrast. The shallow conditions in North Shore are similar to CENA conditions where a strong impedance contrast between soil and bedrock exist near surface. For such conditions, it is expected that Vs_{30}-based amplification may not capture the resonance amplification (Hassani and Atkinson 2018) and T_0 may be a more powerful amplification proxy. Trends in SRA amplification with Vs_{30} and T_0 are therefore of interest. Figure 6-14 shows the linear and nonlinear SRA amplification at all sites from all

earthquake sources with PGA_r differentiated by 3 major categories of Vs_{30} representing soft to stiff site conditions. Figure 6-14 show nonlinearity (deamplification) increases with PGA_r for lower Vs_{30} sites, and less significantly for higher Vs_{30} sites. Similarly, Figure 6-14 shows the trend in SRA amplification differentiated by three categories of T_0 representing deep to shallow site conditions. Deeper sites with long T_0 show stronger nonlinearity at shorter periods, while shallow sites (short T_0) show lower nonlinearity and higher amplification at shorter periods. Figures 6-14 and 6-15 confirm that both Vs_{30} and T_0 in Metro Vancouver can be used to estimate amplification in Metro Vancouver.
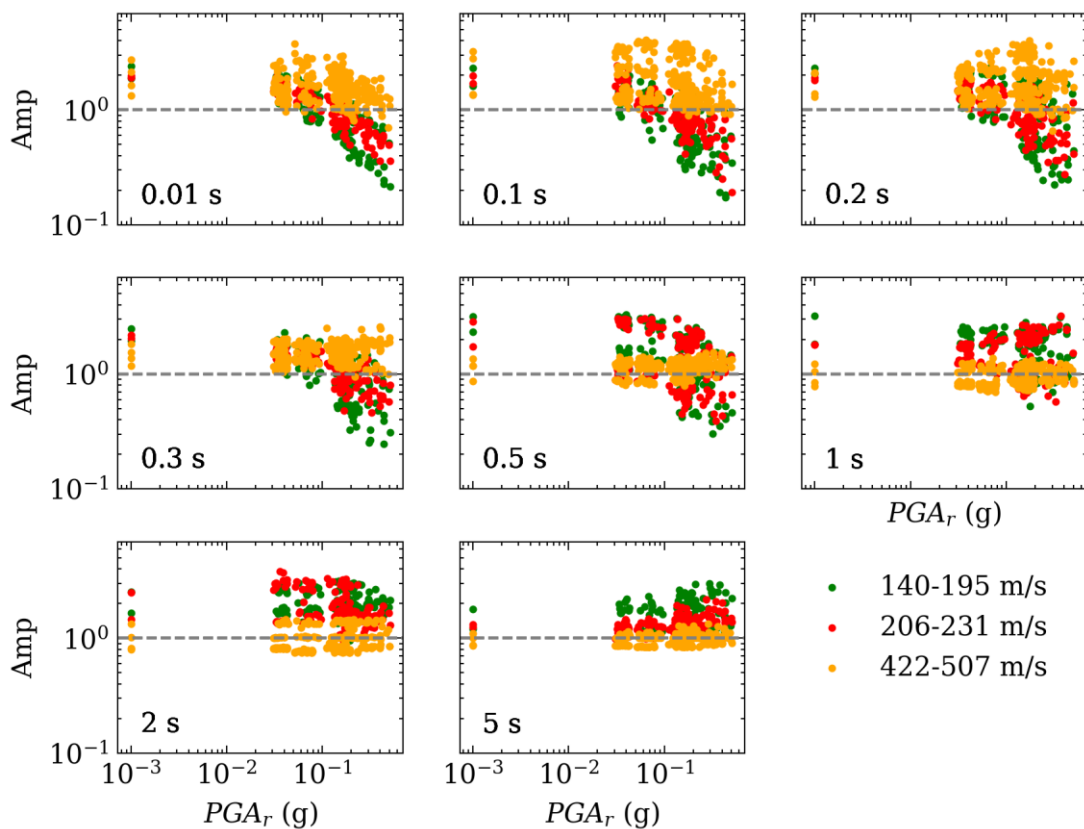
Figure 6-14. SRA linear and nonlinear amplification with PGA_r for different Vs_{30} categories.
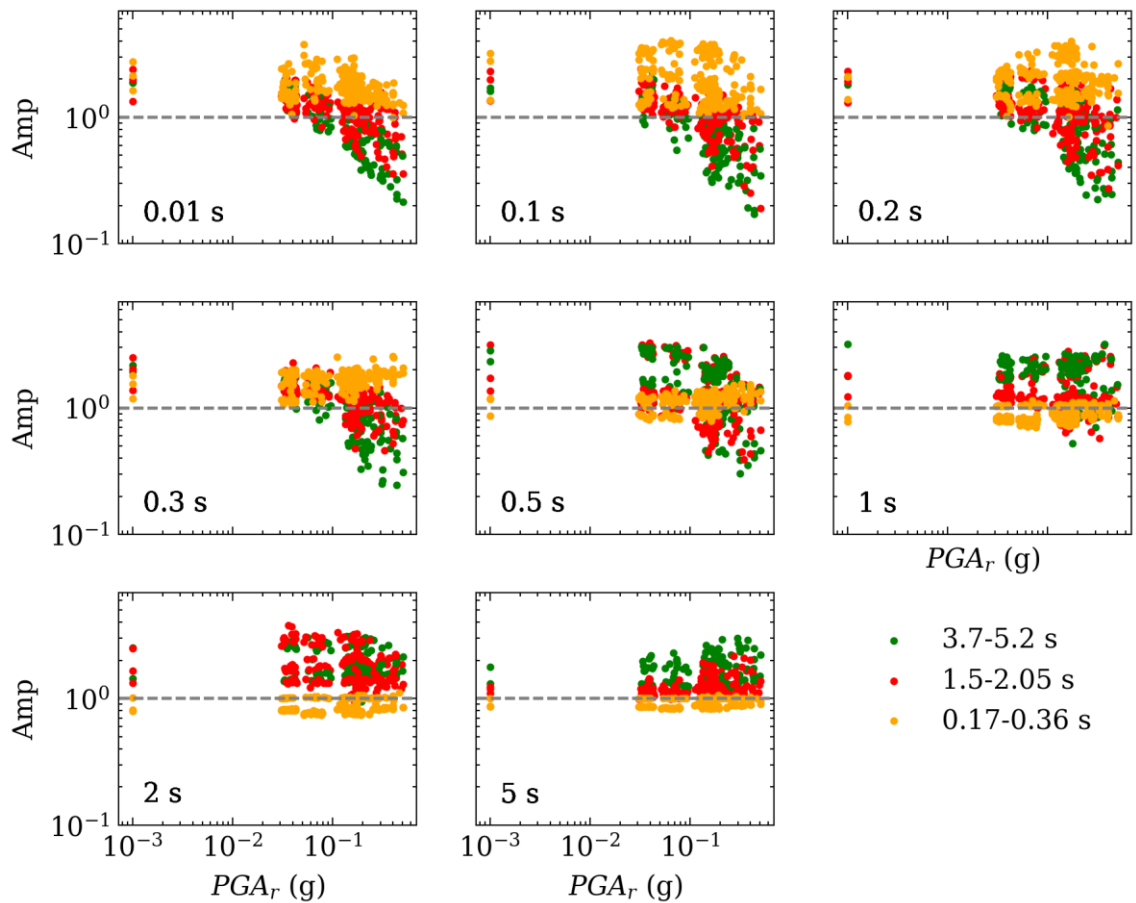
Figure 6-15. SRA linear and nonlinear amplification with PGA$_r$ for different T$_0$ categories.

6.5 Uncertainties and Limitations in SRA

There are several sources of uncertainties and limitations in the presented SRA methodology for Metro Vancouver that could influence the modelled site amplification and are worth exploring. SRA sensitivity analyses are conducted to examine the influence of Vs variability of deeper glacial sediments in the FRD and inclusion of Vs reversals to the predicted site amplification. Uncertainties and limitations of this study's 1D SRA procedure to accomplishing regional site amplification mapping are also discussed.

6.5.1 Sensitivity Analysis on the Effect of Deeper Vs in the FRD on Amplification

Although significant effort has been applied to establish Vs(z) distributions of glacial sediments and Tertiary sedimentary rock beneath the FRD (Chapter 5, Section 6.2), Vs at such deep depths are not well constrained. A SRA parameter sensitivity analysis is conducted considering Vs variability at deep depth in the FRD, in glacial sediment and Tertiary rock model layers. For the deepest two sites in the FRD (FD94-4 and FD94-3), the 1D soil model developed in Section 6.4 applied a constant Vs for the glacial sediment layer (termed the base case here). To investigate the effect of this assumption on the SRA amplification, an alternative 1D soil model that applies the average soil Vs(z) from deep reflection profiling (shown previously in Figure 6-2b) is used (alternative case). In addition, the Tertiary rock (half-space) Vs is adjusted from 760 m/s (base case) to 1500 m/s (alternative case). The two Vs(z) cases for the two deep FRD sites are shown in Figure 6-16a and b. An alternative 1D SRA model for SCPT20-11 site includes adjustment of the half-space Vs to 1500 m/s (Figure 6-16c). Prior to performing SRA for these alternative soil models, adjustment of the input motions to a reference condition of 1500 m/s is also accomplished as described in section 6.3. Only crustal input motions are adjusted to limit the number of SRA analyses.

Figure 6-16(d-f) presents the ratio between the alternative case SRA crustal-source mean amplification (blue profiles in Figure 6-16a-c) to the SRA crustal-source mean amplification of the base case (green profiles), i.e., alternative/base amplification. Note that the amplifications relative to 1500 m/s are converted back to a reference of 760 m/s for comparison with the base case referenced to 760 m/s. The ratio indicates the alternative case linear amplification is higher at shorter periods (T < 0.4 s) and around T_0 at all three sites compared to the amplification of the base case with constant Vs profile and a reference condition of 760 m/s. The maximum amplification ratio is up to 1.4 at the ~3-s T_0 and slightly lower at shorter periods. For the 2 % in 50 years POE ground motions, the alternative/base amplification is less pronounced at shorter period and decreases slightly at intermediate periods. The impact of the deeper Vs structure and reference condition in the

FRD on the SRA amplification decreases, more significantly at shorter periods, with the increase of input motion PGA_r.
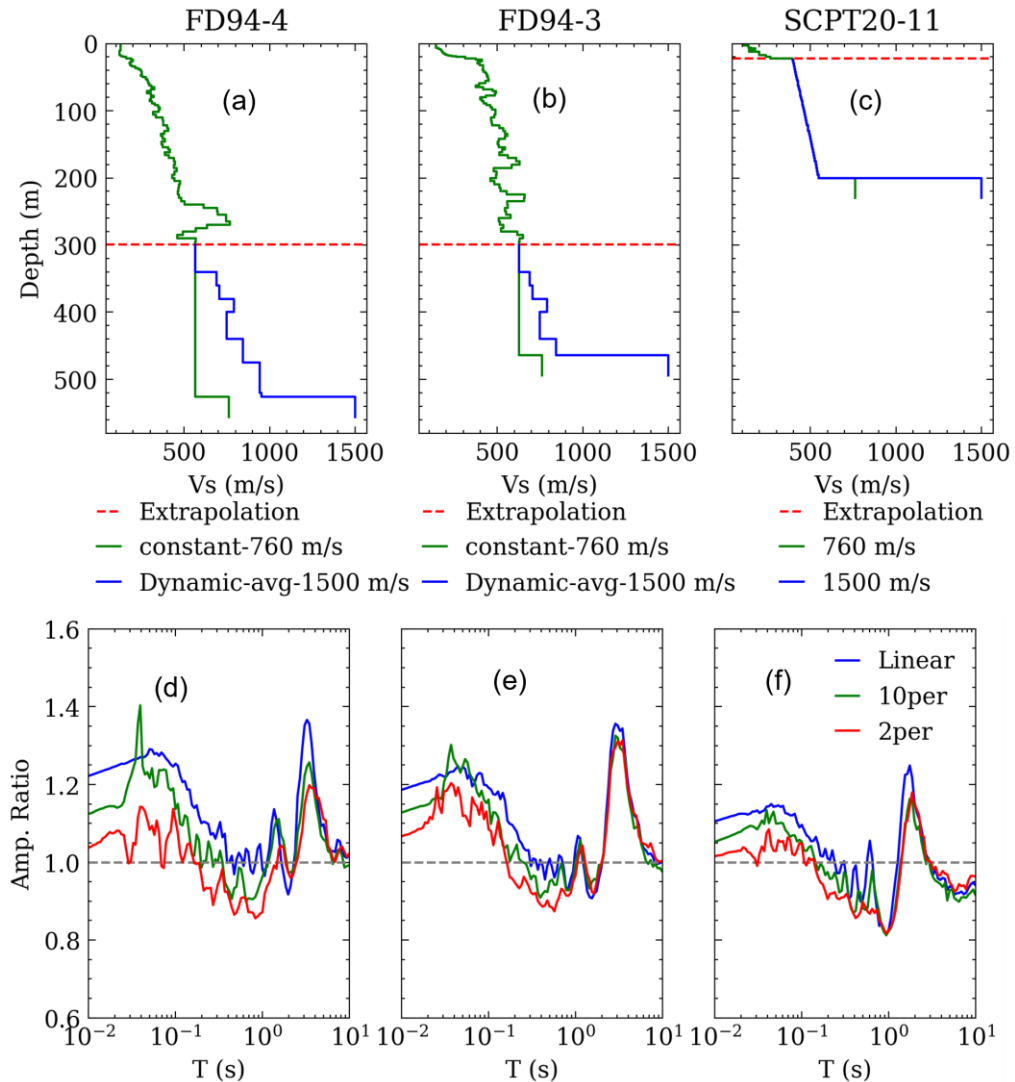
Figure 6-16. Effect of Vs of deeper glacial and Tertiary sediments beneath the FRD on linear and nonlinear SRA amplification. Note the y-axis in (d), (e), and (f) is the ratio of the amplification of the alternative Vs profile (blue line in a-c) to the amplification of the base-case Vs profile (green line in a-c).

6.5.2   Sensitivity Analysis on the Effect of Vs Reversal on Amplification

The measured Vs profiles at 6 out of the 8 sites exhibit Vs reversals in post-glacial and glacial sediments. While these Vs reversals may be due to actual soil conditions, specifically in our glacial simplification of Pleistocene and older interlayered inter/glacial sediments (e.g., FD94-4), they may also be due to data errors in interpretations of the invasive travel-time measurements (e.g., picking of shear wave arrival times). Pehlivan et al. (2015) found that Vs reversals in SRA modeling may lead to reduction (up to 10 %) in median amplification at periods shorter than T_0. To investigate the effect of Vs reversals in Metro Vancouver post-glacial and glacial sediments on SRA amplification, Vs reversals at the 6 sites (base case as shown in Fig 6-2b) are smoothed and removed (alternative case) as shown in Figure 6-17. The smoothing slightly decreases T_0 and slightly increases Vs_{30} at all sites except for FD94-4 where Vs reversal occurs at depth more than 30 m. The Vs reversals occur in post-glacial sediments at SCPT20-11 and CHS13-02 sites, and in glacial sediments at FD94-3, DST14-01, and A294 sites. At FD94-4, Vs reversals occur in both post-glacial and glacial sediments.

The SRA amplifications of the alternative case Vs profiles are calculated and the ratio between the mean linear and nonlinear amplifications at the two POE from the alternative case profiles to the mean amplifications from the base case profiles is shown in Figure 6-18.
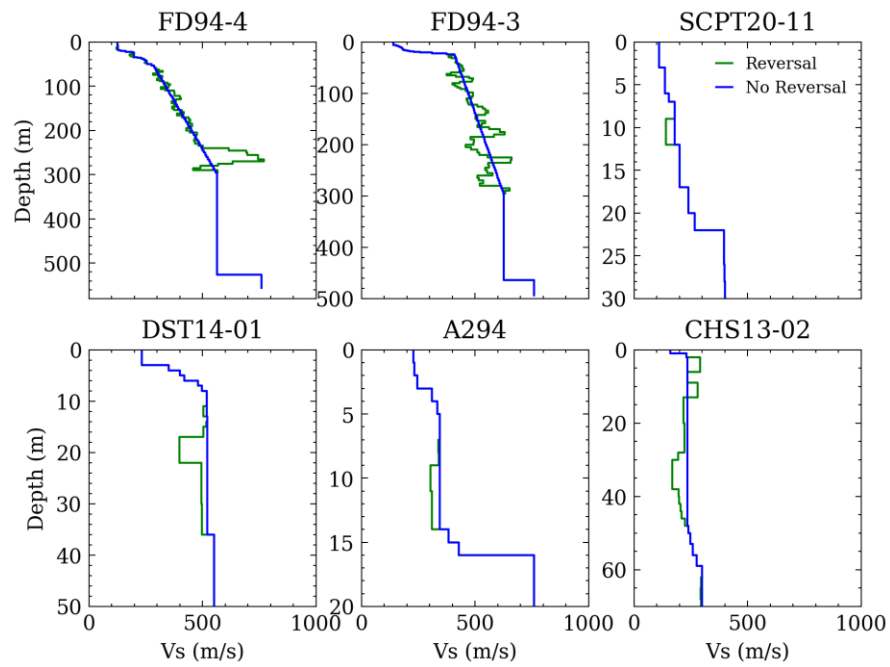
Figure 6-17. Vs profiles base case (green) and alternative case smoothed profiles with no Vs reversals (blue).
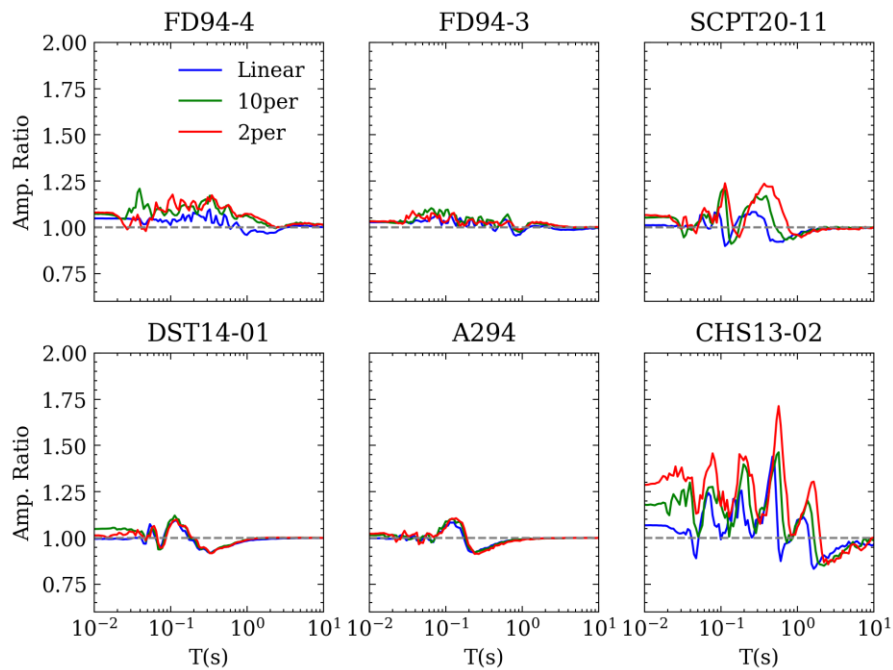
Figure 6-18. Ratio of the amplification of smoothed Vs profiles with no Vs reversal (blue in Fig 6-17) to the amplification of Vs profiles with Vs reversals (green in Fig 6-17).

The removal of Vs reversals in stiff glacial sediments (FD94-3, DST14-01, and A294) leads to a slight increase (up to 10 %) at some spectral periods and slight decrease at other spectral periods in linear and nonlinear amplifications. However, the removal of Vs reversals in soft post-glacial sediments (FD94-4, SCPT20-11, and CHS13-02) results in a pronounced increase (up to 75 %) in the amplification. This increase is most pronounced for motions with highest PGA_r (2 % in 50 yr [2per] POE ground motions). This can be explained by the localized large shear strains that develop at depths where Vs reversals occur in the soft sediments that lead to significant deamplification. When these reversals are removed, lower strains are induced and higher amplification occurs. The results suggest that the removal of Vs reversals in soft post-glacial sediments in Metro Vancouver can have significant impact (up to 75% increase) on SRA amplification, specifically for stronger motions. On the other hand, Vs reversals in glacial sediments have limited effect on the SRA amplification. It should be noted that only crustal input motions are used here. For intraslab input motions with higher PGA_r, the removal of Vs reversals may lead to more than a 75 % increase in amplification at the 2 % in 50 years. When no geologic evidence supports the presence of Vs reversals in post-glacial sediments, it is recommended that Vs reversals be removed from SRA models as they can result in significantly lower amplifications.

In addition to the uncertainties in Vs, other factors related to the soil models can influence SRA results and should be investigated. The depth to bedrock at many locations in Metro Vancouver is large and is also not well constrained. Therefore, some level of uncertainty should be added to this variable to capture its effects on SRA results. The assigned MRD curves can also effect the linear and nonlinear amplification. The MRD curves used in this study for post-glacial sediments are recommended by Anderson et al. (2007). However, the Darendeli (2001) curves may better capture the pressure-dependent behaviour with depth, which is expected to have more influence at very deep sites in FRD. Additionally, most

MRD curves from laboratory testing are limited to lower shear strains of around 0.1-0.3 %. When using constitutive models such as the MKZ, the resulting shear strength at larger strains may not represent the actual shear strength of the soil. The General-Quadratic hyperbolic (GQ/H) model (Groholski et al. 2016) allows correcting for the shear strength at larger strains; however, it requires the shear strength profile of the soil as input which entails certain assumptions specifically at larger depths in the FRD. In general, the GQ/H and MKZ models provide similar results when lower shear strains are expected. The presented uncertainties are specific to SRA modeling assumptions in Metro Vancouver and should be addressed with sensitivity analyses similar to that presented in this section.

In addition to uncertainties, there are limitations to the 1D SRA analysis in Metro Vancouver. It is well known that the Georgia basin beneath Metro Vancouver can produce additional long-period amplification due to the interaction between the 3D basin structure and the incident seismic waves (Molnar et al. 2014a, b). This interaction can lead to surface wave generation at the edges of the basin which cannot be captured by 1D SRA. In such case, 3D modeling provides a better option to predict the long period amplification related to the basin structure. A parallel study (Ghofrani et al. 2019) to quantify basin amplification in Metro Vancouver using 3D simulations is underway. The SRA study related to the shallow 1D amplification in combination with the 3D basin simulations can provide a more completed understanding of regional site amplification in Metro Vancouver.

6.6   Conclusions

In this study, linear and nonlinear regional SRA in Metro Vancouver are investigated. Reference site conditions are studied using the Vs database presented in previous chapters. Reference site conditions with Vs_{30} = 760 m/s for the FRD and Uplands and Vs_{30} = 1500 m/s for North Shore are selected for SRA. To represent the local seismicity in the region, input time histories for crustal, intraslab, and interface earthquakes are developed from a PSHA study, conducted as part of this thesis, which considered different earthquake sources separately. For each earthquake type, time histories are scaled to the 2 and 10 % in 50 years ground motions probabilities of exceedance (POE). SRA linear and nonlinear

amplifications from the three earthquake sources input motions at 8 selected sites are presented and compared to BSSA14 linear and nonlinear site term.

The results indicate that ergodic crustal BSSA14 predicts higher linear amplification compared to SRA amplification at deeper sites in Metro Vancouver, and underestimates the linear amplification at shallow sites, specifically in North Vancouver where a strong impedance exists between glacial sediments and pre-Tertiary rock. In terms of nonlinearity, deep soft sites in Metro Vancouver exhibit stronger nonlinearity and de-amplification at short periods compared to BSSA14 nonlinear model. Although interface records PGA_r is lower than that of crustal records at the 2 % in 50 yr, interface records induce stronger nonlinearity at soft deep sites due to their longer durations and larger induced shear strains.

A sensitivity analysis indicates that amplification at short periods (T < 0.4 s) as well as at longer periods (T ~ T_0) can be affected by the choice of Vs of deeper glacial and Tertiary sediments underneath the FRD. Further, Vs reversals in post-glacial sediments can have significant impact on the SRA results. Unless supported by geologic evidence, reversals in post-glacial sediments should be removed from SRA modeling. Uncertainties in the MRD curves that could influence SRA results are identified.

The presented observations may be further confirmed by additional SRAs at all recommended sites in future. Performing SRA for all recommended sites (or more) will enable development of a region-specific site amplification model based on V_{S30}, T_0, and PGA_r. It is expected that including both V_{S30} and T_0 parameters in the regional site amplification model will result in better model performance. The first region-specific amplification maps (at select spectral periods) for Metro Vancouver could be produced using such a model in combination with regional V_{S30} and T_0 maps produced by the Metro Vancouver microzonation project and PGA_r maps from the PSHAs in this study.

6.7   References

Abrahamson, N. A., Silva, W. J., & Kamai, R. (2014). Summary of the ASK14 ground motion relation for active crustal regions. Earthquake Spectra, 30(3), 1025-1055.

Adams, J., Halchuk, S., Allen, T., Rogers, G. (2015). Canada's 5th Generation Seismic Hazard Model, As Prepared For the 2015 National Building Code of Canada. In Proceedings of the 11th Canadian Conference on Earthquake En- gineering, Victoria, Canada 1–11

Al Atik, L., and N. A. Abrahamson (2021). A methodology for the development of 1D reference VS profiles compatible with ground-motion prediction equations: Application to NGAWest2 GMPEs, Bull. Seismol. Soc. Am., doi: 10.1785/0120200312

Atkinson, G.M., Adams, J. (2013): Ground motion prediction equations for application to the 2015 Canadian national seismic hazard maps, Can. J. Civ. Eng., **40**, 988–998, doi: 10.1139/cjce-2012-0544.

Ancheta, T. D., Darragh, R. B., Stewart, J. P., Seyhan, E., Silva, W. J., Chiou, B. S., ... & Donahue, J. L. (2013). PEER NGA-west2 database (Vol. 172). Berkeley, CA: Pacific Earthquake Engineering Research Center.

Anderson, D. L., Byrne, P. M., DeVall, R. H., Naesgaard, E., Wijewickreme, D., Adebar, P., ... & Yan, L. (2007). Geotechnical design guidelines for buildings on liquefiable sites in accordance with NBC 2005 for Greater Vancouver Region. Greater Vancouver Liquefaction Task Force Report, University of British Columbia.

Atkinson, G.M. and Cassidy, J.F. (2000). "Integrated Use of Seismograph and Strong-Motion Data to Determine Soil Amplification: Response of the Fraser River Delta to the Duvall and Georgia Strait Earthquakes," Bulletin of the Seismological Society of America, **90**(4): 1028–1040.

Baker, J. W. (2011). Conditional mean spectrum: Tool for ground-motion selection. Journal of structural engineering, 137(3), 322-331.

Bard, P. Y., Bora, S. S., Hollender, F., Laurendeau, A., & Traversa, P. (2020). Are the standard VS-Kappa host-to-target adjustments the only way to get consistent hard-rock ground motion prediction?. Pure and Applied Geophysics, 177(5), 2049-2068.

Boore, D.M., Stewart, J.P., Seyhan, E. and Atkinson, G.M. (2014). "NGA-West2 Equations for Predicting PGA, PGV, and 5% Damped PSA for Shallow Crustal Earthquakes," Earthquake Spectra, **30**(3): 1057–1085

Borcherdt, R.D. (1994). Estimates of Site-Dependent Response Spectra for Design (Methodology and Justification). Earthquake Spectra 10:617–653

Boucher C. (2022). Approaches to model non-uniquness and site complexity for non-invasive shear-wave depth profiling. London, Ontario: The University of Western University.

Bozorgnia, Y., Abrahamson, N. A., al Atik, L., Ancheta, T. D., Atkinson, G. M., Baker, J. W., Baltay, A., Boore, D. M., Campbell, K. W., Chiou, B. S. J., Darragh, R., Day, S., Donahue, J., Graves, R. W., Gregor, N., Hanks, T., Idriss, I. M., Kamai, R., Kishida, T., … Youngs, R. (2014). NGA-West2 research project. *Earthquake Spectra*, *30*(3). https://doi.org/10.1193/072113EQS209M

Britton, J.R., Harris, J.B., Hunter, J.A., Luternauer, J.L. (1995). The bedrock surface beneath the Fraser River delta in British Columbia based on seismic measurements. In: Current Research 1995-E. Geological Survey of Canada, pages 83–89

Campbell, K.W. (2009). Estimates of shear-wave Q and K_0 for unconsolidated and semiconsolidated sediments in Eastern North America. Bulletin of the Seismological Society of America 99: 2365–2932.

Campbell, K.W. and Bozorgnia, Y. (2014). "NGA-West2 Ground Motion Model for the Average Horizontal Components of PGA, PGV, and 5% Damped Linear Acceleration Response Spectra," Earthquake Spectra, **30**(3): 1087–1115

Darendeli, M. B. (2001). Development of a new family of normalized modulus reduction and material damping curves Ph. D., University of Texas at Austin

Day, S.M., Graves, R., Bielak, J., Dreger, D., Larsen, S., Olsen, K.B., et al. (2008). Model for basin effects on long-period response spectra in southern California. Earthquake Spectra. 24 (1), 257–277

Di Alessandro, C., Bonilla, L.F., Boore, D.M., Rovelli, A., Scotti, O. (2012). Predominant-Period Site Classification for Response Spectra Prediction Equations in Italy. Bulletin of the Seismological Society of America **102**:680–695. doi: 10.1785/0120110084

Falcone, G., Acunzo, G., Mendicelli, A., Mori, F., Naso, G., Peronace, E., ... & Moscatelli, M. (2021). Seismic amplification maps of Italy based on site-specific microzonation dataset and one-dimensional numerical approach. Engineering Geology, 289, 106170.

Finn, W.D.L., Zhai, E., Thavaraj, T., Hao, X-S., Ventura, C. (2003). 1-D and 2-D analyses of weak motion data in Fraser Delta from 1966 Duvall earthquake. Soil Dynamics and Earthquake Engineering **23**:323–329. doi: 10.1016/S0267-7261(02)00207-5

Ghofrani H., Molnar S., (2019). 3D Sedimentary Basin Effects in the Metro Vancouver Area and Its Seismic Hazard Implications: Updates and Validations of the Georgia Basin Velocity Model, 12CCEE Proceedings.

Ghofrani, H., Atkinson, GM. (2014). Site condition evaluation using horizontal-to-vertical response spectral ratios of earthquakes in the NGA-West2 and Japanese databases. Soil Dynamics and Earthquake Engineering **67**:30–43. doi: 10.1016/J.SOILDYN.2014.08.015

Groholski, DR., Hashash, Y.M.A, Kim, B., Musgrove, M., Harmon, J. and Stewart, J.P. (2016). "Simplified Model for Small-Strain Nonlinearity and Strength in 1D Seismic Site Response Analysis," Journal of Geotechnical and Geoenvironmental Engineering, **142**(9): 04016042

Hashash, Y. M.A., Ilhan, O., Hassani, B., Atkinson, G.M., Harmon, J., Shao, H. (2020a). Significance of site natural period effects for linear site amplification in central and eastern North America: Empirical and simulation-based models. Earthquake Spectra **36**:87–110. doi: 10.1177/8755293019878198

Hashash, Y. M.A., Ilhan, O., Harmon, J. A., Parker, G. A., Stewart, J. P., Rathje, E. M., ... & Silva, W. J. (2020b). Nonlinear site amplification model for ergodic seismic hazard analysis in central and eastern North America. Earthquake Spectra, 36(1), 69-86.

Hashash, Y.M.A., Musgrove, M.I., Harmon, J.A., Ilhan, O., Xing, G., Numanoglu, O., Groholski, D.R., Phillips, C.A., and Park, D. (2020). "DEEPSOIL 7.0, User Manual". Urbana, IL, Board of Trustees of University of Illinois at Urbana-Champaign.

Hassani, B., and G. M. Atkinson (2018). Site-effects model for central and eastern North America based on peak frequency and average shear-wave velocity, Bull. Seismol. Soc. Am. 107, 338-350.

Hunter, J. A., Burns, R. A., Good, R. L., & Pelletier, C. F. (2016). Fraser River Delta–A compilation of shear wave velocities and borehole geophysics logs in unconsolidated sediments of the Fraser River Delta, British Columbia. Geological Survey of Canada Open File, 1-112.

Harmon, J., Hashash, Y.M.A., Stewart, J.P., Rathje, E.M., Campbell, K.W., Silva, W.J., Xu, B., Musgrove, M. and Ilhan, O. (2019a). Site amplification functions for central and Eastern North America—Part I: Simulation data set development. Earthquake Spectra 35: 787–814.

Harmon, J., Hashash, Y.M.A., Stewart, J.P., Rathje, E.M., Campbell, K.W., Silva, W.J., Musgrove, M. and Ilhan, O. (2019b). Site amplification functions for central and eastern North America—Part II: Modular simulation-based models. Earthquake Spectra 35: 815–847.

Jackson, F., Molnar, S., Ghofrani, H., Atkinson, G.M., Cassidy, J.F., Assatourians, K. (2017). Ground Motions of the December 2015 M 4.7 Vancouver Island Earthquake: Attenuation and Site Response. Bulletin of the Seismological Society of America 107:2903–2916

Kamai, R., Abrahamson, N. A., & Silva, W. J. (2014). Nonlinear horizontal site amplification for constraining the NGA-West2 GMPEs. Earthquake Spectra, 30(3), 1223-1240.

Kim, B. (2019). Mapping of ground motion amplifications for the Fraser River delta in Greater Vancouver, Canada. Earthquake Engineering and Engineering Vibration, 18(4), 703-717.

Kolaj, M., Allen, T., Mayfield, R., Adams, J., & Halchuk, S. (2019). Ground-motion models for the 6th Generation Seismic Hazard Model of Canada. In 12th Canadian Conference on Earthquake Engineering.

Matasovic, N. (1993). Seismic response of composite horizontally-layered soil deposits Ph.D. Thesis, University of California, Los Angeles

Mazzoni, S., Kishida, T., Stewart, J. P., Contreras, V., Darragh, R. B., Ancheta, T. D., ... & Bozorgnia, Y. (2022). Relational database used for ground-motion model development in the NGA-Sub project. Earthquake Spectra, 38(2), 1529-1548.

Molnar, S., Cassidy J.F., Olsen, K.B., Dosso, S.E. and He, J. (2014a). "Earthquake Ground Motion and 3D Georgia Basin Amplification in Southwest British Columbia: Deep Juan de Fuca Plate Scenario Earthquakes," Bulletin of the Seismological Society of America, **104**(1): 301–320.

Molnar, S., Cassidy J.F., Olsen, K.B., Dosso, S.E. and He, J. (2014b). "Earthquake Ground Motion and 3D Georgia Basin Amplification in Southwest British Columbia: Shallow Blind-Thrust Scenario Earthquakes," Bulletin of the Seismological Society of America, **104**(1): 321–335

Molnar, S., Assaf, J., Sirohey, A., & Adhikari, S. R. (2020). Overview of local site effects and seismic microzonation mapping in Metropolitan Vancouver, British Columbia, Canada. Engineering Geology, 270, 105568.

Pehlivan, M., Y. Hashash, J. Harmon, E. M. Rathje, J. P. Stewart, W. J. Silva, K. W. Campbell, and S. Nikolaou (2015). Influence of shear wave velocity reversals on one-dimensional site response of spatially varied profiles, Proc. 6th Int. Conf. on Earthq. Geotech. Eng., Christchurch, New Zealand, 1–4 November, 8 pp.

Petersen, M. D., Shumway, A. M., Powers, P. M., Mueller, C. S., Moschetti, M. P., Frankel, A. D., Rezaeian, S., McNamara, D. E., Luco, N., Boyd, O. S., Rukstales, K. S., Jaiswal, K. S., Thompson, E. M., Hoover, S. M., Clayton, B. S., Field, E. H., & Zeng, Y. (2020). The 2018 update of the US National Seismic Hazard Model: Overview of model and implications. *Earthquake Spectra*, *36*(1). https://doi.org/10.1177/8755293019878199

Seed, H. B. and Idriss, I. M. (1970). "Soil moduli and damping factors for dynamic response analyses." Report No. EERC 70-10, Earthquake Engineering Research Center, University of California, Berkeley, California, 40p.

Seyhan, E. and Stewart, J.P. (2014). Semi-empirical nonlinear site amplification from NGA-West2 data and simulations. Earthquake Spectra 30: 1241–1256.

Sirohey, A. (2022). Soil amplification and peak frequencies from thousands of passive seismic measurements across metro Vancouver, British Columbia, Canada. London, Ontario: The University of Western University.

Stewart, J.P., Afshari, K. and Goulet, C.A. (2017). Non-ergodic site response in seismic hazard analysis. Earthquake Spectra 33: 1385–1414

Trifunac, M. D., & Brady, A. G. (1975). A study on the duration of strong earthquake ground motion. Bulletin of the Seismological Society of America, 65(3), 581-626.

Walling, M., Silva, W. and Abrahamson, N. (2008). Nonlinear site amplification factors for constraining the NGA models. Earthquake Spectra 24: 243–255.

Williams, T., & Abrahamson, N. (2021). Site-Response Analysis Using the Shear-Wave Velocity Profile Correction Approach. Bulletin of the Seismological Society of America, 111(4), 1989-2004.

Vucetic, M. and Dobry, R. (1991). Effect of soil plasticity on cyclic response. Journal of Geotechnical Engineering; 117(1): 89-107.

Zhu, C., Pilz, M., & Cotton, F. (2020). Which is a better proxy, site period or depth to bedrock, in modelling linear site response in addition to the average shear-wave velocity?. Bulletin of Earthquake Engineering, 18(3), 797-820.

Chapter 7

7 Summary, Conclusions, and Recommendations

7.1 Summary and Conclusions

This thesis utilizes the most comprehensive database of seismic site condition measures to develop important predictive site characteristic models for site-specific and regional applications and facilitate the development of a region-specific amplification model in Metro Vancouver.

First, the applicability of multi-method non-invasive seismic *in situ* testing methods to retrieve important seismic site characteristic metrics in the FRD such as the depth to glacial till (z_{gl}) and Vs(z) are investigated. Single station MHVSR measurements for amplification spectra and peak frequency(ies) were performed at 14 sites with known z_{gl} in addition to active-source MASW and passive-source MAM array testing for Vs(z) at 16 sites. A model is developed to predict z_{gl} based on the 2nd peak frequency of MHVSR for shallow FRD sites. Using joint inversion of multi-methods, deep constrained Vs profiles to significant depths are obtained. The results indicate that non-invasive measurements can produce reliable deep Vs profiles up to 220 m compared to invasive methods in the FRD.

SCPT measurements in Metro Vancouver were compiled and used to evaluate existing CPT-to-Vs models developed for other regions. The results demonstrate that the models are biased when applied to Metro Vancouver data. Instead, a multi-approach to regression considering traditional linear and nonlinear methods along with two machine learning algorithms was performed to derive unbiased region-specific CPT-to-Vs models. Region-specific CPT-to-Vs models are developed and the results promote the use of machine learning approaches in geotechnical applications.

A comprehensive Vs(z) database for Metro Vancouver was compiled and utilized to obtain generic Vs(z) relationships for major geologies in the region. Further, a Vs_{30} database was established from direct Vs(z) measurements, Vs(z) from CPTs, and Rayleigh wave

fundamental-mode dispersion curves. Two hybrid proxy-Vs_{30} models (geology-topographic slope, geology-z_{gl}) were developed to map Vs_{30} in Metro Vancouver. Residual analysis indicates that the geology-z_{gl} model outperforms the geology-slope model in predicting Vs_{30} in Metro Vancouver. Recommendations on applying the geology-z_{gl} model to produce the first Vs_{30} map of Metro Vancouver are provided.

Finally, regional prediction of site-specific ground motions (amplification) was accomplished by performing 1D linear and nonlinear site response analyses (SRA) in Metro Vancouver. Reference site conditions Vs_{30} of 1500 m/s for pre-Tertiary igneous rock in the North Shore and 760 m/s for Tertiary sedimentary rock elsewhere were assigned based on comparison of $Vs(z)$ for the two geologic bedrock types with implicit $Vs(z)$ in CanadaSHM6 GMMs. Input time histories compatible with CanadaSHM6 for crustal, intraslab, and interface earthquakes were selected and scaled to the two selected reference site conditions at three sites and two probability of exceedance (POE) hazard levels (2 and 10 % in 50 years); a procedure to obtain time histories at any location in the region is proposed. A suite of 1D SRAs were conducted at 8 selected sites and the results were compared to ergodic GMM (BSSA14) site amplification. The ergodic site amplification model overestimates site amplification for deep soft sites and underestimates amplification for shallow sites in Metro Vancouver. The approach proposed to achieve mapping of 1D site amplification for Metro Vancouver for the first time involves performing SRAs at 51 recommended sites to develop a region-specific model to predict 1D site amplification based on Vs_{30}, T_0, and PGA_r. The following major conclusions can be drawn from the work presented in this thesis:

1- The MHVSR 2nd peak frequency ($f_{1,HVSR}$) scales well with the depth to glacial till (z_{gl}) at shallow sites in the FRD. At the few available deeper sites ($z_{gl} > \sim 60$ m), $f_{1,HVSR}$ does not accurately predict z_{gl}. Our developed z_{gl} model can be used with inexpensive MHVSR measurements to map out the depth to glaciated sediments around the edges of the FRD and constrain the geometry for 1D and 2D site response analyses in future. Further, the z_{gl} model can be applied to other regions in

the world, specifically deltaic settings, with similar Vs(z) relationship to that in the FRD.

2- Non-invasive active- and passive-source seismic testing is demonstrated to be robust in retrieving deep Vs(z) in the FRD. The agreement within 10 % between inverted Vs from three non-invasive methods and invasive downhole Vs to a depth of 220 m, deeper than most available Vs profiles in the FRD, is notable.

3- Region-specific CPT-to-Vs models are developed for Metro Vancouver. Further, machine learning approaches can provide improved predictions from large (CPT) datasets compared to traditional regressions.

4- z_{gl} is a more predictive Vs_{30} proxy than topographic slope. A model to map Vs_{30} using the combination of geology (proxy of Vs) and z_{gl} (soil thickness) is developed.

5- Vs(z) distribution and relationships of major geologic units were updated (post-glacial sediments) or determined for the first time (glacial sediments, sedimentary and igneous rocks). Vs(z) of both geologic rock types established that Vs_{30} of Tertiary sedimentary rock is lower than pre-Tertiary igneous rock (as expected) such that one single reference site condition across Metro Vancouver is not appropriate.

6- Regional prediction of site-specific ground motions via 1D SRA for Metro Vancouver is more challenging than any other Canadian city in terms of the regional probabilistic seismic hazard (three earthquake source types), significant thickness (hundreds of meters) of both post-glacial and glacial sediments, and lack of a single reference site condition (sedimentary and igneous rock types).

7- The use of an ergodic (BSSA14 GMM) site amplification model for western North America underestimates linear site amplification at the site natural period (T_0) for shallow sites, specifically in the North Shore, and overestimates linear amplification for soft deep sites.

8- In addition, deep soft sites in Metro Vancouver exhibit stronger nonlinearity (deamplification) at shorter periods relative to western North America GMM model. Nonlinear site amplification of the ergodic model is more applicable for shallow sites in Metro Vancouver.

9- Unless supported by geologic evidence, Vs reversals in post-glacial sediments should be removed from SRA modeling. Vs reversals in glacial sediments have less effect on SRA amplification.

7.2 Recommendations for future research

The seismic site characteristic data acquired within the Metro Vancouver seismic microzonation mapping project allows further investigations that will enhance understanding of seismic site effects in Metro Vancouver. Recommendations for future research include:

1- Obtaining larger passive-source array measurements in FRD to constrain Vs at deep depths (lower frequencies than $f_{1,HVSR}$) beneath the FRD.

2- Exploring correlations between $f_{0,HVSR}$, $f_{1,HVSR}$, f_0, and depths to glacial sediments and bedrock elsewhere in the region from available borehole data and MHVSR measurements (Sirohey 2022). Such correlations can be very useful in defining soil model depths for SRA.

3- Developing soil-type specific CPT-to-Vs correlations from the compiled SCPT database.

4- Investigating the correlation between Vs_{30} and $f_{0,HVSR}$ from the extensive available MHVSR measurements in the region.

5- Investigating the applicability of remote sensing techniques (e.g., topographic slope, terrain classification, and geographical features) with machine learning

methods to develop province wide site characteristic prediction models (e.g., Vs_{30}, f_0) based on the large *in situ* project's database.

6- Completing linear and nonlinear SRA at more (51 recommended) sites in combination with additional SRA sensitivity analyses on the effects of modeling choices and soil model variability (using randomizations) to the predicted site amplification.

7- Proposing a region-specific site amplification model based on Vs_{30}, T_0, and PGA_r and comparing the model to limited observed ground motions from recorded earthquakes.

8- Incorporating the developed site amplification model into regional PSHA and comparison with the national-scale CanadaSHM6 PSHA results.

7.3   References

Sirohey, A. (2022). Soil amplification and peak frequencies from thousands of passive seismic measurements across metro Vancouver, British Columbia, Canada. London, Ontario: The University of Western University, ETD 8810.

Appendix A

Table A-1. MHVSR peak frequencies with nearby borehole characteristics used to develop Eq. 3-5.

MHVSR site	Latitude (°N)	Longitude (°E)	$f_{0,HSVR}$ (Hz)	$f_{1,HVSR}$ (Hz)	Glacial sediment depth (z_{gl}) (m)	Borehole site	Borehole distance from site (m)
VNC4_UWO6	49.21016	-123.112	0.59	3.347	10.7	AH20-03-VWP	16
VNC5_UWO6	49.2089	-123.112	0.779	2.134	17.1	AH20-10-ENV	20
94-3_Sheri1*	49.1715	-123.056	0.39	2	19	FD94-3	Within meters
VNC7_UWO6	49.20819	-123.111	0.513	1.911	22.95	SCPT20-11	28
VNC10_UWO6	49.20721	-123.111	0.506	1.626	27	CPT20-12	39
RMD3_UWO1	49.20035	-123.113	0.416	1.399	32	FD92-2	23
FD977_UWO1	49.1118	-122.912	0.307	1.396	32	FD97-7	44
RMD56_UWO1	49.1982	-123.138	0.247	1.44	35	FD90-1	80
RMD69_UWO6	49.19569	-123.122	0.282	1.036	44	RAN18546	55
FD97-2_Sheri*	49.0645	-123.157	0.3	1	50	FD97-2	Within meters
TS409a	49.04831	-123.11	0.286	1.162	51	FD86-5	12
FD952_UWO7	49.06811	-123.152	0.287	1.008	52	FD95-2	8
RMD6_UWO1	49.19882	-123.114		1.226	53	FD96-2	47
RI072b	49.20233	-123.048		1.094	56	FD97-4	57
RMD31_UWO1	49.17597	-123.114	0.229	0.907	236	FD94-4	33
RMD961_UWO6	49.16398	-123.138	0.227	0.836	305	FD96-1	7
RMD14_UWO7	49.12398	-123.078	0.229	0.66	313.9	BH13-01	19

*: digital MHVSR curves are not available. MHVSR peak frequencies provided by co-author Sheri Molnar.
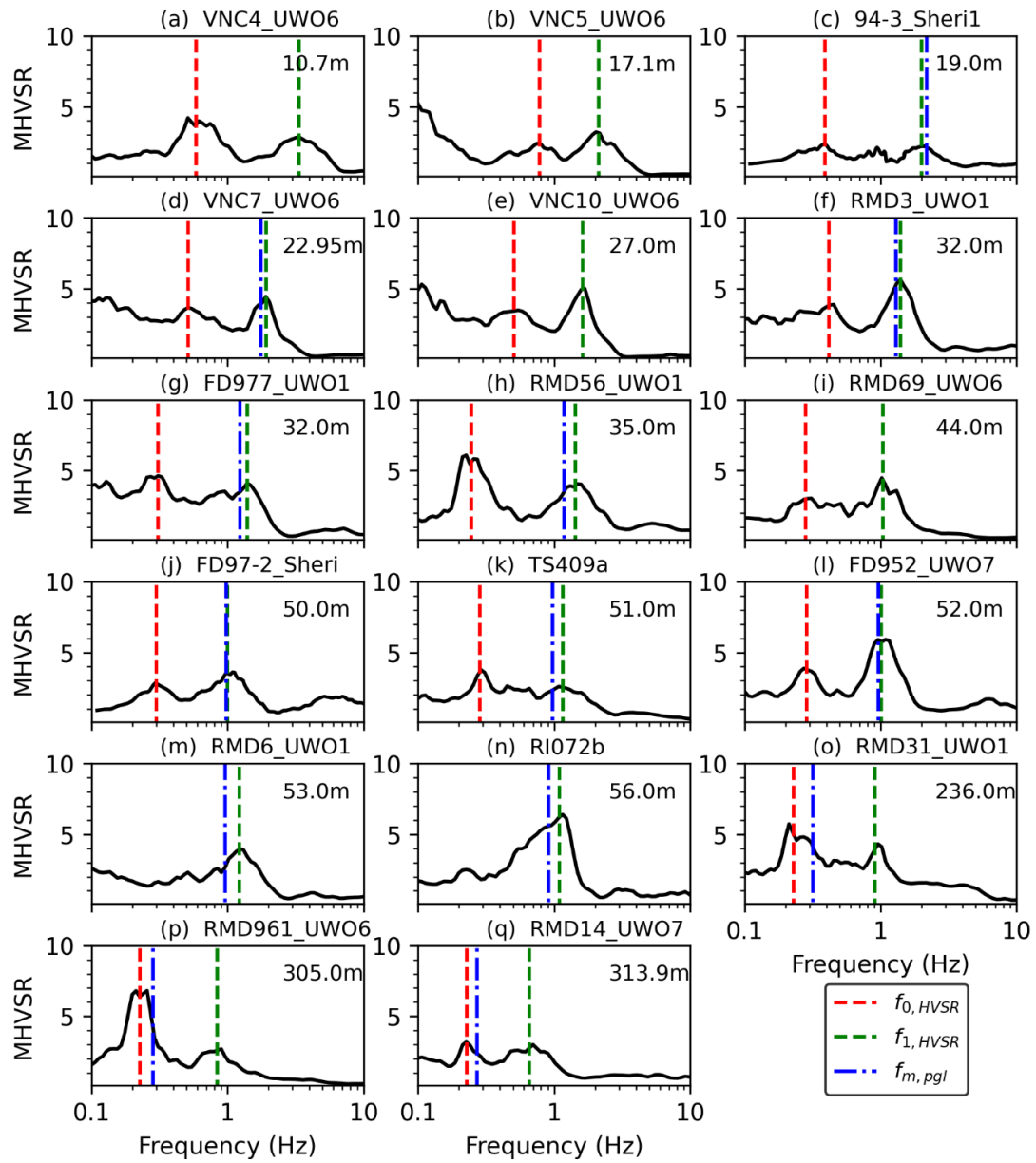
Figure A-1. MHVSRs at the 17 sites with picked peak frequencies (see legend) and depth to glacial sediments (text in upper right of each plot). The forward-predicted $f_{m,pgl}$ for boreholes with available Vs profiles is also shown.

Appendix B

Table B-1. Multi-linear regression (MLR) coefficients of 5 CPT-Vs relationships for Metro Vancouver.

Model	Equation of $\ln(V_s)$	a ± standard error	b ± standard error	c ± standard error	d ± standard error
A07	a+ b. $\ln(q_t)$+c. $\ln(I_c)$ +d. $\ln(z)$	3.25 ± 0.0897	0.15 ± 0.00909	0.214 ± 0.0348	0.193 ± 0.00652
MG15_q_t	a+ b. $\ln(q_t)$+c. $\ln(f_s)$ +d. $\ln(z)$	3.8 ± 0.0264	0.0905 ± 0.00415	0.0134 ± 0.00579	0.224 ± 0.00375
MG15_q_c	a+ b. $\ln(q_c)$+c. $\ln(f_s)$ +d. $\ln(z)$	3.81 ± 0.0259	0.0884 ± 0.00408	0.0132 ± 0.00583	0.226 ± 0.00376
W12_q_t	a+ b. $\ln(q_t)$+c. $\ln(f_s)$ +d. $\ln(\sigma'_v)$	3.03 ± 0.0323	0.104 ± 0.00417	-0.0174 ± 0.00597	0.275 ± 0.00458
W12_q_c	a+ b. $\ln(q_c)$+c. $\ln(f_s)$ +d. $\ln(\sigma'_v)$	3.05 ± 0.0321	0.102 ± 0.00411	-0.018 ± 0.00601	0.277 ± 0.00461

Vs in m/s; z in meters; q_c, q_t, f_s and σ'_v in kPa. I_c unitless.

Table B-2. Nonlinear regression (NLR) coefficients of 5 CPT-Vs relationships for Metro Vancouver.

Model	Equation of Vs	a ± standard error	b ± standard error	c ± standard error	d ± standard error
A07	$a\ q_t^b\ I_c^c\ z^d$	37.2 ± 3.4	0.111 ± 0.00943	0.0951 ± 0.0354	0.217 ± 0.00757
MG15_q_t	$a\ q_t^b\ f_s^c\ z^d$	47.1 ± 1.44	0.0866 ± 0.00428	0.00147 ± 0.00587	0.234 ± 0.00439
MG15_q_c	$a\ q_c^b\ f_s^c\ z^d$	48 ± 1.44	0.0843 ± 0.00421	0.00136 ± 0.00592	0.235 ± 0.00442
W12_q_t	$a\ q_t^b\ f_s^c\ \sigma_v'^d$	22.8 ± 0.886	0.095 ± 0.00432	-0.0238 ± 0.00609	0.279 ± 0.00521
W12_q_c	$a\ q_c^b\ f_s^c\ \sigma_v'^d$	23.1 ± 0.893	0.0927 ± 0.00426	-0.0241 ± 0.00615	0.28 ± 0.00525

Table B-3. Random Forest regression (RFR) hyper-tuned model parameters of 5 CPT-Vs relationships for Metro Vancouver .

Model_Name	n_estimators	max_depth	max_features	max_samples
A07	150	6	2	0.67
R09	150	6	2	0.67
MG15_q_t	400	6	2	0.67
MG15_q_c	400	6	2	0.67
W12_q_t	500	6	2	0.67
W12_q_c	500	6	2	0.67

n_estimators: number of trees; **max_depth**: maximum depth of a tree; **max_features**: number of predictor variables used in each node split; **max_samples**: ratio of the training data used in building each tree.

Table B-4. Extreme Gradient Boosting regression (XGBR) hyper-tuned model parameters of 5 CPT-Vs relationships for Metro Vancouver .

Model_Name	n_estimators	max_depth	min_child_weight	eta	colsample_bynode	subsample
A07	100	4	5	0.05	2	0.67
R09	200	4	4	0.025	2	0.67
MG15_q_t	200	4	5	0.025	2	0.67
MG15_q_c	200	4	4	0.025	2	0.67
W12_q_t	100	4	4	0.05	2	0.67
W12_q_c	100	4	5	0.05	2	0.67

n_estimators: number of trees; **max_depth**: maximum depth of a tree; **min_child_weight**: minimum sum of instance weight (hessian) needed in a child. **eta**: Step size shrinkage used in update to prevents overfitting **colsample_bynode**: number of predictor variables used in each node split; **subsample**: ratio of the training data used in building each tree

Appendix C
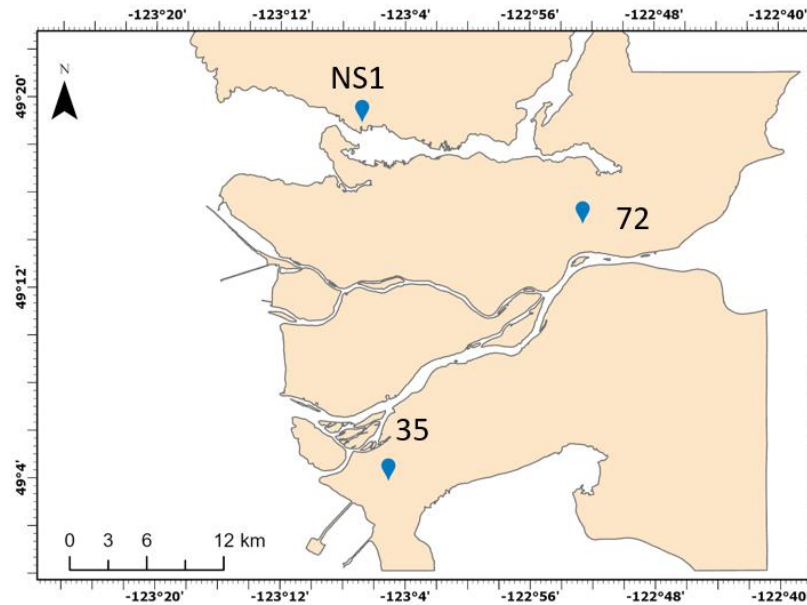
Figure C-1. Selected reference sites 35 and 72 (Vs₃₀ = 760 m/s) and NS1 (Vs₃₀ = 1500 m/s) for developing input time histories.
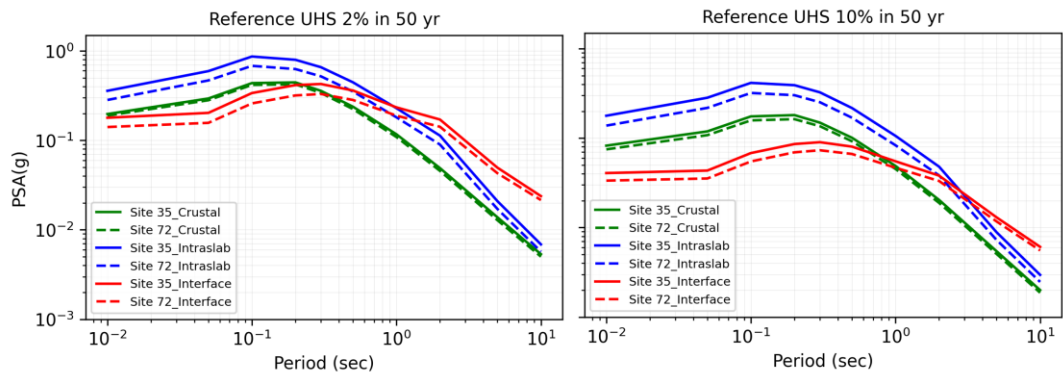
Figure C-2. Individual UHS at the 2 and 10 % in 50 yr POE at reference sites 35 and 72 (Vs₃₀ = 760 m/s).
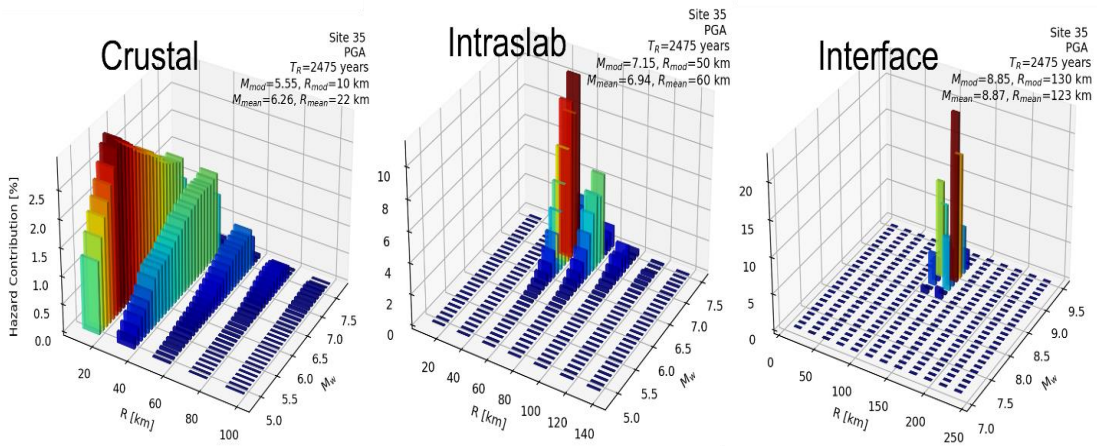
Figure C-3. Example disaggregation of PGA at site 35 for 2 % in 50 yr POE (2475 years return period).
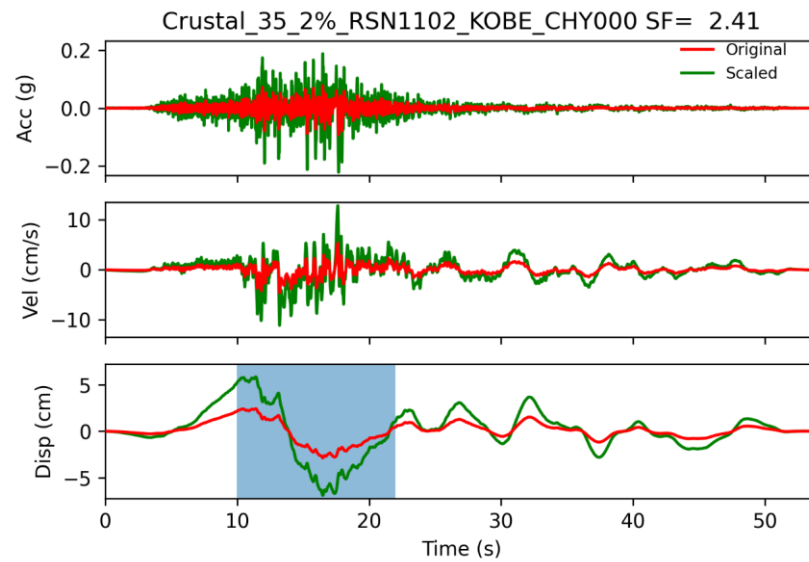
Figure C-4. Original and scaled example crustal acceleration, velocity, and displacement time series (M$_w$=6.9 and R$_{rup}$=50 km) with significant duration (D5_95) as a blue shaded box for site 35 at 2 % in 50 yr POE.
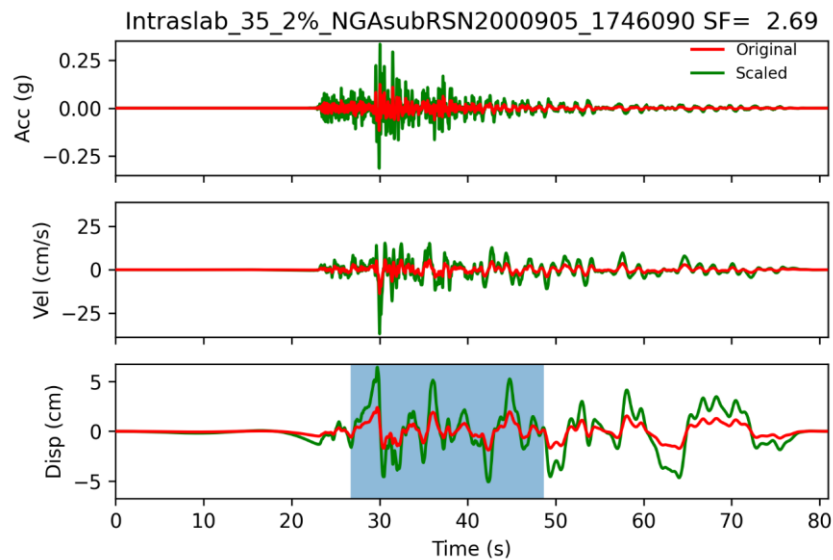
Figure C-5. Original and scaled example intraslab acceleration, velocity, and displacement time series (M$_w$=6.55 and R$_{rup}$=43 km) with significant duration (D5_95) as a blue shaded box for site 35 at 2 % in 50 yr POE.
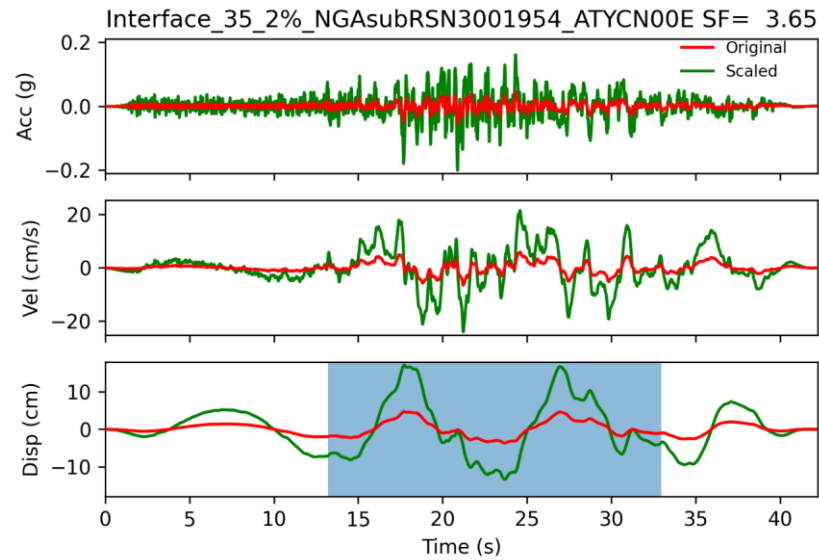
Figure C-6. Original and scaled example interface acceleration, velocity, and displacement time series (M$_w$=7.99 and R$_{rup}$=126 km) with significant duration (D5_95) as a blue shaded box for reference site 35 at 2 % in 50 yr POE.
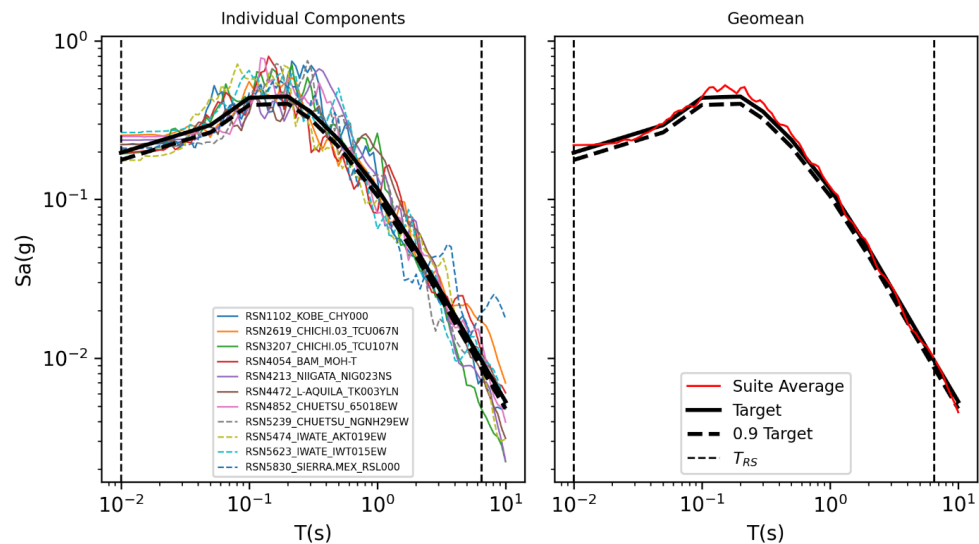
Figure C-7. Individual target UHS for shallow crustal earthquakes for reference site 35 at 2 % in 50 yr POE compared to PSA spectra of 11 crustal earthquakes (left) and their geometric mean (right) in log-log scale.
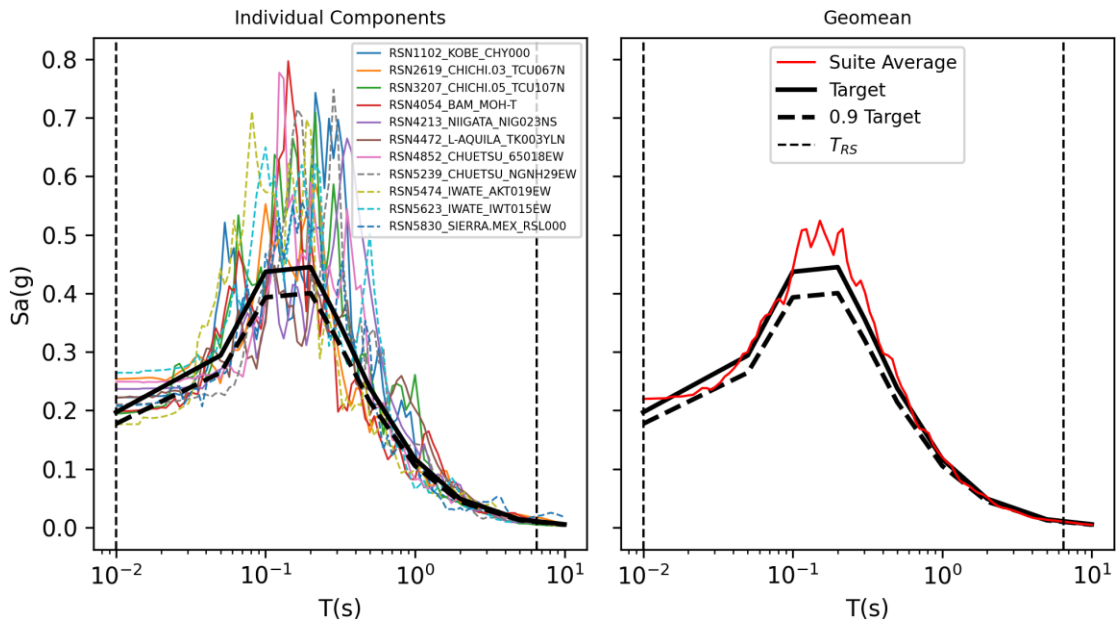
Figure C-8. Same as Figure C-7, log-lin scale.

Table C-1. Characteristics of the 11 selected crustal earthquake recordings for reference site 35 and POE 2 % in 50 yr (Figure C-7 and C-8).

RSN[*]	Earthquake Name	Year	M_w	Station Name	R_{rup} (km)	Vs_{30} (m/s)	Comp[+]	SF
1102	Kobe, Japan	1995	6.9	Chihaya	50	609	00°	2.41
2619	Chi-Chi, Taiwan-03	1999	6.2	TCU067	28	434	N	1.2
3207	Chi-Chi, Taiwan-05	1999	6.2	TCU107	56	409	N	2.09
4054	Bam, Iran	2003	6.6	Mohammad Abad-e-Madkoon	46	575	T	2.75
4213	Niigata, Japan	2004	6.63	NIG023	26	655	NS	0.59
4472	L'Aquila, Italy	2009	6.3	Celano	21	613	YLN	2.41
4852	Chuetsu-oki, Japan	2007	6.8	Joetsu, Aramaki District	33	606	EW	0.98
5239	Chuetsu-oki, Japan	2007	6.8	NGNH29	47	465	EW	2.02
5474	Iwate, Japan	2008	6.9	AKT019	29	640	EW	0.99
5623	Iwate, Japan	2008	6.9	IWT015	21	567	EW	1.09
5830	El Mayor-Cucapah, California	2010	7.2	RANCHO SAN LUIS	45	524	00°	3.39

Table C-2. Characteristics of the 11 selected crustal earthquake recordings for reference site 35 and POE 10 % in 50 yr.

RSN*	Earthquake Name	Year	M_w	Station Name	R_{rup} (km)	Vs_{30} (m/s)	Comp+	SF
1102	Kobe, Japan	1995	6.9	Chihaya	50	609	00°	0.96
2619	Chi-Chi, Taiwan-03	1999	6.2	TCU067	28	434	N	0.47
2954	Chi-Chi, Taiwan-05	1999	6.2	CHY046	71	442	E	0.69
2956	Chi-Chi, Taiwan-05	1999	6.2	CHY050	86	539	N	1.84
3207	Chi-Chi, Taiwan-05	1999	6.2	TCU107	56	409	N	0.82
3916	Tottori, Japan	2000	6.61	OKY013	69	472	EW	0.72
4054	Bam, Iran	2003	6.6	Mohammad Abad-e-Madkoon	46	575	T	1.09
5239	Chuetsu-oki, Japan	2007	6.8	NGNH29	47	465	NS	0.92
5288	Chuetsu-oki, Japan	2007	6.8	NIGH15	50	686	NS	1.68
5830	El Mayor-Cucapah, California	2010	7.2	RANCHO SAN LUIS	45	524	90°	1.3
6002	El Mayor-Cucapah, California	2010	7.2	RANCHO SAN LUIS	90	743	90°	1.62

Table C-3. Characteristics of the 11 selected crustal earthquake recordings for reference site 72 and POE 2 % in 50 yr.

RSN*	Earthquake Name	Year	M_w	Station Name	R_{rup} (km)	Vs_{30} (m/s)	Comp+	SF
1102	Kobe, Japan	1995	6.9	Chihaya	50	609	00°	2.24
2619	Chi-Chi, Taiwan-03	1999	6.2	TCU067	28	434	N	1.11
3207	Chi-Chi, Taiwan-05	1999	6.2	TCU107	56	409	N	1.95
4054	Bam, Iran	2003	6.6	Mohammad Abad-e-Madkoon	46	575	T	2.55
4213	Niigata, Japan	2004	6.63	NIG023	26	655	NS	0.54
4472	L'Aquila, Italy	2009	6.3	Celano	21	613	YLN	2.24
4852	Chuetsu-oki, Japan	2007	6.8	Joetsu, Aramaki District	33	606	EW	0.92

5239	Chuetsu-oki, Japan	2007	6.8	NGNH29	47	465	EW	1.88
5474	Iwate, Japan	2008	6.9	AKT019	29	640	EW	0.92
5623	Iwate, Japan	2008	6.9	IWT015	21	567	EW	1.01
5830	El Mayor-Cucapah, California	2010	7.2	RANCHO SAN LUIS	45	524	00°	3.15

*RSN is the record sequence number in the PEER database. ⁺component azimuth as reported in the PEER database.

Table C-4. Characteristics of the 11 selected crustal earthquake recordings for reference site 72 and POE 10 % in 50 yr.

RSN*	Earthquake Name	Year	M_w	Station Name	R_{rup} (km)	Vs_{30} (m/s)	Comp⁺	SF
1102	Kobe, Japan	1995	6.9	Chihaya	50	609	00°	0.89
2619	Chi-Chi, Taiwan-03	1999	6.2	TCU067	28	434	N	0.44
2954	Chi-Chi, Taiwan-05	1999	6.2	CHY046	71	442	E	0.64
2956	Chi-Chi, Taiwan-05	1999	6.2	CHY050	86	539	N	1.7
3207	Chi-Chi, Taiwan-05	1999	6.2	TCU107	56	409	N	0.76
3916	Tottori, Japan	2000	6.61	OKY013	69	472	EW	0.67
4054	Bam, Iran	2003	6.6	Mohammad Abad-e-Madkoon	46	575	T	1.01
5239	Chuetsu-oki, Japan	2007	6.8	NGNH29	47	465	NS	0.85
5288	Chuetsu-oki, Japan	2007	6.8	NIGH15	50	686	EW	1.56
5830	El Mayor-Cucapah, California	2010	7.2	RANCHO SAN LUIS	45	524	90°	1.2
6002	El Mayor-Cucapah, California	2010	7.2	RANCHO SAN LUIS	90	743	90°	1.5

*RSN is the record sequence number in the PEER database. ⁺component azimuth as reported in the PEER database.

Table C-5. Characteristics of the 11 selected intraslab earthquake recordings for reference site 35 and POE 2 % in 50 yr.

NGAsubRSN*	Earthquake Name/ Location	Year	M_w	Station Name	R_{rup} (km)	Vs_{30} (m/s)	Comp⁺	SF
2000905	Ferndale, California	2010	6.55	1746	43	362	90°	2.69
3001493	184, Michoacan, Mexico	1997	7.15	LA UNION	90	517	90°	3.92
4007352^	Miyagi_Pre.Off, Japan	2011	7.15	KANEGA SAKI	114	486	NS2	1.64

4007390^	Miyagi_Pre.Off, Japan	2011	7.15	ONODA	101	305	EW2	0.99
4016859^	Miyagi_Pre.Off, Japan	2011	7.15	HARAM ACHI	99	535	EW	1.54
4027318^	Geiyo, Japan	2001	6.83	KAWAU CHI	45	366	EW	2.9
4027361^	Geiyo, Japan	2001	6.83	ONOMIC HI	65	535	EW	4.38
4027554^	Geiyo, Japan	2001	6.83	MUIKAI CHI	85	482	EW	3.58
4027602^	Geiyo, Japan	2001	6.83	KANO	93	367	NS	4.15
6001243	2575090, Antofagasta, Chile	2007	6.74	MEJILLO NE	46	745	NS	2.87
6001245	2575090 Antofagasta, Chile	2007	6.74	MICHILL A	48	1087	EW	2.59

*NGAsubRSN is the record sequence number in the NGA-Subduction database. +component azimuth as reported in the NGA-Subduction database. ^downloaded from KiK-net/K-NET.

Table C-6. Characteristics of the 11 selected intraslab earthquake recordings for reference site 35 and POE 10 % in 50 yr.

NGAsubRSN	Earthquake Name/ Location	Year	M_w	Station Name	R_{rup} (km)	Vs_{30} (m/s)	Comp	SF
2000037	Nisqually, Cascadia	2001	6.8	ELW	84	438	E	2.75
2000052	Nisqually, Cascadia	2001	6.8	MURR	47	521	N	2.64
3001493	184, Michoacan, Mexico	1997	7.15	LA UNION	90	517	00°	1.99
4007391^	Miyagi_Pre.Off, Japan	2011	7.15	TAJIRI	82	593	NS2	0.59
4016859^	Miyagi_Pre.Off	2011	7.15	HARAM ACHI	99	535	EW	0.68
4027443^	Geiyo, Japan	2001	6.83	OHTOY O	96	526	NS	3.44
4027602^	Geiyo, Japan	2001	6.83	KANO	93	367	NS	1.84
6001245	2575090, Antofagasta, Chile	2007	6.74	MICHILL A	48	1087	EW	1.15
6001246	2575090, Antofagasta, Chile	2007	6.74	TOCOPI LLA PUERTO (SOQUI MICH)	95	605	EW	2.2
7006045	Pingtung.Doublet1 , Japan	2006	7.02	KAU042	51	816	N	0.89
7006355	Pingtung.Doublet2 , Japan	2006	6.94	CHY100	107	344	E	2.14

Table C-7. Characteristics of the 11 selected intraslab earthquake recordings for reference site 72 and POE 2 % in 50 yr.

NGAsubRSN	Earthquake Name/ Location	Year	M_w	Station Name	R_{rup} (km)	Vs_{30} (m/s)	Comp	SF
2000052	Nisqually, Cascadia	2001	6.8	MURR	47	521	E	3.57
3001294	143, El Salvador	2014	7.32	644	120	517	02	3.31
3001493	184, Michoacan, Mexico	1997	7.15	LA UNION	90	517	00°	3.64
4007352^	Miyagi_Pre.Off, Japan	2011	7.15	KANEG ASAKI	114	486	NS2	1.33
4016859^	Miyagi_Pre.Off, Japan	2011	7.15	HARAM ACHI	99	535	EW	1.24
4027361^	Geiyo, Japan	2001	6.83	ONOMIC HI	65	535	EW	3.53
4027554^	Geiyo, Japan	2001	6.83	MUIKAI CHI	85	482	EW	2.89
4027602^	Geiyo, Japan	2001	6.83	KANO	93	367	NS	3.36
6001243	2575090, Antofagasta, Chile	2007	6.74	MEJILLO NE	46	745	NS	2.32
6001245	2575090, Antofagasta, Chile	2007	6.74	MICHILL A	48	1087	EW	2.09
7006045	Pingtung.Doubl et1, Japan	2006	7.02	KAU042	51	816	N	1.6

Table C-8. Characteristics of the 11 selected intraslab earthquake recordings for reference site 72 and POE 10 % in 50 yr.

NGAsubRSN	Earthquake Name/ Location	Year	M_w	Station Name	R_{rup} (km)	Vs_{30} (m/s)	Comp	SF
2000037	Nisqually, Cascadia	2001	6.8	ELW	84	438	E	2.27
2000052	Nisqually, Cascadia	2001	6.8	MURR	47	521	NN	2.18
3001493	184, Michoacan, Mexico	1997	7.15	LA UNION	90	517	00°	1.65
4007391^	Miyagi_Pre.Off, Japan	2011	7.15	TAJIRI	82	593	NS2	0.49

4016859^	Miyagi_Pre.Off, Japan	2011	7.15	HARAM ACHI	99	535	EW	0.56
4027443^	Geiyo, Japan	2001	6.83	OHTOY O	96	526	NS	2.85
4027602^	Geiyo, Japan	2001	6.83	KANO	93	367	NS	1.52
6001245	2575090, Antofagasta, Chile	2007	6.74	MICHILL A	48	1087	EW	0.94
6001246	2575090, Antofagasta, Chile	2007	6.74	TOCOPI LLA PUERTO (SOQUI MICH)	95	605	EW	1.82
7006045	Pingtung.Doublet1, Japan	2006	7.02	KAU042	51	816	N	0.73
7006355	Pingtung.Doublet2, Japan	2006	6.94	CHY100	107	344	E	1.77

*NGAsubRSN is the record sequence number in the NGA-Subduction database. +component azimuth as reported in the NGA-Subduction database. ^downloaded from KiK-net/K-NET.

Table C-9. Characteristics of the 11 selected interface earthquake recordings for reference site 35 and POE 2 % in 50 yr.

NGAsubRSN	Earthquake Name/ Location	Year	M_w	Station Name	R_{rup} (km)	Vs_{30} (m/s)	Comp	SF
3001954	Michoacan, Mexico	1985	7.99	ATOYAC, Iglesia	126	429	00°	3.65
3001963	Michoacan, Mexico	1985	7.99	TEACAL CO	181	517	00°	3.62
4000330^	Tohoku, Japan	2011	9.12	ROKKAS YO	146	434	EW2	3.31
4000401^	Tohoku, Japan	2011	9.12	TOMIOK A	168	421	EW2	2.39
4000713^	Tohoku, Japan	2011	9.12	KYOWA	167	606	NS	3.5
4000717^	Tohoku, Japan	2011	9.12	YOKOTE	138	571	EW	2.98
4001035^	Tohoku, Japan	2011	9.12	FIJINO	152	589	EW	3.82
4022854^	Tokachi-oki, Japan	2003	8.29	HOBETS U	122	542	NS2	3.09
4028580^	Tokachi-oki, Japan	2003	8.29	TOMUR AUSHI	117	673	NS	3.96
4028605	Tokachi-oki, Japan	2003	8.29	OIWAKE	138	351	NS	1.67
6001396	Iquique, Chile	2014	8.15	TAC2	107	382	EW	3

*NGAsubRSN is the record sequence number in the NGA-Subduction database. +component azimuth as reported in the NGA-Subduction database. ^downloaded from KiK-net/K-NET.

Table C-10. Characteristics of the 11 selected interface earthquake recordings for reference site 35 and POE 10 % in 50 yr.

NGAsubRSN	Earthquake Name/ Location	Year	M_w	Station Name	R_{rup} (km)	Vs_{30} (m/s)	Comp	SF

3001963	Michoacan, Mexico	1985	7.99	TEACAL CO	181	517	00°	0.81
4000400^	Tohoku, Japan	2011	9.12	TAKAY AMA	179	624	EW2	1.16
4000721^	Tohoku, Japan	2011	9.12	ANI	174	577	NS	1.95
4000813^	Tohoku, Japan	2011	9.12	KANEY AMA	158	494	NS	1.18
4001246^	Tohoku, Japan	2011	9.12	SHIMOY ACHI	145	428	NS	0.74
4022854^	Tokachi-oki, Japan	2003	8.29	HOBETS U	122	542	NS2	0.69
4022895^	Tokachi-oki, Japan	2003	8.29	FURANO	149	403	NS2	1.42
4022900^	Tokachi-oki, Japan	2003	8.29	BIEI-E	147	771	EW2	1.14
4028522^	Tokachi-oki, Japan	2003	8.29	TENNIN KYO	152	459	NS	0.91
4028580^	Tokachi-oki, Japan	2003	8.29	TOMUR AUSHI	117	673	NS	0.89
6001388	Iquique, Chile	2014	8.15	PB16	101	605	E	1.35

*NGAsubRSN is the record sequence number in the NGA-Subduction database. +component azimuth as reported in the NGA-Subduction database. ^downloaded from KiK-net/K-NET.

Table C-11. Characteristics of the 11 selected interface earthquake recordings for reference site 72 and POE 2 % in 50 yr.

NGAsubRSN	Earthquake Name/ Location	Year	M_w	Station Name	R_{rup} (km)	Vs_{30} (m/s)	Comp	SF
3001954	Michoacan, Mexico	1985	7.99	ATOYAC , Iglesia	126	429	00°	2.95
3001963	Michoacan, Mexico	1985	7.99	TEACAL CO	181	517	00°	2.92
4000330^	Tohoku, Japan	2011	9.12	ROKKAS YO	146	434	EW2	2.68
4000485^	Tohoku, Japan	2011	9.12	KIYOKA WA	154	793	EW2	3.91
4000713^	Tohoku, Japan	2011	9.12	KYOWA	167	606	NS	2.83
4000717^	Tohoku, Japan	2011	9.12	YOKOTE	138	571	EW	2.41
4001246^	Tohoku, Japan	2011	9.12	SHIMOY ACHI	145	428	EW	2.41
4022854^	Tokachi-oki, Japan	2003	8.29	HOBETS U	122	542	NS2	2.49
4028522^	Tokachi-oki, Japan	2003	8.29	TENNIN KYO	152	459	NS	3.28
4028580^	Tokachi-oki, Japan	2003	8.29	TOMUR AUSHI	117	673	NS	3.2
4028581	Tokachi-oki, Japan	2003	8.29	HIDAKA	107	360	NS	2

*NGAsubRSN is the record sequence number in the NGA-Subduction database. +component azimuth as reported in the NGA-Subduction database. ^downloaded from KiK-net/K-NET.

Table C-12. Characteristics of the 11 selected interface earthquake recordings for reference site 72 and POE 10 % in 50 yr.

NGAsubRSN	Earthquake Name/ Location	Year	M_w	Station Name	R_{rup} (km)	Vs_{30} (m/s)	Comp	SF
3001963	Michoacan, Mexico	1985	7.99	TEACAL CO	181	517	00°	0.68
4000400^	Tohoku, Japan	2011	9.12	TAKAY AMA	179	624	EW2	0.97
4000719^	Tohoku, Japan	2011	9.12	OGACHI	138	431	NS	0.83
4000721^	Tohoku, Japan	2011	9.12	ANI	174	577	NS	1.64
4000813^	Tohoku, Japan	2011	9.12	KANEY AMA	158	494	NS	0.99
4001246^	Tohoku, Japan	2011	9.12	SHIMOY ACHI	145	428	NS	0.62
4022854^	Tokachi-oki, Japan	2003	8.29	HOBETS U	122	542	NS2	0.58
4022895^	Tokachi-oki, Japan	2003	8.29	FURANO	149	403	NS2	1.19
4022900^	Tokachi-oki, Japan	2003	8.29	BIEI-E	147	771	EW2	0.95
4028522^	Tokachi-oki, Japan	2003	8.29	TENNIN KYO	152	459	NS	0.76
6001388	Iquique, Chile	2014	8.15	PB16	101	605	E	1.13

[*]NGAsubRSN is the record sequence number in the NGA-Subduction database. [+]component azimuth as reported in the NGA-Subduction database. ^downloaded from KiK-net/K-NET.

Table C-13. Characteristics of the 11 selected crustal earthquake recordings for reference site NS1 and POE 2 % in 50 yr.

RSN[*]	Earthquake Name	Year	M_w	Station Name	R_{rup} (km)	Vs_{30} (m/s)	Comp[+]	SF
1102	Kobe, Japan	1995	6.9	Chihaya	50	609	00°	1.74
2820	Chi-Chi, Taiwan-04	1999	6.2	Chihaya	40	665	E	2.3
2935	Chi-Chi, Taiwan-04	1999	6.2	KAU050	38	665	E	1.91
3472	Chi-Chi, Taiwan-06	1999	6.3	TTN051	26	615	N	1.19
3920	Tottori, Japan	2000	6.61	TCU076	71	1047	EW	3.47
4054	Bam, Iran	2003	6.6	OKYH02	46	575	T	1.99
4472	L'Aquila, Italy	2009	6.3	Mohammad Abad-e-Madkoon	21	613	YLN	1.74
5288	Chuetsu-oki, Japan	2007	6.8	Celano	50	686	EW	3.09
5474	Iwate, Japan	2008	6.9	NIGH15	29	640	EW	0.71
5623	Iwate, Japan	2008	6.9	AKT019	21	567	EW	0.79
5830	El Mayor-Cucapah, California	2010	7.2	IWT015	45	524	90°	2.37

*RSN is the record sequence number in the PEER database. + component azimuth as reported in the PEER database.

Table C-14. Characteristics of the 11 selected crustal earthquake recordings for reference site NS1 and POE 10 % in 50 yr.

RSN*	Earthquake Name	Year	M_w	Station Name	R_{rup} (km)	Vs_{30} (m/s)	Comp+	SF
1102	Kobe, Japan	1995	6.9	Chihaya	50	609	00°	0.7
2820	Chi-Chi, Taiwan-04	1999	6.2	KAU050	40	665	E	0.93
2935	Chi-Chi, Taiwan-04	1999	6.2	TTN051	38	665	E	0.77
2946	Chi-Chi, Taiwan-05	1999	6.2	CHY029	60	545	N	0.64
3920	Tottori, Japan	2000	6.61	OKYH02	71	1047	EW	1.39
4054	Bam, Iran	2003	6.6	Mohammad Abad-e-Madkoon	46	575	T	0.8
4472	L'Aquila, Italy	2009	6.3	Celano	21	613	YLN	0.7
5288	Chuetsu-oki, Japan	2007	6.8	NIGH15	50	686	EW	1.24
5292	Chuetsu-oki, Japan	2007	6.8	NIGH19	60	625	EW	1.21
5446	Chuetsu-oki, Japan	2007	6.8	YMTH05	106	533	NS	2.32
5830	El Mayor-Cucapah, California	2010	7.2	RANCHO SAN LUIS	45	524	90°	0.95

*RSN is the record sequence number in the PEER database. + component azimuth as reported in the PEER database.

Table C-15. Characteristics of the 11 selected intraslab earthquake recordings for reference site NS1 and POE 2 % in 50 yr

NGAsubRSN	Earthquake Name/ Location	Year	M_w	Station Name	R_{rup} (km)	Vs_{30} (m/s)	Comp	SF
2000036	Nisqually, Cascadia	2001	6.8	EARN	89	506	N	3.56
2000052	Nisqually, Cascadia	2001	6.8	MURR	47	521	N	4.12
3001294	143, El Salvador	2014	7.32	644	120	517	02	2.82
3001493	184, Michoacan, Mexico	1997	7.15	LA UNION	90	517	90°	2.71
4016859^	Miyagi_Pre.Off, Japan	2011	7.15	HARAM ACHI	99	535	EW	1.06
4017058^	Miyagi_Pre.Off, Japan	2011	7.15	TAIWA	88	579	EW	0.72
4027352^	Geiyo, Japan	2001	6.83	KOHNU	79	611	EW	3.9
4027361^	Geiyo, Japan	2001	6.83	ONOMIC HI	65	535	EW	3.02

NGAsubRSN	Earthquake Name/ Location	Year	M_w	Station Name	R_{rup} (km)	Vs_{30} (m/s)	Comp	SF
6001243	2575090, Antofagasta, Chile	2007	6.74	MEJILLONE	46	745	NS	1.99
6001245	2575090, Antofagasta, Chile	2007	6.74	MICHILLA	48	1087	EW	1.79
7006045	Pingtung.Doublet1, Japan	2006	7.02	KAU042	51	816	N	1.38

*NGAsubRSN is the record sequence number in the NGA-Subduction database. +component azimuth as reported in the NGA-Subduction database. ^downloaded from KiK-net/K-NET.

Table C-16. Characteristics of the 11 selected intraslab earthquake recordings for reference site NS1 and POE 10 % in 50 yr

NGAsubRSN	Earthquake Name/ Location	Year	M_w	Station Name	R_{rup} (km)	Vs_{30} (m/s)	Comp	SF
2000036	Nisqually, Cascadia	2001	6.8	EARN	89	506	N	1.56
2000052	Nisqually, Cascadia	2001	6.8	MURR	47	521	N	1.81
3001294	143, El Salvador	2014	7.32	644	120	517	02	1.24
3001493	184, Michoacan, Mexico	1997	7.15	LA UNION	90	517	E	1.37
4016859	Miyagi_Pre.Off, Japan	2011	7.15	HARAMACHI	99	535	EW	0.47
4027352	Geiyo, Japan	2001	6.83	TAIWA	79	611	NS	2.02
4027361	Geiyo, Japan	2001	6.83	KOHNU	65	535	EW	1.32
4027443	Geiyo, Japan	2001	6.83	ONOMICHI	96	526	NS	2.36
4027552	Geiyo, Japan	2001	6.83	MEJILLONE	107	661	NS	3.5
6001245	2575090, Antofagasta, Chile	2007	6.74	MICHILLA	48	1087	EW	0.79
7006045	Pingtung.Doublet1, Japan	2006	7.02	KAU042	51	816	N	0.6

*NGAsubRSN is the record sequence number in the NGA-Subduction database. +component azimuth as reported in the NGA-Subduction database. ^downloaded from KiK-net/K-NET

Table C-17. Characteristics of the 11 selected interface earthquake recordings for reference site NS1 and POE 2 % in 50 yr.

NGAsubRSN	Earthquake Name/ Location	Year	M_w	Station Name	R_{rup} (km)	Vs_{30} (m/s)	Comp	SF
3001963	Michoacan, Mexico	1985	7.99	TEACALCO	181	517	00°	2.59
4000357^	Tohoku, Japan	2011	9.12	ATSUSHIOKANOU	138	508	EW2	2.27
4000400^	Tohoku, Japan	2011	9.12	TAKAYAMA	179	624	EW2	3.71

4000485	Tohoku, Japan	2011	9.12	KIYOKA WA	154	793	EW2	3.44
4000713^	Tohoku, Japan	2011	9.12	KYOWA	167	606	NS	2.5
4000843^	Tohoku, Japan	2011	9.12	SAKAM OTO	187	663	EW	2.72
4001242^	Tohoku, Japan	2011	9.12	YAMAG ATA	120	539	EW	1.44
4022854^	Tokachi-oki, Japan	2003	8.29	HOBETS U	122	542	NS2	2.21
4022900^	Tokachi-oki, Japan	2003	8.29	BIEI-E	147	771	NS2	3.91
4028580^	Tokachi-oki, Japan	2003	8.29	TOMUR AUSHI	117	673	EW	3.01
6001388	Iquique, Chile	2014	8.15	PB16	101	605	N	3.77

[*]NGAsubRSN is the record sequence number in the NGA-Subduction database. [+]component azimuth as reported in the NGA-Subduction database. ^downloaded from KiK-net/K-NET.

Table C-18. Characteristics of the 11 selected interface earthquake recordings for reference site NS1 and POE 10 % in 50 yr.

NGAsubRSN	Earthquake Name/ Location	Year	M_w	Station Name	R_{rup} (km)	Vs_{30} (m/s)	Comp	SF
3001963	Michoacan, Mexico	1985	7.99	TEACAL CO	181	517	00°	0.62
4000400^	Tohoku, Japan	2011	9.12	TAKAY AMA	179	624	EW2	0.89
4000483^	Tohoku, Japan	2011	9.12	YAMAKI TA-C	169	731	EW2	1.21
4000569^	Tohoku, Japan	2011	9.12	MUIKA	186	686	NS2	2.3
4000717^	Tohoku, Japan	2011	9.12	YOKOTE	138	571	EW	0.52
4000721^	Tohoku, Japan	2011	9.12	ANI	174	577	NS	1.51
4022763^	Tokachi-oki, Japan	2003	8.29	TAKINO UE-N	181	1136	NS2	3.04
4022900^	Tokachi-oki, Japan	2003	8.29	BIEI-E	147	771	EW2	0.88
4028527^	Tokachi-oki, Japan	2003	8.29	TAKINO UE	181	728	NS	3.02
4028580^	Tokachi-oki, Japan	2003	8.29	TOMUR AUSHI	117	673	EW	0.73
6001388	Iquique, Chile	2014	8.15	PB16	101	605	E	1.04

[*]NGAsubRSN is the record sequence number in the NGA-Subduction database. [+]component azimuth as reported in the NGA-Subduction database. ^downloaded from KiK-net/K-NET.

Curriculum Vitae

Name:	Jamal Assaf

Post-secondary Education and Degrees:

Lebanese University, Beirut, Lebanon
2010-2016 Bachelors in Civil Engineering

Université Libre de Bruxelles,
Bruxelles, Belgium
2014-2016 MSc., Civil Engineering construction

Western University
Dept. Civil and Environmental Engineering
London, Ontario, Canada
2016- 2022
Ph.D., Geotechnical Engineering

Honors and Awards:

Milos Novak award
2018-2019

Related Work Experience
2016-2020

Teaching Assistant
The University of Western Ontario
Statics, Earthquake Engineering, Geotechnical Design Engineering, Lateral design

Journal Articles

Assaf, J., Molnar, S., & El Naggar, M. H. (2023). CPT-Vs correlations for post-glacial sediments in Metropolitan Vancouver. Soil Dynamics and Earthquake Engineering, 165, 107693. https://doi.org/10.1016/j.soildyn.2022.107693

Assaf, J., Molnar, S., El Naggar, M. H., & Sirohey, A. (2022). Seismic site characterization in Fraser River Delta in Metropolitan Vancouver. Soil Dynamics and Earthquake Engineering, 161, 107384. https://doi.org/https://doi.org/10.1016/j.soildyn.2022.107384

Molnar, S., Sirohey, A., **Assaf, J.**, Bard, P.-Y., Castellaro, S., Cornou, C., Cox, B., Guillier, B., Hassani, B., Kawase, H., Matsushima, S., Sánchez-Sesma, F. J., & Yong, A. (2022). A review of the microtremor horizontal-to-vertical spectral ratio (MHVSR) method. Journal of Seismology, 26(4), 653–685. https://doi.org/10.1007/s10950-021-10062-9

Molnar, S., **Assaf, J**., Sirohey, A., & Adhikari, S. R. (2020). Overview of local site effects and seismic microzonation mapping in Metropolitan Vancouver, British Columbia, Canada. Engineering Geology, 270, 5, https://doi.org/10.1016/j.enggeo.2020.105568.

Conference Papers with presentation

Assaf, J., Molnar, S., El Naggar, M.H., Sirohey, A. (2019). Seismic Site Characterization at Strong Motion Stations in Metro Vancouver, 12th Canadian Conference of Earthquake Engineering, Quebec City, Quebec, 8 pages.

Assaf, J., Molnar, S., El Naggar, M.H. (2018). Comprehensive earthquake site amplification assessment for Greater Vancouver, 71st Canadian Geotechnical conference, Edmonton, Alberta, 8 p.

Technical Reports

Assaf, J., Sirohey, A., Ghofrani, H., Molnar, S. (2022). Compilation and systematic processing of earthquake and microtremor HVSR amplification at Metro Vancouver strong-motion stations. ISSN 2816-6027. (https://metrovanmicromap.ca)

Invited Lecture

Assaf, J. (2020). Vancouver Seismic Microzonation Project: Local site effect, College of Architecture and Civil Engineering, Beijing University of Technology, 20 May 2020, virtual online.

Presentations

Assaf, **J.,** Molnar, S., El Naggar, M.H., (2019). Shear Wave Velocity Profiling at Seismic Strong Motion Stations in Vancouver, Western Geotechnical Centrifuge Grand Opening, London, Ontario, Poster.

Molnar, S., **Assaf**, **J.**, Fallah Yeznabad, A. (2018). Seismic microzonation mapping project for Metro Vancouver, British Columbia, Canada. European Seismological Commission Meeting, Valletta, Malta, Sept 2-7 2018, Oral.